Application of anthropogenic uranium radioisotopes in tracing water mass movement in the Arctic-North Atlantic Ocean

Lin, Gang

Publication date:
2023

Document Version
Publisher's PDF, also known as Version of record

DTU

DTU Sustain

Application of anthropogenic uranium radioisotopes in tracing water mass movement in the Arctic-North Atlantic Ocean

Gang Lin

PhD Thesis

Application of anthropogenic uranium radioisotopes in tracing water mass movement in the Arctic-North Atlantic Ocean

Gang Lin

PhD Thesis
September 2023

DTU Sustain
Department of Environmental and Resource Engineering
Technical University of Denmark

Application of anthropogenic uranium radioisotopes in tracing water mass movement in the Arctic-North Atlantic Ocean

Gang Lin

PhD Thesis, September, 2023

Address: DTU Sustain
Department of Environmental and Resource Engineering
Technical University of Denmark
Bygningstorvet, Building 115
2800 Kgs. Lyngby
Denmark

Phone reception: +45 4525 1600

Homepage: https://www.sustain.dtu.dk
E-mail: info@sustain.dtu.dk

Supervisor

Senior Researcher **Jixin Qiao**

Department of Environmental and Resource Engineering, Technical University of Denmark, Risø Campus, Roskilde, Denmark

Co-Supervisor

Professor **Colin Andrew Stedmon**

National Institute of Aquatic Resources, Technical University of Denmark, Lyngby, Denmark

Opponents

Professor **Charlotte Scheutz**

Department of Environmental and Resource Engineering, Technical University of Denmark, Lyngby, Denmark

Senior Scientist **Galina Lujaniene**

State Research Institute Center for Physical Sciences and Technology, Vilnius, Lithuania

Senior Scientist **Hilde Elise Heldal**

Department of Contaminants and Biohazards, Institute of Marine Research, Bergen, Norway

Preface

All works presented in the PhD thesis were conducted at the Climate and Monitoring Section, Department of Environmental and Resource Engineering, Technical University of Denmark between December 2019 - September 2023. These works were funded by Independent Research Fund Denmark (No. 9040-938 00266B), the European Union H2020 as part of the EU Project ARICE grant agreement No. 730965 and the RADIATE project from the EU Research and Innovation programme HORIZON 2020 under grant agreement No 824096, proposal NO. 21002412-ST and No. 21002394-ST.

This PhD thesis is organized in two parts: the first part is a synopsis of the findings in published papers or unpublished manuscripts within this PhD project; the second part consists of four independent papers, i.e., **Papers (I - IV)** as listed below. This thesis introduces the scientific backgrounds, the known results from previous studies and research challenges at first. And the synopsis of the novel and important findings from the four papers is shown. The obtained results provide new perspectives and insights for the current research.

Paper I: Lin, G., Lin, M., Qiao, J., Sejr, M.K., Steier, P., Meire, L., Stedmon, C.A., 2022. Estimation of Atlantic Water transit times in East Greenland fjords using a ^{233}U-^{236}U tracer approach. *Chemical Geology, 607,* 121007.

Paper II: Lin, G., Qiao, J., Steier, P., Danielsen, M., Guðnason, K., Joensen, H.P., Stedmon, C.A., 2022. Tracing Atlantic water transit time in the subarctic and Arctic Atlantic using ^{99}Tc-^{233}U-^{236}U. *Science of the Total Environment, 851,* 158276.

Paper III: Lin, G., Qiao, J., Dodd, P.A., Gonçalves-Araujo, R., Granskog, M.A., Steier, P., Stedmon, C.A., 2023. Tracing Atlantic water transit times in the Arctic Ocean: coupling reprocessing-derived ^{236}U and colored dissolved organic matter to distinguish different pathways. *Earth and Planetary Science Letters*, 118415.

Paper IV: Lin, G., Qiao, J., Steier, P., Danielsen, M., Guðnason, K., Tracing Atlantic water in and out of the Nordic Seas with reprocessing-derived ^{236}U. Manuscript in preparation.

Acknowledgements

Time flies at Risø, which is a beautiful and natural place for my PhD study. I am glad to spend almost 4 years to do the challenging research here. Calm sea in Roskilde fjord with various birds gives a deep impression for me. My research at DTU combines radiochemistry and oceanography to study water mass movement in the Arctic Ocean. Different from warm seawater near Risø Campus, cold seawater in the Arctic Ocean tells me a different world. Glacier, sea ice and polar bear satisfy my imagination of the Arctic. The earth is full of seawater, which is like an explorer, deciphering the unknown mysteries of this planet. This is why I am fascinated by marine research, and DTU provides the opportunity to achieve my dream.

I am sincerely grateful to my supervisor, Dr. Jixin Qiao, who is a wise and patient scientist. Although I met many difficulties at first, you still guided me patiently. You always welcome me to discuss any issues at your office whenever I need. Your strong logic and profound knowledge of radiochemistry helps get my ideas into shape when I feel confused, and your academic enthusiasm encourages me to overcome these challenges in my PhD project. I learn how to become an excellent scientific researcher from your rigorous academic attitude. It is my honor to be your PhD student.

I would like to deeply thank my co-supervisor, Pro. Colin Stedmon, who is a smart and nice scientist at DTU Aqua. I still remember when I wrote the first paper on the Arctic cruise. I obtained many ideas from the discussion with you. Your active thinking and rich oceanographic knowledge made me surprise. You guide me to combine various methods to study the ocean, broadening my academic horizon. I learn from your suggestions and comments on my papers how to make them more understandable for people that had different backgrounds.

I want to thank Pro. Xiaolin Hou, who is like an encyclopedia in my research group. Not only do you have a deep understanding for radiochemistry, but you also have many insights into different study fields. Each conversation with you makes me surprise that

you know everything. I would never forget what you told me. “Don’t limit yourself to your own study field, but open up your mind and be willing to know about different knowledge.”

I want to say thanks to Dr. Kasper Grann Andersson, who is a kind Senior Researcher in my research group. When I was anxious, you always patiently listened to my blah blah blah and gave some advice, even though you always said that you were not from the chemical background.

I should give a special thank to Dr. Peter Steier, who provides irreplaceable helps on AMS measurement and the data quality at VERA, University of Vienna. I also appreciate Dr. Paul A. Dodd and Dr. Laura de Steur from Nowegian Polar Institute for their supports in the Fram Strait 2021 sampling expedition.

I also thank Dr. Rafael Gonçalves-Araujo, Dr. Mats A. Granskog, Dr. Magnús Danielsen, Dr. Kjartan Guðnason, Dr. Hans Pauli Joensen, Pro. Mikael Kristian Sejr and Dr. Lorenz Meire for your contributions on my papers, including the supports of providing data, seawater samples and paper comments.

A warm gratitude is given to my colleagues and friends in my research group at Risø Campus (they are still here: Christian, Eike, Guillaume, Hanne, Jesper, Josephine, Jixin, Kasper, Liga, Matic, Mette, Peter, Sven, Svend, Xiaolin; they have left: Emilie, Feng, Gunnar, Ines, Jakathamani, Jianhua, Jingjing, José Luis, Liuchao, Lucas, Mathias, Matteo, Mengting, Stanislas, Yanyun, Yijing, Yixuan and Zhao). And I also thank all people in the Climate and Monitoring Section, DTU Sustain and the former DTU Nutech. All of you give me many unforgettable memories in Denmark. I do feel what is “hygge” here.

Importantly, I would like to appreciate to my beloved family. Although we can’t meet each other physically in the past 4 years due to the Covid-19 situation, you are the spiritual harbor in my heart, supporting me in my PhD study. I love you forever.

Summary

A faster decline of sea ice extent in the Arctic in recent years is caused by the rapid warming of global climate. The northward Atlantic water carries a large amount of heat from the lower latitudes of the North Atlantic Ocean, and the release of heat in the Arctic Ocean plays a key role in the sea ice melting process. Atlantic water losses the heat to be cold and dense and thus sinks to deep water layer in the Arctic and subpolar region. Colder and deeper dense water outflows back into the North Atlantic Ocean, and this circulation is defined as the Atlantic Meridional Overturning Circulation (AMOC). It is one of important part of global thermohaline circulation, which profoundly contributes to global climate. Therefore, insights on the transport pathways and timescales of Atlantic water in the Arctic and North Atlantic oceans are significant for understanding the AMOC and the influence on melting of sea ice.

Anthropogenic uranium (U) isotopes, namely ^{233}U and ^{236}U, are promising oceanic tracers owning to their long half-lives and conservative behavior in the open ocean, and their transient signals are useful to investigate water mass movement in a large spatial scale. Unique point-source signal from nuclear reprocessing plants (NRPs) at Sellafield (SF) and La Hague (LH) of European coast is herein exploited to study the transport of Atlantic water in the Arctic and North Atlantic oceans. Combining nutrients, salinity, colored dissolved organic matter (CDOM) and ^{99}Tc, two ^{233}U-^{236}U tracer approaches were developed to estimate Atlantic water transit time. The first approach estimated the transit time of Atlantic water through comparing the original NRPs-derived ^{236}U ($^{236}U_{NRPs}$) concentrations in seawater sample and the reconstructed historic concentrations in three $^{236}U_{NRPs}$ input functions at the Barents Sea Opening **(Paper I)**. CDOM helps distinguish different Atlantic branch waters based on the terrestrial-derived and marine-derived CDOM, and therefore constrains the corresponding input functions **(Paper III)**. The $^{236}U_{NRPs}$ input functions were reconstructed through some assumptions of hydrologic features, whereas the second approach chose to use the ratio of ^{99}Tc and ^{236}U from the

NRPs discharge instead of the reconstructed input functions, avoiding the potential uncertainties from these assumptions **(Paper II)**.

Based on the developed new approaches, average Atlantic water transit times in surface water were obtained in the Fram Strait (14 years), East Greenland fjords (16 years) and the coasts of East Greenland (16 – 17 years), West Greenland (22 years), Iceland and Faroe Islands (25 years) **(Papers I, II and III)**. Our observation of ^{233}U and ^{236}U suggested that the surface outflowing water from the Arctic Ocean transported to the North Atlantic Ocean along the coast of Greenland, but the intermediate dense water outflowing through the sill of the Denmark Strait had a mixed composition of Arctic Atlantic Water, Recirculating Atlantic Water from the eastern Fram Strait and the deep and bottom waters in the Fram Strait **(Paper IV)**. The outflowing dense water moved to the North Atlantic Ocean along the seafloor and contributed to the North Atlantic Deep Water.

Dansk sammenfatning

Den globale opvarmning har i de senere år resulteret i en hurtigere forsvinden af havis i det arktiske område. Det nordgående atlantiske vand medbringer en stor mængde varme fra lavere breddegrader af det nordlige Atlanterhav, og frigørelsen af varme i Ishavet spiller en hovedrolle i afisningsprocessen. Vand fra Atlanterhavet mister varme og bliver ved afkølingen fortættet, og synker ned i et dybt vandlag i den arktiske og subpolare region. Koldere og dybere fortættet vand flyder tilbage til det nordlige Atlanterhav, og denne cirkulation defineres som 'the Atlantic Meridional Overturning Circulation' (AMOC). Dette er en af de vigtigste dele af den globale termohaline cirkulation, som bidrager væsentligt til det globale klima. Derfor er transporten af atlantisk vand i de arktiske og nordatlantiske have, og derunder transportvejene og tidsskalaen, væsentlige for forståelse af AMOC og dettes indflydelse på smeltningen af havis.

Antropogene uran (U) isotoper, herunder ^{233}U og ^{236}U, er lovende oceanografiske tracere, grundet deres lange halveringstider og konservative opførsel i det åbne ocean og kan dermed være nyttige til at undersøge bevægelser af vandmasser i stor skala. Det unikke punktkilde-signal fra nukleare oparbejdningsanlæg ('reprocessing plants' – NRPs) ved Sellafield (SF) og La Hague (LH) på europæiske kyster anvendes til at studere transporten af atlantisk vand i de arktiske og nordatlantiske have. Ved kombination af næringsstoffer, salinitet, 'colored dissolved organic matter' (CDOM) og ^{99}Tc udvikledes to ^{233}U-^{236}U tracermetoder til estimering af bevægelsestiden for atlantisk havvand. Den første metode estimerer bevægelsestiden af atlantisk havvand ved sammenligning af de originale NRP-afledte ^{236}U ($^{236}U_{NRPs}$) koncentrationer i havvandsprøven med de rekonstruerede historiske koncentrationer i tre $^{236}U_{NRPs}$ inputfunktioner af Barents Sea Opening (Paper I). CDOM hjælper til at skelne mellem forskellige atlantiske vandgrene, på basis af terrestrisk afledt og marint afledt CDOM, og begrænser derved de tilsvarende inputfunktioner (Paper III). $^{236}U_{NRPs}$ input funktionerne blev rekonstrueret ved antagelse af nogle hydrologiske egenskaber, men den anden metode anvendte forholdet mellem

^{99}Tc og ^{236}U fra NRP-udledningen i stedet for rekonstruerede inputfunktioner, hvorved man undgik potentielle usikkerheder fra antagelser (Paper II).

På basis af de nye udviklede metoder, blev bevægelsestider for atlantisk overfladevand bestemt i Fram-strædet (14 år), østgrønlandske fjorde (16 år), de østgrønlandske kyster (16-17 år), Vestgrønland (22 år), og Island og Færøerne (25 år) (Papers I, II og III). Vores observation af ^{233}U og ^{236}U indikerer, at det udflydende overfladevand fra det Aktiske hav transporteres til det nordlige Atlanterhav langs kysten af Grønland, men det mellemliggende fortættede vand, som flyder ud gennem tærsklen af Danmarksstrædet, har en blandet sammensætning af arktisk atlantisk vand, recirkulerende atlantisk vand fra det østlige Fram-stræde og dyb- og bundvand i Fram-strædet (Paper IV). Det udflydende fortættede vand bevæger sig til det nordlige Atlanterhav langs med havbunden og bidrager til det nordatlantiske dybvand.

Table of Contents

Abbreviations

a_{350}	Absorption coefficient at 350 nm
AAW	Arctic Atlantic Water
AMOC	Atlantic Meridional Overturning Circulation
AMS	Accelerator mass spectrometry
AO	Arctic Oscillation
Ar	Argon
BSBW	Barents Sea Branch Water
BW	Bottom water
C	Carbon
CDOM	Colored dissolved organic matter
CFCs	Chlorofluorocarbons
Cs	Cesium
DOM	Dissolved organic matter
DSOW	Demark Strait Overflow Water
DW	Deep water
EGC	East Greenland Current
FSBW	Fram Strait Branch Water
Ga	Gallium
GF	Global fallout
GSR	Greenland-Scotland Ridge
He	Helium
I	Iodine
ISOW	Iceland Scotland Overflow Water
K_d	Distribution coefficient
LH	La Hague
N	Nitrate
NADW	North Atlantic Deep Water
NCC	Norwegian Coastal Current
Nd	Neodymium
NIIC	North Icelandic Irminger Current
Np	Neptunium
NRPs	Nuclear reprocessing plants
NSDW	Nordic Seas Deep Water
NwAC	Norwegian Atlantic Current
O	Oxygen
OW	Outflowing waters
P	Phosphate
Pa	Protactinium
PSW	Polar Surface Water
RAW	Recirculating Atlantic Water

S	Salinity
SF	Sellafield
SF_6	Sulfur hexafluoride
Sm	Samarium
Sr	Strontium
Tc	Technetium
TTD	Transit time distribution
U	Uranium
VSMOW	Vienna-Standard mean ocean water
Θ	Potential temperature
σ_Θ	Potential density
$^{236}U_{GF}$	Global fallout-derived uranium-236
$^{236}U_{NRPS}$	Reprocessing-derived uranium-236
^{3}H	Tritium

1. Introduction

1.1 Water mass in the Arctic and North Atlantic oceans

1.1.1 Environmental setting

The Arctic Ocean (9.5×10^6 km^2) surrounded by the Eurasian Continent and the American Continent is a semi-enclosed ocean (Coachman and Aagaard, 1974), which consists of the central Arctic Ocean and several marginal seas, including Barents Sea, White Sea, Kara Sea, Laptev Sea, East Siberian Sea, Chukchi Sea, Beaufort Sea and Lincoln Sea **(Figure 1)**. Their areas, volumes and mean depths are summarized in the **Table 1** (Rudels, 2021). The Eurasian shelf is broad extending more than 800 km offshore while the North American shelf is narrow (50-90 km) (Coachman and Aagaard, 1974). The majority of the marginal seas are therefore located on the Eurasian continental shelf. The central Arctic Ocean is split into two basins: the Amerasian Basin and the Eurasian Basin, separated by the Lomonosov Ridge **(Figure 1)**. The major compositions of the Amerasian Basin are the Beaufort Sea, Canada Basin, Alpha Ridge and Mendeleev Ridge, Makarov Basin. The Eurasian Basin consists of Nansen Basin, Gakkel Ridge, and the Amundsen Basin, where the deepest part (~ 4500 m) of the Arctic Ocean is found.

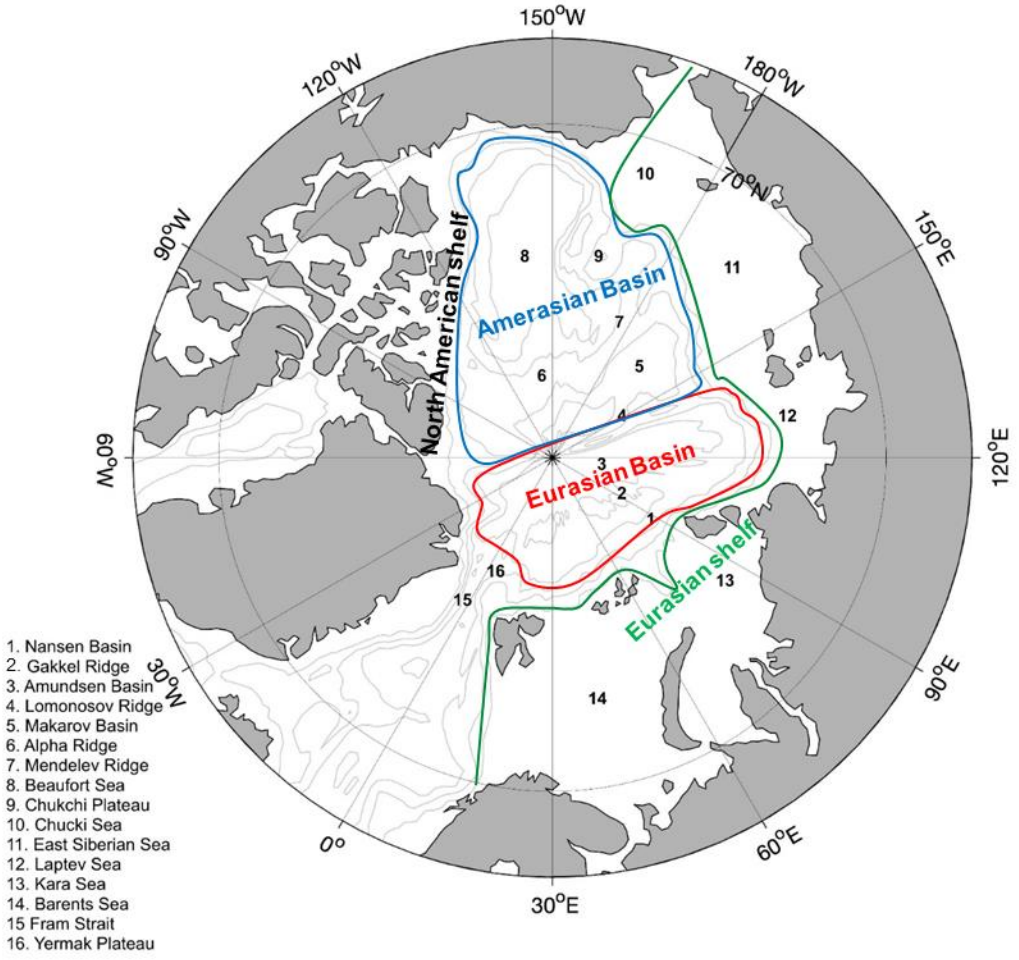

Figure 1. The submarine terrain and marginal seas in the Arctic Ocean (modified from Stedmon et al., 2021).

The Arctic Ocean connects the North Atlantic and North Pacific oceans with water exchange. It is constricted with four gateways, three where water flows into the Arctic (Barents Sea, Eastern Fram Strait and Bering Strait), and two where water flows out to the North Atlantic (Western Fram Strait and Canadian Archipelago). As the sole connection between the Arctic Ocean and the Pacific Ocean, the Bering Strait is located between the Eastern Siberia and the Alaska with a narrow (~ 85 km) and a shallow sill (~

45 m) (Coachman and Aagaard, 1974). The Fram Strait located between Greenland and Svalbard Islands is a crucial gateway for water exchange between the Arctic Ocean and the North Atlantic Ocean with a deeper (~ 2.6 km) and wider section (~ 450 km) (Jakobsson, 2002; Jakobsson et al., 2003; Rachold et al., 2004). There is a steep continental slope in the eastern Fram Strait, while the western Fram Strait has a wide northeastern Greenland shelf, including the Westwind Trough and the Norske Trough. The Barents Sea is a shelf sea with shallower shelf in the eastern and northern parts of the Barents Sea. However, several deep canyons reached 300 – 400 m depths are located in the western parts (Coachman and Aagaard, 1974). The Canadian Archipelago consists of broken islands between Greenland and the American continent, and thus provides 16 reticular passages for polar water to the North Atlantic Ocean through the Baffin Bay. These passages are more than 700 m deep with the different widths ranged in 10 – 120 km (Collin, 1963).

Table 1. Area, volume and mean depth in the marginal seas of the Arctic Ocean (Jakobsson, 2002; Jakobsson et al., 2003; Rachold et al., 2004)

Seas	Area × 10^3 [km^2]	Volume × 10^3 [km^2]	Mean depth [m]
Barents Sea	1512	302	200
White Sea	85	5	56
Kara Sea	926	121	131
Laptev Sea	498	24	48
East Siberian Sea	987	57	58
Chukchi Sea	620	50	80
Beaufort Sea	178	22	124
Lincoln Sea	64	16	257
Central Arctic Ocean	4489	12339	2748

The Nordic Seas are the important transition region between the Arctic and the North Atlantic oceans. It is surrounded by Greenland, Iceland, Faroe Islands, British Islands, Scandinavian Peninsula and Svalbard Islands. The island of Jan Mayen is located in the central part on the intertwined ridges that are the northern extension of the mid Atlantic ridge and that separate the region into three seas: Norwegian Sea, Greenland Sea and Iceland Sea. The southern boundary is the Greenland-Scotland Ridge (GSR) which separates the Nordic Seas from other deeper basins and deep sea plains of the North Atlantic Ocean. These deep sea basins and plains are commonly deeper than 5000 m. The limited sill depths in the Denmark Strait (650 m), the passage between Iceland and Faroe Islands (~ 480 m) and the Faroe-Bank Channel (820 – 830 m) control the water to the deep region of the North Atlantic Ocean, which is separated into the eastern and western parts by the mid-Atlantic ridge (Coachman and Aagaard, 1974). The adjacent Irminger Sea and Labrador Sea in the northwestern North Atlantic Ocean receive waters from the Nordic Seas. Conversely, the North Sea as a shallow shelf sea in the northeastern North Atlantic Ocean provides a passage for the inflowing water to the Nordic Seas.

1.1.2 Water mass distribution and movement

A body of water has a common formation history and the distinct properties compared with surrounding waters and thus is defined as water mass. Although water mass occupies a part of region in the ocean with a certain volume, the region is not solely occupied by single water mass. The movement of water mass results in mixing of different water masses in the ocean. Various physical-chemical properties contribute to water mass classification, including physical tracers (e.g. potential temperature (Θ), salinity (S) and potential density (σ_Θ)) and chemical tracers (e.g. nutrient, dissolved organic matter (DOM) and isotopes). Besides these tracers, the geographical location is also important for distinguishing water mass.

The basic circulation pattern and water mass distribution in the Arctic and North Atlantic oceans have been introduced and summarized in Rudels (2021) **(Figure 2)**. Warm Atlantic water shows a clockwise movement in surface layer of the North Atlantic Ocean as a subtropical gyre. The North Equatorial Current moves westward to the Gulf Stream system. As a part of the subtropical gyre, Atlantic water transports along the coast of the North America. And it flows eastward as the North Atlantic Drift, which bifurcates into two parts: 1) a northward flow transporting to the subpolar gyre and Nordic Seas 2) and an eastward flow reaching the European coast. The inflows to the Nordic Seas occur east and west of the Iceland and Faroe Islands across the GSR. A part of eastward flow of the North Atlantic Drift turns southward as the Canary Current, and another part moves into the North Sea through the English Channel. Surface Atlantic waters in the eastern and western North Atlantic Ocean are defined as Eastern North Atlantic Central Water (Θ: 8.0 – 18.0 °C; S: 35.2 – 36.7) and Western North Atlantic Central Water (Θ: 7.0 – 20.0 °C; S: 35.0 – 36.7), respectively (Emery, 2001) **(Figure 3 and Table 2)**.

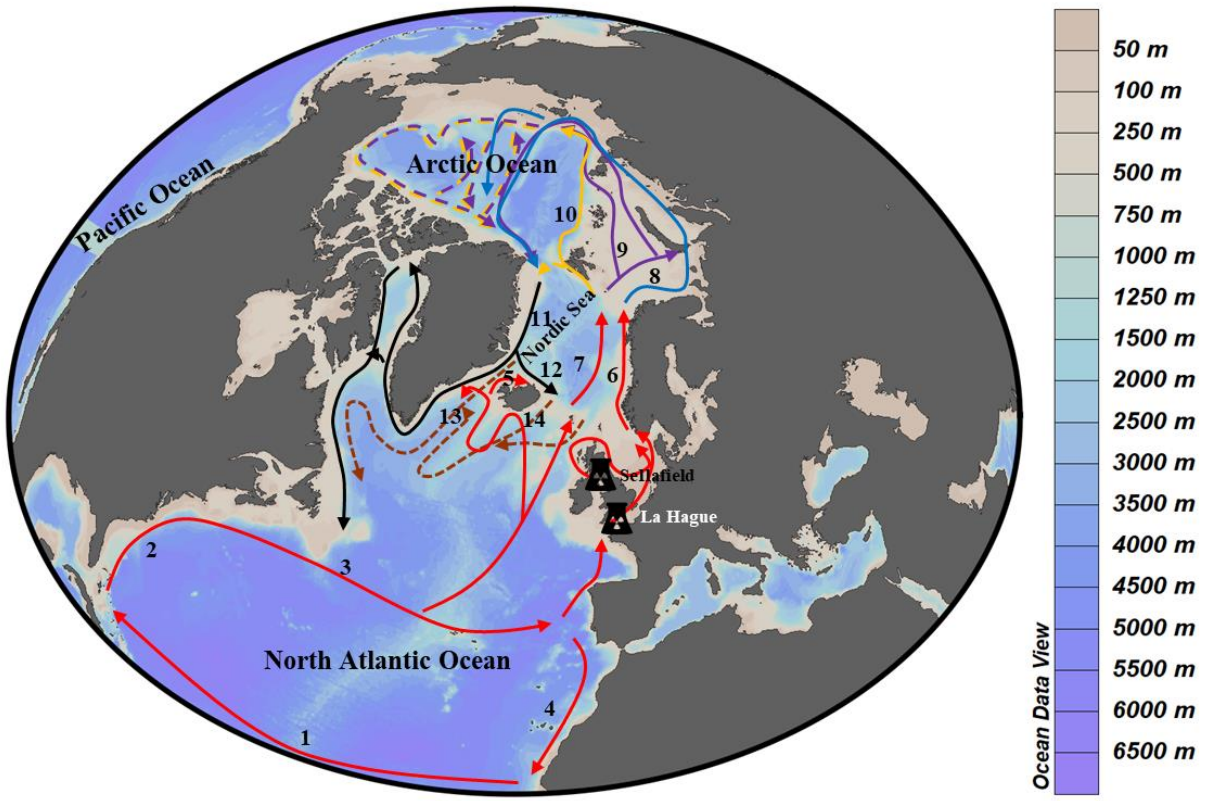

Figure 2. Circulation pattern in the Arctic and North Atlantic oceans. Currents are marked in black numbers (1: North Equatorial Current; 2: Gulf Stream; 3: North Atlantic Drift; 4: Canary Current; 5: North Icelandic Irminger Current; 6: Norwegian Coastal Current; 7: Norwegian Atlantic Current; 8: the extension of Norwegian Coastal Current in the Arctic Ocean; 9: Barents Sea Branch Water; 10: Fram Strait Branch Water; 11: East Greenland Current; 12: East Iceland Current; 13: Demark Strait Overflow Water; 14: Iceland Scotland Overflow Water). Sellafield and La Hague refer to two main nuclear reprocessing plants on European coast; Red arrows refer to Atlantic water; Blue, purple and orange arrows refers to different Atlantic branch waters in the Arctic Ocean; Black arrows refer to the outflowing water from the Arctic Ocean; Brown arrows refers to deep and bottom waters outflowing from the Nordic Seas. Produced with Ocean Data View (Schlitzer, 2016).

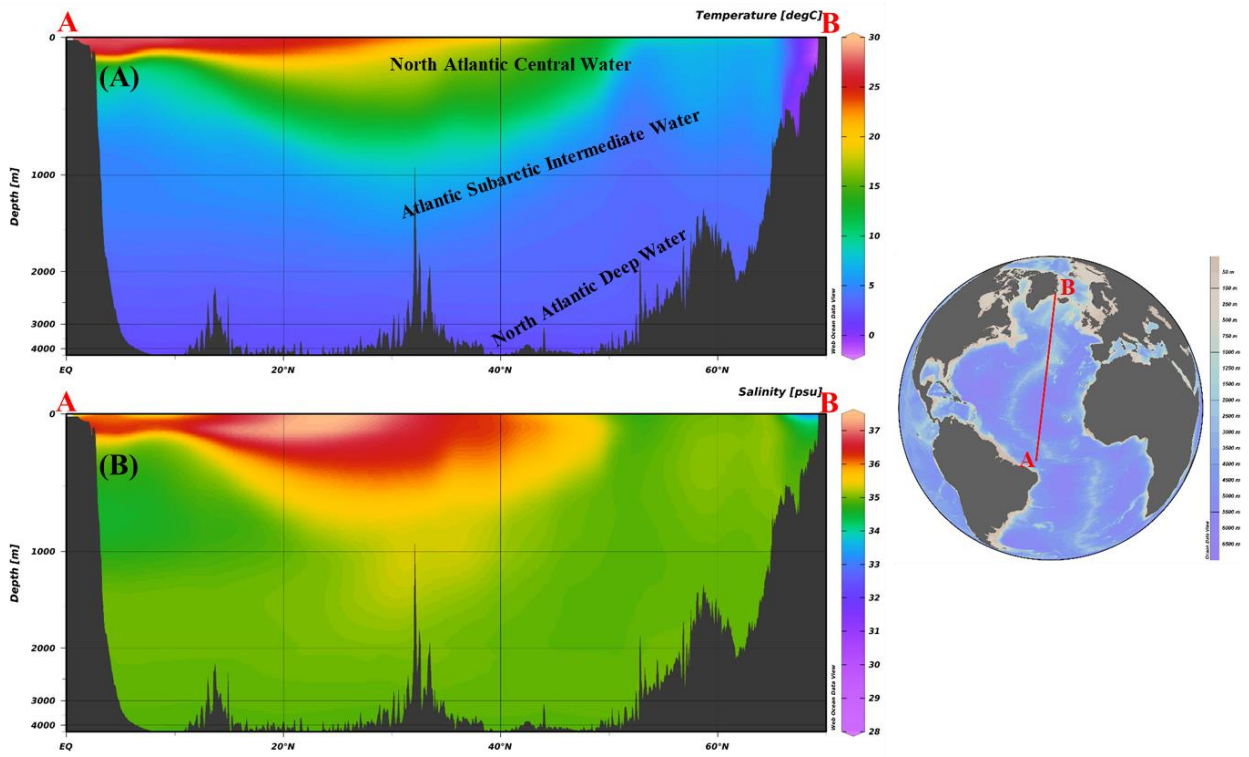

Figure 3. Transects of annual mean temperature (A) and salinity (B) in the North Atlantic Ocean. Data of annual mean temperature and salinity from 1955 to 2010 with a revolution of 0.25° based on Ocean Data View (https://odv.awi.de/data/ocean/world-ocean-atlas-2018).

One branch of the northward North Atlantic Drift transports to the southeastern Greenland coast without entering the Nordic Seas. Other inflowing Atlantic waters in the western Iceland coast, the Norwegian coast and offshore are the North Icelandic Irminger Current (NIIC), the Norwegian Coastal Current (NCC) and the Norwegian Atlantic Current (NwAC), respectively (Rudels, 2021) **(Figure 2)**. Atlantic water across the GSR forms the NIIC and the NwAC with high Θ and S, but the NCC starting from the North Sea and the Baltic Sea is less saline. Both the offshore NwAC and the coastal NCC move northward to the Barents Sea Opening, where the NwAC bifurcates into two branch waters: 1) a branch water on shelf (Barents Sea Branch Water, BSBW) and 2) a branch water on the shelf edge through the Fram Strait (Fram Strait Branch Water, FSBW) **(Figure 2)**. However, there is a westward branch water of FSBW from East to West Fram

Strait without the circulation in the Arctic Ocean. This has a high Θ (> 2 °C), S and σ_Θ ($27.70 < \sigma_\Theta \leqslant 27.97$) and is defined as Recirculating Atlantic Water (RAW) **(Table 2)**.

The bifurcation of the BSBW occurs in the Barents Sea and thus forms two branch waters, which mix with the NCC on the coast and the FSBW on the shelf edge, respectively (Loeng, 1991). The coastal Atlantic water carries the river inputs into the central Arctic Ocean and mixes with Pacific water and sea ice meltwater. Pacific water inflows from the Bering Strait and moves to the Arctic Ocean with different pathways, and one part contributes to dilute Atlantic water in the central Arctic Ocean (Jones et al., 2003). The mixing of Atlantic, Pacific, sea ice melt and river waters occurs in the surface layer of the Arctic Ocean and forms Polar Surface Water (PSW) characterized by low Θ ($\leqslant$ 0 °C), S and σ_Θ ($\leqslant$ 27.70) (Rudels et al., 2005) **(Figure 4 and Table 2)**. For the offshore Atlantic water, it transports in the intermediate layer underlying PSW as Arctic Atlantic Water (AAW) characterized by high Θ ($0\ °C < \Theta \leqslant 2\ °C$), S and σ_Θ ($27.70 < \sigma_\Theta \leqslant 27.97$) (Rudels et al., 2005) **(Figure 4 and Table 2)**. The majority of outflowing waters passes over the western Fram Strait as the East Greenland Current (EGC). The Fram Strait as a gateway has a complicated construction for water mass. In surface and intermediate layers, RAW dominates the eastern Fram Strait, while the western Fram Strait is occupied by PSW and AAW. Besides inflowing Nordic Seas Deep Water (NSDW) in deep layer near the eastern continental slope of the eastern Fram Strait, other waters in deep layer outflow from the Arctic Ocean, including Arctic Intermediate Water, Upper Polar Deep Water, Eurasian Basin Deep Water and Canada Basin Deep Water **(Figure 4 and Table 2)**. Surface EGC transports to the North Atlantic Ocean through the Greenland coast and Baffin Bay. Deeper EGC outflows through passing over sills of the GSR, and forms Denmark Strait Overflow Water (DSOW) and Iceland Scotland Overflow Water (ISOW), which merge and move along the seafloor to the North Atlantic Ocean as the North Atlantic Deep Water (NADW) (Θ: 1.5 – 4.0 °C; S: 34.8 – 35.0) (Emery, 2001) **(Figure 2)**.

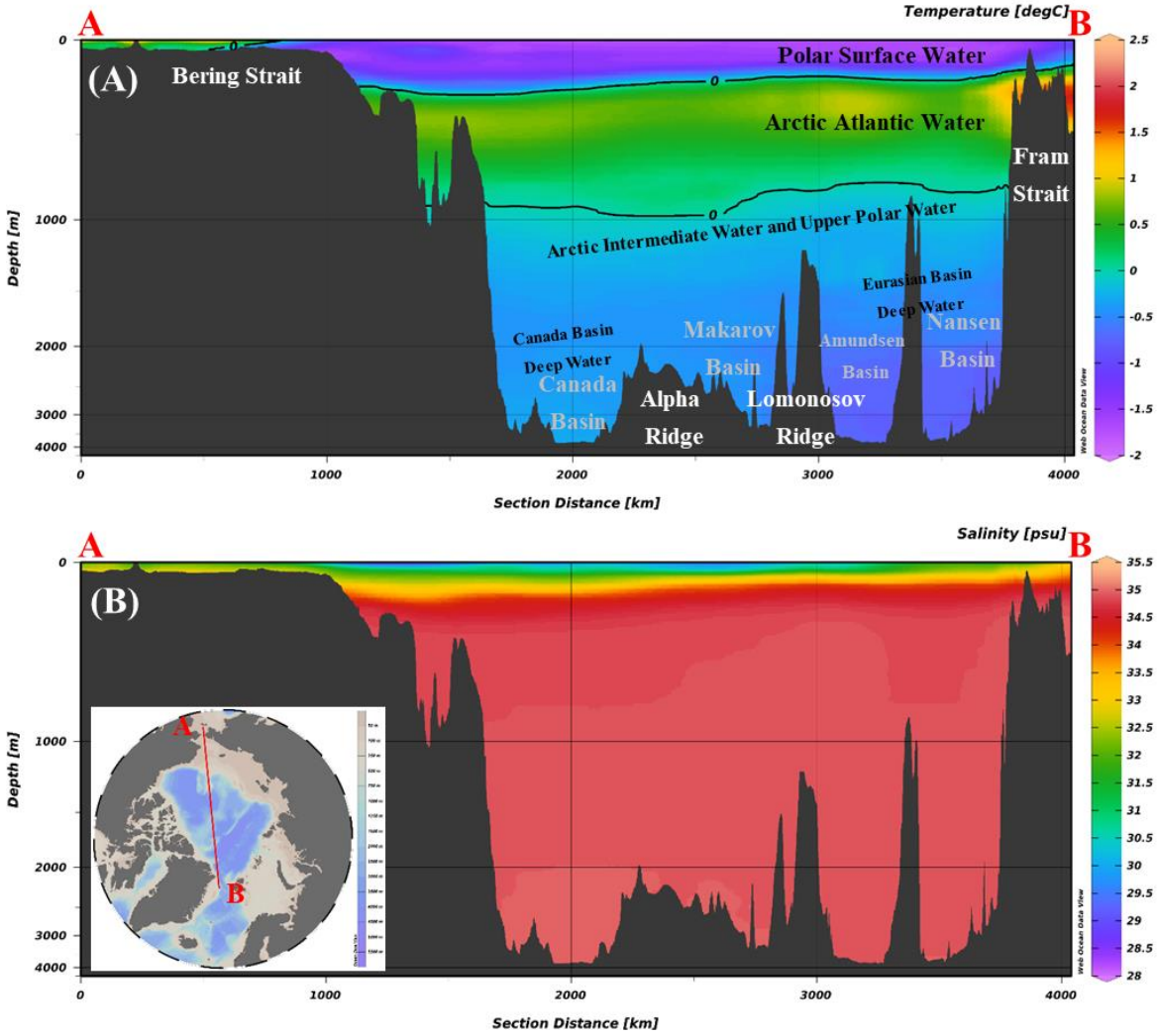

Figure 4. Transects of annual mean temperature (A) and salinity (B) in the Arctic Ocean. Data of annual mean temperature and salinity from 1955 to 2010 with a revolution of 0.25° based on Ocean data view.

Table 2. Water mass properties in the Arctic and North Atlantic oceans (Emery, 2001; Rudels et al., 2005).

Regions	Water masses	Θ [°C]	Salinity
North Atlantic Ocean	Atlantic Subarctic Upper Water	0.0 - 4.0	34 - 35
	Western North Atlantic Central Water	7.0 - 20.0	35.0 -36.7
	Eastern North Atlantic Central Water	8.0 - 18.0	35.2 - 36.7

	Western Atlantic Subarctic intermediate Water	3.0 - 9.0	34.0 - 35.1
	Eastern Atlantic Subarctic intermediate Water	3.0 - 9.0	34.4 - 35.3
	North Atlantic Deep Water	1.5 - 4.0	34.8 - 35.0
Fram Strait (Arctic Ocean)	(Warm) Polar Surface Water ($\sigma_\Theta \leq 27.7$)	≤ 0 ($0 < \Theta \leq 2$)	
	Recirculating Atlantic Water/Atlantic Water ($27.7 < \sigma_\Theta \leq 27.97$)	< 2	
	Arctic Atlantic Water ($27.7 < \sigma_\Theta \leq 27.97$)	$0 < \Theta \leq 2$	
	Arctic Intermediate Water and Upper Polar Deep Water ($27.7 < \sigma_\Theta$, $\sigma_{0.5} \leq 30.444$)	≤ 0	
	Nordic Seas Deep Water ($30.444 < \sigma_{0.5}$)		≤ 34.915
	Canada Basin Deep Water ($30.444 < \sigma_{0.5}$, $\sigma_{1.5} \leq 35.142$)		> 34.915
	Eurasian Basin Deep Water ($30.444 < \sigma_{0.5}$, $35.142 < \sigma_{1.5}$)		> 34.916

1.1.3 Research challenges

Global average air temperature has significantly increased in recent decades, and a faster increasing rate of warming occurs in the Arctic compared with other regions, which is called Arctic Amplification (England et al., 2021; Rantanen et al., 2022). The direct manifestation is the fast decline of sea ice extent from the Arctic edge to the central Arctic with the thinning thickness (Massonnet et al., 2018). Sea ice is dynamic and flows in the Arctic Ocean due to the drive of wind and current. Seawater freezes and rejects the salt from ice layer in winter, but the sea ice may melt in other regions in summer, suggesting that the movement of seasonal sea ice is important for the redistribution of freshwater in the Arctic (Aagaard and Carmack, 1989). The northward Atlantic water carries a large amount of heat from the low latitude region to the Arctic and thus promotes sea ice melt, and enhance of upward heat flux from Atlantic water promotes the process since 2000s (Polyakov et al., 2017). The consistency between the Arctic sea ice loss and heat loss highlights the importance of the circulation of inflowing warm Atlantic

water to sea ice melt (Smedsrud et al., 2022) **(Figure 5)**. Atlantic water continuously releases heat from the ocean to the atmosphere during its transit in the Arctic. The remaining heat from the upstream Atlantic water contributes to the downstream melting of sea ice, even terminating glaciers on Greenland coast (Mouginot et al., 2015; Lindeman et al., 2020), revealing that the upstream change of Atlantic water properties is crucial for the Arctic sea ice cover. Insights on timescales of Atlantic water movement from upstream region to downstream region in the Arctic are therefore important for understanding these processes.

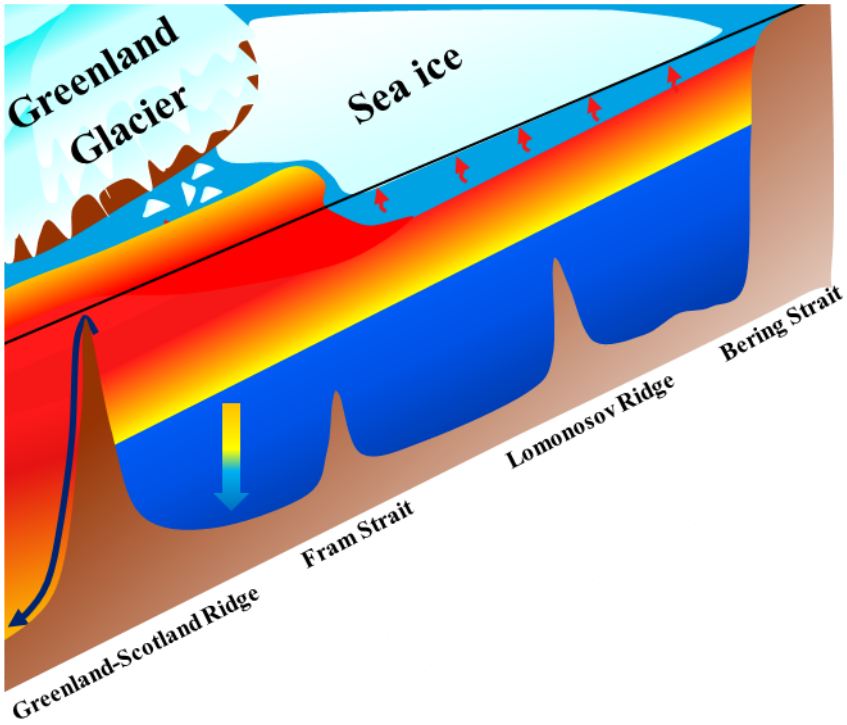

Figure 5. A schematic overview of Atlantic water influence in the Arctic and North Atlantic oceans. Wavy lines: the loss of heat from the northward Atlantic water; Colored arrow: Atlantic water becomes cool, dense and sink; Dark blue arrow: dense outflowing waters.

In addition, after losing heat, the northward warm Atlantic water becomes cool and dense. Denser cold water sinks and overflows south back to the North Atlantic Ocean. The circulation is defined as the Atlantic Meridional Overturning Circulation (AMOC), which is a key component of global thermohaline circulation and plays an important role in global climate change (Intergovernmental Panel on Climate Change Fifth Assessment Report, 2014). Based on the global circulation, the AMOC brings heat to various parts of the globe, in particular Europe, which is warmer than other regions in the northern hemisphere. The AMOC variations are linked to the loss of sea ice and Greenland Ice Sheet in the Arctic (Rignot and Kanagaratnam, 2006; Delworth et al., 2016; Sévellec et al., 2017; Liu et al., 2020; Liu and Fedorov, 2022), highlighting the significance for understanding the circulation of the AMOC. The AMOC is not a simply and tightly connected circulation system but the connection of various regional circulations and gyres with different AMOC pathways (Bower et al., 2019). The Nordic Seas are crucial region for connecting the upper (warm Atlantic water in surface) and lower limbs (cold and dense water in deep) of the AMOC, requiring a strengthened understanding of pathways of the inflowing and outflowing waters passed over the GSR.

1.2 Chemical tracers in the Arctic and North Atlantic oceans

Investigation of timescales and pathways of northward Atlantic water needs an appropriate selection for oceanic tracers. Traditional physical tracers (Θ, S, σ_θ) provide a fast and simple approach to define and trace water mass in the ocean (Rudels, et al., 2005). Assuming no interaction between the air and seawater, the physical properties of a water mass only change due to the mixing of different water masses when it moves from its original location. These physical parameters are commonly integrated in oceanic models to reveal and predict a dynamic trajectory of water mass movement (Aksenov et al., 2016; Fuentes-Franco and Koenigk). Revealing a detailed pathway, quantifying water fraction and estimating water transit time are main aims for tracing water mass movement. However, the stable regional distribution of physical tracers is not enough to decipher the complicated movement of water mass, and therefore the combined use of chemical tracer is essential for investigating water mass movement.

1.2.1 Natural tracers

1.2.1.1 Nutrients

As the traditional tracers, nutrients have been invoked to trace Pacific water in the Arctic (Wheeler et a., 1997; Yamamoto-Kawai et al., 2006; Stedmon et al., 2015). Different from Atlantic water, nitrate is depleted in Pacific water, where phosphate is enriched (Jones et al., 1998). Although their environmental behaviors are not conservative, relationship between concentrations of nitrate and phosphate in Pacific water and Atlantic water is conservative (Jones et al., 1998) **(Figure 6)**. Two parallel lines indicate the nitrate vs. phosphate correlations in pure Pacific water and pure Atlantic water, respectively. Besides Pacific water and Atlantic water, freshwater from river runoff, precipitation and sea ice melted is also one of important component in the Arctic

seawater. Compared with Pacific water and Atlantic water, the contribution of freshwater is small, and the relationship of nitrate and phosphate is proven the same to Atlantic water (Jones et al., 1998). Based on the conservative relationship, Pacific water signal can be isolated from the mixed water in the Arctic Ocean. Significant difference of salinity in Atlantic water and freshwater enables the separation of their water fractions (Jones et al., 2008; Dodd et al., 2012). Quantitative estimation of water fraction shows a common distribution of Pacific water in upper ~200 m of the Arctic Ocean through using nitrate and phosphate approach (N:P approach) (Jones et al., 2008; Dodd et al., 2012).

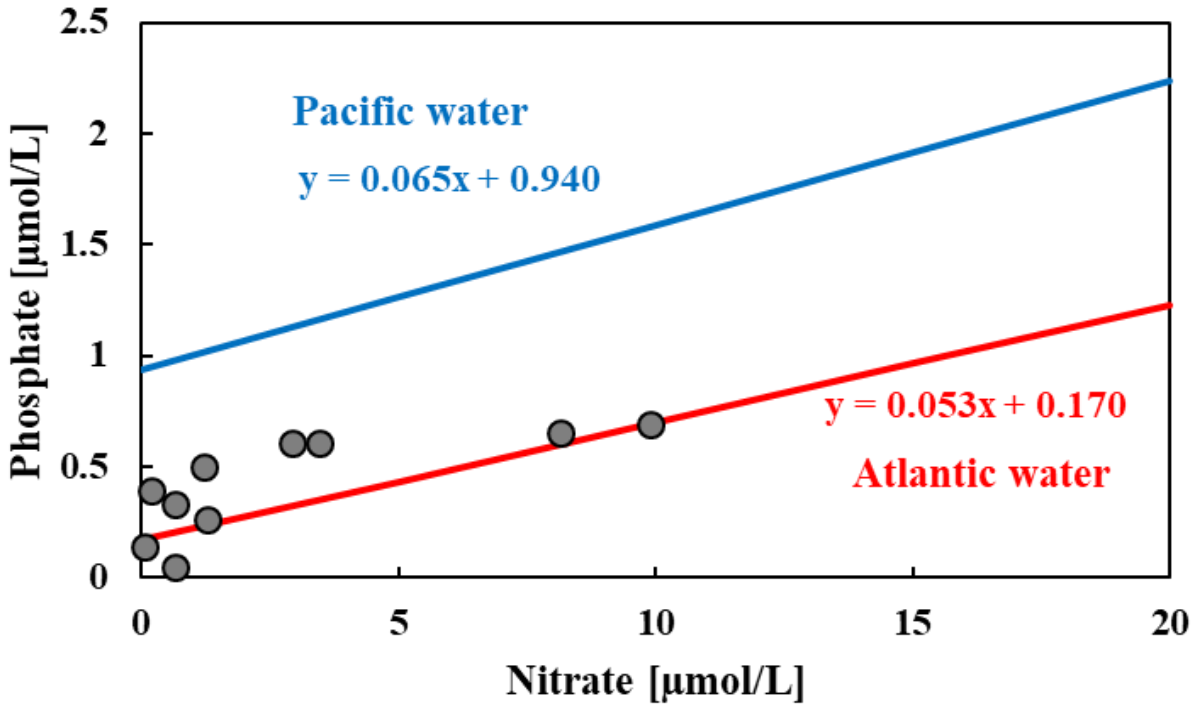

Figure 6. Relationship between nitrate and phosphate in Atlantic water and Pacific water entering the Arctic (modified from Dodd et al., 2012). Gray dots are measured seawater samples in East Greenland fjords.

1.2.1.2 Colored dissolved organic matter

One pathway for Atlantic water is along the Siberian shelf and here waters are influenced by riverine discharge. Arctic rivers are stained brown due to high concentrations of dissolved organic matter leached from their catchments. The contribution of river water can be traced by measuring light absorption of colored dissolved organic matter, CDOM **(Figures 7)** (Stedmon et al 2011; Granskog et al 2012). This offers an approach to distinguish circulation pathways for different Atlantic branch waters. A part of Atlantic water moved along the Siberia coastline entrains the terrestrial high levels of CDOM in the estuary of Siberian rivers and subsequently transports into the central Arctic Ocean. Conversely, another part of offshore Atlantic water can not receive the terrestrial CDOM or carrys its limited dispersion from the coast to the shelf edge. The significantly different characteristics for terrestrial and marine CDOM levels in the Arctic allows us to use it as an attempt to identify the coastal and offshore Atlantic waters.

The absorption coefficient at 350 nm (a_{350}) is commonly used to reflect the content of CDOM in seawater (Granskog et al 2012; Stedmon et al., 2015; Gonçalves-Araujo et al., 2016). Values in the Arctic outflow with a river CDOM contribution vary between 0.37 and 0.86 m^{-1} while the absorption in the inflowing Atlantic waters is between 0.10 and 0.34 m^{-1} **(Figure 7)**. A sub-fraction of CDOM also emits a fluorescence **(Figure 8)**, and this signal can be measured using in situ fluorometers and provide high resolution sections tracing the distribution of DOM (Anderson and Amon 2015; Stedmon et al., 2021). In the Arctic Ocean there is a strong positive correlation between CDOM and meteoric water fraction, suggesting that CDOM is a good oceanic tracer for water mass, especially for the Siberian river water in the Arctic (Granskog et al., 2012; Stedmon et al., 2015).

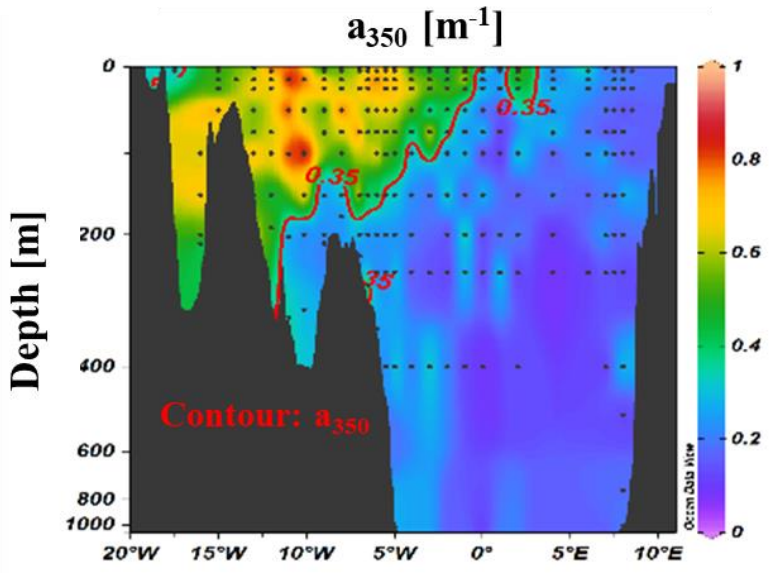

Figure 7. Observed absorption coefficient of dissolved colored organic matter at 350 nm in the Fram Strait in 2021.

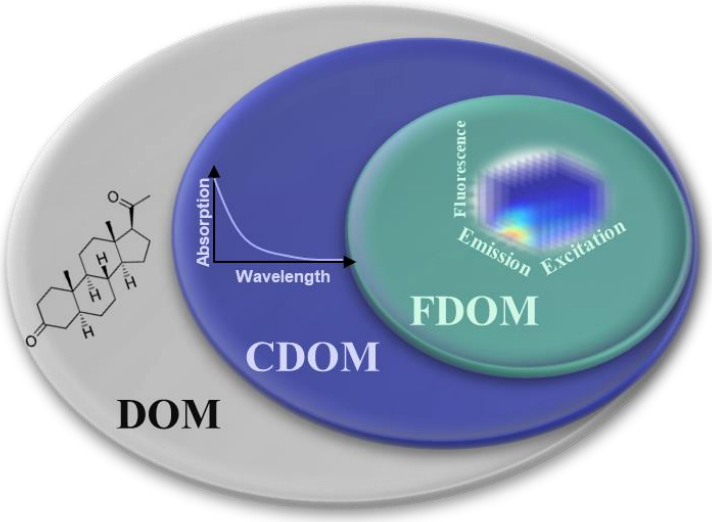

Figure 8. Schematic diagram of dissolved organic matter (DOM), colored dissolved organic matter (CDOM) and fluorescent dissolved organic matter (FDOM).

1.2.1.3 Isotopes

Various isotopes have been applied in tracing waters in the Arctic and North Atlantic oceans, such as oxygen isotopes and neodymium isotopes (Jones et al., 2008; Voelker et al., 2015; Laukert et al., 2017a; Zieringer et al., 2019). A successful use of oxygen (O) isotopes is to identify meteoric water and sea ice meltwater in freshwater from the Arctic Ocean (Jones et al., 2008; Dodd et al., 2012). The deviation from the Vienna-Standard mean ocean water (VSMOW) ($\delta^{18}O$) replaces the direct ratio of $^{18}O/^{16}O$ to compare the characteristics in various waters. Compared with the slightly enriched ^{18}O in sea ice meltwater, the ^{18}O in meteoric water is significantly depleted relative to the value of VSMOW due to a considerable isotopic fractionation, and hence $\delta^{18}O$ values are negative between -10 – -30 ‰ (Östlund and Hut, 1984). The large difference of $\delta^{18}O$ values in meteoric water and sea ice meltwater helps estimate their fractions. And the $\delta^{18}O$ values in Atlantic water and Pacific water are constantly close to 0 ‰ (Östlund and Hut, 1984; Yamamoto-Kawai et al., 2008; Dodd et al., 2012).

As a meteoric water tracer in the Arctic, $\delta^{18}O$ is combined with N: P approach or neodymium (Nd) isotopes to strengthen the quantification of water fractions (Jones et al., 2008; Laukert et al., 2019). Nd isotopes are quasi-conservative oceanic tracers for water mass movement attributed to the labelled signatures from the input of weathered continental material and its shorter intermediate average oceanic residence time relative to global circulation (Frank, 2002; Goldstein and Hemming, 2003; Tachikawa et al., 2003; Arsouze et al., 2009; Rempfer et al., 2011). ^{143}Nd decays from the samarium (Sm) isotope, and the change of $^{143}Nd/^{144}Nd$ ratio in rock is caused by differentiation of Sm and Nd in their melting or fractional crystallization and the ingrowth of ^{143}Nd (Jacobsen and Wasserburg, 1980). Similarly, the deviation of $^{143}Nd/^{144}Nd$ ratio expressed as ε_{Nd} is used for comparison instead. Various ε_{Nd} values for every specific water sources (i.e. -14.5 in NCC, -5.5 in Pacific water, -6.1 in Ob river, -5.2 in Yenisei river, -15 – -16 in Lena river, -6.0 in Kolyma river, -12.9 in Mackenzie river) highlight the application of Nd isotopes in tracing water mass movement (Dahlqvist et al., 2007; Porcelli et al., 2009;

Zimmermann et al., 2009; Persson et al., 2011; Petrova, 2015). The combination of Nd isotopes and O isotopes reveals the lateral advection of water masses in the Arctic Ocean and the mixing of warm Atlantic water in the Fram Strait with Pacific water (< ~ 30%), river water (< ~ 8%) and local Greenland freshwater (~ 6%) (Laukert et al., 2017b).

Although the use of isotopes of O and Nd has presented much of results in water mass movement, the shown information addresses the water fraction quantification with corresponding transport pathways. Timescale is also a crucial information for water mass movement. Cosmogenicly isotopes Carbon-14 (^{14}C) and Argon-40 (^{40}Ar) are used to estimate water mass timescale through a known radioactive decay rate in the seawater isolated from atmosphere (Broecker and Peng, 1982; Koeve et al., 2015; Holzer et al., 2019). And the estimated water age has a large timescale for ocean circulation over ~ 100 years.

1.2.2 Anthropogenic tracers

In the context of the rapid climate change in the past few decades, a relatively short timescale information for water mass movement may be more urgent, forcing us to use anthropogenic chemical tracers to obtain it. Anthropogenic tracers are produced from human activities, such as industrial production, nuclear facilities and nuclear weapons testing. A known annual release of anthropogenic tracers enables us to anchor the source year of water mass by comparing the historic release and measured tracers in the seawater. According to the passage for anthropogenic tracer source entering the ocean, they are divided into two types: 1) diffuse-source tracers and 2) point-source tracers.

1.2.2.1 Diffuse-source tracers

Diffuse-source tracers derive from atmospheric fallout, which deposits all over the world. As synthetic compounds, chlorofluorocarbons (CFCs) and sulfur hexafluoride (SF_6) have

been used in refrigerators as industrial coolants after the 1930s and electrical industry since the 1960s, respectively, and thus emitted into the atmosphere (Fine, 2011). Their concentrations in the seawater are influenced by dilution and the source years, which are calculated from the moments when the exchange of CFCs/SF_6 between the air and the ocean ceases. They have been used in estimating the ventilation age of water mass in the Arctic and North Atlantic oceans through transit time distribution (TTD) approach (Tanhua et al., 2009; Fine et al., 2011; Jeansson et al., 2023). Based on the mathematical framework, TTD approach is used to characterize the advective, diffused and lateral transport of water fluids in the ocean (Haine and Hall, 2002; Waugh et al., 2003). Estimated ventilation times in the intermediate seawater of the Eurasian Basin (~ 200 years) and the Canadian Basin (~ 300 years) contribute to calculate the inventory of anthropogenic carbon dioxide (Tanhua et al., 2009). Nuclear bomb-derived tritium (^3H) and its decay product helium-3 (^3He) have also been used for water mass age estimation that defined the elapsed time since the water parcel is cut off from the air (Jenkins and Clarke, 1976). Although the timescale of water mass is estimated by diffuse-source tracers, the wide deposition from atmospheric fallout results in the fact that they can not track a specific water mass.

1.2.2.2 Point-source tracers

Compared with diffuse-source tracers, point-source tracers applied in the Arctic and North Atlantic oceans are dominantly anthropogenic radioisotopes originating from the two nuclear reprocessing plants (NRPs) at Sellafield (United Kingdom) and La Hague (France). The geographical constrain makes these point-source tracers as asset for Atlantic water from the western European coast. Previous results showed that NRPs-derived anthropogenic radioisotopes flowed into the North Sea, the Nordic Seas and the Arctic Ocean, and even moved back the North Atlantic Ocean in deep layer (Aarkrog et al., 1987; Dahlgaard, 1995; Kershaw and Baxter, 1995; Hou et al., 2000; Smith et al., 2011; Casacuberta et al., 2014; Wefing et al., 2021). Therefore, NRPs-derived

anthropogenic radioisotopes provide the unique signal to trace Atlantic water movement in the Arctic and North Atlantic oceans.

Among anthropogenic radioisotopes, ^{90}Sr, ^{99}Tc, ^{129}I, ^{137}Cs and ^{236}U are common oceanic tracers adopted in the past few decades (Dahlgaard, 1995; Casacuberta and Smith, 2023). Although the global fallout (GF) from atmospheric nuclear weapons testing increased the background levels of some (e.g., ^{90}Sr, ^{137}Cs and ^{236}U) of these tracers in the ocean, the substantial and continuous discharges from NRPs facilitate their uses in the Arctic and North Atlantic oceans as Atlantic water tracer. The distribution coefficient (K_d) is used to assess the conservative degree for a marine tracer, and calculated as the ratio of its mass concentration in sediment/biota and seawater (International Atomic Energy Agency IAEA, 2004). Therefore, small K_d reflects highly conservative property of a tracer in the marine system. Comparatively, Cs (K_d = 2000) is less conservative and easily absorbed by suspended solid and thus deposits in the marine sediment. Sr (K_d = 200), Tc (K_d = 200), I (K_d = 100) and U (K_d = 500) are more conservative in the open ocean. In addition, discharges of ^{90}Sr (SF: 6.6 PBq; LH: 1.1 PBq), ^{99}Tc (SF: 1.7 PBq; LH: 0.2 PBq), ^{129}I (SF: 4667 kg; LH: 1673 kg), ^{137}Cs (SF: 41.3 PBq; LH: 1.0 PBq) and ^{236}U (SF: 237 ± 21 kg; LH: 46 kg) from NRPs have different temporal patterns in the past few decades (Michel et al., 2012; Shi et al., 2012; OSPAR, 2019; Castrillejo et al., 2020) **(Figure 9)**. Only the NRPs discharge of ^{129}I dominantly derives from LH, and the discharge from SF is the main NRPs source for ^{90}Sr, ^{99}Tc, ^{137}Cs and ^{236}U. NRPs discharges of ^{90}Sr and ^{137}Cs dominate in the 1970s – 1990s, while ^{99}Tc has two distinct peaks in the periods of 1970 – 1980 and 1994 – 2004. Discharges of ^{129}I and ^{236}U present monotonically increasing and decreasing trends after 1990s and 1970s, respectively. Compared with ^{137}Cs (t½ = 30.2 yr) and ^{90}Sr (t½ = 28.8 yr), ^{99}Tc (t½ = 0.211 Myr), ^{129}I (t½ = 15.7 Myr) and ^{236}U (t½ = 23.4 Myr) have much longer half-lives, which allows to trace Atlantic water in the Arctic and North Atlantic oceans, even the South Atlantic Ocean, for a longer timeframe.

Compared with ^{99}Tc and ^{129}I, more releases from GF contribute to short-lived ^{137}Cs (1000 PBq) and ^{90}Sr (380 PBq) (UNSCEAR, 2000; Aarkrog, 2003). And long-lived ^{99}Tc (>

90%) and ^{129}I (98%) have a dominated source from NRPs, which is advantageous to trace Atlantic water with negligible interference from GF (Michel et al., 2012; Shi et al., 2012; OSPAR, 2019). The source of long-lived ^{236}U, however, has a higher contribution from GF (900 – 1400 kg) (Sakaguchi et al., 2009 and 2012), implying that GF interference to the use of NRPs-derived ^{236}U ($^{236}U_{NRPs}$) as a point source should be considered. The $^{233}U/^{236}U$ ratio can be used to fractionate the GF and NRPs contributions to ^{236}U due to the different $^{233}U/^{236}U$ isotopic signatures produced in nuclear weapon testing versus civil nuclear industry (Hain et al., 2020; Qiao et al., 2020).

With the technical development of accelerator mass spectrometry (AMS), a long-lived ^{233}U ($t_{½}$ = 0.159 Myr) has been measured in environmental samples recently, and ^{233}U can be produced from various nuclear reactions and decay processes (e.g. ^{235}U (n, 3n) ^{233}U, ^{238}U (n, 2n) $^{237}U \rightarrow {}^{237}Np \rightarrow {}^{233}Pa \rightarrow {}^{233}U$, ^{234}U (n, 2n) ^{233}U) (Hain et al., 2020). Compared with the significantly low natural production of ^{233}U, anthropogenic source from ^{233}U-fueled devices thermonuclear weapons dominates the contribution of ^{233}U through the ^{235}U (n, 3n) ^{233}U reaction. GF of atmospheric nuclear weapons testing was reported to release approximately 7 – 15 kg of ^{233}U, as estimated from the sediment cores in the Baltic Sea (Lin et al., 2021). Small cross-sections in nuclear reactions seriously suppress the ^{233}U production in the nuclear power plants, reactors and reprocessing plants. However, considerable amounts of ^{236}U can be produced from these nuclear facilities and thermonuclear weapons and thus form a clear difference of $^{233}U/^{236}U$ atomic ratios in the sources from nuclear facilities ($1 – 10 \times 10^{-7}$) and thermonuclear weapons-induced global fallout ($1.4 \pm 0.15 \times 10^{-2}$ after the 1970s) (Hain et al., 2020, HELCOM MORS Discharge basement, 2020). Based on the unique characteristic of $^{233}U/^{236}U$ ratio, it has been used for revealing the unknown reactor release in the Baltic Sea (Qiao et al., 2021) and different water masses in the Arctic Ocean (Chamizo et al., 2022).

Transit time of Atlantic water from the Barents Sea Opening have been estimated using coupled anthropogenic radioisotopes in Nansen Basin (^{129}I-^{236}U: 3 – 12 years in PSW and 15 – 45 years of mean ages in AAW; ^{129}I-^{137}Cs: 4 – 9 years in PSW and 10 – 30 years of

mean ages in AAW), Amundsen Basin (^{129}I-^{236}U: 9 – 16 years in PSW and 18 – 28 years of mean ages in AAW; ^{129}I-^{137}Cs: 7 – 9 years in PSW and 20 – 30 years of mean ages in AAW), Makarov Basin (^{129}I-^{236}U: 2 – 14 years in PSW and 18 – 23 years of mean ages in AAW; ^{129}I-^{137}Cs: 4 – 12 years in PSW and 18 – 22 years of mean ages in AAW) and Canada Basin (^{129}I-^{236}U: 14 – 20 years in PSW and 29 years of mean ages in AAW; ^{129}I-^{137}Cs: 33 – 46 years of mean ages in AAW) of the Arctic Ocean through mixing model and TTD model (Smith et al., 2011; Wefing et al., 2021). GF contributions of ^{236}U and ^{137}Cs and less conservative behavior of short-lived ^{137}Cs may potentially add uncertainties in the transit time estimates. The use of long-lived and isolated $^{236}U_{NRPs}$ signal is expected to tackle challenges. A dominant NRPs discharge of ^{236}U in the 1970s – 1980s makes up the shortcoming of ^{129}I due to its limited discharge before the 1990s.

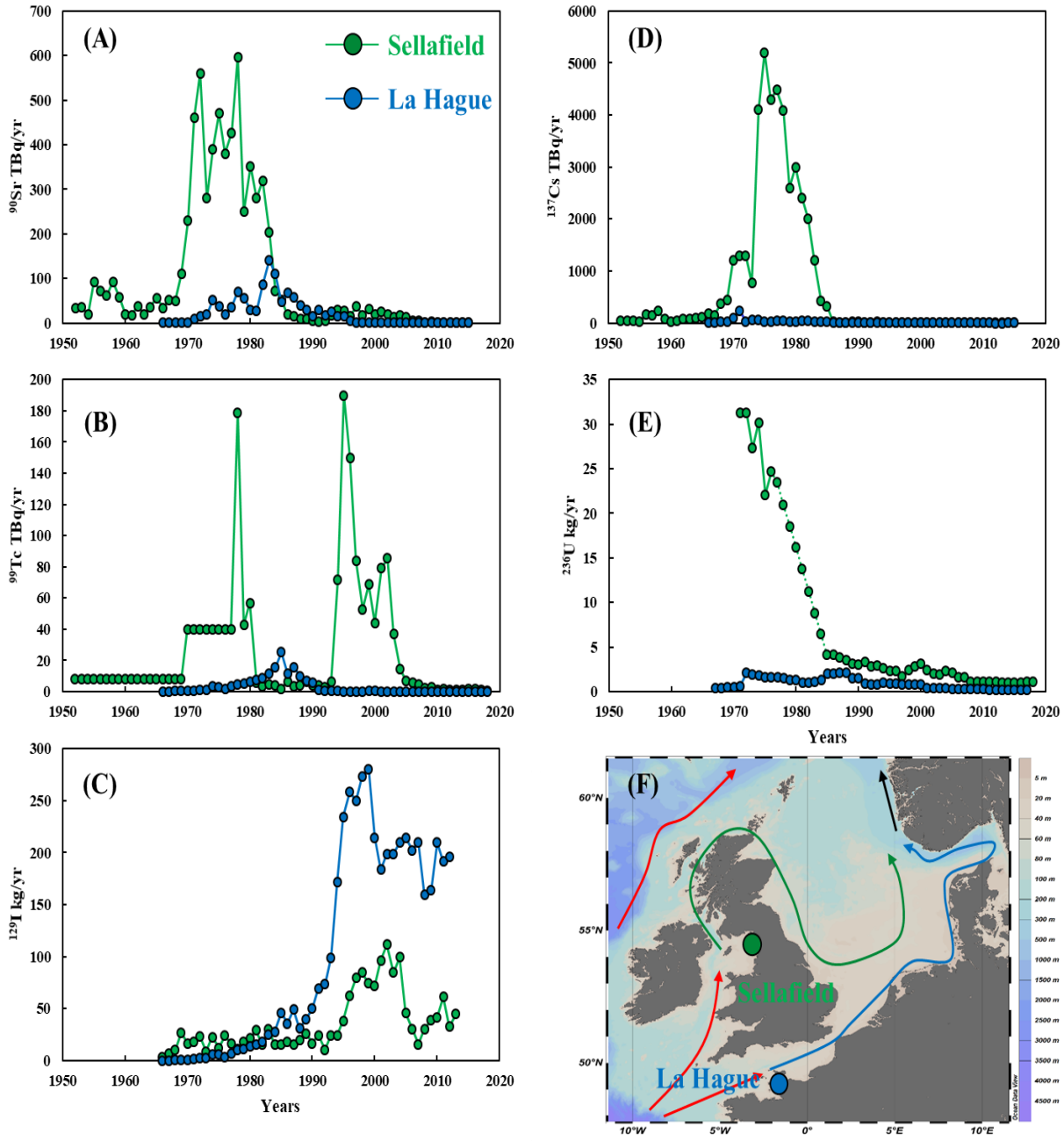

Figure 9. Historic discharges of ^{90}Sr (A), ^{99}Tc (B), ^{137}Cs (C), ^{129}I (D) and ^{236}U (E) from the two main European nuclear reprocessing plants at Sellafield and La Hague and circulation pattern in the North Sea (F). Red arrows refer to normal Atlantic water; Green arrow refers to Sellafield branch water; Blue arrow refers to La Hague branch water; Black arrow refers to the Norwegian Coastal Current.

1.3 Research objectives

Environmental challenges highlight the importance of understanding Atlantic water transport pathways and timescales in the Arctic-North Atlantic Ocean. Limitations in existing oceanic tracers set demands to develop independent tracer approach to compare, and to be applied for achieving more insights on water mass movement in the Arctic-North Atlantic Ocean. Therefore, our research in this project aims to achieve the following objectives:

- Develop ^{233}U-^{236}U tracer approaches to trace Atlantic water transit time in the Arctic through combining nutrient-salinity or another anthropogenic isotope ^{99}Tc;
- Identify the transport pathways of different Atlantic branch waters for improving the robustness of Atlantic water transit time estimate through coupling ^{233}U-^{236}U and CDOM;
- Investigating Atlantic water transport pathways through observations of ^{233}U and ^{236}U in the Arctic and North Atlantic oceans, especially for the outflowing Atlantic waters from the Arctic Ocean.

2. Materials and Methods

2.1 Sample collection in the Arctic and North Atlantic oceans

2.1.1 Seawater samples

A total of 424 seawater samples were collected in the Arctic-North Atlantic Ocean, including the Mid-North Atlantic Ocean, the Norwegian Sea, the Arctic Ocean, the Fram Strait and the sea around Greenland, Iceland and Faroe Islands **(Figure 10)**. A large scale coverage of sampling was useful to investigate the transport of Atlantic water. Seawater samples in the Mid-North Atlantic Ocean were obtained in December, 2017 – February, 2018 through JC156-GA13 cruise. Sampling in the Arctic Ocean was carried out in August - September, 2021 through the R/V Akademik Tryoshnikov. The sample collection in the Norwegian Sea and the sea around Iceland were carried out in May, 2020 and May – August, 2019 and 2020 by the R/V G.O. Sars and the R/V Bjarni Sæmundsson, respectively. Seawater sampling in the Fram Strait was carried out in August – September during 2019 – 2021 on expeditions aboard the R/V Kronprins Haakon by Norwegian Polar Institute. Seawater in East Greenland fjords (the Kong Oscars and Franz Josef fjord system) was collected in August, 2018 through the Royal Danish Naval Vessel HMDS Lauge Koch. And the samples in the sea around Greenland and Faroe Islands were collected in 2019 and 2017 – 2021, respectively. All seawater samplings were carried out through the collaboration of Technical University of Denmark with Aarhus University, Denmark, Norwegian Polar Institute and Institute of Marine Research, Norway, Marine and Freshwater Research Institute, Iceland, and University of Faroe Islands.

2.1.2 Freshwater in river and sea ice

To consider the influence of anthropogenic U in river water and sea ice, two river water samples in East Greenland fjords and three sea ice core samples in the western Fram Strait were collected in August, 2018 and August, 2021 through the Royal Danish Naval Vessel HMDS Lauge Koch and the R/V Kronprins Haakon, respectively **(Figure 10)**.

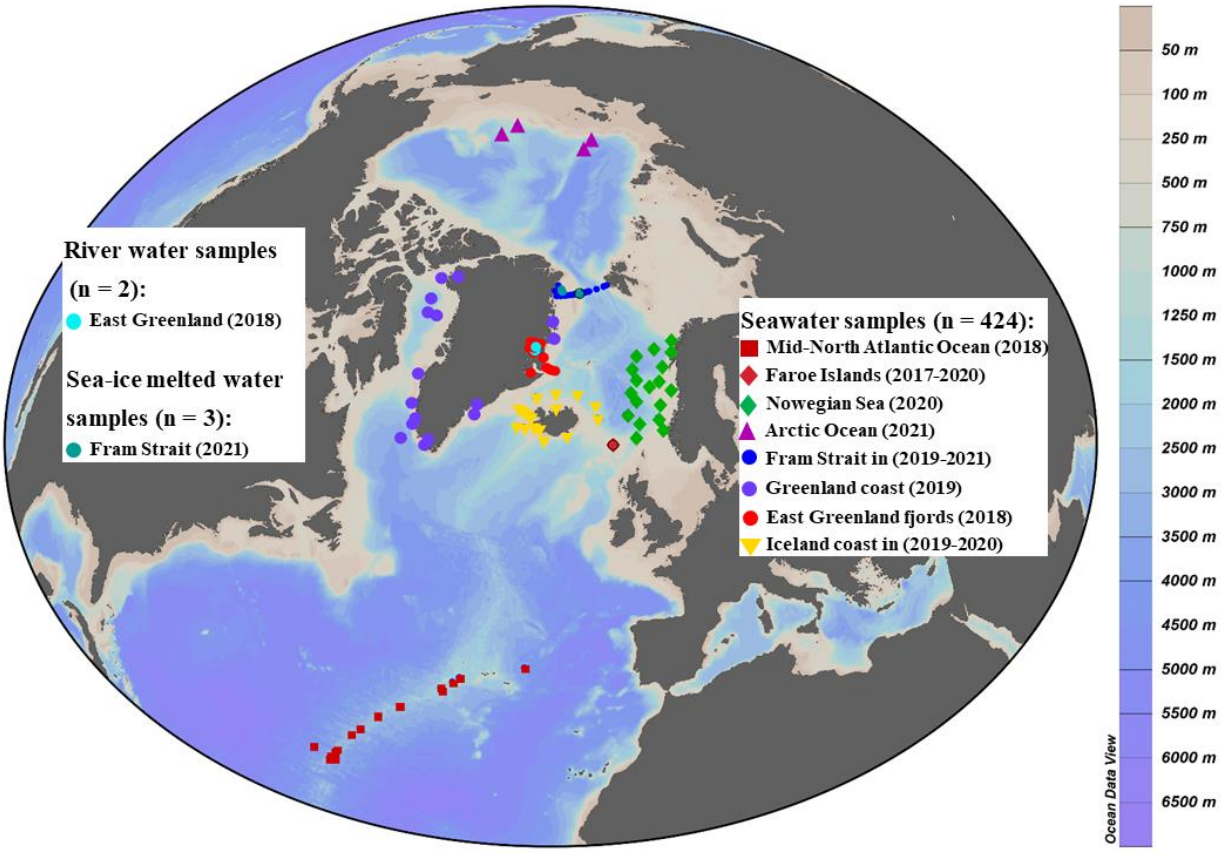

Figure 10. Sample locations in the Arctic and North Atlantic oceans covered in this study.

2.2 Research approaches

Two novel ^{233}U-^{236}U tracer approaches have been developed to estimate transit times of Atlantic waters in the Arctic and North Atlantic oceans through combining nutrient, CDOM and ^{99}Tc. Detailed processes of preparation for the determination of uranium isotopes, nutrient, CDOM and ^{99}Tc have been described in the independent scientific **Papers (I, II and III)**. In addition, the data of nitrate and phosphate was provided by Colin A. Stedmon (DTU Aqua). CDOM absorbance in the Fram Strait was measured by Rafael Gonçalves-Araujo (DTU Aqua) and Colin A. Stedmon (DTU Aqua). And ^{99}Tc as another anthropogenic radioisotope was measured by colleagues of the Climate and Monitoring Section at Risø (DTU).

2.2.1 ^{233}U-^{236}U-nutrient approach

Compared with the diffuse-source of GF, a point-source for $^{236}U_{NRPs}$ concentration provides a better use for tracing Atlantic water transit time. All transit times in this thesis refers to the tracer ages assuming an advective transport due to the strong stratification in the Arctic. To avoid the ubiquitous interference of GF, $^{236}U_{NRPs}$ signal is isolated by the following equations (eqs. 1 – 4) using the atomic ratio of $^{233}U/^{236}U$ (Qiao et al., 2020).

$$P_{GF} = \frac{(R_{NRPs}^{233/236} - R_S^{233/236})}{(R_{NRPs}^{233/236} - R_{GF}^{233/236})} \approx \frac{R_S^{233/236}}{R_{GF}^{233/236}} \qquad (1)$$

$$P_{NRPs} = 1 - P_{GF} \qquad (2)$$

$$C_{s,GF}^{236} = C_s^{236} \times P_{GF} = \frac{C_S^{233}}{R_{GF}^{233/236}} \qquad (3)$$

$$C_{s,NRPs}^{236} = C_s^{236} \times P_{NRPs} = C_s^{236} - C_{s,GF}^{236} \qquad (4)$$

where P_{GF} and P_{NRPs} refer to the proportions of GF and NRPs in ^{236}U; $R_S^{233/236}$, $R_{NRPs}^{233/236}$ and $R_{GF}^{233/236}$ are the corresponding $^{233}U/^{236}U$ atomic ratios for the measured sample, and the endmember values in NRPs (1×10^{-7}) and GF ($1.40 \pm 1.5 \times 10^{-2}$), respectively (Hain et al., 2020; HELCOM MORS Discharge basement, 2020); C_s^{233}, C_s^{236}, $C_{s,GF}^{236}$, and $C_{s,NRPs}^{236}$ are concentrations of ^{233}U, and total ^{236}U, GF-derived ($^{236}U_{GF}$) and $^{236}U_{NRPs}$ in the sample, respectively. Based on uncertainty propagation (BIPM et al., 2008), the uncertainties can be calculated through the equations, which are described in **supporting information of Paper I.**

Besides the influence of the dilution from Pacific water and freshwater (river water, ice meltwater and precipitation), the historic discharges of ^{236}U from SF and LH is crucial to establish the ^{233}U-^{236}U tracer approach. Due to lack of documentation, the discharges of ^{236}U from SF and LH were reconstructed through the ^{236}U observations in shell collected nearby SF and LH (Castrillejo et al., 2020). And the historic input functions of ^{236}U in SF and LH branch waters are estimated through the assumed water flow **(Figure 11A)**. The $^{236}U_{GF}$ concentrations estimated in the North Sea are subtracted for obtaining the $^{236}U_{NRPs}$ concentrations in SF and LH branch waters (Christl et al., 2015). However, SF and LH branch waters mix with the pure GF-dominated Atlantic water in the Barents Sea Opening before entering the Arctic Ocean and thus form three Atlantic branch waters (NCC, BSBW and FSBW) in different mixing patterns (Casacuberta et al., 2018) **(Figure 11B, Table 3)**. Thus, the input functions of ^{236}U concentrations in the NCC, BSBW and FSBW are obtained through the following equations (eqs. 5 – 7). And their uncertainties are propagated from the $^{236}U/^{238}U$ ratios in the record of shell and the mixing pattern in the Barents Sea Opening (Casacuberta et al., 2018; Castrillejo et al., 2020). The reconstructed input functions of $^{236}U_{NRPs}$ concentrations in the Barents Sea Opening present a monotonically decreasing trend since the 1970s with different concentrations in Atlantic branch waters (NCC > BSBW > FSBW) **(Figure 11B)**.

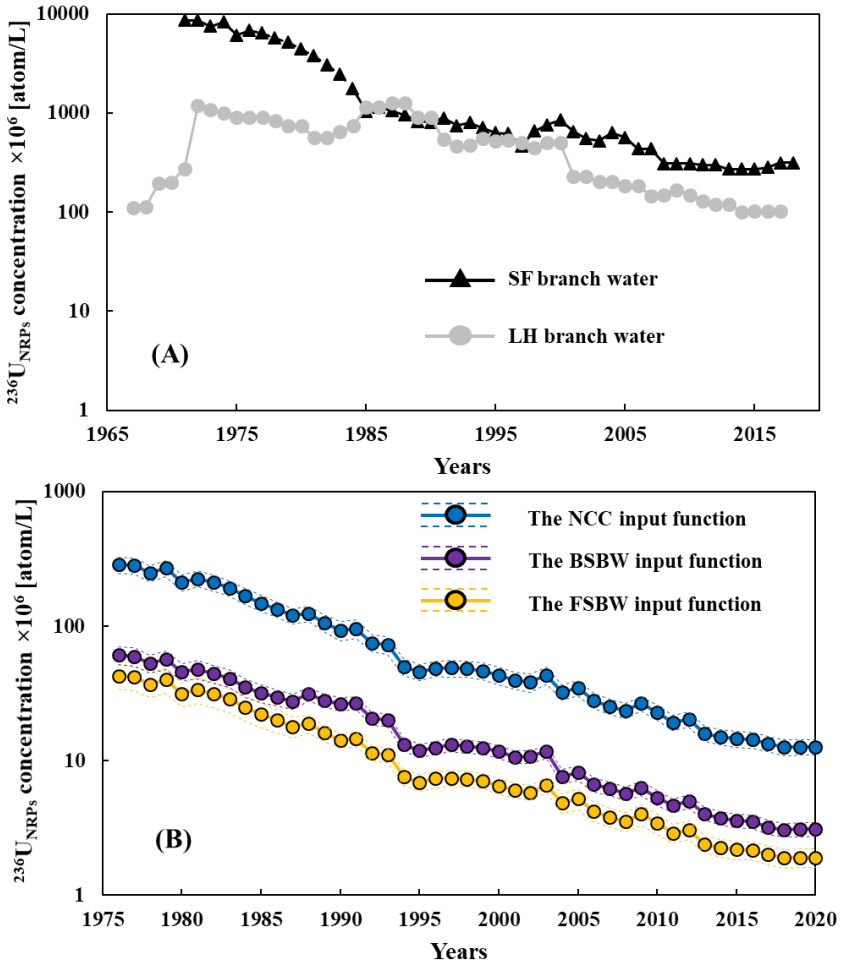

Figure 11. The reconstructed historic change of $^{236}U_{NRPs}$ concentrations in SF and LH branch waters (A) and the Barents Sea Opening (B). SF: Sellafield; LH: La Hague; NCC: Norwegian Coastal Current; BSBW: Barents Sea Branch Water; FSBW: Fram Strait Branch Water.

Table 3. Water mixing pattern in the Barents Sea Opening

Atlantic branch waters	LH branch (%)	SF branch (%)	Atlantic water (%)
Norwegian Coastal Current (NCC)	5.2 ± 1.1	2.7 ± 0.4	92.1 ± 1.1
Barents Sea Branch Water (BSBW)	1.7 ± 0.2	0.5 ± 0.1	97.7 ± 0.2
Fram Strait Branch Water (FSBW)	0.8 ± 0.1	0.4 ± 0.1	98.7 ± 0.2

** NCC was defined as Arctic Shelf Break Branch (Casacuberta et al., 2018, Wefing et al., 2019), Atlantic water (AW) only has pure GF signal*

$$^{236}U_{NCC} = 5.2\% \times {}^{236}U_{LH} + 2.7\% \times {}^{236}U_{SF} + 92.1\% \times {}^{236}U_{AW} \quad (5)$$

$$^{236}U_{BSBW} = 1.7\% \times {}^{236}U_{LH} + 0.5\% \times {}^{236}U_{SF} + 97.7\% \times {}^{236}U_{AW} \quad (6)$$

$$^{236}U_{FSBW} = 0.8\% \times {}^{236}U_{LH} + 0.4\% \times {}^{236}U_{SF} + 98.7\% \times {}^{236}U_{AW} \quad (7)$$

Due to the monotonically decreasing input of $^{236}U_{NRPs}$ and the dilution from Pacific water and other freshwaters, the $^{236}U_{NRPs}$ concentration in the downstream seawater is lower than that in the endmember of the Barents Sea Opening during the same period. To estimate Atlantic water transit time from the Barents Sea Opening, the proportion of Atlantic water is used to calibrate the dilution effect. Here, we use nitrate, phosphate and salinity to calculate the fraction of Atlantic water for obtaining the original $^{236}U_{NRPs}$ concentration in the endmember of the Barents Sea Opening. And Atlantic water fraction can be calculated through the equations 8 – 12 (Dodd et al., 2012):

$$P_{aw} = 0.53N + 0.170 \quad (8)$$

$$P_{pw} = 0.65N + 0.940 \quad (9)$$

$$f_{aw} + f_{pw} + f_{fw} = 1 \quad (10)$$

$$f_{aw}P_{aw} + f_{fw}P_{aw} + f_{pw}P_{pw} = P_s \quad (11)$$

$$f_{aw}S_{aw} + f_{pw}S_{pw} + f_{fw}S_{fw} = S_s \quad (12)$$

where P_{aw}, P_{pw} and P_s are the phosphate concentrations in the endmember of Atlantic water and Pacific water and our measured seawater samples; f_{aw}, f_{pw} and f_{fw} are Atlantic water fraction, Pacific water fraction and freshwater fraction, respectively; S_{aw}, S_{pw}, S_{fw}

and S_s are the salinities in the endmember of Atlantic water (34.9), Pacific water (32) and freshwater (0) and our measured seawater samples.

The Atlantic water endmember concentration of $^{236}U_{NRPs}$ ($^{236}U_{NRPs\text{-}aw}$) in the downstream seawater can be obtained by the equations 13 – 14:

$$f_{aw}{}^{236}U_{NRPs\text{-}aw} + f_{pw}{}^{236}U_{NRPs\text{-}pw} + f_{fw}{}^{236}U_{NRPs\text{-}fw} = {}^{236}U_{NRPs} \quad (13)$$

$$^{236}U_{NRPs\text{-}aw} = {}^{236}U_{RP}/\, f_{aw} \quad (14)$$

where $^{236}U_{NRPs\text{-}aw}$, $^{236}U_{NRPs\text{-}pw}$ and $^{236}U_{NRPs\text{-}fw}$ are $^{236}U_{NRPs}$ concentrations in the endmember of Atlantic water, Pacific water (0) and freshwater (0), respectively. And the values in Pacific water and freshwater are assumed as zero due to the assumption that Pacific water and freshwater do not carry the signal from nuclear reprocessing plants.

Therefore, $^{236}U_{NRPs\text{-}aw}$ concentration in the downstream seawater of the Arctic area is only affected by the source year of Atlantic water from the Barents Sea Opening. Through comparison of the $^{236}U_{NRPs\text{-}aw}$ concentrations in the seawater samples and the input functions, the corresponding year for the matched value is obtained **(Figure 12)**.

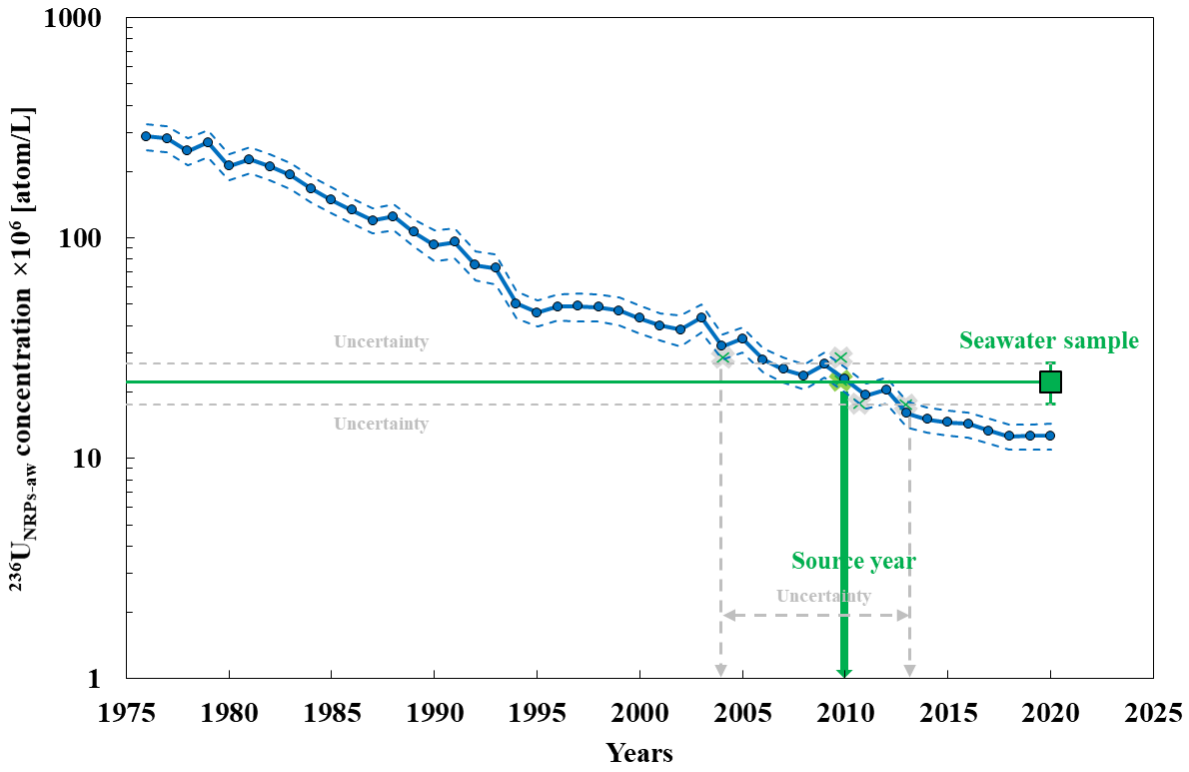

Figure 12. A seawater sample in the Fram Strait for Atlantic water transit time estimation with uncertainty. Estimated $^{236}U_{NRPs-aw}$ concentration in sample is only influenced by the endmember concentrations of $^{236}U_{NRPs-aw}$ which is time-depend following the NCC (or others) input function(s). Dashed lines refer to uncertainties.

2.2.2 Colored dissolved organic matter as an auxiliary for ^{233}U-^{236}U-nutrient approach

Atlantic water enters to the Arctic Ocean as three separate branches which can be assigned to different NRPs contributions and thus formulating different input functions (Casacuberta et al., 2018). These NRPs input functions are crucial for using radioisotopes to track Atlantic water transport pathways and estimate their transit times. However, the dilution and various historic discharges of NRPs result in unclear boundary of NRPs signal in seawater among different input functions. Compared with the weak background signal from marine organic matter, the terrestrial CDOM supplies a prominent signal in

the Arctic seawater from the Arctic rivers, especially the Siberian rivers (Stedmon et al., 2011), and thus becomes a riverine freshwater tracer (Granskog et al., 2012; Stedmon et al 2015; Gonçalves-Araujo et al., 2016; Charette et al 2020). Importantly, the exported high CDOM levels on the Siberian coast can be entrained by Atlantic water, which transports to the Fram Strait across the Arctic basins as part of the Transpolar Drift (Charette et al 2020). Therefore, CDOM is expected to be a tracer for the coastal Atlantic water (NCC) on the Siberian shelf, and hereby is used to distinguish different input functions for NRPs signal in seawater.

CDOM absorbance showed a clear difference (a_{350}: 0.06 – 0.86 m^{-1}) in the Fram Strait, it was significantly higher in upper 200 m of the western Fram Strait **(Figure 13 J-L)**. And the distribution of higher CDOM absorbance ($\geqslant$ 0.35 m^{-1}) changed to be wider and deeper from 2019 to 2021. Wefing et al. (2019 and 2021) assumed that the NCC input function and the BSBW/FSBW input function dominated the NRPs signal in PSW and AAW, respectively, due to the difference in $^{129}I/^{236}U$ ratio and salinity. However, $^{129}I/^{236}U$ ratio can be influenced by the historic NRPs discharge from SF and LH, and salinity is also diluted by Pacific water and sea-ice meltwater. Compared to this assumption, CDOM is a direct tracer for identifying these Atlantic branch waters in different pathways.

Atlantic water dominates the eastern Fram Strait, so CDOM absorbance ($a_{350} < 0.35$ m^{-1}) in the eastern Fram Strait can be used as the background signal of marine organic matter **(Figure 13 J-L)**. And high CDOM absorbance ($\geqslant$ 0.35 m^{-1}) in the Fram Strait is considered to be influence by the NCC entrained the terrestrial CDOM. It can be defined as "Arctic High CDOM Water". Consequently, $^{236}U_{NRPs}$ in the Arctic High CDOM Water derives from the NCC input functions. Recently, a study proposed a potential mixture of the NCC input function with the BSBW or FSBW input function in the Barents Sea through comparing concentrations of ^{129}I and ^{236}U in the Amundsen Basin and the input functions (Wefing et al., 2022). The circulation in the Barents Sea shows two branch waters in BSBW: 1) one coastward branch water and 2) a northward branch water toward

the shelf edge (Loeng, 1991). We suggest a mixture of the NCC and BSBW input functions in the Barents Sea, and they are the source of $^{236}U_{NRPs}$ in Arctic High CDOM Water.

The remaining waters were characterized by low CDOM absorbance ($a_{350} < 0.35\ m^{-1}$) in the Fram Strait, but their variabilities of potential temperature (Θ) **(Figure 13 D-F)**, potential density **(Figure 13 G-I)** and ^{236}U concentrations **(Figure 13 P-R)** revealed a further water classification. Compared with $^{236}U_{NRPs}$ concentrations in the western Fram Strait, they are lower in the eastern Fram Strait due to the westward Atlantic water (without the transportation in the Arctic Ocean). The westward Atlantic water is defined as (dense) Recirculating Atlantic Water and Atlantic water through potential temperature and density. In addition, Atlantic water on the coast of Svalbard Islands has a high Θ (> 2) but low σ_Θ ($\leqslant$ 27.7). For these Atlantic waters, they have same source of $^{236}U_{NRPs}$ from the FSBW input function. Therefore, they are integrated and redefined as "Atlantic Low CDOM Water" ($a_{350} < 0.35\ m^{-}1$; $2 < \theta$ and $27.7 < \sigma_\Theta \leqslant 27.97$ or $0 < \Theta$, $27.97 < \sigma_\Theta$, $\sigma_{0.5} \leqslant 30.444$, Θ and S decrease with depth).

For the Arctic-derived low CDOM waters, we propose that their sources of $^{236}U_{NRPs}$ are the offshore Atlantic water from the BSBW and the FSBW. Compared with a low ^{236}U concentration ($< \sim 10 \times 10^6$ atom/L) in deeper water, a part of seawater has a higher ^{236}U concentration ($\geqslant 15 \times 10^6$ atom/L) in upper ~1000 m **(Figure 13P-R)**. Higher concentration of ^{236}U derives from a strong advective transport from the BSBW and FSBW. And the low concentration of ^{236}U in deeper water may originate from the mixture of the vertical dispersion of the BSBW and FSBW and the natural background seawater. It is noted that surface seawater in upper 200 m has a lower ^{236}U concentration ($< 15 \times 10^6$ atom/L) due to the dilution from Pacific water, river water and sea-ice meltwater. These surface waters has a low density ($\sigma_\Theta \leqslant 27.7$) compared with that in deeper water. Seawater in low CDOM levels has a higher ^{236}U concentration ($\geqslant 15 \times 10^6$ atom/L) or a low σ_Θ ($\leqslant$ 27.7) and thus is defined as "Arctic Low CDOM / High ^{236}U

Water". And the remainder of waters in the Fram Strait is defined as "Low CDOM / Low ^{236}U Water". Characteristics of the defined water classes in the Fram Strait are shown in **Table 3**.

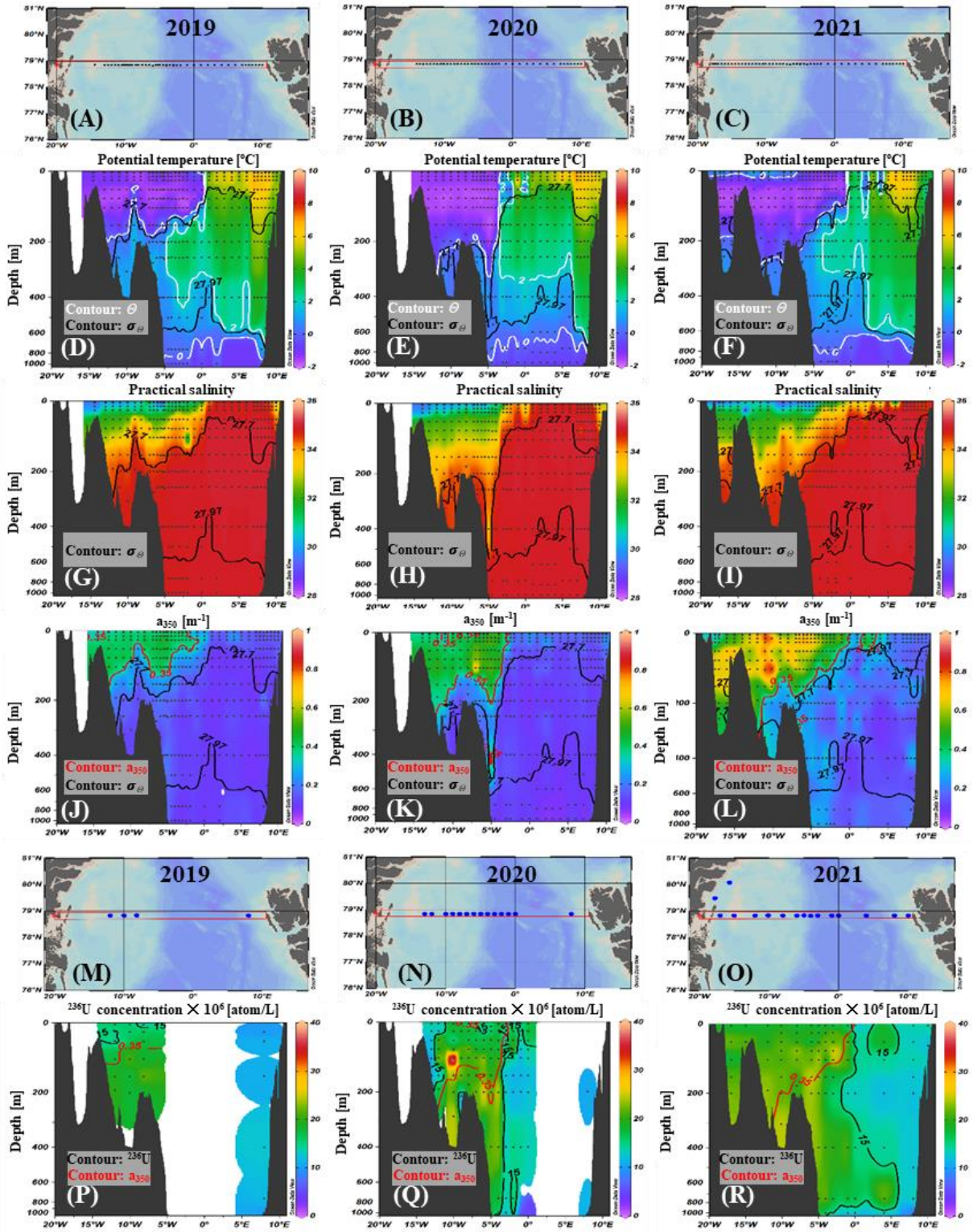

Figure 13. A transect (A – C) of potential temperature (D – F), salinity (G – I) and a_{350} (J – L), the uranium stations (M – O) and ^{236}U concentrations (P – R) in the Fram Strait during 2019 – 2021.

Table 3. Characteristics of the different water classes in the Fram Strait.

Properties	Years	Arctic High CDOM Water* (n = 108)	Atlantic Low CDOM Water (n = 40)	Arctic Low CDOM / High ^{236}U Water (n = 79)	Arctic Low CDOM / Low ^{236}U Water (n = 14)
Average Θ [°C]	2019	-1.3 ± 0.23	5.62 ± 1.43	-0.19 ± 0.74	
	2020	-1.36 ± 0.65	3.32 ± 0.71	0.12 ± 0.90	-0.71 ± 0.02
	2021	-0.84 ± 1.03	3.55 ± 1.40	0.33 ± 0.92	-0.65 ± 0.08
Average S_p	2019	31.45 ± 1.16	34.95 ± 0.09	34.28 ± 0.34	
	2020	32.11 ± 1.23	34.75 ± 0.30	34.41 ± 0.53	34.92 ± 0.003
	2021	32.12 ± 1.63	34.78 ± 0.55	34.69 ± 0.27	34.92 ± 0.01
Average a_{350} [m^{-1}]	2019	0.40 ± 0.03	0.12 ± 0.02	0.22 ± 0.05	
	2020	0.46 ± 0.07	0.13 ± 0.06	0.17 ± 0.06	0.11 ± 0.02
	2021	0.61 ± 0.13	0.16 ± 0.08	0.24 ± 0.07	0.18 ± 0.08
Average $^{236}U_{NRPs}$ concentration × 10^6 [atom/L]	2019	9.82 ± 1.48	2.86 ± 1.83	11.38 ± 3.01	
	2020	9.48 ± 4.02	5.63 ± 2.10	8.86 ± 4.50	1.27 ± 0.76
	2021	13.49 ± 2.83	7.64 ± 1.72	13.67 ± 2.54	3.92 ± 1.64
Average estimated $^{236}U_{NRPs\text{-}aw}$ concentration× 10^6 [atom/L]	2019	17.16 ± 3.43	2.90 ± 1.87	12.17 ± 3.73	
	2020	14.92 ± 5.89	6.11 ± 2.67	11.38 ± 5.06	1.47 ± 0.91
	2021	20.74 ± 6.18	8.12 ± 2.09	14.16 ± 2.47	3.26 ± 2.35
Corresponding source waters		NCC-BSBW	FSBW	BSBW-FSBW	

** Two surface seawater samples in 2020 with lower a_{350} values (< 0.35 m^{-1}) are also included in "Arctic High CDOM Water" due to the local dilution from sea ice meltwater.*

2.2.3 ^{99}Tc-^{233}U-^{236}U approach

Unique point-source of NRPs signal provides an opportunity for $^{236}U_{NRPs}$ to trace Atlantic water movement in the Arctic areas. However, the dilution of Pacific water and freshwater needs to be calibrated to obtain reliable estimates on the source year of Atlantic water in the downstream regions. To eliminate uncertainties in calculating the

water fraction, we can use the time-dependent isotopic ratios of a tracer pair in the NRPs discharge to trace Atlantic water. The ratio of $^{236}U_{NRPs}$ and another conservative radioisotope is solely affected by the historic NRPs discharge. Both ^{99}Tc and ^{129}I are the conservative and long-lived NRPs-dominated radioisotopes (Raisbeck and Yiou, 1999; Hou et al., 2000; Shi et al., 2012). ^{99}Tc dominantly derives from SF, and the main source of ^{129}I is LH (OSPAR, 2019). The reconstructed discharge of $^{236}U_{NRPs}$ from the record of shell show a dominated source from SF (Castrillejo et al., 2020), so the atomic ratio of $^{99}Tc/^{236}U_{NRPs}$ is selected in this study. Although SF is the main source for ^{99}Tc and $^{236}U_{NRPs}$, the discharge from LH still has a less contribution. Therefore, the reconstruction of temporal change in discharge ratios of $^{99}Tc/^{236}U_{NRPs}$ is considered under three scenarios: 1) the sole source from SF; 2) the contribution of both SF and LH; 3) the mixture from SF and LH with a 2-year transit time for SF **(Figure 14)**. And the transit times from SF branch water and LH branch water to the Barents Sea Opening are considered to be 5 and 3 years, respectively (Casacuberta et al., 2018). Two years lag is assumed for the mixture of branch waters of SF and LH. Therefore, the third scenario agrees with an actual situation. The temporal change of discharge ratios of $^{99}Tc/^{236}U_{NRPs}$ presents two significant peak values in 1995 and 2002, respectively **(Figure 14)**. The source year is constrained through comparison of $^{99}Tc/^{236}U_{NRPs}$ ratios in seawater samples and the reconstructed discharge ratios, and Atlantic water transit time can be estimated through aligning the time series of measurement to the historic temporal trend **(Figure 14)**.

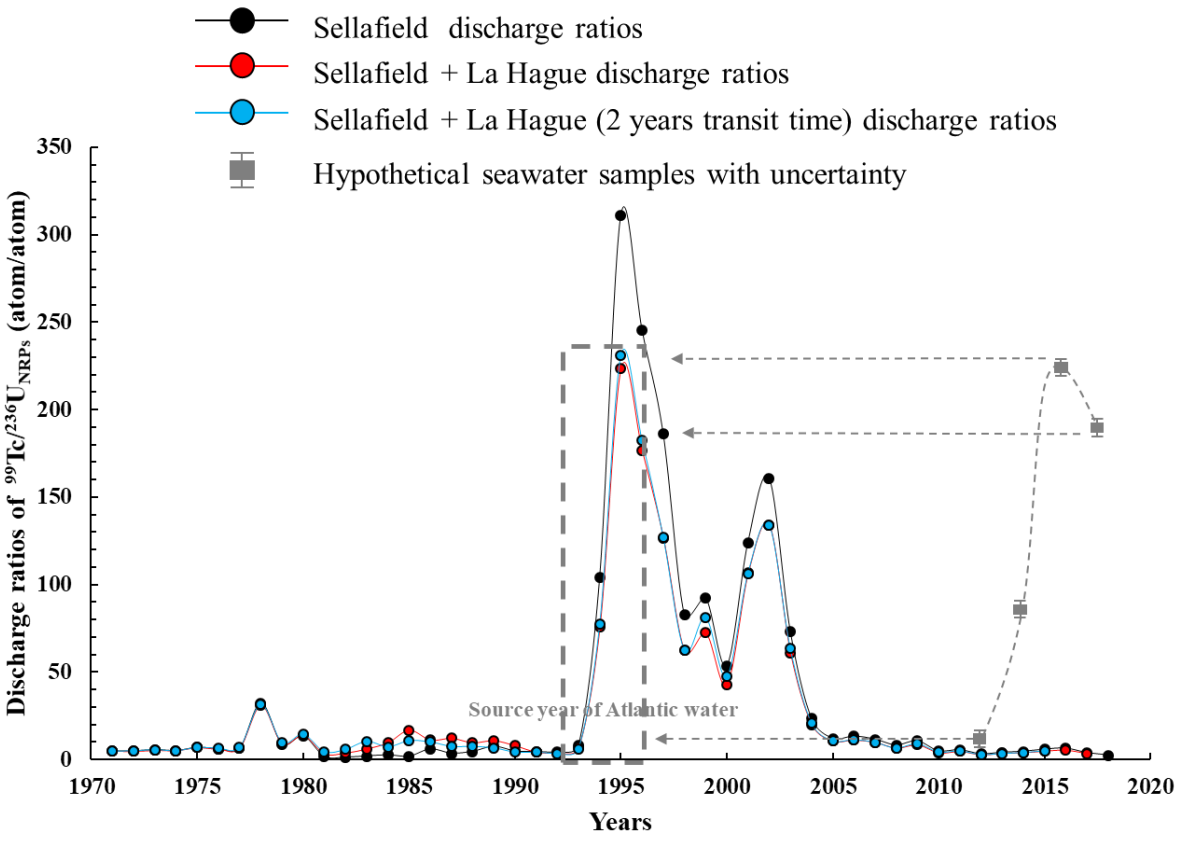

Figure 14. The approach of Atlantic water transit time estimation based on comparison between time series $^{99}Tc/^{236}U_{NRPs}$ atomic ratios in seawater samples of Greenland coast and corresponding discharge ratios from reprocessing plants.

3. Results and Discussions

3.1 Spatiotemporal distributions of ^{233}U and ^{236}U in Arctic and North Atlantic oceans

The distribution of ^{233}U concentration in the Arctic and North Atlantic oceans ranged from 1.06 – 62.85 × 10^4 atom/L **(Figure 15)**. For the surface seawater (0 – 10 m), ^{233}U concentrations were more various in the Norwegian Sea. This might be related to the input of freshwater from the European coast and the mixture of multiple currents from different latitudes. For the water column samples, ^{233}U concentrations primarily distributed within 0 – 20 × 10^4 atom/L, and ^{233}U concentrations were generally lower than 10 × 10^4 atom/L in the areas 2 and 7. ^{233}U concentrations showed slightly higher levels at 400 – 500 m depth of the areas 3, 4 and 5. These changes were resulted by both the latitudinal deposition and a strongly advective transport in the Arctic Ocean. The areas 2 and 7 were located in high (77°N – 81°N) and low (26°N – 39°N) latitudes zones, respectively, where weaker deposition of GF could be implied by other radioisotopes (Aoyama et al., 2006; Snyder et al., 2010). In addition, the freshwater contribution from Pacific water, river discharge and precipitation facilitated a stronger stratification in the Arctic region (Serreze et al., 2006). Atlantic water carried higher ^{233}U concentration from the mid-latitude area into the Arctic, and advectively transported at the intermediate layer. Consequently, the slightly high distribution of ^{233}U concentration was observed at 400 – 500 m depth.

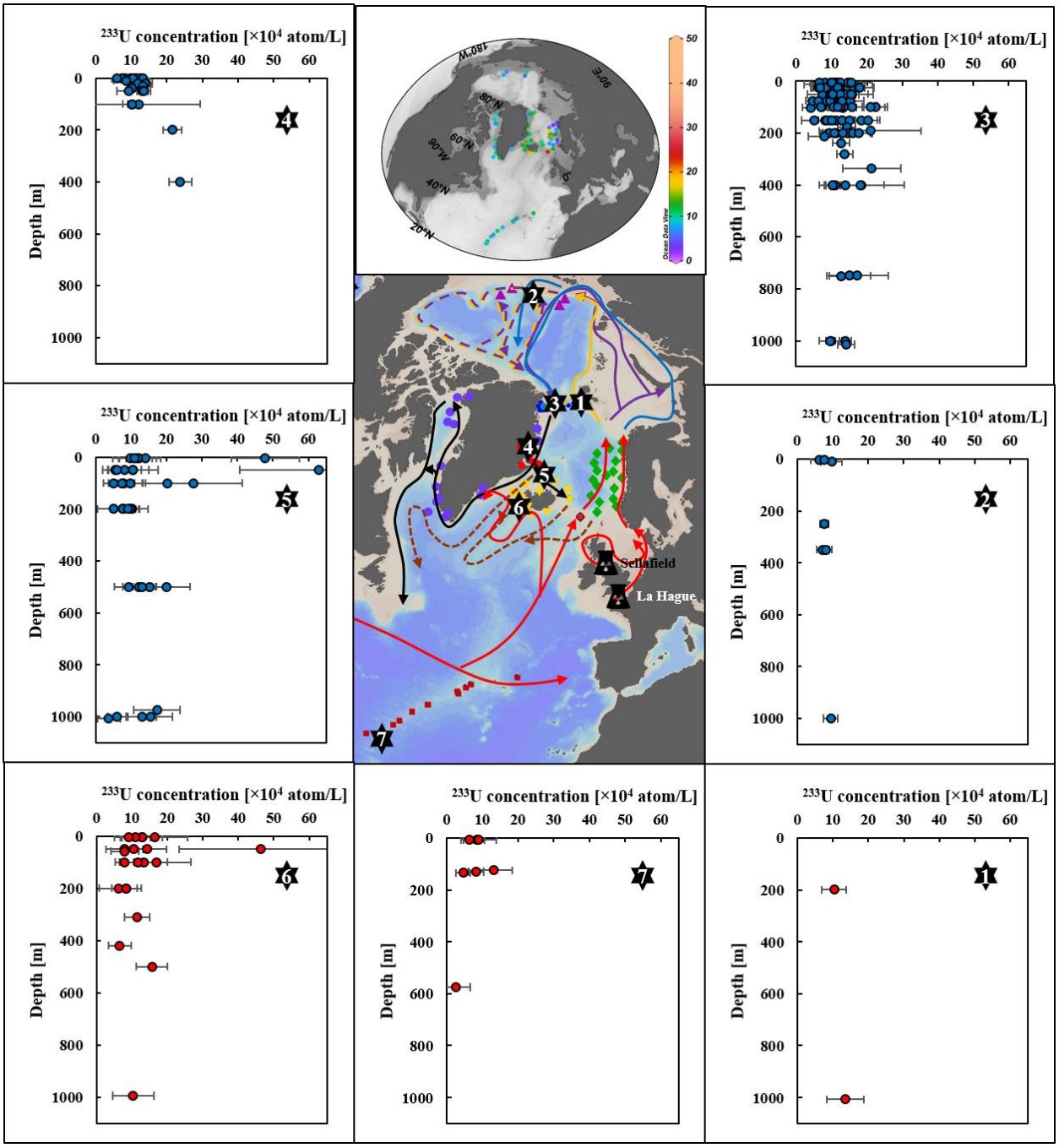

Figure 15. The distribution of ^{233}U concentration in surface seawater samples (0 – 10 m) and column seawater samples of the Arctic-North Atlantic Ocean.

The measured concentrations of ^{236}U varied within 1.64 – 120.27 × 10^6 atom/L, but their dominant ranges were 10 – 20 × 10^6 atom/L **(Figure 16)**. And high values (> 20 × 10^6

atom/L) were observed in the coastal water of the Norway and Greenland and the surface water of the Mid-North Atlantic Ocean. For the surface seawater, ^{236}U concentrations gradually decreased following the order: the Norwegian coast, the Arctic Ocean and the Greenland coast, the northern sea around Iceland and the Norwegian offshore, the southern sea around Iceland and the Mid-North Atlantic Ocean. For the water column samples, the slightly higher concentrations of ^{236}U were found at 100 – 500 m depths of the areas 3, 4, 5 and 7. To interpret these difference, it was necessary to separate ^{236}U into $^{236}U_{GF}$ and $^{236}U_{NRPs}$ using the ratios of $^{233}U/^{236}U$.

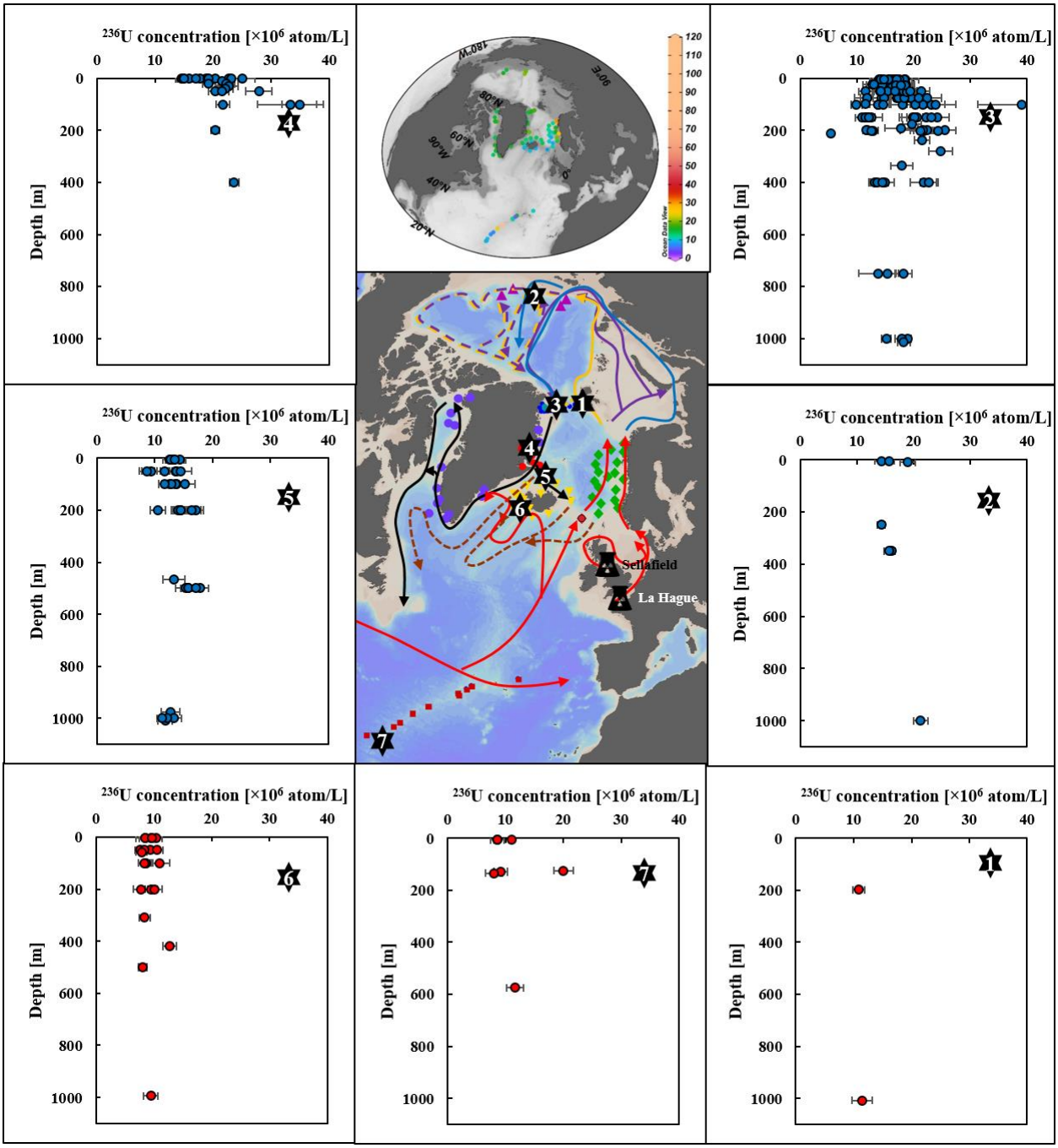

Figure 16. The distribution of ^{236}U concentration in surface seawater samples (0 – 10 m) and column seawater samples of the Arctic-North Atlantic Ocean.

GF and NRPs contributions in ^{236}U were important to be distinguished for investigating water movement. The difference of $^{233}U/^{236}U$ atomic ratios in the endmembers of NRPs

(10^{-7} – 10^{-6}) and GF ($1.40 \pm 0.15 \times 10^{-2}$) had been successfully used to separate NRPs and GF signals for ^{236}U, respectively (Hain et al., 2020; Qiao et al., 2020; HELCOM, 2020). Our observation of $^{233}U/^{236}U$ ratios showed a range between 5.00×10^{-4} – 6.73×10^{-2}, revealing variable contributions of NRPs and GF in the Arctic-North Atlantic Ocean.

GF-derived ^{236}U ($^{236}U_{GF}$) concentrations (0.75 – 16.99×10^6 atom/L) showed a similar regional change to ^{233}U concentration **(Figure 17)**. They also had a more various distribution in surface water of the Norwegian Sea. Although the historic deposition of ^{233}U was unknown, the concentration of $^{236}U_{GF}$ had been reconstructed in seawater of the North Sea (50°N – 60°N) based on 2-D GRACE model (Christl et al., 2015). The modelling results showed a monotonically decreasing trend since the year of 1966, and $^{236}U_{GF}$ concentration reached ~10×10^6 atom/L in the 2010s. Our observation results indicate a dominant distribution of $^{236}U_{GF}$ concentration between 5 – 10×10^6 atom/L during 2018 – 2021, which was consistent with the modelling results (Christl et al., 2015). $^{236}U_{GF}$ concentrations in the depth profiles should show a gradually decreasing trend from surface water to bottom water, but in the regions 3 – 5 they were slightly higher at 400 – 500 m depths, suggesting the advective transport of Atlantic water carrying older $^{236}U_{GF}$ signal from the mid-latitude area.

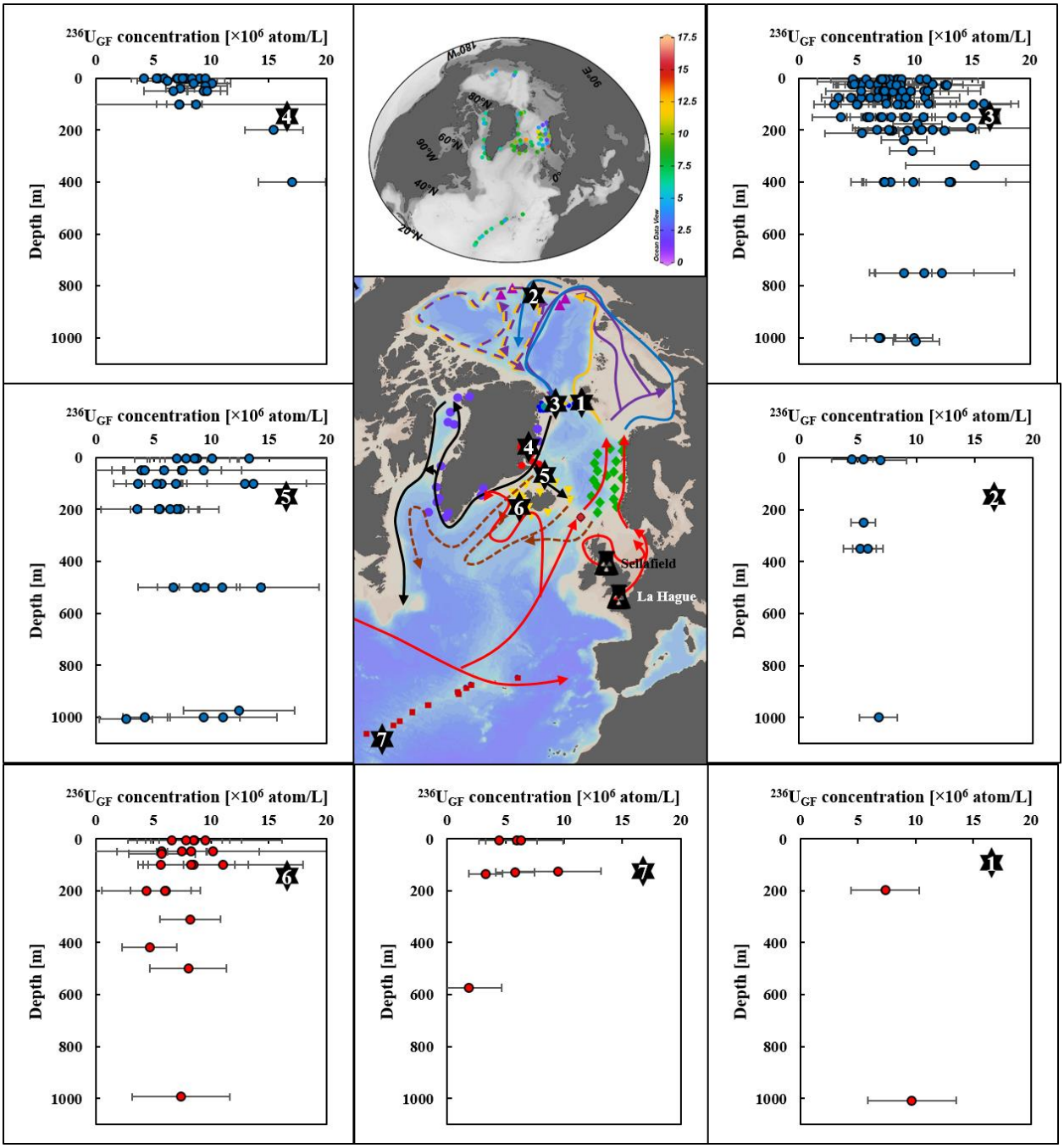

Figure 17. The distribution of $^{236}U_{GF}$ concentration in surface seawater samples (0 – 10 m) and column seawater samples of the Arctic-North Atlantic Ocean.

On the other hand, $^{236}U_{NRPs}$ concentrations were estimated to be in the range of 0 – 115.94 × 10^6 atom/L **(Figure 18)**, demonstrating similar spatial distribution pattern to

that of ^{236}U. The SF and LH branch waters carrying higher $^{236}U_{NRPs}$ concentration mixed in the North Sea (Christl et al., 2017; Castrillejo et al., 2020), and further transported northward to the Arctic Ocean along the Norwegian coast **(Figure 9F)**. These $^{236}U_{NRPs}$–tagged Atlantic waters dispersed in the Arctic Ocean and outflowed from the western Fram Strait to the North Atlantic Ocean along the Greenland coast. And the $^{236}U_{NRPs}$ concentration distribution in surface water agreed with the current circulation in the Arctic and North Atlantic oceans. In addition, significantly higher $^{236}U_{NRPs}$ concentrations were found in the Mid-North Atlantic Ocean, implying that a potential unreported NRPs release in low latitude area. For the slightly enhance of $^{236}U_{NRPs}$ concentration at 100 – 500 m depths of areas 3, 4, and 5, there were two potential reasons. At first, $^{236}U_{NRPs}$ concentration in surface water of the upper 100 m was diluted by other waters (e.g. Pacific water, river water and ice meltwater). And the influence of dilution was minor for these $^{236}U_{NRPs}$–tagged Atlantic waters at 100 – 500 m depths. Secondly, the historic discharge of $^{236}U_{NRPs}$ revealed a monotonically decreasing trend after the 1970s. The higher $^{236}U_{NRPs}$ concentration at 100 – 500 m depths might be due to the stagnated NRPs signal from older years. In short, the distribution of $^{236}U_{NRPs}$ concentrations agreed with the current circulation pattern, thus highlighting its tracer application for Atlantic water in the Arctic and North Atlantic oceans.

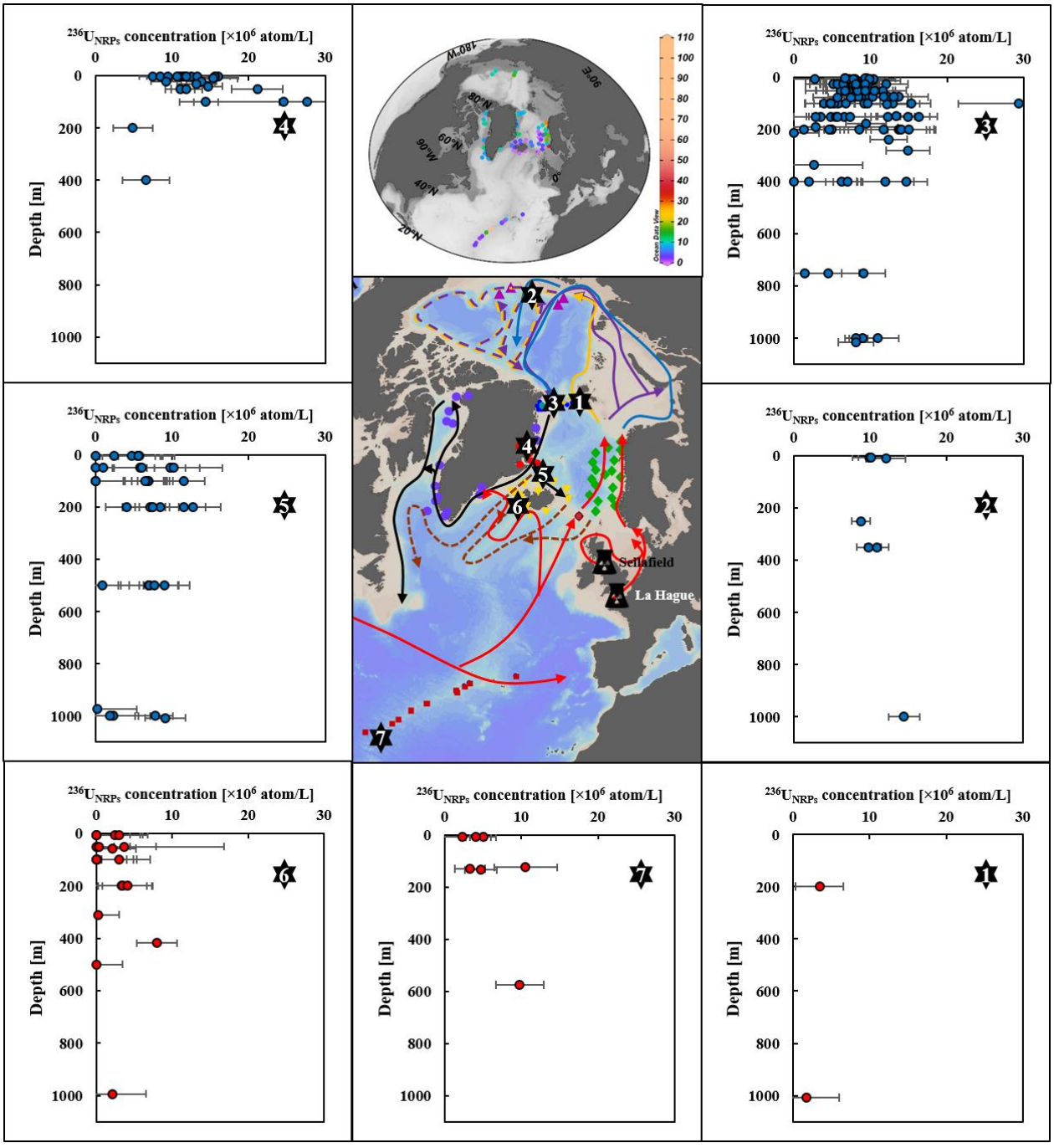

Figure 18. The distribution of $^{236}U_{NRPs}$ concentration in surface seawater samples (0 – 10 m) and column seawater samples of the Arctic-North Atlantic Ocean.

3.2 Transit times of Atlantic waters in Arctic and North Atlantic oceans

Atlantic water transit times in the Arctic and North Atlantic oceans are estimated by two ^{233}U-^{236}U approaches, and the results are summarized in **Table 4**. Previous estimated results in the Fram Strait of the northeastern Greenland coast are compared for validating these approaches.

For the ^{233}U-^{236}U-nutrinets approach, we compare the estimated result in Arctic High CDOM Water (~ upper 200 m) of the western Fram Strait with the reported estimation in PSW (upper 100 m) (Wefing et al., 2019). The source year in the Fram Strait is estimated in 2006 (uncertainties: 2000 – 2015), so Atlantic water transit time is 14 years (5 – 20 years) **(Table 4)**. Compared with the estimation (12 – 19 years) based on the ^{129}I and ^{236}U (Wefing et al., 2019), our estimation shows a similar result (14 years), suggesting that this approach can be successfully used to estimate Atlantic water transit time. And the combination of CDOM has a better constraint of NRPs input functions for Atlantic water, which improves the estimated results using ^{233}U-^{236}U-nutrinets approach **(Figure 13 and Table 3)**.

For the ^{233}U-^{236}U-^{99}Tc approach, the estimated results in surface seawater of upper 10 m of East Greenland coast are compared with the previous results in PSW of the western Fram Strait (12 – 19 years) (Wefing et al., 2019). Assuming with a 5 years transit time from SF to the Barents Sea Opening, an earlier estimation based on the use of ^{129}I and ^{236}U shows that Atlantic water transit times on the northeastern Greenland coast (the western Fram Strait) are 17–24 years (Casacuberta et al., 2018; Wefing et al., 2019), which agrees with our estimation (16 – 17 years) on East Greenland coast. This suggests that this approach is reliable for estimating Atlantic water transit time in the Arctic and North Atlantic oceans.

Table 4. The estimated Atlantic water transit times in the Arctic and North Atlantic oceans.

	Depth/water class	Approaches	Initial point	Input functions/Discharges	Average transit time of Atlantic water (years)
Fram Strait	Arctic High CDOM Water in upper ~ 200 m	^{233}U-^{236}U-nutrients	Barents Sea Opening	50% NCC - 50% BSBW	14 (5 - 20)
Fram Strait	Arctic Low CDOM / High ^{236}U Water at ~ 200 - 1000 m depths	^{233}U-^{236}U-nutrients	Barents Sea Opening	50% BSBW - 50% FSBW	26 (18 - 30)
East Greenland fjords	Cold polar water in upper ~ 100 m of outer Fjords	^{233}U-^{236}U-nutrients	Barents Sea Opening	50% NCC - 50% BSBW	16 (12 - 24)
East Greenland fjords	Warm Atlantic water in upper ~ 100 m of inner Fjords	^{233}U-^{236}U-nutrients	Barents Sea Opening	50% BSBW - 50% FSBW	24 (24 -25)
East Greenland coast	Upper 10 m	^{99}Tc-^{233}U-^{236}U	Sellafield	Discharge raito of $^{99}Tc/^{236}U_{NRPs}$	16 -17 (14 - 18)
West Greenland coast	Upper 10 m	^{99}Tc-^{233}U-^{236}U	Sellafield	Discharge raito of $^{99}Tc/^{236}U_{NRPs}$	22 (20 -24)
Iceland coast	Upper 10 m	^{99}Tc-^{233}U-^{236}U	Sellafield	Discharge raito of $^{99}Tc/^{236}U_{NRPs}$	25
Faroe Islands coast	Upper 10 m	^{99}Tc-^{233}U-^{236}U	Sellafield	Discharge raito of $^{99}Tc/^{236}U_{NRPs}$	25

3.3 Approach comparison for Atlantic water transit time estimate

For the ^{233}U-^{236}U tracer approaches, the first approach estimates Atlantic water transit time through combining with nutrient, CDOM and salinity, and the second approach combines with another anthropogenic radioisotope ^{99}Tc. The use of the first approach assumes the constant water flux near two NRPs (Castrillejo et al., 2020) and a constant water mixing pattern in the Barents Sea Opening (Casacuberta et al., 2018) for reconstructing NRPs input functions, and thus may introduce uncertainties for the estimation of Atlantic water transit time. Conversely, the ^{99}Tc-^{233}U-^{236}U approach directly uses the NRPs discharge ratios to estimate Atlantic water transit time, and the NRPs discharge ratios are only influenced by the historic releases from NRPs without the impact of dilution. This eliminates the uncertainties from different assumptions which may not reflect the actually complicated hydrologic dynamic in the Arctic and North Atlantic oceans.

Compared with the sample preparation and measurement for ^{99}Tc in the second approach, those for nutrient, CDOM and salinity in the first approach are faster and more cost-effective (Chen et al., 1994; Hansen and Koroleff, 1999; Schnetger and Lehners 2014). And less water volume (<1 L for nutrient, CDOM and salinity; 200 L for ^{99}Tc) is also used in the first approach. However, the second approach provides a lower uncertainty for transit time estimation. The first approach uses nitrate and phosphate to estimate the fraction of Atlantic water in the Arctic area, but the denitrification on shelf water results in the considerable errors in the fraction estimation of Pacific water and Atlantic water (Jones et al., 1998; Bauch et al., 2011; Alkire et al., 2015). Although the determination of ^{99}Tc is currently tedious and costly, with the improvement of preparation procedures and measurement techniques in the future, the situation could be improved. For example, with the use of advanced AMS measurement, less water volume ($\leqslant$ 10 L) is needed for ^{99}Tc in the advanced AMS measurement (Hain et al., 2022).

Comparatively, the first approach is more applicable to a large number of samples, such as the following scenarios: 1) a large-scale sampling for the comparison of dataset with the modelling results in the Arctic area, 2) a high-resolution water collection for the regional estimation and 3) a limited water budget and ship time schedule during the sampling expedition. The second approach may be advantageous in the following cases: 1) more precise estimation for Atlantic water transit time with enough supporting in sampling and analysis resources and 2) application in the subpolar region and the North Atlantic Ocean due to the mixture of NRPs-tagged Atlantic water and pure GF-dominated Atlantic water.

3.4 An improved understanding for water mass movement in Arctic and North Atlantic oceans

3.4.1 Interpretation of CDOM variation

The unclear mixing patterns of the NCC and BSBW input functions in Arctic High CDOM Water and the BSBW and FSBW in Low CDOM / High ^{236}U Water influence the accuracy of the estimated Atlantic water transit times. Instead, a higher $^{236}U_{NRPs\text{-}aw}$ concentration in same water class indicates to a longer transit time and transport pathway, avoiding the impact of the unclear mixing patterns. Our observation in the Fram Strait during 2019 – 2021 shows significantly different trends in the correlation of $^{236}U_{NRPs\text{-}aw}$ vs. a_{350} between the Arctic High CDOM Water ($a_{350} > 0.35$ m^{-1}) and other low CDOM waters (< 0.25 m^{-1}) **(Figure 19A)**. It is noted that a part of seawater has intermediate CDOM level ($0.25 < a_{350} < 0.35$ m^{-1}) without any correlation to $^{236}U_{NRPs\text{-}aw}$ concentrations. This part of seawater may be in the boundary between high and low CDOM waters. Based on the analysis of a linear regression, the slope in other low CDOM waters (slope = 58.67) is approximately two times than that in the Arctic High CDOM Water (slope = 23.07). High slope in other low CDOM waters suggests that CDOM levels slightly increase with a longer transit time and transport pathway. In contrast, although samples in Arctic High CDOM Water have a high degree of scatter, low slope in Arctic High CDOM Water still reveals that a longer transit time and transport pathway may facilitate more accumulation of CDOM. CDOM absorbance and salinity have a strong negative correlation at the Arctic river mouths, suggesting that high levels of CDOM from the Arctic rivers are released to the Arctic Ocean (Matsuoka et al., 2017), as also evidenced in our results **(Figure 19B)**. In the Arctic High CDOM Water, Atlantic water transports along the Siberian coast and carries riverine high levels of CDOM into the central Arctic Ocean. A longer transit time and transport pathway for the coastal Atlantic water facilitate more contributions of high CDOM levels from the Siberian rivers. However, other low CDOM waters in the Fram Strait are affected by the

offshore Atlantic water, which is hardly to receive a large amount of CDOM from the Siberian rivers. Therefore, the influence of transit time and transport pathway is limited.

For the variation of CDOM, the impact of Atlantic water transit time and transport pathway is significant in the Arctic High CDOM Water. The annual comparison in the Arctic High CDOM Water shows that estimated $^{236}U_{NRPs\text{-}aw}$ concentrations and a_{350} values in 2021 are higher than those in 2019 and 2020 **(Figure 19C)**, implying the annual change for Atlantic water transit time and transport pathway. Previous studies suggested that the Arctic Oscillation (AO) affected the circulation pattern in the Arctic Ocean and thus resulted in various pathways of Atlantic water in different years (Karcher et al., 2012; Smith et al., 2021). Longer pathways for Atlantic water passed through the East Siberian Sea and the Mendeleev Ridge associate with a positive mean AO index from January – March, and Atlantic water flows through shorter pathways along the Lomonosov Ridge under the context of a negative mean AO index. The AO index-influenced pathways may have a further impact on CDOM levels.

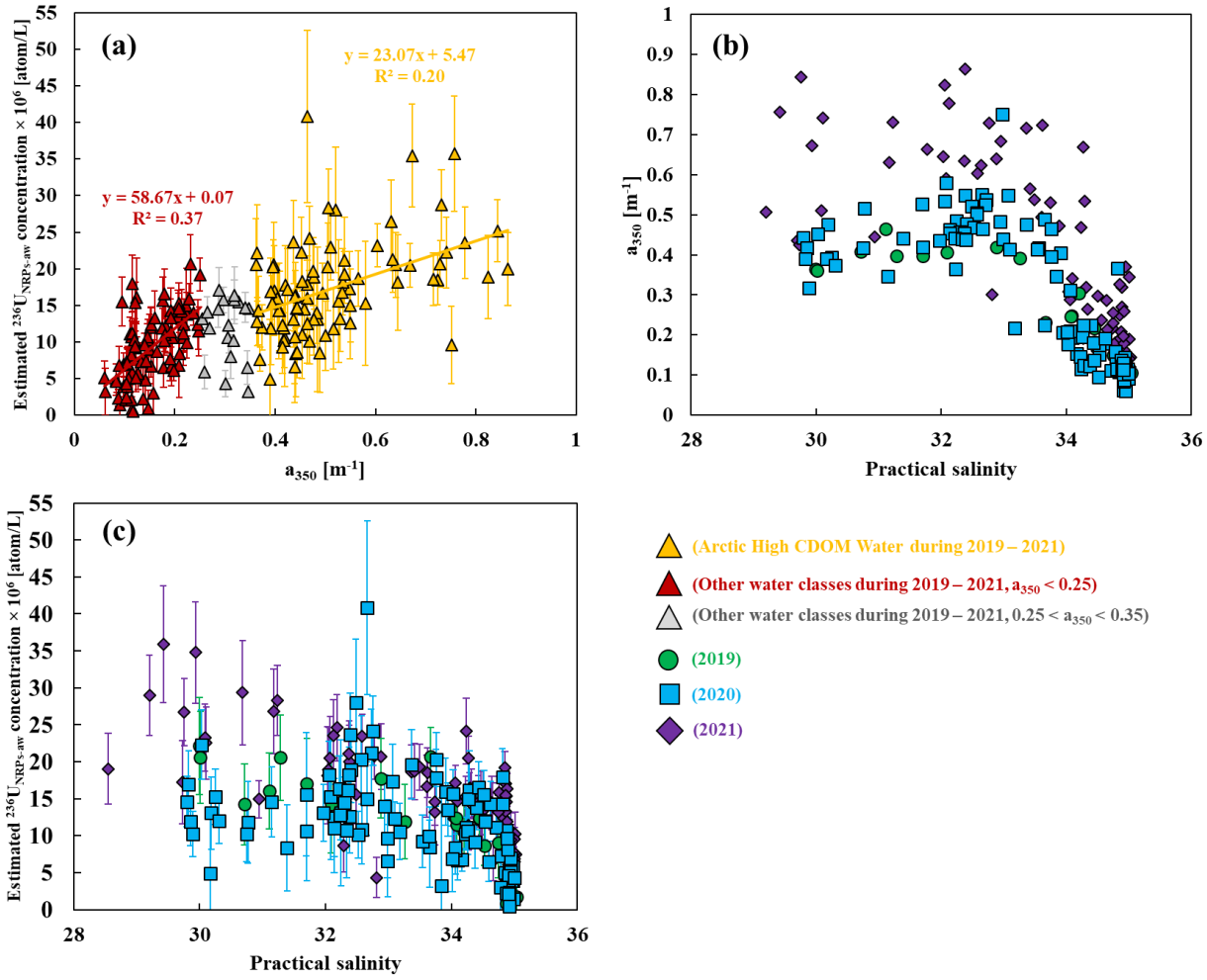

Figure 19. Correlation between estimated $^{236}U_{NRPs\text{-}aw}$ concentrations and a_{350} (A), and their variations with practical salinity (B – C).

3.4.2 Understanding of the outflowing waters transport from the Arctic Ocean

In the sea around the northern Iceland, the circulation pattern is complicated (Casanova-Masjoan et al., 2020). The outflowing EGC at the mid-East Greenland coast bifurcate into two branch waters: 1) a continuously southwestward EGC and 2) a southeastward East Iceland Current (EIC) **(Figure 1)**. And a southwestward North Icelandic Jet outflows from the Nordic Seas through the Denmark Strait, where the northeastward

NIIC inflows along the coast of Iceland. We average $^{236}U_{NRPs}$ concentrations and salinity of these outflowing waters (OW) at each depth to reveal the transport and mixing of these waters. For the OW at 5 – 100 m depth, our observation of $^{236}U_{NRPs}$ concentration and salinity shows that they derive from a mixture of PSW, the NIIC and the RAW, but the contribution of PSW is relatively lower **(Figure 20A)**. And PSW dominantly originates from the shelf break rather than the shelf (coastline).

The RAW contribution gradually increases with depth from 5 m – 100 m **(Figure 20B)**. Compared with at 5 – 100 m depth, $^{236}U_{NRPs}$ concentration in the OW increases at 200 m depth, suggesting an increasing contribution from the Arctic-derived AAW instead of PSW **(Figure 20B)**. AAW in the Fram Strait has mixed with various AAW in different pathways and RAW, so the upstream AAW in the Arctic Ocean is selected as the endmember of AAW. From the depth of 200 m to 1000 m, $^{236}U_{NRPs}$ concentrations show a decreasing trend with a slightly increase of salinity, implying more contributions from RAW at deeper depth compared with Arctic-derived AAW **(Figure 20B)**. The distribution of AAW in the eastern and western Arctic Ocean and the RAW reveals their potential transport pathways to the sea around the northern Iceland. Both the NIIC ($1.22 \pm 1.46 \times 10^6$ atom/L, 34.97 ± 0.14) and the Deep water (DW) & Bottom water (BW) in the Fram Strait ($1.27 \pm 0.76 \times 10^6$ atom/L, 34.92 ± 0.00) are characterized by low $^{236}U_{NRPs}$ concentration and high salinity. And the NIIC has a higher contribution in shallower layer, but the DW & BW from the Fram Strait have an impact for deeper layer.

For the water column samples in the sill of the Denmark Strait, the NIIC has more contributions in seawater of the upper 200 m **(Figure 20C)**. And the distribution of seawater at 500 m depth in the northern Denmark Strait is between the AAW and RAW, but the bottom water (975 m) at same station suggests a dominant source from the DW & BW in the Fram Strait. Due to a large uncertainty, it is not clear that the source of low $^{236}U_{NRPs}$ concentration in the Denmark Strait is from the contribution of the NIIC or the mixture of RAW and DW & BW. To interpret the source, the potential density (σ_θ) in the seawater of the Denmark Strait and the NIIC is compared **(Figure 20C)**. The potential

density in the NIIC is significantly lower than that in the seawater at 500 – 975 m of the Denmark Strait. Considering the difference of density, the high-density seawater from the Fram Strait likely contributes to the similar density seawater in the Denmark Strait. Therefore, we propose that the mixture of AAW with RAW and DW & BW form the DSOW, which transports to the North Atlantic Ocean as North Atlantic Deep Water (NADW) through the sill of the Denmark Strait (650 m).

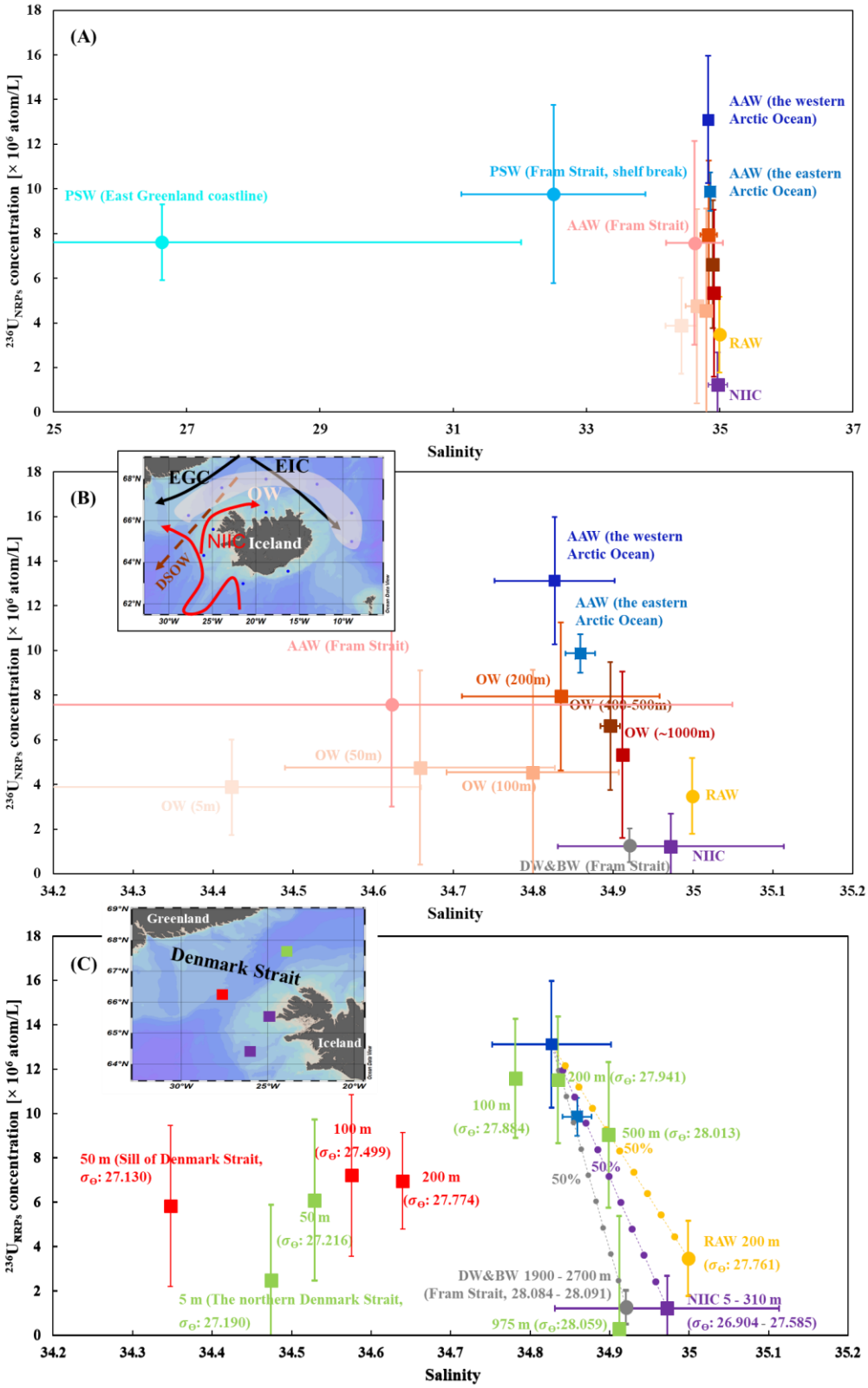

Figure 20. Characteristic of average $^{236}U_{NRPs}$ concentration and salinity in seawater around Iceland with different water source. Seawater mixing pattern between Polar Surface Water, Recirculating

Atlantic Water and North Icelandic Irminger Current (A); Seawater mixing pattern between the western Arctic Atlantic Water (Chamizo et al., 2022), the eastern Arctic Atlantic Water, Recirculating Atlantic Water, North Icelandic Irminger Current and Fram Strait deep and bottom waters (B); Seawater samples in the Denmark Strait for each depth (C); PSW: Polar Surface Water; AAW: Arctic Atlantic Water; NCC: Norwegian Coastal Current; NwAC: Norwegian Atlantic Current; RAW: Recirculating Atlantic Water; EGC: East Greenland Current; NIIC: North Icelandic Irminger Current.

3.5 Perspectives

While this study demonstrates the potential utility of ^{233}U-^{236}U as tracers to investigate the Atlantic water movement in the Arctic and North Atlantic oceans, it is essential to address existing limitations and future perspectives:

- High uncertainty (> 30%) of $^{236}U_{NRPs}$ propagated from ^{233}U influences its use in trace Atlantic water, especially for deeper waters. Larger water volume (10 – 20L) can improve the high uncertainty for ^{233}U measurement. The measurement technology of ^{233}U is also continuously developing, and advanced AMS measurement for ^{233}U is expected to improve analytical precision in the future.
- The first approach can not avoid and reduce the uncertainty from the water fractionation due to the denitrification on the shelf. To obtain a more conservative result, new approaches of water fractionation could be applied in the Arctic Ocean through dissolved Nd and its isotopes or dissolved gallium (Ga) (Laukert et al., 2017; Whitmore et al., 2020). As a conservative-type tracer, water fractionation based on dissolved Ga avoids the interference of denitrification. New combination with isotopes of Nd or Ga is useful to reduce the uncertainty for estimating Atlantic water transit time in the first method. In addition, the mixing patterns of different $^{236}U_{NRPs}$ input functions in the Barents Sea are important to estimate Atlantic water transit time, but their proportions are still unclear. Using modelling result or the record from coral to reconstruct the historic $^{236}U_{NRPs}$ concentrations in the Barents Sea is expected to solve the problem.
- For the second approach, more conservative isotopes can be used to combine, such as ^{129}I. However, ^{129}I dominantly derives from NRPs at LH, which differs from ^{236}U and ^{99}Tc. The incompletely mixture of LH and SF branch waters in the North Sea require a detailed water mixing pattern for them. This needs a precious simulation from ocean model. In addition, our observation of the transient anthropogenic uranium isotopes only reveals water mass movement and mixing within limited timeframe in the Arctic and North Atlantic oceans. However, the

dynamic processes of water mass movement and water mixing highlight the importance of combining the ocean modeling with observations. The Norwegian Earth System Model (NorESM) is coupled global climate three-dimensional model, which is composed of the components of atmosphere, ocean, sea ice, land and others (Seland et al., 2020). It has been used to simulate the transport pathway of ^{90}Sr along water flows (Atlantic water and Ob river water) in the Arctic and North Atlantic oceans (Gao et al., 2009). This model is therefore expected to trace the water mass movement and mixing under defined scenarios of climate change through projecting the dispersion of $^{236}U_{NRPs}$ and other NRPs-derived radioisotopes.

- A part of Atlantic waters recirculates in the Arctic Ocean, but other Atlantic waters directly sink in the Nordic Seas. Transport processes of the sinking Atlantic waters in deep and bottom layers of the Nordic Seas lack of the attention. More collections of water column samples in the basin regions of the Nordic Seas are meaningful to understand the transit process of AMOC. Traditional tracers (such as CFCs and SF_6) focus on the ventilation process of the AMOC in the Nordic Seas, but they are not applicable tracer to reveal the horizontal transport in the deep and bottom layers. The transient anthropogenic uranium isotopes provide an appropriate tool to reflect the inflowing and outflowing Atlantic water in various pathways.
- Compared with traditional water classification by Rudel et al. (2005), the new definition of water classes highlights different Atlantic waters transport pathways and thus constrains the corresponding NRPs signal and their input functions. This is meaningful for other studies using NRPs-derived radioisotopes to trace Atlantic water in the Arctic Ocean. In addition, various anthropogenic pollutants (such as microplastic and persistent organic pollutants) are transported into the Arctic Ocean by Atlantic water from the European coast, entering different water layers through different Atlantic water transport pathways (Ma et al., 2018; Ross et al., 2021; Yakushev et al., 2021; Huserbråten et al., 2022; Zhang et al., 2022). Our

work in this thesis also provides a constraint for the dispersion of these pollutants along different Atlantic water transport pathways, improving our understanding on the pollutant dynamics in the Arctic Ocean.

4. Conclusions

A large-scale investigation of ^{233}U and ^{236}U in seawater of the Arctic and North Atlantic oceans was carried out to trace water mass movement in this thesis. Combining other parameters (temperature, salinity, density, nitrate, phosphate, ^{99}Tc and CDOM), we achieved the following:

- Two new ^{233}U-^{236}U tracer approaches were developed for Atlantic water transit time estimation in the Arctic area. The first approach combines with nitrate and phosphate to estimate Atlantic water transit time. Atlantic water fraction calculated from the nitrate and phosphate is used to calibrate the dilution of $^{236}U_{NRPs}$ concentration, and the estimated $^{236}U_{NRPs\text{-}aw}$ concentration is compared with input functions of $^{236}U_{NRPs}$ concentration for anchoring the source year of Atlantic water. The second approach estimates Atlantic water transit time through combining ^{99}Tc. ^{99}Tc and $^{236}U_{NRPs}$ are dominated by the European NRP at SF, and their atomic ratios are only affected by the historic discharge. Time-series observation of $^{99}Tc/^{236}U_{NRPs}$ atomic ratios in the same area is used to compare with the temporal trend of from the NRPs discharge, thus to constrain the source year of Atlantic water. Our estimated results with both approaches are similar to those in earlier study, suggesting that two independent approaches are reliable for estimating Atlantic water transit time. In addition, compared with the second approach, the measurement of first approach is faster and cost-effective, requiring less water volume, but the estimated results could possibility be biased due to the assumptions in hydrologic conditions. The second approach is expected to provide a more precise estimation in the Arctic Ocean, even in the North and South Atlantic oceans, avoiding the uncertainties from different assumptions of hydrologic conditions.
- A new approach defining water class was used to constrain the transport pathways of different Atlantic branch waters in the Arctic Ocean through the combination of

CDOM, ^{236}U, potential temperature and density, which was useful to select the appropriate NRPs input functions for estimating Atlantic water transit time in the downstream seawater. This improves our understanding on Atlantic water movement and its traceability in the Arctic Ocean.

- A positive correlation between estimated $^{236}U_{NRPs\text{-}aw}$ concentration and a_{350} in the Fram Strait reveals the potential facilitation of longer Atlantic water transit time and transport pathway for obtaining more contributions of CDOM in the Arctic Ocean, especially in Arctic High CDOM Water. As high levels of CDOM from the Siberian rivers carrying a large amount of terrestrial CDOM are entrained on the shelf through the coastal Atlantic branch water. And longer transit time and transport pathway enable the Atlantic water to capture more terrestrial CDOM.
- Compared with ^{236}U carrying a mixed signature from GF and NRPs, isolated $^{236}U_{NRPs}$ based on the use of $^{233}U/^{236}U$ atomic ratio is a superior point-source tracer to explore the transport of Atlantic water in the Arctic-North Atlantic Ocean without the ubiquitous interference of GF. For the outflowing waters from the Arctic Ocean, there are different transport pathways in PSW and the underlying waters. One branch of PSW outflows along the Greenland coast to the North Atlantic Ocean, and another branch moves eastward the north Iceland. Other underlying waters (AAW, RAW and deep and bottom waters) outflow from the GSR and contribute to the formation of DSOW.

5. References

Aarkrog, A., Boelskifte, S., Dahlgaard, H., Duniec, S., Hallstadius, L., Holm, E., Smith, J.N., 1987. Technetium-99 and Cesium-134 as long distance tracers in Arctic waters. *Estuarine, Coastal and Shelf Science*, *24*(5), 637-647.

Aagaard, K., Carmack, E.C., 1989. The role of sea ice and other fresh water in the Arctic circulation. *Journal of Geophysical Research: Oceans*, *94*(C10), 14485-14498.

Aarkrog, A., 2003. Input of anthropogenic radionuclides into the World Ocean. *Deep Sea Research Part II: Topical Studies in Oceanography*, *50*(17-21), 2597-2606.

Aksenov, Y., Karcher, M., Proshutinsky, A., Gerdes, R., De Cuevas, B., Golubeva, E., Kauker, F., Nguyen, A.T., Platov, G.A., Wadley, M., Watanabe, E., 2016. Arctic pathways of Pacific Water: Arctic Ocean Model Intercomparison experiments. *Journal of Geophysical Research: Oceans*, *121*(1), 27-59.

Alkire, M.B., Morison, J., Andersen, R., 2015. Variability in the meteoric water, sea-ice melt, and Pacific water contributions to the central Arctic Ocean, 2000–2014. *Journal of Geophysical Research: Oceans*, *120*(3), 1573-1598.

Aoyama, M., Hirose, K., Igarashi, Y., 2006. Re-construction and updating our understanding on the global weapons tests ^{137}Cs fallout. *Journal of Environmental Monitoring*, *8*(4), 431-438.

Arsouze, T., Dutay, J.C., Lacan, F., Jeandel, C., 2009. Reconstructing the Nd oceanic cycle using a coupled dynamical–biogeochemical model. *Biogeosciences*, *6*(12), 2829-2846.

Bauch, D., van der Loeff, M.R., Andersen, N., Torres-Valdes, S., Bakker, K., Abrahamsen, E.P., 2011. Origin of freshwater and polynya water in the Arctic Ocean halocline in summer 2007. *Progress in Oceanography*, *91*(4), 482-495.

BIPM, IEC, IFCC, ISO, IUPAC, IUPAP, OIML, 2008. Evaluation of measurement data—Guide to the expression of uncertainty in measurement. Jt. Comm. Guid. Metrol. 100, 1–116.

Bower, A., Lozier, S., Biastoch, A., Drouin, K., Foukal, N., Furey, H., Lankhorst, M., Rühs, S., Zou, S., 2019. Lagrangian views of the pathways of the Atlantic Meridional Overturning Circulation. *Journal of Geophysical Research: Oceans*, *124*(8), 5313-5335.

Broecker, W.S., Peng, T.H., 1982. *Tracers in the Sea* (Vol. 690). Palisades, New York: Lamont-Doherty Geological Observatory, Columbia University.

Casacuberta, N., Christl, M., Lachner, J., Van Der Loeff, M.R., Masque, P., Synal, H.A., 2014. A first transect of ^{236}U in the North Atlantic Ocean. *Geochimica et Cosmochimica Acta*, *133*, 34-46.

Casacuberta, N., Christl, M., Vockenhuber, C., Wefing, A.M., Wacker, L., Masqué, P., Synal, H.A., Rutgers van der Loeff, M., 2018. Tracing the three Atlantic branches entering the Arctic Ocean with ^{129}I and ^{236}U. *Journal of Geophysical Research: Oceans*, *123*(9), 6909-6921.

Casacuberta, N., Smith, J.N., 2023. Nuclear Reprocessing Tracers Illuminate Flow Features and Connectivity Between the Arctic and Subpolar North Atlantic Oceans. *Annual Review of Marine Science*, *15*, 203-221.

Casanova-Masjoan, M., Pérez-Hernández, M.D., Pickart, R.S., Valdimarsson, H., Ólafsdóttir, S.R., Macrander, A., Grisolía-Santos, D., Torres, D.J., Jónsson, S., Våge, K., Lin, P., 2020. Along-stream, seasonal, and interannual variability of the North Icelandic Irminger Current and East Icelandic Current around Iceland. *Journal of Geophysical Research: Oceans*, *125*(9), e2020JC016283.

Castrillejo, M., Witbaard, R., Casacuberta, N., Richardson, C.A., Dekker, R., Synal, H.A., Christl, M., 2020. Unravelling 5 decades of anthropogenic ^{236}U discharge from nuclear reprocessing plants. *Science of the Total Environment*, *717*, 137094.

Chamizo, E., Christl, M., López-Lora, M., Casacuberta, N., Wefing, A.M., Kenna, T.C., 2022. The potential of ^{233}U/^{236}U as a water mass tracer in the Arctic Ocean. *Journal of Geophysical Research: Oceans*, *127*(3), e2021JC017790.

Change, I.C., 2014. Mitigation of climate change. *Contribution of working group III to the fifth assessment report of the intergovernmental panel on climate change*, *1454*, 147.

Charette, M.A., Kipp, L.E., Jensen, L.T., Dabrowski, J.S., Whitmore, L.M., Fitzsimmons, J.N., Williford, T., Ulfsbo, A., Jones, E., Bundy, R.M., Vivancos, S.M., 2020. The transpolar drift as a source of riverine and shelf-derived trace elements to the central Arctic Ocean. *Journal of Geophysical Research: Oceans*, *125*(5), e2019JC015920.

Chen, Q., Dahlgaard, H., Nielsen, S.P., 1994. Determination of ^{99}Tc in sea water at ultra low levels. *Analytica chimica acta*, *285*(1-2), 177-180.

Christl, M., Casacuberta, N., Vockenhuber, C., Elsässer, C., Bailly du Bois, P., Herrmann, J., Synal, H.A., 2015. Reconstruction of the ^{236}U input function for the N ortheast A tlantic O cean: Implications for ^{129}I/^{236}U and ^{236}U/^{238}U-based tracer ages. *Journal of Geophysical Research: Oceans*, *120*(11), 7282-7299.

Christl, M., Casacuberta, N., Lachner, J., Herrmann, J., Synal, H.A., 2017. Anthropogenic ^{236}U in the North Sea–a closer look into a source region. *Environmental Science & Technology*, *51*(21), 12146-12153.

Coachman, L.K., Aagaard, K., 1974. Physical oceanography of Arctic and subarctic seas. In *Marine geology and oceanography of the Arctic seas* (pp. 1-72). Berlin, Heidelberg: Springer Berlin Heidelberg.

Collin, A. E. 1963. The waters of the Canadian Arctic Archipelago. Proceedings of the Arctic Basin Symposium, October, 1962. Washington, D.C.: Arctic Institute of North America. 128-136.

Dahlgaard, H., 1995. Transfer of European coastal pollution to the Arctic: radioactive tracers. *Marine Pollution Bulletin*, *31*(1-3), 3-7.

Dahlqvist, R., Andersson, P., Porcelli, D., 2007. Nd isotopes in Bering Strait and Chukchi Sea water. Geochim. Cosmochim. Acta, 71, A196.

Delworth, T.L., Zeng, F., Vecchi, G.A., Yang, X., Zhang, L., Zhang, R., 2016. The North Atlantic Oscillation as a driver of rapid climate change in the Northern Hemisphere. *Nature Geoscience*, *9*(7), 509-512.

Dodd, P.A., Rabe, B., Hansen, E., Falck, E., Mackensen, A., Rohling, E., Gransk, C., Kristiansen, S., 2012. The freshwater composition of the Fram Strait outflow derived from a decade of tracer measurements. *Journal of Geophysical Research: Oceans*, *117*(C11).

Emery, W.J., 2001. Water types and water masses. *Encyclopedia of ocean sciences*, *6*, 3179-3187.

England, M.R., Eisenman, I., Lutsko, N.J., Wagner, T.J., 2021. The recent emergence of Arctic Amplification. *Geophysical Research Letters*, *48*(15), e2021GL094086.

Fine, R.A., 2011. Observations of CFCs and SF_6 as ocean tracers. *Annual review of marine science*, *3*, 173-195.

Frank, M., 2002. Radiogenic isotopes: Tracers of past ocean circulation and erosional input. *Reviews of geophysics*, *40*(1), 1-1.

Fuentes-Franco, R., Koenigk, T., 2019. Sensitivity of the Arctic freshwater content and transport to model resolution. *Climate Dynamics*, *53*, 1765-1781.

Gao, Y., Drange, H., Johannessen, O.M., Pettersson, L.H., 2009. Sources and pathways of ^{90}Sr in the North Atlantic–Arctic region: Present day and global warming. *Journal of environmental radioactivity*, *100*(5), 375-395.

Goldstein, S.L., Hemming, S.R., 2003. Long-lived isotopic tracers in oceanography, paleoceanography, and ice-sheet dynamics. *Treatise on geochemistry*, *6*, 625.

Gonçalves-Araujo, R., Granskog, M.A., Bracher, A., Azetsu-Scott, K., Dodd, P.A., Stedmon, C.A., 2016. Using fluorescent dissolved organic matter to trace and distinguish the origin of Arctic surface waters. *Scientific Reports*, *6*(1), 33978.

Granskog, M.A., Stedmon, C.A., Dodd, P.A., Amon, R.M., Pavlov, A.K., de Steur, L., Hansen, E., 2012. Characteristics of colored dissolved organic matter (CDOM) in the Arctic outflow in the Fram Strait: Assessing the changes and fate of terrigenous CDOM in the Arctic Ocean. *Journal of Geophysical Research: Oceans*, *117*(C12).

Hain, K., Steier, P., Froehlich, M.B., Golser, R., Hou, X., Lachner, J., Nomura, T., Qiao, J., Quinto, F., Sakaguchi, A., 2020. $^{233}U/^{236}U$ signature allows to distinguish environmental emissions of civil nuclear industry from weapons fallout. *Nature communications*, *11*(1), 1275.

Hain, K., Martschini, M., Gülce, F., Honda, M., Lachner, J., Kern, M., Pitters, J., Quinto, F., Sakaguchi, A., Steier, P., Wiederin, A., 2022. Developing accelerator mass spectrometry capabilities for anthropogenic radionuclide analysis to extend the set of oceanographic tracers. *Frontiers in Marine Science*, *9*, 837515.

Haine, T.W., Hall, T.M., 2002. A generalized transport theory: Water-mass composition and age. *Journal of physical oceanography*, *32*(6), 1932-1946.

Hansen, H. P., Koroleff, F., 1999. Determination of nutrients, in Methods of Seawater Analysis, 3rd ed., edited by K. Grasshoff, K. Kremling, and M. Ehrhardt, pp. 159–228, Wiley-VCH, Weinheim, Germany.

HELCOM MORS Discharge database [WWW Document]. n.d. https://helcom.fi/baltic-sea-trends/data-maps/databases/ (accessed 5.20.2020).

Holzer, M., DeVries, T., Smethie Jr, W., 2019. The ocean's global ^{39}Ar distribution estimated with an ocean circulation inverse model. *Geophysical Research Letters*, *46*(13), 7491-7499.

Hou, X.L., Dahlgaard, H., Nielsen, S.P., 2000. Iodine-129 time series in Danish, Norwegian and northwest Greenland coast and the Baltic Sea by seaweed. *Estuarine, Coastal and Shelf Science*, *51*(5), 571-584.

https://odv.awi.de/data/ocean/world-ocean-atlas-2018.

Huserbråten, M.B., Hattermann, T., Broms, C., Albretsen, J., 2022. Trans-polar drift-pathways of riverine European microplastic. *Scientific reports*, *12*(1), 1-10.

International Atomic Energy Agency (IAEA), 2004. Sediment distribution coefficients and concentration factors for biota in the marine environment. Technical Reports Series No. 422 9–25.

Jacobsen, S.B., Wasserburg, G.J., 1980. Sm-Nd isotopic evolution of chondrites. *Earth and Planetary Science Letters*, *50*(1), 139-155.

Jakobsson, M., 2002. Hypsometry and volume of the Arctic Ocean and its constituent seas. *Geochemistry, Geophysics, Geosystems* 3 (5), 1-18.

Jakobsson, M., Grantz, A., Kristoffersen, Y., Macnab, M., 2003. Bathymetry and physiography of the Arctic Ocean and its constituent seas. Springer.

Jeansson, E., Tanhua, T., Olsen, A., Smethie Jr, W.M., Rajasakaren, B., Ólafsdóttir, S.R., Ólafsson, J., 2023. Decadal Changes in Ventilation and Anthropogenic Carbon in the Nordic Seas. *Journal of Geophysical Research: Oceans*, *128*(3), e2022JC019318.

Jenkins, W.J., Clarke, W.B., 1976, June. The distribution of ^{3}He in the western Atlantic Ocean. In *Deep Sea Research and Oceanographic Abstracts* (Vol. 23, No. 6, pp. 481-494). Elsevier.

Jones, E.P., Anderson, L.G., Swift, J.H., 1998. Distribution of Atlantic and Pacific waters in the upper Arctic Ocean: Implications for circulation. *Geophysical Research Letters*, *25*(6), 765-768.

Jones, E.P., Swift, J.H., Anderson, L.G., Lipizer, M., Civitarese, G., Falkner, K.K., Kattner, G., McLaughlin, F., 2003. Tracing Pacific water in the North Atlantic Ocean. *Journal of Geophysical Research: Oceans*, *108(C4)*.

Jones, E.P., Anderson, L.G., Jutterström, S., Mintrop, L., Swift, J.H., 2008. Pacific freshwater, river water and sea ice meltwater across Arctic Ocean basins: Results from the 2005 Beringia Expedition. *Journal of Geophysical Research: Oceans*, *113*(C8).

Karcher, M., Smith, J.N., Kauker, F., Gerdes, R., Smethie Jr, W.M., 2012. Recent changes in Arctic Ocean circulation revealed by iodine-129 observations and modeling. *Journal of Geophysical Research: Oceans*, *117*(C8).

Kershaw, P., Baxter, A., 1995. The transfer of reprocessing wastes from north-west Europe to the Arctic. *Deep Sea Research Part II: Topical Studies in Oceanography*, *42*(6), 1413-1448.

Koeve, W., Wagner, H., Kähler, P., Oschlies, A., 2015. ^{14}C-age tracers in global ocean circulation models. *Geoscientific Model Development*, *8*(7), 2079-2094.

Laukert, G., Frank, M., Bauch, D., Hathorne, E.C., Gutjahr, M., Janout, M., Hölemann, J., 2017a. Transport and transformation of riverine neodymium isotope and rare earth element signatures in high latitude estuaries: a case study from the Laptev Sea. *Earth and Planetary Science Letters*, *477*, 205-217.

Laukert, G., Frank, M., Bauch, D., Hathorne, E.C., Rabe, B., von Appen, W.J., Wegner, C., Zieringer, M., Kassens, H., 2017b. Ocean circulation and freshwater pathways in the Arctic Mediterranean based on a combined Nd isotope, REE and oxygen isotope section across Fram Strait. *Geochimica et Cosmochimica Acta*, *202*, 285-309.

Laukert, G., Makhotin, M., Petrova, M.V., Frank, M., Hathorne, E.C., Bauch, D., Böning, P., Kassens, H., 2019. Water mass transformation in the Barents Sea inferred from radiogenic neodymium isotopes, rare earth elements and stable oxygen isotopes. *Chemical Geology*, *511*, 416-430.

Lin, M., Qiao, J., Hou, X., Dellwig, O., Steier, P., Hain, K., Golser, R., Zhu, L., 2021. 70-year anthropogenic uranium imprints of nuclear activities in Baltic Sea sediments. *Environmental Science & Technology*, *55*(13), 8918-8927.

Lindeman, M.R., Straneo, F., Wilson, N.J., Toole, J.M., Krishfield, R.A., Beaird, N.L., Kanzow, T., Schaffer, J., 2020. Ocean circulation and variability beneath Nioghalvfjerdsbræ (79 North Glacier) ice tongue. *Journal of Geophysical Research: Oceans*, *125*(8), e2020JC016091.

Liu, W., Fedorov, A.V., Xie, S.P., Hu, S., 2020. Climate impacts of a weakened Atlantic Meridional Overturning Circulation in a warming climate. *Science advances*, *6*(26), eaaz4876.

Liu, W., Fedorov, A., 2022. Interaction between Arctic sea ice and the Atlantic meridional overturning circulation in a warming climate. *Climate Dynamics*, 1-17.

Loeng, H., 1991. Features of the physical oceanographic conditions of the Barents Sea, Polar Research, 10:1, 5-18.

Ma, Y., Adelman, D.A., Bauerfeind, E., Cabrerizo, A., McDonough, C.A., Muir, D., Soltwedel, T., Sun, C., Wagner, C.C., Sunderland, E.M., Lohmann, R., 2018. Concentrations and water mass transport of legacy POPs in the Arctic Ocean. *Geophysical Research Letters*, *45*(23), 12-972.

Massonnet, F., Vancoppenolle, M., Goosse, H., Docquier, D., Fichefet, T., Blanchard-Wrigglesworth, E., 2018. Arctic sea-ice change tied to its mean state through thermodynamic processes. *Nature Climate Change*, *8*(7), 599-603.

Matsuoka, A., Boss, E., Babin, M., Karp-Boss, L., Hafez, M., Chekalyuk, A., Proctor, C.W., Werdell, P.J., Bricaud, A., 2017. Pan-Arctic optical characteristics of colored dissolved organic matter: Tracing

dissolved organic carbon in changing Arctic waters using satellite ocean color data. *Remote Sensing of Environment, 200*, 89-101.

Michel, R., Daraoui, A., Gorny, M., Jakob, D., Sachse, R., Tosch, L., Nies, H., Goroncy, I., Herrmann, J., Synal, H.A., Stocker, M., 2012. Iodine-129 and iodine-127 in European seawaters and in precipitation from Northern Germany. *Science of the total environment*, *419*, 151-169.

Mouginot, J., Rignot, E., Scheuchl, B., Fenty, I., Khazendar, A., Morlighem, M., Buzzi, A., Paden, J., 2015. Fast retreat of zachariæ isstrøm, northeast Greenland. *Science*, *350*(6266), 1357-1361.

OSPAR, 2019. Liquid Discharges from Nuclear Installations [WWW Document]. https://www.ospar.org.

Persson, P.O., Andersson, P.S., Porcelli, D., Semiletov, I., 2011, April. The influence of Lena River water inflow and shelf sediment-sea water exchange for the Nd isotopic composition in the Laptev Sea and Arctic Ocean. In *Geophysical Research Abstracts* (Vol. 13).

Petrova, M., 2015. *Neodymium isotopes and rare earth element distribution in the Barents Sea, Arctic Ocean* (Doctoral dissertation, Saint Petersburg State University/University of Hamburg).

Polyakov, I.V., Pnyushkov, A.V., Alkire, M.B., Ashik, I.M., Baumann, T.M., Carmack, E.C., Goszczko, I., Guthrie, J., Ivanov, V.V., Kanzow, T., Krishfield, R., 2017. Greater role for Atlantic inflows on sea-ice loss in the Eurasian Basin of the Arctic Ocean. *Science*, *356*(6335), 285-291.

Porcelli, D., Andersson, P.S., Baskaran, M., Frank, M., Björk, G., Semiletov, I., 2009. The distribution of neodymium isotopes in Arctic Ocean basins. *Geochimica et Cosmochimica Acta*, *73*(9), 2645-2659.

Qiao, J., Hain, K., Steier, P., 2020. First dataset of ^{236}U and ^{233}U around the Greenland coast: A 5-year snapshot (2012–2016). *Chemosphere*, *257*, 127185.

Qiao, J., Zhang, H., Steier, P., Hain, K., Hou, X., Vartti, V.P., Henderson, G.M., Eriksson, M., Aldahan, A., Possnert, G., Golser, R., 2021. An unknown source of reactor radionuclides in the Baltic Sea revealed by multi-isotope fingerprints. *Nature Communications*, *12*(1), 823.

Rachold, V., Eicken, H., Gordeev, V.V., Grigoriev, M.N., Hubberten, H.W., Lisitzin, A.P., Shevchenko, V.P., Schirrmeister, L., 2004. Modern terrigenous organic carbon input to the Arctic Ocean. In *The organic carbon cycle in the Arctic Ocean* (pp. 33-55). Berlin, Heidelberg: Springer Berlin Heidelberg.

Raisbeck, G.M., Yiou, F., 1999. ^{129}I in the oceans: origins and applications. *Science of the Total Environment, 237*, pp.31-41.

Rantanen, M., Karpechko, A.Y., Lipponen, A., Nordling, K., Hyvärinen, O., Ruosteenoja, K., Vihma, T., Laaksonen, A., 2022. The Arctic has warmed nearly four times faster than the globe since 1979. *Communications Earth & Environment*, *3*(1), 168.

Rempfer, J., Stocker, T.F., Joos, F., Dutay, J.C., Siddall, M., 2011. Modelling Nd-isotopes with a coarse resolution ocean circulation model: Sensitivities to model parameters and source/sink distributions. *Geochimica et Cosmochimica Acta*, *75*(20), 5927-5950.

Rignot, E., Kanagaratnam, P., 2006. Changes in the velocity structure of the Greenland Ice Sheet. *Science*, *311*(5763), 986-990.

Ross, P.S., Chastain, S., Vassilenko, E., Etemadifar, A., Zimmermann, S., Quesnel, S.A., Eert, J., Solomon, E., Patankar, S., Posacka, A.M., Williams, B., 2021. Pervasive distribution of polyester fibres in the Arctic Ocean is driven by Atlantic inputs. *Nature communications*, *12*(1), 1-9.

Rudels, B., Björk, G., Nilsson, J., Winsor, P., Lake, I., Nohr, C., 2005. The interaction between waters from the Arctic Ocean and the Nordic Seas north of Fram Strait and along the East Greenland Current: results from the Arctic Ocean-02 Oden expedition. Journal of Marine Systems, 55(1-2), 1-30.

Rudels, B., 2021. *The Physical Oceanography of the Arctic Mediterranean Sea: Explorations, Observations, Interpretations*. Elsevier.

Sakaguchi, A., Kawai, K., Steier, P., Quinto, F., Mino, K., Tomita, J., Hoshi, M., Whitehead, N., Yamamoto, M., 2009. First results on ^{236}U levels in global fallout. *Science of the Total Environment*, *407*(14), 4238-4242.

Sakaguchi, A., Kadokura, A., Steier, P., Takahashi, Y., Shizuma, K., Hoshi, M., Nakakuki, T., Yamamoto, M., 2012. Uranium-236 as a new oceanic tracer: a first depth profile in the Japan Sea and comparison with caesium-137. *Earth and Planetary Science Letters*, *333*, 165-170.

Schlitzer, R., 2016. Ocean data view. Retrieved from http://odv.awi.de.

Schnetger, B., Lehners, C., 2014. Determination of nitrate plus nitrite in small volume marine water samples using vanadium (III) chloride as a reduction agent. *Marine Chemistry*, *160*, 91-98.

Seland, Ø., Bentsen, M., Olivié, D., Toniazzo, T., Gjermundsen, A., Graff, L.S., Debernard, J.B., Gupta, A.K., He, Y.C., Kirkevåg, A., Schwinger, J., 2020. Overview of the Norwegian Earth System Model (NorESM2) and key climate response of CMIP6 DECK, historical, and scenario simulations. *Geoscientific Model Development*, *13*(12), 6165-6200.

Serreze, M.C., Barrett, A.P., Slater, A.G., Woodgate, R.A., Aagaard, K., Lammers, R.B., Steele, M., Moritz, R., Meredith, M., Lee, C.M., 2006. The large-scale freshwater cycle of the Arctic. *Journal of Geophysical Research: Oceans*, *111*(C11).

Shi, K., Hou, X., Roos, P., Wu, W., 2012. Determination of technetium-99 in environmental samples: a review. *Analytica Chimica Acta*, *709*, 1-20.

Smedsrud, L.H., Muilwijk, M., Brakstad, A., Madonna, E., Lauvset, S.K., Spensberger, C., Born, A., Eldevik, T., Drange, H., Jeansson, E., Li, C., 2022. Nordic Seas heat loss, Atlantic inflow, and Arctic sea ice cover over the last century. *Reviews of Geophysics*, *60*(1), e2020RG000725.

Smith, J.N., McLaughlin, F.A., Smethie Jr, W.M., Moran, S.B., Lepore, K., 2011. Iodine-129, ^{137}Cs, and CFC-11 tracer transit time distributions in the Arctic Ocean. *Journal of Geophysical Research: Oceans*, *116*(C4).

Smith, J.N., Karcher, M., Casacuberta, N., Williams, W.J., Kenna, T., Smethie Jr, W.M., 2021. A changing Arctic Ocean: how measured and modeled ^{129}I distributions indicate fundamental shifts in circulation between 1994 and 2015. *Journal of Geophysical Research: Oceans*, *126*(3), e2020JC016740.

Snyder, G., Aldahan, A., Possnert, G., 2010. Global distribution and long-term fate of anthropogenic ^{129}I in marine and surface water reservoirs. *Geochemistry, Geophysics, Geosystems*, *11*(4).

Stedmon, C.A., Amon, R.M.W., Rinehart, A.J., Walker, S.A., 2011. The supply and characteristics of colored dissolved organic matter (CDOM) in the Arctic Ocean: Pan Arctic trends and differences. *Marine Chemistry*, *124*(1-4), 108-118.

Stedmon, C.A., Granskog, M.A., Dodd, P.A., 2015. An approach to estimate the freshwater contribution from glacial melt and precipitation in E ast G reenland shelf waters using colored dissolved organic matter (CDOM). *Journal of Geophysical Research: Oceans*, *120*(2), 1107-1117.

Stedmon, C.A., Amon, R.M., Bauch, D., Bracher, A., Gonçalves-Araujo, R., Hoppmann, M., Krishfield, R., Laney, S., Rabe, B., Reader, H., Granskog, M.A., 2021. Insights into water mass origins in the central Arctic Ocean from in-situ dissolved organic matter fluorescence. *Journal of Geophysical Research: Oceans*, *126*(7), e2021JC017407.

Sévellec, F., Fedorov, A.V., Liu, W., 2017. Arctic sea-ice decline weakens the Atlantic meridional overturning circulation. *Nature Climate Change*, *7*(8), 604-610.

Tachikawa, K., Athias, V., Jeandel, C., 2003. Neodymium budget in the modern ocean and paleo-oceanographic implications. *Journal of Geophysical Research: Oceans*, *108*(C8).

Tanhua, T., Jones, E.P., Jeansson, E., Jutterström, S., Smethie Jr, W.M., Wallace, D.W., Anderson, L.G., 2009. Ventilation of the Arctic Ocean: Mean ages and inventories of anthropogenic CO_2 and CFC-11. *Journal of Geophysical Research: Oceans*, *114*(C1).

UNSCEAR, 2000. Sources and Effects of Ionizing Radiation.

Voelker, A.H., Colman, A., Olack, G., Waniek, J.J., Hodell, D., 2015. Oxygen and hydrogen isotope signatures of Northeast Atlantic water masses. *Deep Sea Research Part II: Topical Studies in Oceanography*, *116*, 89-106.

Waugh, D.W., Hall, T.M., Haine, T.W., 2003. Relationships among tracer ages. *Journal of Geophysical Research: Oceans*, *108*(C5).

Wefing, A.M., Christl, M., Vockenhuber, C., Rutgers van der Loeff, M., Casacuberta, N., 2019. Tracing Atlantic waters using ^{129}I and ^{236}U in the Fram Strait in 2016. *Journal of Geophysical Research: Oceans*, *124*(2), 882-896.

Wefing, A.M., Casacuberta, N., Christl, M., Gruber, N., Smith, J.N., 2021. Circulation timescales of Atlantic Water in the Arctic Ocean determined from anthropogenic radionuclides. *Ocean Science*, *17*(1), 111-129.

Wefing, A.M., Casacuberta, N., Christl, M., Dodd, P.A., 2022. Water mass composition in Fram Strait determined from the combination of ^{129}I and ^{236}U: Changes between 2016, 2018, and 2019. *Frontiers in Marine Science*, *9*, 973507.

Wheeler, P.A., Watkins, J.M., Hansing, R.L., 1997. Nutrients, organic carbon and organic nitrogen in the upper water column of the Arctic Ocean: implications for the sources of dissolved organic carbon. *Deep Sea Research Part II: Topical Studies in Oceanography*, *44*(8), 1571-1592.

Whitmore, L.M., Pasqualini, A., Newton, R., Shiller, A.M., 2020. Gallium: A new tracer of Pacific water in the Arctic Ocean. *Journal of Geophysical Research: Oceans*, *125*(7), e2019JC015842.

Yakushev, E., Gebruk, A., Osadchiev, A., Pakhomova, S., Lusher, A., Berezina, A., van Bavel, B., Vorozheikina, E., Chernykh, D., Kolbasova, G., Razgon, I., 2021. Microplastics distribution in the Eurasian Arctic is affected by Atlantic waters and Siberian rivers. *Communications earth & environment*, *2*(1), 1-10.

Yamamoto-Kawai, M., Carmack, E., McLaughlin, F., 2006. Nitrogen balance and Arctic throughflow. *Nature*, *443*(7107), 43-43.

Yamamoto-Kawai, M., McLaughlin, F.A., Carmack, E.C., Nishino, S., Shimada, K., 2008. Freshwater budget of the Canada Basin, Arctic Ocean, from salinity, δ18O, and nutrients. *Journal of Geophysical Research: Oceans*, *113*(C1).

Zhang, L., Ma, Y., Vojta, S., Morales-McDevitt, M., Hoppmann, M., Soltwedel, T., Kirk, J., De Silva, A., Muir, D., Lohmann, R., 2023. Presence, sources and transport of polycyclic aromatic hydrocarbons in the Arctic Ocean. *Geophysical Research Letters*, *50*(1), e2022GL101496.

Zieringer, M., Frank, M., Stumpf, R., Hathorne, E.C., 2019. The distribution of neodymium isotopes and concentrations in the eastern tropical North Atlantic. *Chemical Geology*, *511*, 265-278.

Zimmermann, B., Porcelli, D., Frank, M., Andersson, P.S., Baskaran, M., Lee, D.C., Halliday, A.N., 2009. Hafnium isotopes in Arctic Ocean water. *Geochimica et Cosmochimica Acta*, *73*(11), 3218-3233.

Östlund, H.G., Hut, G., 1984. Arctic Ocean water mass balance from isotope data. *Journal of Geophysical Research: Oceans*, *89*(C4), 6373-6381.

7. Papers

I: Lin, G., Lin, M., Qiao, J., Sejr, M.K., Steier, P., Meire, L., Stedmon, C.A., 2022. Estimation of Atlantic Water transit times in East Greenland fjords using a ^{233}U-^{236}U tracer approach. *Chemical Geology*, *607*, 121007.

II: Lin, G., Qiao, J., Steier, P., Danielsen, M., Guðnason, K., Joensen, H.P., Stedmon, C.A., 2022. Tracing Atlantic water transit time in the subarctic and Arctic Atlantic using ^{99}Tc-^{233}U-^{236}U. *Science of The Total Environment*, *851*, 158276.

III: Lin, G., Qiao, J., Dodd, P.A., Gonçalves-Araujo, R., Granskog, M.A., Steier, P., Stedmon, C.A., 2023. Tracing Atlantic water transit times in the Arctic Ocean: coupling reprocessing-derived ^{236}U and colored dissolved organic matter to distinguish different pathways. *Earth and Planetary Science Letters*, 118415.

IV: Lin, G., Qiao, J., Steier, P., Danielsen, M., Guðnason, K., Tracing Atlantic water in and out of the Nordic Seas with reprocessing-derived ^{236}U. Manuscript in preparation.

Paper I

Estimation of Atlantic Water transit times in East Greenland fjords using a ^{233}U-^{236}U tracer approach

Gang Lin[a], Mu Lin[a], Jixin Qiao[a,*], Mikael K. Sejr[b,c], Peter Steier[d], Lorenz Meire[e,f], Colin A. Stedmon[g]

[a]Department of Environmental and Resource Engineering, Technical University of Denmark, DK-4000 Roskilde, Denmark

[b]Department of Bioscience, Aarhus University, Vejlsøvej 25, 8600 Silkeborg, Denmark

[c]Arctic Research Centre, Aarhus University, Aarhus, Denmark

[d]VERA Laboratory, Faculty of Physics, Isotope Physics, University of Vienna, Währinger Straße 17, A-1090 Vienna, Austria

[e]Greenland Climate Research Centre, Greenland Institute of Natural Resources, Kivioq 2, P.O. Box 570, 3900 Nuuk, Greenland

[f]Department of Estuarine and Delta Systems, Royal Netherlands Institute of Sea Research, Yerseke, Netherlands

[g]National Institute of Aquatic Resources, Technical University of Denmark, Kemitorvet, 2800 Kgs. Lyngby, Denmark

Chemical Geology 607 (2022) 121007

Contents lists available at ScienceDirect

Chemical Geology

journal homepage: www.elsevier.com/locate/chemgeo

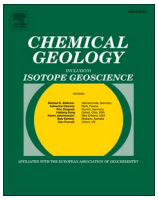

Estimation of Atlantic Water transit times in East Greenland fjords using a ^{233}U-^{236}U tracer approach

Gang Lin [a], Mu Lin [a], Jixin Qiao [a,*], Mikael K. Sejr [b,c], Peter Steier [d], Lorenz Meire [e,f], Colin A. Stedmon [g]

[a] Department of Environmental and Resource Engineering, Technical University of Denmark, DK-4000 Roskilde, Denmark
[b] Department of Bioscience, Aarhus University, Vejlsøvej 25, 8600 Silkeborg, Denmark
[c] Arctic Research Centre, Aarhus University, Aarhus, Denmark
[d] VERA Laboratory, Faculty of Physics, Isotope Physics, University of Vienna, Währinger Straße 17, A-1090 Vienna, Austria
[e] Greenland Climate Research Centre, Greenland Institute of Natural Resources, Kivioq 2, P.O. Box 570, 3900 Nuuk, Greenland
[f] Department of Estuarine and Delta Systems, Royal Netherlands Institute of Sea Research, Yerseke, Netherlands
[g] National Institute of Aquatic Resources, Technical University of Denmark, Kemitorvet, 2800 Kgs. Lyngby, Denmark

ARTICLE INFO

Editor: Don Porcelli

Keywords:
^{233}U
^{236}U
Nutrients
East Greenland fjords
Atlantic Water transit time
Arctic Ocean

ABSTRACT

Water mass composition and transit times of outflowing waters from the Arctic Ocean can reflect changes of polar climate and ocean circulation upstream. In this study we apply a novel approach using anthropogenic uranium tracers (^{233}U and ^{236}U), combined with salinity, and nutrients (nitrate and phosphate) to estimate transit times of waters from the Atlantic passing through the Arctic and into East Greenland fjords. In Polar Surface Water (PSW, typically found in surface ~150 m of the fjords) the dominant source of ^{236}U is European reprocessing plants (63%) while in Arctic Atlantic Water (AAW, typically directly below PSW in these fjords) it is much less (26%) and the ^{236}U signal is dominated by the global fallout contribution. Here we isolate the ^{236}U signal from reprocessing plants using $^{236}U/^{233}U$ ratios and use the temporal development in ^{236}U discharges to estimate transit times for Atlantic Water entering the Arctic Ocean and exiting as either PSW or AAW on the Greenland Shelf. PSW, which flows into the fjords from the shelf, has a transit time of between 6 and 14 years from the Arctic entrance (Barents Sea Opening, 74°N, 19°E). The transit time of AAW, which is entrained into upwelling subglacial discharge in the inner parts of the fjords, is in the order of 24–25 years since entrance in the Barents Sea. The findings indicate the potential of this novel ^{233}U-^{236}U approach to trace Atlantic Water circulation in the Arctic Ocean. The method offers independent transit time estimates to compare with circulation models and indicates the potential time lag between documented recent change in properties of water leaving the Arctic Ocean and the upstream processes contributing to these changes.

1. Introduction

Changes in the supply and distribution of heat and freshwater in the Arctic Ocean can potentially influence global ocean circulation and climate (Aagaard and Carmack, 1989; Rahmstorf, 2002; Tsubouchi et al., 2021; Wang, 2021). Inflowing waters from the Atlantic and Pacific bring heat to the Arctic Ocean and result in loss of sea ice (Beszczynska-Möller et al., 2011; Polyakov et al., 2017; Skagseth et al., 2020). As Pacific Water is less saline than Atlantic Water, it contributes together with precipitation and river discharge, as a source of freshwater (Serreze et al., 2006). These freshwater contributions serve to maintain a density stratification in the Arctic Ocean, and also supply freshwater to the North Atlantic via the Canadian Archipelago and the East Greenland Shelf. Here the freshwater supply can potentially influence Atlantic meridional overturning circulation (Rahmstorf, 2002; Ionita et al., 2016). Atlantic, Pacific and fresh waters are integrated into Polar Surface Water (PSW) with sub-zero temperature and variable salinity that are transported by the outflowing East Greenland Current. The fjords of Northeast Greenland often have a layer of PSW lying above warmer Arctic Atlantic Water (AAW, more saline and with temperatures above 0 °C) which represents Atlantic Water that has entered the Arctic Ocean and recirculated out. AAW is located at intermediate depths (~300–800 m) in the Arctic Ocean below PSW (Rudels et al., 2004). Warmer AAW (0–2 °C) carries more heat which facilitates the melt of sea ice (Polyakov

* Corresponding author.
E-mail address: jiqi@dtu.dk (J. Qiao).

https://doi.org/10.1016/j.chemgeo.2022.121007
Received 6 March 2022; Received in revised form 6 June 2022; Accepted 26 June 2022
Available online 30 June 2022

et al., 2017). Measurements of surface and subsurface waters of these fjords can reflect the changing properties of PSW and AAW exiting the Arctic Ocean and transported along the East Greenland Shelf (Sejr et al., 2017). These properties are currently changing in response to changes occurring upstream in the Arctic Ocean. The clearest trends are from 2000 onwards. PSW entering the fjords from the shelf and has freshened (Sejr et al., 2017) and the thickness of the PSW layer has thinned (Gjelstrup et al., 2022). There is also a greater presence of AAW, particularly evident as warmer bottom water temperatures on the shelf and in fjords (Schaffer et al., 2017, 2020; Gjelstrup et al., 2022). The transport of Atlantic Water in PSW and AAW plays a significant role in the Arctic climate and environment, so a good tracer approach is necessary for investigating and estimating its circulation pattern and transit time to explain the hydrographic and biogeochemical processes.

Significant amounts of radioisotopes have been discharged to the North Atlantic Ocean from the two European reprocessing plants (RP) at Sellafield (SF, United Kingdom) and La Hague (LH, France). This imparts a signature on Atlantic Water as it moves northwards toward the Arctic (Fig. 1). Discharges of several radioisotopes from the two plants have varied over the last 50 years, and this presents an opportunity to use these radioisotopes as transient tracers to resolve circulation patterns and timescales (Smith et al., 2011; Christl et al., 2012; Christl et al., 2015; Casacuberta et al., 2018; Wefing et al., 2019; Wefing et al., 2021). In the North Atlantic and Arctic Oceans, ^{129}I-^{236}U tracer pair has been used to trace the path of three branches of Atlantic Water (Casacuberta et al., 2018). Wefing et al. (2019 and 2021) estimated the transit times of

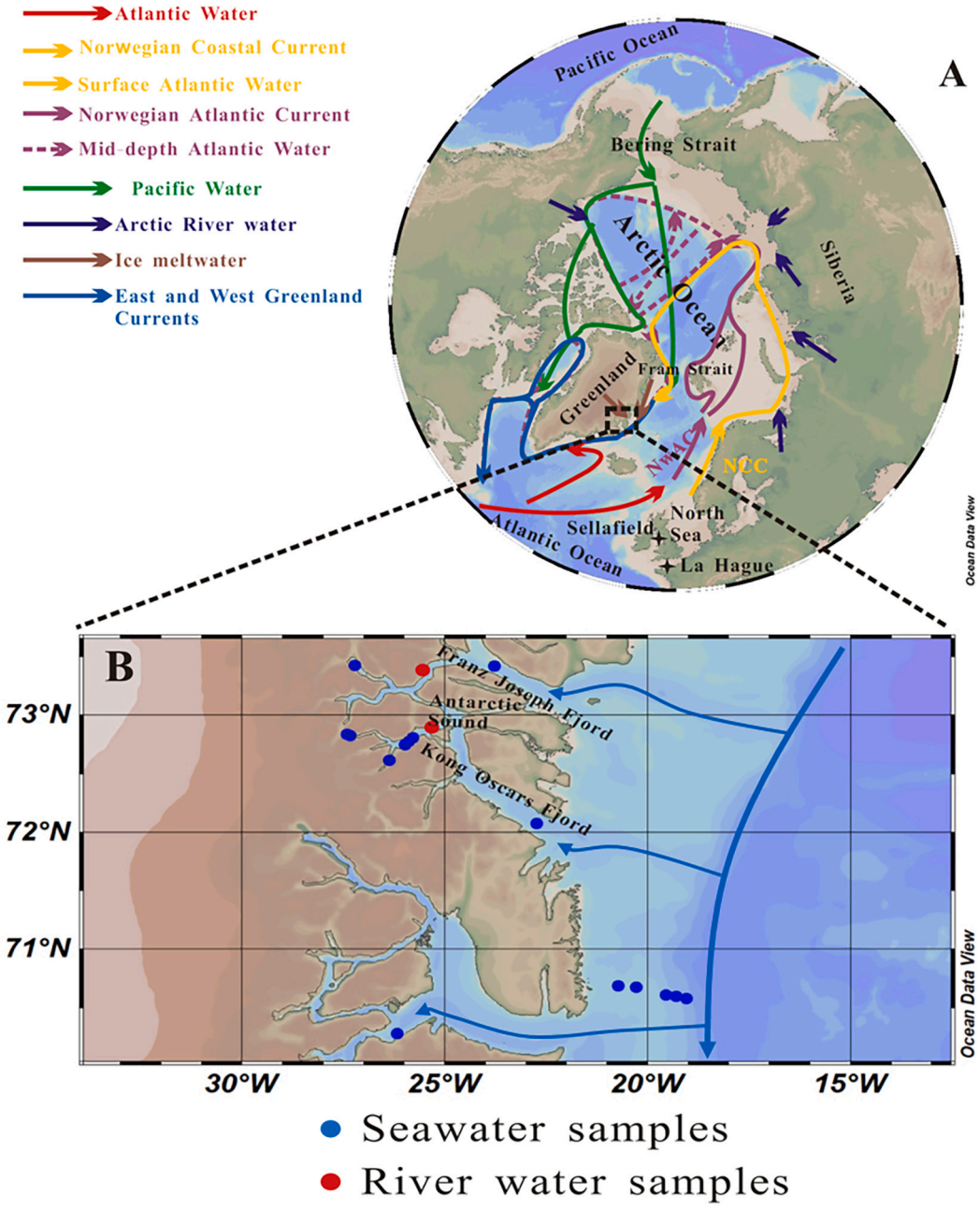

Fig. 1. Simplified depiction of general circulation pattern in the North Atlantic and Arctic Ocean (A), location of sampling sites (B). Currents and water masses in the Arctic Ocean are Norwegian Coastal Current (NCC; orange), Norwegian Atlantic Current (NwAC; purple), Pacific Water (green), Arctic rivers water (dark blue), ice meltwater (brown) and East and West Greenland Current (mixture of Atlantic Water, Pacific Water, Arctic rivers water and ice meltwater, blue). Solid arrows are surface water, and dotted arrows are deeper water. Black crosses mark two main European reprocessing plants at Sellafield and La Hague. (For interpretation of the references to colour in this figure legend, the reader is referred to the web version of this article.)

Atlantic Water in the Arctic Ocean and the Fram Strait using a binary mixing model with $^{129}I/^{236}U$ ratios and ^{236}U concentrations as signatures. The transit times of Atlantic Water in PSW from the entrance of the Arctic Ocean (74°N, 19°E) to the Amundsen Basin and the western Fram Strait were reported to be 9–16 years and 12–17 years respectively (Wefing et al., 2021). The corresponding transit time for Atlantic Water in AAW was estimated to be 16–23 years (Wefing et al., 2019).

While this approach offers estimates of transport times to compare with models of ocean circulation, it assumes that the two elements (I and U) have the same physiochemical behaviors in seawater and that $^{129}I/^{236}U$ ratios are not altered by processes other than mixing along the transport pathways. However, iodine and uranium have different biogeochemical properties in seawater (Tsungogai and Henmi, 1971; Klimkhammer and Palmer, 1991; Rutgers van der Loeff and Geibert, 2008). Iodine is readily enriched in waters containing high content of organic matter (Schwehr et al., 2005), while uranium behaves non-conservatively in anoxic waters (Dunk et al., 2002; Lin et al., 2021a; Andersson et al., 1995). In open areas of the Arctic Ocean, both iodine and uranium may behave conservatively. Whereas in estuarine environments, such as the Siberian coast, contribution of organic matter from Siberian rivers may alter the behavior of iodine and uranium to be non-conservative at different extents, thus changing $^{129}I/^{236}U$ ratios.

In addition, the current oceanic tracer studies using ^{236}U suffer from methodological difficulties to distinguish different ^{236}U sources. Besides the natural inventory of 35 kg ^{236}U in the Earth's crust (Steier et al., 2008), the dominating sources of anthropogenic ^{236}U in the environment are the global fallout (GF) from atmospheric nuclear weapons testing since 1950s (900–1400 kg in total) and the discharges from SF (237 ± 21 kg) and LH (46 kg) which were primarily released into the North Atlantic Ocean (Steier et al., 2008; Sakaguchi et al., 2009; Castrillejo et al., 2020).

RP signal that is discharged into the northeastern North Atlantic Ocean tags Atlantic Water thus makes it easily identifiable. A previous study indicated that radioactive releases from SF were transported by Scottish Coastal Current from the Irish Sea to the northern Scotland coast and the North Sea (Christl et al., 2017). A branch of Scottish Coastal Current carrying SF signal enters the North Sea and mixes with the releases from LH transported by the English Channel Current. SF and LH signals are partly merged in the North Sea, transported northward by the Norwegian Coastal Current (NCC) to the Barents Sea, and subsequently advected to the surface and subsurface layer of the Arctic Ocean to form PSW (Wefing et al., 2021). The branches of Scottish Coastal Current (SF) and English Channel Current (LH) also join the Norwegian Atlantic Current (NwAC), and further enter the intermediate layer of the Arctic Ocean forming AAW (Wefing et al., 2021).

The ubiquitous ^{236}U contributions from GF inevitably introduce uncertainties in transit time estimates for Atlantic Water in the Arctic Ocean, especially in the coastal regions of the Arctic fjords which may receive more GF input from the terrestrial areas via glaciers melt and river runoff. The uranium isotope signature in glacial meltwater likely varies from pre-post nuclear weapons testing to present due to the changing GF contribution. It can therefore be beneficial to isolate the RP-derived ^{236}U rather than assume a constant value for GF-derived ^{236}U. This can be achieved by applying a uranium dual tracer (^{233}U-^{236}U) approach.

In contrast to ^{236}U, almost all ^{233}U is supplied by GF (Hain et al., 2020), which results in large difference in $^{236}U/^{233}U$ atomic ratios between GF (71.4 ± 7.7) and RP (LH, 1–10 × 10^6) (Hain et al., 2020; HELCOM MORS Discharge database [WWW Document], 2020; Qiao et al., 2020). $^{236}U/^{233}U$ ratios can therefore be used to distinguish contributions of ^{236}U from GF and RP, and thereby refine the ^{236}U approach for trace Atlantic Water transit times. Atlantic Water contains both RP and GF derived ^{236}U whereas other waters only contain a GF-derived ^{236}U signal. The time-dependent variation of RP-derived ^{236}U in discharge and subsequently also in recipient Atlantic Water can be used to estimate the contribution and transit time of Atlantic Water in the Arctic and subpolar regions. Compared to other radioisotopes, such as ^{90}Sr (half-life 28.8 a) and ^{137}Cs (half-life 30.2 a) (Dahlgaard, 1995), ^{233}U and ^{236}U have superior properties including very long half-lives (^{233}U: 0.159 Ma; ^{236}U: 23.4 Ma) and high solubility in the open ocean (Sakaguchi et al., 2012; Eigl et al., 2013; Casacuberta et al., 2014; Hain et al., 2020). Importantly, being isotopes of the same element, $^{236}U/^{233}U$ ratios are not affected by geochemical processes along the transport (Hain et al., 2020; Qiao et al., 2020). Different from anthropogenic chemical tracers, such as chlorofluorocarbons (CFCs) and sulfur hexafluoride (SF6) (Fine, 2011) which enter the ocean everywhere by air-sea exchange, anthropogenic radioisotope tracers have the advantage of constrained source functions from RP, thus provide reliability in their tracer applications for water mass transport. In the case of ^{233}U-^{236}U, the dominant point-source release of ^{236}U from SF and LH make them suitable to trace large-scale water mass transport in the North Atlantic-Arctic Ocean.

In our previous work, ^{236}U source terms were estimated for the Greenland coast based on ^{233}U and ^{236}U data in the surface seawater (0–10 m), wherein dominating ^{236}U contribution (~ 70%) were found from RP and ~ 30% from GF (Qiao et al., 2020). In this work, we aim to explore the opportunity of using the ^{233}U-^{236}U tracer approach to estimate the transit times of Atlantic Water in the Arctic Ocean. The measurements arise from opportunistic sampling in a Northeast Greenland fjord complex (Fig. 1). Isotope measurements where combined with salinity, nitrate and phosphate measurements to resolve mixing and transit times. We recognize that the study region might not be ideal to prove a new approach for RP-derived radioisotopes as it is quite far downstream from the source of RP. We believe it is still relevant to demonstrate the potential of the proposed ^{233}U-^{236}U tracer approach in oceanic studies.

2. Materials and methods

2.1. Study area and sampling

The study region is located halfway along the East Greenland coast in the Kong Oscars and Franz Josef fjord system (Fig. 1A and B). Sampling was carried out on board the Royal Danish Naval vessel HMDS Lauge Koch in August 2018. Water profiles of salinity and temperature were collected using a SeaBird SBE25 CTD (conductivity, temperature, depth), and water samples were collected using 10-L Niskin bottles.

A total of 26 seawater samples (5–10 L) were collected in the East Greenland coast for uranium isotopes analyses among which 13 were water column samples and 13 were surface water samples (Table S1). Two additional river water samples were taken from the Antarctic Sound in the Kong Oscar fjord complex. Seawater samples were stored in 10-L precleaned plastic bottles after first rinsing with sample water and sent back to the laboratory for ^{233}U, ^{236}U and ^{238}U processing. In addition, seawater samples for nutrient measurement were collected in acid-washed polyethylene bottles and frozen at −20 °C. Ten seawater samples were analyzed through using an autoanalyzer (Skalar) based on the approach of Hansen and Koroleff (1999). The average precision on nitrate and phosphate measurement is 1%. Due to opportunistic sampling for uranium measurement, only 10 samples for nutrient analyses can be matched.

2.2. Determination of ^{233}U, ^{236}U, and ^{238}U

To determine ^{233}U and ^{236}U, an optimized radiochemical procedure was utilized to extract U isotopes from 5 to 10 L seawater samples (See supporting information) (Qiao et al., 2015; Lin et al., 2021b). The accelerator mass spectrometry (AMS) measurement of $^{236}U/^{238}U$ and $^{233}U/^{238}U$ measurement was carried out at the Vienna Environmental Research Accelerator (VERA) facility in the University of Vienna. The detailed setup and method of AMS measurement has been reported elsewhere (Steier et al., 2010; Steier et al., 2019; Hain et al., 2020). Each

sample was measured by AMS for three cycles with counting times of 300–1000 s for ^{236}U and 2000–4500 s for ^{233}U in each cycle, respectively, to obtained average atomic ratios of $^{236}U/^{238}U$ and $^{233}U/^{238}U$. Typically, relative uncertainties of $^{236}U/^{238}U$ and $^{233}U/^{238}U$ ratios obtained in this work were below 10% and 30%, respectively. In case of higher uncertainties obtained, the measured values were deemed as outliers. To obtain ^{233}U and ^{236}U concentrations in seawater samples, ^{238}U concentration in seawater samples were measured using inductively coupled plasma mass spectrometry (ICP-MS) (ICP-QQQ 8800, Agilent) after dilution with 0.5 M HNO_3 (Qiao and Xu, 2018). Indium or bismuth was utilized as the internal standard.

Satisfactory chemical yields for U (60–80%) monitored via ^{238}U were

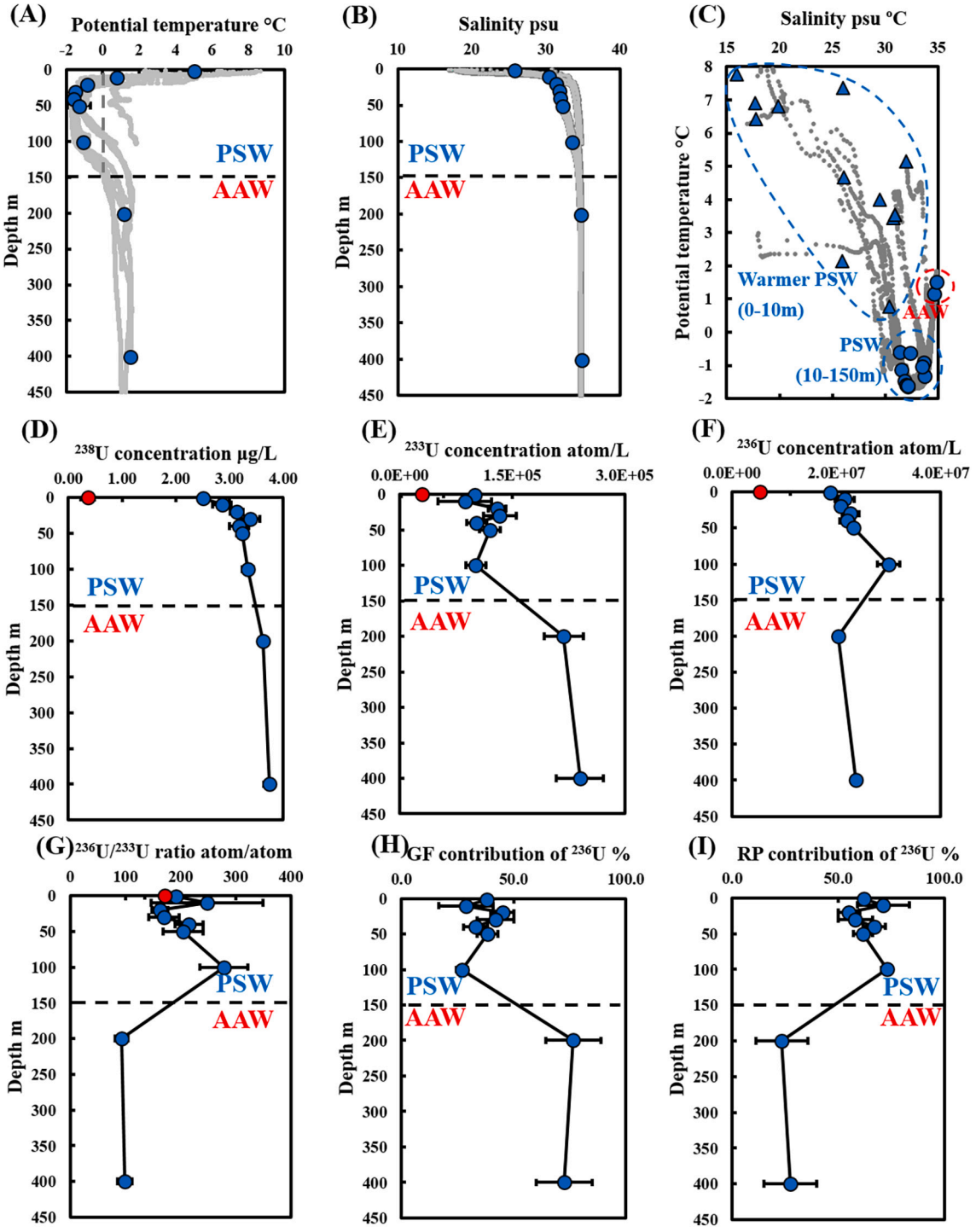

Fig. 2. The depth profiles of different measured and calculated parameters. The profiles are divided into two main layers: Polar Surface Water (PSW, $\theta < 0$ °C) and Arctic Atlantic Water (AAW, $0 < \theta < 2$ °C). The parameters are potential temperature θ (A), salinity (B), the diagram of potential temperature-salinity (C, triangle data at 1–10 m depths, circle dots data at 10–100 m depths), ^{238}U concentration (D), ^{233}U concentration (E), ^{236}U concentration (F), $^{236}U/^{233}U$ atomic ratio (G), global fallout (GF) contribution of ^{236}U (H), reprocessing plants (RP) contribution of ^{236}U (I). All dots present the averaged values with uncertainties for the river (red) and seawater (blue) samples at the same depth. Grey profiles represent the full profiles measured by the in situ sensors. (For interpretation of the references to colour in this figure legend, the reader is referred to the web version of this article.)

achieved for the samples analyzed in this work. The chemical yield of uranium during the chemical separation was estimated as the ratio of ^{238}U mass in the eluate and ^{238}U mass in the original seawater sample. Herein, we assume uranium was quantitatively recovered during the AMS target preparation after the chemical separation, which was verified in our earlier study (Qiao et al., 2015). Blank samples were prepared along with each batch (typically $n = 7$) of samples following the same procedure as for the seawater. To reduce the background levels of ^{233}U and ^{236}U, special measures were implemented, including purification of chemicals, utilization of laminar flow bench, and acid boiling for glassware. Under such well-controlled conditions, the count rates of ^{236}U and ^{233}U in the monitored blank samples were typically <30% of the corresponding samples. The removed contribution from laboratory background and the combined uncertainties of ^{233}U/^{238}U and ^{236}U/^{238}U is calculated based on the law of uncertainty propagation, details are summarized in the supporting information.

3. Results

3.1. Water column properties

Practical salinity (S) and potential temperature (θ) of seawater in the East Greenland fjords ranged from 16.02 to 34.89 psu and from −1.63 °C to 7.78 °C, respectively. As the entire study area once beyond the local impact of marine terminating glaciers showed a common stratified and spatially homogeneous structure (as evident from S and θ profiles shown in Fig. 2). Uranium results in multiple samples collected at the same depth ($n = 13$ at 1 m; $n = 2$ at 20 m; $n = 3$ at 50 and 100 m, respectively) were averaged into one value with a combined uncertainty, except for the single sample at 10, 30, 40, 200 and 400 m, respectively (Fig. 2, Table S1). Down the water column, θ quickly decreased from 7.78 °C to −1.63 °C within 0–50 m depth, and then gradually increased to 1.54 °C at 400 m depth (Fig. 2A). In the depth profile of salinity, there was a steep increase (16.02–30.42) in the upper 10 m depth followed by a gentle increase (30.42–34.89) in the subsurface and deep waters (Fig. 2B). Measurements from stations where no uranium samples were collected are shown in grey and emphasize the lateral homogeneity of the sampled region (Fig. 2A-B).

The East Greenland fjords and their neighboring shelf waters are mainly affected by the East Greenland Current from the Arctic Ocean via the Fram Strait, where the surface (and subsurface) and deeper layer are dominated by PSW and AAW, respectively (Rudels, 2009; Wefing et al., 2019). These waters can be distinguished (Fig. 2C), based on different potential temperature and salinity. Waters sampled here that had a temperature < 0 °C and salinity <34 were defined as PSW. Warmer (0–2 °C) and more saline samples were defined as AAW. At the very surface (upper 10 m) the properties of PSW were influenced by surface warming and entrainment of meltwater (Fig. 2). The radioisotope samples can be segregated into originating from one of the two layers, PSW distributed at 0–150 m and AAW distributed below 150 m depth (Fig. 2).

3.2. Uranium isotopes

^{238}U concentrations in the seawater samples varied between 1.26 and 3.74 μg/L (Fig. 2D, Table S1) and revealed a strong linear correlation with salinity ($R^2 = 0.90$, slope = 0.109, $p < 0.01$). Atomic ratios of ^{236}U/^{238}U (2.22–5.36 × 10^{-9}) and ^{233}U/^{238}U (1.10–2.52 × 10^{-11}) were higher than their expected natural background levels (e.g., 10^{-14}–10^{-13} of ^{236}U/^{238}U in natural seawater and 10^{-13}–10^{-11} of ^{233}U/^{238}U in minerals) (Steier et al., 2008; Hain et al., 2020; Villa-Alfageme et al., 2019), indicating the contribution of anthropogenic U in these waters. ^{233}U concentrations, ranging within 5.90–14.1 × 10^4 atom/L, showed no systematic change with depth in PSW, but were significantly higher (21.6–23.8 × 10^4 atom/L) in AAW (Fig. 2E). ^{236}U concentrations gradually increased from 14.5 ± 0.9 × 10^6 atom/L to 34.9 ± 3.0 × 10^6 atom/L in PSW, but decreased again (20.4–23.6 × 10^6 atom/L) in AAW (Fig. 2F). Relatively higher ^{236}U/^{233}U ratios were observed in PSW (137–344) than those in AAW (94–99), indicating that the upper 100 m of the East Greenland fjords received more RP signals than the deep waters (Fig. 2G). ^{233}U and ^{236}U concentrations in East Greenland river water were (2.53–3.46) × 10^4 atom/L and (3.31–7.33) × 10^6 atom/L, respectively (Fig. 2E and F, Table S1).

3.3. Source terms of ^{236}U

Qiao et al. (2020) developed an approach to distinguish the source terms of ^{236}U in the surface seawater of Greenland coast using atomic ratios of ^{233}U/^{236}U. Here we use the following equations modified from Qiao et al. (2020) to calculate the GF and RP fraction, and GF and RP-derived ^{236}U concentration.

$$P_{GF} = \frac{R_{GF}^{236/233}\left(R_{RP}^{236/233} - R_S^{236/233}\right)}{R_S^{236/233}\left(R_{RP}^{236/233} - R_{GF}^{236/233}\right)} \approx \frac{R_{GF}^{236/233}}{R_S^{236/233}} \quad (1)$$

$$P_{RP} = 1 - P_{GF} \quad (2)$$

$$C_{s,GF}^{236} = C_s^{236} \times P_{GF} = R_{GF}^{236/233} \times C_S^{233} \quad (3)$$

$$C_{s,RP}^{236} = C_s^{236} \times P_{RP} = C_s^{236} - C_{s,GF}^{236} \quad (4)$$

where P_{GF} and P_{RP} are GF and RP fraction in the seawater sample; $R_S^{236/233}$ is the ^{236}U/^{233}U atomic ratio of the seawater sample; $R_{RP}^{236/233}$ is RP endmember with the representative value of 1 × 10^7; $R_{GF}^{236/233}$ is GF endmember with the representative value of 71.4 ± 7.7 (Hain et al., 2020); C_s^{233} is the measured ^{233}U concentration in the seawater sample; and C_s^{236}, C_{GF}^{236}, and C_{RP}^{236} are total, GF-derived and RP-derived ^{236}U concentration in the seawater samples, respectively. We acknowledge that $R_{GF}^{236/233}$ in Atlantic Water might be either different or variable over the last 50 years, thus might introduce additional uncertainties in this endmember algorithm. Nevertheless, as the most intensive deposition of global fallout was in the mid-1960s, it is likely that the distribution of GF ^{236}U and ^{233}U reached nearly steady state in the modern ocean surface (as indicated by other radionuclides from GF as well, such as ^{137}Cs and ^{90}Sr). Therefore, we expect that the uncertainties in the GF endmember in the Atlantic Water should be reasonably low. This is partially supported by the comparable ^{236}U/^{233}U ratios in corals and sediments from the Pacific Ocean since 1970s to the represented GF value (Hain et al., 2020; Qiao et al., 2022). Therefore, in this work, we adopted the uncertainty (11%) as derived from the representative GF ^{236}U/^{233}U ratio (71.4 ± 7.7) without giving additional uncertainty in the calculation.

The combined uncertainties of GF and RP contributions of ^{236}U are estimated through the law of uncertainty propagation (BIPM et al., 2008):

$$\begin{aligned} u(P_{GF}) &= \sqrt{\left(\frac{\partial P_{GF}}{\partial R_{GF}^{236/233}}\right)^2 \times u^2\left(R_{GF}^{236/233}\right) + \left(\frac{\partial P_{GF}}{\partial R_S^{236/233}}\right)^2 \times u^2\left(R_S^{236/233}\right)} \\ &= \sqrt{\left(\frac{1}{R_S^{236/233}}\right)^2 \times u^2\left(R_{GF}^{236/233}\right) + \frac{\left(R_{GF}^{236/233}\right)^2}{\left(R_S^{236/233}\right)^4} \times u^2\left(R_S^{236/233}\right)} \end{aligned} \quad (5)$$

$$u(P_{RP}) = \sqrt{\left(\frac{\partial P_{RP}}{\partial P_{GF}}\right)^2 \times u^2(P_{GF})} = u(P_{GF}) \quad (6)$$

where $u(P_{GF})$ and $u(P_{RP})$ are the combined uncertainties of GF-derived and RP-derived ^{236}U concentrations, respectively; and $u(R_{GF}^{236/233})$ and $u(R_S^{236/233})$ are the uncertainties for the representative ^{236}U/^{233}U ratio of GF (7.7) and the measurement samples.

The relative uncertainties of GF and RP contributions of ^{236}U range from 14 to 42% and 7–51%, respectively. And the average weights for GF contribution of ^{236}U in GF and the seawater sample are 0.33 and 0.67, respectively. In addition, the combined uncertainties of GF-derived and RP-derived ^{236}U concentrations are estimated through the law of uncertainty propagation (BIPM et al., 2008):

$$\mathrm{u}\left(C^{236}_{s,GF}\right) = \sqrt{\left(\frac{\partial C^{236}_{s,GF}}{\partial C^{233}_{s}}\right)^2 \times u^2\left(C^{233}_{s}\right) + \left(\frac{\partial C^{236}_{s,GF}}{\partial R^{236/233}_{GF}}\right)^2 \times u^2\left(R^{236/233}_{GF}\right)} = \sqrt{\left(R^{236/233}_{GF}\right)^2 \times u^2\left(C^{233}_{s}\right) + \left(C^{233}_{S}\right)^2 \times u^2\left(R^{236/233}_{GF}\right)} \quad (7)$$

$$\mathrm{u}\left(C^{236}_{s,RP}\right) = \sqrt{\left(\frac{\partial C^{236}_{s,RP}}{\partial C^{236}_{s}}\right)^2 \times u^2\left(C^{236}_{s}\right) + \left(\frac{\partial C^{236}_{s,RP}}{\partial C^{236}_{s,GF}}\right)^2 \times u^2\left(C^{236}_{s,GF}\right)} = \sqrt{u^2\left(C^{236}_{s}\right) + u^2\left(C^{236}_{s,GF}\right)} \quad (8)$$

where $u(C^{236}_{s,\ GF})$ and $u(C^{236}_{s,\ RP})$ are the combined uncertainties of GF-derived and RP-derived ^{236}U concentrations, respectively; $u(C^{233}_{s})$ and $u(C^{233}_{s})$ are the measurement uncertainties of ^{233}U and ^{236}U concentrations, respectively; and $u(R^{236/233}_{GF})$ is the uncertainty for the representative ^{236}U/^{233}U ratio of GF (7.7).

The relative uncertainties of GF-derived and RP-derived ^{236}U concentrations vary from 15 to 42% and 11–53%, respectively. The average weights for ^{236}U/^{233}U atomic ratio in the seawater sample and GF are 0.68 and 0.32, respectively.

Based on these equations, the proportion of ^{236}U derived from GF and RP in East Greenland fjords can be calculated (Table S1). The GF contributions of ^{236}U in PSW of East Greenland fjords range from 21 ± 6 – 52 ± 8%, with the RP contributions representing the remainder (Fig. 2G and H). Distinct changes in ^{236}U source distribution were observed in AAW: GF contributions of ^{236}U increased by a factor of 2 and became the dominating (72 ± 12 – 76 ± 12%) source, whereas the RP contributions decreased to <30%.

4. Discussion

4.1. ^{233}U and ^{236}U in Polar Surface Water, Arctic Atlantic Water, and freshwater

Notable differences (approximate factor of 2) were observed in the ^{233}U concentration and ^{236}U/^{233}U ratio between PSW and AAW (Fig. 2E and G). In comparison, the variability in ^{236}U concentration down the water columns was much lower. As ^{233}U was mainly deposited in GF in 1950s–1960s (Hain et al., 2020; Lin et al., 2021a), lower ^{233}U concentrations can be expected in the comparatively younger PSW. Salinity measurements indicate that while PSW is less saline (Fig. 2B), even dilution with freshwater devoid of ^{233}U cannot explain the lower concentrations in PSW. The differences in the ratios likely reflect the differences in the source and transport pathways of anthropogenic uranium. Higher ^{236}U/^{233}U ratios in the PSW indicate a greater RP contribution in the upper 100 m due to the dominating supply from the NCC to surface water of the Arctic Ocean. The NCC supplies PSW with a greater RP ^{236}U contribution than that supplied by the NwAC to AAW (Fig. 2I) (Casacuberta et al., 2018; Wefing et al., 2021). In contrast, ^{236}U in AAW is predominantly from GF contribution (ca. 74%) (Fig. 2H) reflecting the older GF-derived signal (primarily deposited in 1960s) (Sakaguchi et al., 2016), which was mostly likely advected into deeper water columns by Atlantic Water tagged with the GF in other locations.

The averaged concentration (with standard deviation) of ^{236}U in the upper 10 m of East Greenland fjords (18.9 ± 3.3 × 10^6 atom/L) is comparable to those reported for the Amundsen Basin (24.7 ± 3.6 × 10^6 atom/L) (Casacuberta et al., 2016), the western Fram Strait (20.8 ± 0.8 × 10^6 atom/L) (Wefing et al., 2019) and East Greenland coastal surface waters (18.8 ± 6.4 × 10^6 atom/L) (Qiao et al., 2020). All these values are higher than the expected if ^{236}U concentrations in the Arctic Ocean solely resulted from GF. This indicates the importance of an additional ^{236}U contribution from RP in Europe. The averaged values of GF-derived ^{236}U (7.0 ± 1.5 × 10^6 atom/L) and RP-derived ^{236}U (11.9 ± 2.6 × 10^6 atom/L) obtained for surface seawater (0–10 m) is comparable to those reported earlier from 2012 to 2016 (GF-derived ^{236}U concentration: 5.5 ± 1.9 × 10^6 atom/L and RP-derived ^{236}U concentration: 13.3 ± 4.5 × 10^6 atom/L) (Qiao et al., 2020).

4.2. Estimation of Atlantic Water transit time

4.2.1. End-member mixing algorithm

Here we attempt to use RP-derived ^{236}U concentration calculated from ^{233}U-^{236}U tracer to estimate the transit time of Atlantic Water in PSW of the East Greenland fjords. As the RP signal is unique and constrained to the Atlantic Water, we can use this to examine its dilution with water from other sources. First, we define the end member to be Atlantic Water transported in the NCC and NwAC as this has been shown to be the dominant transport pathway of RP-^{236}U from the Atlantic into the Arctic (Wefing et al., 2021). Other waters (Pacific Water and freshwater including river runoff, sea ice and glacier melt water) only contain a GF signal, so their RP-^{236}U concentrations are considered to be negligible. The RP contribution of ^{236}U in Atlantic Water ($^{236}U_{RP\text{-}AW}$) is a time-dependent value and can be derived from the ^{236}U discharges from SF and LH (see supporting information; Christl et al., 2015; Casacuberta et al., 2018; Castrillejo et al., 2020), and assumptions on mixing in the North Sea and transport northwards to the Arctic, to derive Arctic input functions for NCC and NwAC (Casacuberta et al., 2018; Wefing et al., 2021). The uncertainty of $^{236}U_{RP\text{-}AW}$ can also be estimated from uncertainties of the shell record of ^{236}U/^{238}U ratios near SF and LH, and marine mixing pattern of SF branch water, LH branch water and GF (Casacuberta et al., 2018; Castrillejo et al., 2020). As shown in Fig. S1, the temporal evolutions of $^{236}U_{RP\text{-}AW}$ in both NCC (carrying tracer signal to PSW) and NwAC (carrying tracer signal to AAW) branch waters demonstrate monotonous decreasing trend over the period of 1976–2016. This means that Atlantic Water fraction contained in each sample with known RP-^{236}U concentration is only dependent on the endmember value of $^{236}U_{RP\text{-}AW}$, i.e., the source year of RP-^{236}U in the Atlantic Water (Fig. 3). Consequently, with known Atlantic Water fraction, the transit time of Atlantic Water from the entrance of Arctic Ocean to the study location can be obtained.

4.2.2. Source year estimation based on N:P-derived Atlantic Water fraction

In this study, we use nitrate and phosphate concentrations (Table S1) to estimate the Atlantic Water fraction according to Eqs. (9)–(13) (Dodd et al., 2012) thus to constrain its source year (black and grey lines in Fig. 3). The uncertainty for Atlantic Water fraction estimation with this method was approximately 10% (Dodd et al., 2012).

$$f_{AW} + f_{PW} + f_{FW} = 1 \quad (9)$$

$$f_{AW}P_{AW} + f_{FW}P_{AW} + f_{PW}P_{PW} = P_S \quad (10)$$

$$f_{AW}S_{AW} + f_{PW}S_{PW} + f_{FW}S_{FW} = S_S \quad (11)$$

where P_{AW} and P_{PW} are phosphate concentrations in Atlantic Water and Pacific Water; f_{AW}, f_{PW} and f_{FW} are Atlantic Water fraction, Pacific Water fraction and freshwater fraction in the sample collected (2018); S_{AW}, S_{PW}, S_{FW} and S_s are salinity in Atlantic Water, Pacific Water, freshwater and seawater samples, respectively. Here we assume P_{FW} is equal to P_{AW}. The calculated fractions of Atlantic Water in each sample are summarized in Table S1. In addition, phosphate concentrations for Atlantic Water and Pacific Water are based on the following equations:

$$P_{AW} = M_{AW}N + C_{AW} \quad (12)$$

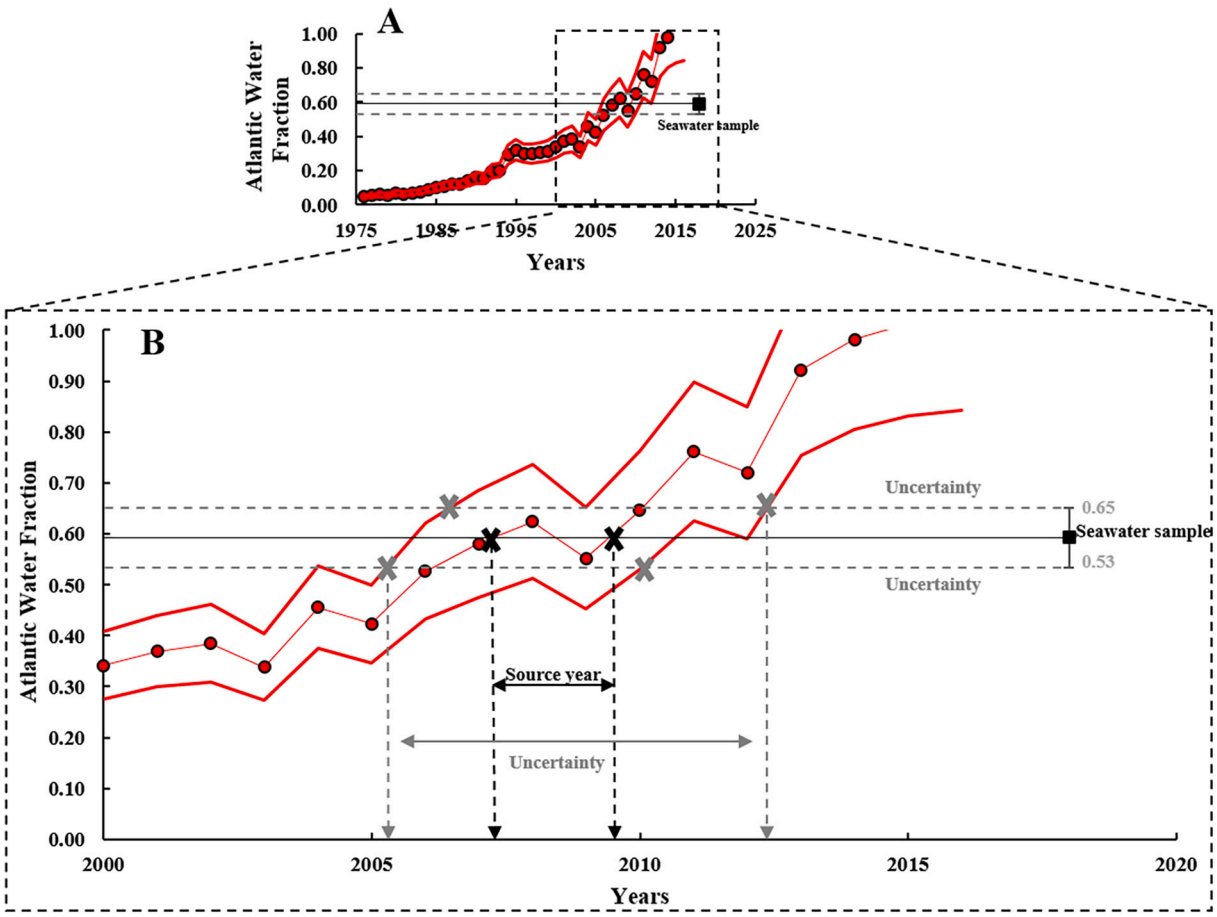

Fig. 3. An example of the fraction estimation of Atlantic Water (red dots and thin red line) with uncertainty (thick red lines) (A) and the detailed change during 2000–2020 (B). The estimation of Atlantic Water fraction for a sample with known RP-^{236}U concentration is only dependent on the end member value of $^{236}U_{RP\text{-}AW}$ which is time-depend following the NCC or NwAC input function (as shown Fig. S1). (For interpretation of the references to colour in this figure legend, the reader is referred to the web version of this article.)

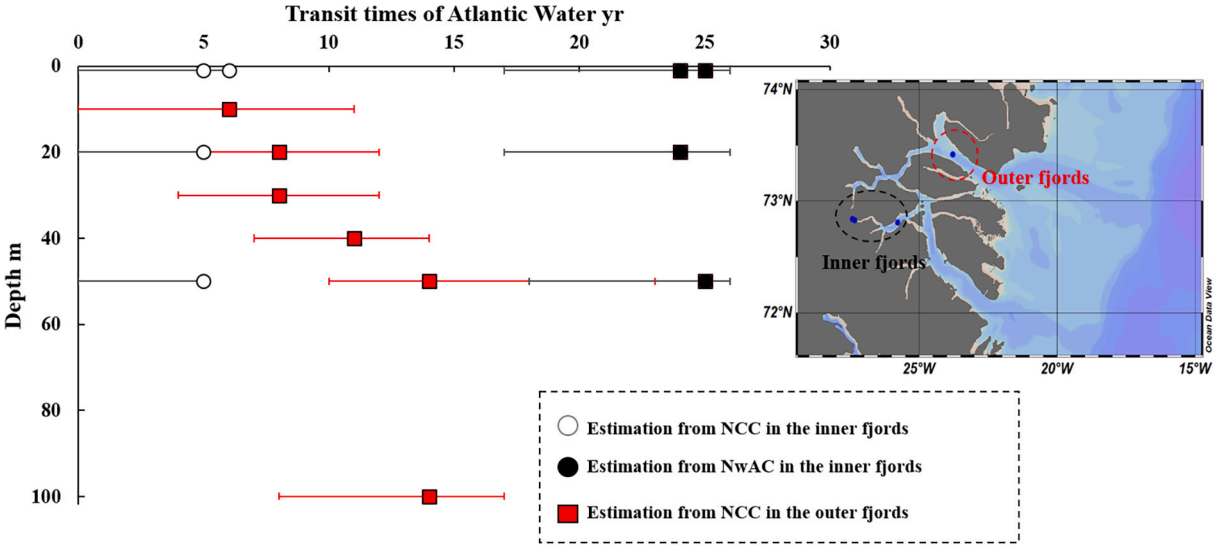

Fig. 4. Estimates of Atlantic Water transit times in the fjords based on the input functions of Norwegian Coastal Current (NCC) and Norwegian Atlantic Current (NwAC). For Polar Surface Water (PSW) in the inner fjords, transit times are estimated with both the NCC $^{236}U_{RP\text{-}AW}$ input function (open circles) and the NwAC $^{236}U_{RP\text{-}AW}$ input function (black circles). For PSW in the outer fjords transit times are estimated with the NCC $^{236}U_{RP\text{-}AW}$ input function (red squares). (For interpretation of the references to colour in this figure legend, the reader is referred to the web version of this article.)

$$P_{PW} = M_{PW}N + C_{PW} \quad (13)$$

where N is nitrate concentration in the seawater samples; M_{AW} (M_{PW}) and C_{AW} (C_{PW}) are the slope and intercept of Atlantic Water (Pacific Water) N:P relationship.

Based on the end member values in NCC branch water, the source years of Atlantic Water in PSW (upper 100 m) in the East Greenland fjords are estimated between 2004 and 2012 (uncertainties of source years: 1995–2018), suggesting that the transit times from the entrance of the Arctic Ocean are 0 years (ranging from 0 to 6 years considering uncertainties) in the inner fjords and 6–14 years (ranging from 0 to 23 years considering uncertainties) in the outer fjords (Fig. 4 open circle and red square symbols). Compared with previous results (12–17 years, Wefing et al., 2021) in polar waters on the Greenland shelf estimated from ^{129}I and ^{236}U, our results in the PSW of the fjords show a wider range. It is worth noting that the estimated transit times in the inner fjords seem not reasonable, which might be due to the impact of upwelling of AAW (see detailed explanation in Section 4.3). For the outer fjords, transit times of Atlantic Water increase with depths, which may be related to different transport pathways (Fig. 4).

4.3. The impact of upwelling on transit time estimation of Atlantic Water

While the majority of estimations of Atlantic Water transit times in the fjords are reasonable, there are however exceptions. The four samples (open circle in Fig. 4) from the inner parts of the fjords have unrealistically short transit times ($\leq$ 6 years). Comparison with other samples at the same depth reveals that these samples have higher fractions of Atlantic Water (e.g. 93% at inner fjord vs. 63% at outer fjord at 50 m depth) and freshwater (e.g. 7% at inner fjord vs. 5% at outer fjord at 50 m depth) but lower Pacific Water contributions (e.g. -1% at inner fjord vs. 32% at outer fjord at 50 m depth) (Fig. 5A-C). This might be

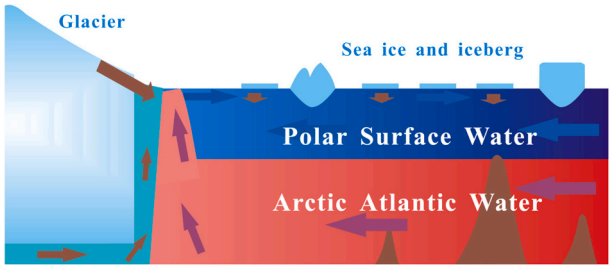

Fig. 6. Schematic of water column stratification in East Greenland fjords.

because these waters are influenced by subglacial discharge, which causes upwelling at the terminus and entrains AAW to the surface, restricting the lateral extent of polar waters (Fig. 6). This is also reflected by lower RP-^{236}U concentrations in these samples compared to those from the remaining part of the fjord (e.g., 14.4 ± 1.6 × 10^6 atom/L in the inner fjord vs. 27.6 ± 3.6 × 10^6 atom/L in the outer fjord at 100 m depth), revealing that the RP ^{236}U signal is diluted by upwelling entrained Greenlandic meltwater (no RP signal) and older AAW (low RP signal) (Fig. 5B). The entrainment of AAW from upwelling and lack of surface Atlantic Water contribution implies that transit time estimate for samples in the inner fjords should be further constrained by taking into account fjord circulation and re-considering the use of the appropriate input function. In the inner parts of the fjords where glacial upwelling entrains AAW to the surface and the influence of Pacific Water (PW) is limited, and the NwAC $^{236}U_{RP\text{-}AW}$ input function is more appropriate to use.

AAW on the East Greenland Shelf with (temperature 1.17–1.54 °C and salinity 34.71–34.89 in Fig. 2A-B), has its origins in the NwAC (Wefing et al., 2019; Wefing et al., 2021), which has its own RP ^{236}U input function at the entrance of Arctic (74°N, 19°E) (Fig. S2, supporting

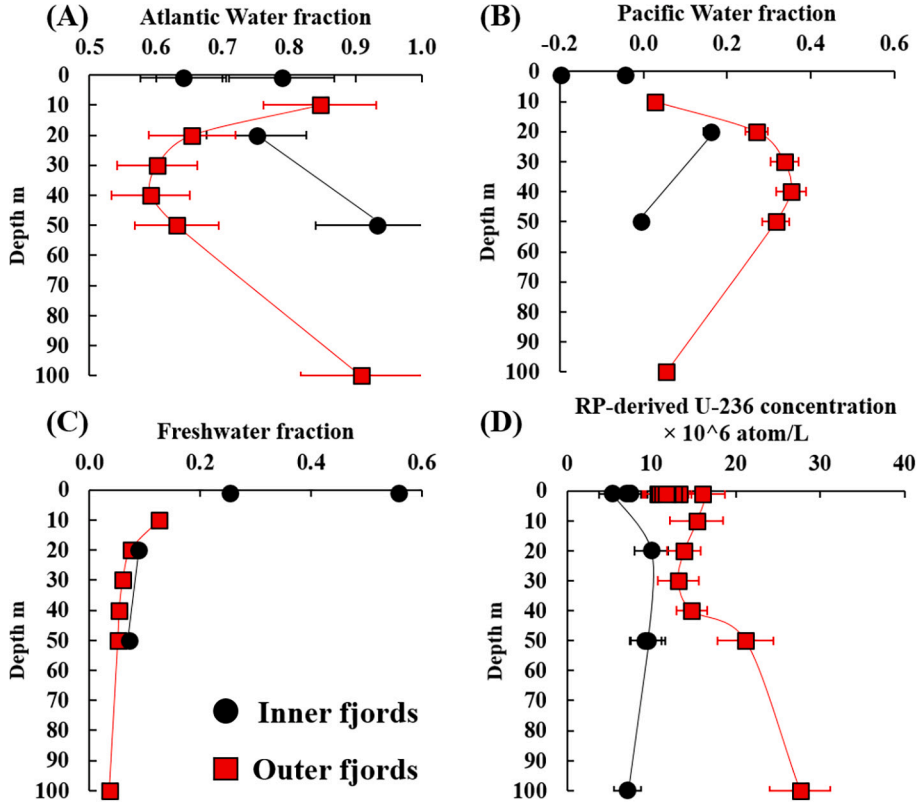

Fig. 5. The fractions of Atlantic Water (A), Pacific Water (B) and freshwater (C) in the profiles of the inner fjords (black circles) and the outer fjords (red squares) estimated from nitrate, phosphate and salinity and RP-derived ^{236}U concentrations in the profile of the inner fjords (black circles) and the outer fjords (red squares) (D). (For interpretation of the references to colour in this figure legend, the reader is referred to the web version of this article.)

information). Replacing the NCC input function with NwAC for the surface water samples in the inner fjord, results in transit times on the order of 24–25 years (ranging from 17 to 27 years considering uncertainties) (Fig. 4, black dot). Our estimations are slightly higher than the transit times for the AAW (16–23 years) on the western Fram Strait (Wefing et al., 2019). This is reasonable as it takes extra time for Atlantic Water exiting from western Fram Strait to reach East Greenland fjords. In this study, we assume the purely advective transport in the Arctic Ocean due to the strong stratification and vertical mixing was considered limited. Therefore, single NwAC input function can be considered in the AAW. In addition, the Returning Atlantic Current (RAC) can reach Northeast Greenland fjords through the Fram Strait without entering the Arctic Ocean (Schaffer et al., 2017), implying possible appearance of younger Atlantic Water in this region. However, it is not clear whether RAC is present in the study area, as so far no report has verified the contribution of RAC in East Greenland fjords. Therefore, contribution of RAC fraction (if any) was not considered in our Atlantic Water transit time estimation.

4.4. The limitations and uncertainties of the ^{233}U-^{236}U tracer approach

Although the approach provides plausible transit times which are comparable with published data, there are still limitations and uncertainties associated with these estimates. The proposed ^{233}U-^{236}U tracer approach is based on the assumption of purely advective transport of input function signals to the study region. One can question the validity of this assumption, but the observed widespread stratification in the region hints to limited deep vertical mixing in these waters sampled. The nutrient based approach used here to isolate the Atlantic Water fraction also has considerable limitations. It assumes the preferential loss of nitrate (to denitfircation), relative to phosphate, only occurs on shelf waters influenced by the Pacific inflow (Jones et al., 1998). However, there is clear evidence that Siberian shelf waters can also contribute (Alkire et al., 2015; Bauch et al., 2011) and that there may be considerable errors in the estimates of Pacific water in the central Arctic (Alkire et al., 2015; Whitmore et al., 2020). Similarly it is unclear if interactions with Greenland shelf sediments during passage over fjord sills can generate an artificial Pacific Water signal. With this in mind it would certainly be relevant to expand on this explorative study to include greater coverage of additional tracers for water fractionation and better geographical coverage of sampling to map source waters. Additional chemical tracers (such as ^{99}Tc, ^{137}Cs and ^{129}I) could also add to further validate this new ^{233}U-^{236}U tracer approach.

We also acknowledge that part of the relatively high uncertainty (up to 40%) in the current transit time estimation can be due to the ultra-low levels of ^{233}U in environmental samples and limitation in achieving high precision in $^{236}U/^{233}U$ (currently at level of 30%) measurement by AMS. This could in part be rectified by using larger sample volume to achieve increased detection efficiency in the AMS measurement. Finally the approach also hinges on the validity of the input function estimates and mixing of SF and LH branch water. Nevertheless, our results (6–14 years) in the outer fjords agree well with previous study, indicating success in our exploration to use ^{233}U and ^{236}U to estimate transit times of Atlantic Water in East Greenland fjords. Therefore, the paired anthropogenic uranium (^{233}U and ^{236}U) tracer approach, combining with salinity and nutrients (nitrate and phosphate), may hold promise as a technique to isolate RP ^{236}U and estimate Atlantic water transit times in Arctic and subpolar regions.

5. Conclusions and perspectives

In this work, we developed a new approach based on paired tracer ^{233}U-^{236}U and nutrient data for estimating Atlantic Water transit time in the Arctic Ocean. ^{233}U was used to isolate reprocessing contribution of ^{236}U to exclusively trace the Atlantic Water, and nitrate and phosphate were measured to constrain the Atlantic Water fraction, thereby to derive the transit time based on the time-dependent variation of ^{236}U in the Atlantic Water end member. The significantly distinct source term distribution of ^{236}U in PSW (63% from RP contributions) and in AAW (74% from GF contributions) makes the ^{233}U-^{236}U signal very useful fingerprint to distinguish these two water bodies in the Arctic region.

Based on the estimation with the ^{233}U-^{236}U approach, the transit time of Atlantic Water in outer East Greenland fjords is 6–14 years, while that in inner East Greenland fjords is 24–25 years. These estimates were in good agreement with earlier studies in the northeastern Greenland coast (Wefing et al., 2019). The estimates in this work using the ^{233}U-^{236}U tracer pair offer a first approximation of transit times which can be constrained in the future by further sampling with higher spatial resolution and comparison with ocean circulation model results.

The transit times estimated in this work provide an indication of the time lag that can be expected between alterations in the waters entering the Arctic to a subsequent effect on the water leaving the Arctic Ocean on the East Greenland shelf. As transit times for Atlantic Water are on the order of 24–25 years any changes in the Atlantic waters flowing into the Arctic, can be expect to materialize in outflowing waters approximately 25 years later. Although it should also be noted that variability in ocean circulation conditions directly upstream of the Greenland shelf, in the central Arctic, likely have a greater influence on water properties in the region. Although this extrapolation may be speculative and further investigations are needed, these measurements provide an indication of the potential timescale of propagation of a signal from the Atlantic to the Greenland shelf.

Declaration of Competing Interest

The authors declare that they have no known competing financial interests or personal relationships that could have appeared to influence the work reported in this paper.

Acknowledgements

We acknowledge the financial support of the Independent Research Fund Denmark (9040-00266B). Part of the AMS measurements at VERA were supported by the RADIATE project from the EU Research and Innovation programme HORIZON 2020 under grant agreement No 824096, proposal No. 21002394-ST. L.M. was funded by research programme VENI with project number 016.Veni.192.150, which is financed by the Dutch Research Council (NWO). We also thank the captain and crews of the Royal Danish Naval vessel HMDS Lauge Koch for their support with sampling at Northeast Greenland.

Appendix A. Supplementary data

Supplementary data to this article can be found online at https://doi.org/10.1016/j.chemgeo.2022.121007.

References

Aagaard, K., Carmack, E.C., 1989. The role of sea ice and other fresh water in the Arctic circulation. J. Geophys. Res. Ocean 94 (10), 14485–14498. https://doi.org/10.1029/JC094iC10p14485.

Alkire, M.B., Morison, J., Andersen, R., 2015. Variability in the meteoric water, sea-ice melt, and Pacific Water contributions to the Central Arctic Ocean, 2000-2014. J. Geophys. Res. Oceans 120 (3), 1573–1598. https://doi.org/10.1002/2014JC010023.

Andersson, P.S., Wasserburg, G.J., Chen, J.H., Papanastassiou, D.A., Ingri, J., 1995. ^{238}U-^{234}U and ^{232}Th-^{230}Th in the Baltic Sea and in river water. Earth Planet. Sci. Lett. 130, 217–234. https://doi.org/10.1016/0012-821X(94)00262-W.

Bauch, D., van der Loeff, M.R., Andersen, N., Torres-Valdes, S., Bakker, K., Abrahamsen, E.P., 2011. Origin of freshwater and polynya water in the Arctic Ocean halocline in summer 2007. Prog. Oceanogr. 91 (4), 482–495. https://doi.org/10.1016/j.pocean.2011.07.017.

Beszczynska-Möller, A., Woodgate, R.A., Lee, C., Melling, H., Karcher, M., 2011. A synthesis of exchanges through the main oceanic gateways to the Arctic Ocean. Oceanography 24 (3), 82–99. https://doi.org/10.5670/oceanog.2011.59.

BIPM, IEC, IFCC, ISO, IUPAC, IUPAP, OIML, 2008. Evaluation of measurement data—Guide to the expression of uncertainty in measurement. Jt. Comm. Guid. Metrol. 100, 1–116.
Casacuberta, N., Christl, M., Lachner, J., van der Loeff, M.R., Masqué, P., Synal, H.-A., 2014. A first transect of ^{236}U in the North Atlantic Ocean. Geochim. Cosmochim. Acta 133, 34–46. https://doi.org/10.1016/j.gca.2014.02.012.
Casacuberta, N., Masqué, P., Henderson, G., Rutgers van der Loeff, M., Bauch, D., Vockenhuber, C., Daraoui, A., Walther, C., Synal, H.-A., Christl, M., 2016. First ^{236}U data from the Arctic Ocean and use of ^{236}U/^{238}U and ^{129}I/^{236}U as a new dual tracer. Earth Planet. Sci. Lett. 440, 127–134. https://doi.org/10.1016/j.epsl.2016.02.020.
Casacuberta, N., Christl, M., Vockenhuber, C., Wefing, A.-M., Wacker, L., Masqué, P., Synal, H.-A., van der Loeff, M.R., 2018. Tracing the three Atlantic branches entering the Arctic Ocean with ^{129}I and ^{236}U. J. Geophys. Res. Oceans 123, 6909–6921. https://doi.org/10.1029/2018JC014168.
Castrillejo, M., Witbaard, R., Casacuberta, N., Richardson, C.A., Dekker, R., Synal, H.-A., Christl, M., 2020. Unravelling 5 decades of anthropogenic ^{236}U discharge from nuclear reprocessing plants. Sci. Total Environ. 717, 137094. https://doi.org/10.1016/j.scitotenv.2020.137094 (2020).
Christl, M., Lachner, J., Vockenhuber, C., Lechtenfeld, O., Stimac, I., van der Loeff, M.R., Synal, H.-A., 2012. A depth profile of uranium-236 in the Atlantic Ocean. Geochim. Cosmochim. Acta 77, 98–107. https://doi.org/10.1016/j.gca.2011.11.009.
Christl, M., Casacuberta, N., Vockenhuber, C., Elsässer, C., Bailly du Bois, P., Herrmann, J., Synal, H.A., 2015. Reconstruction of the ^{236}U input function for the Northeast Atlantic Ocean: Implications for ^{129}I/^{236}U and ^{236}U/^{238}U-based tracer ages. J. Geophys. Res. Oceans 120, 7282–7299. https://doi.org/10.1002/2015JC011116.
Christl, M., Casacuberta, N., Lachner, J., Herrmann, J., Synal, H.-A., 2017. Anthropogenic ^{236}U in the North Sea—a closer look into a source region. Environ. Sci. Technol. 51, 12146–12153. https://doi.org/10.1021/acs.est.7b03168.
Dahlgaard, H., 1995. Transfer of European coastal pollution to the arctic: Radioactive tracers. Mar. Pollut. Bull. 31, 3–7. https://doi.org/10.1016/0025-326X(95)00003-6.
Dodd, P.A., Rabe, B., Hansen, E., Falck, E., Mackensen, A., Rohling, E., Stedmon, C.A., Kristiansen, S., 2012. The freshwater composition of the Fram Strait outflow derived from a decade of tracer measurements. J. Geophys. Res. 117, C11005. https://doi.org/10.1029/2012JC008011.
Dunk, R.M., Mills, R.A., Jenkins, W.J., 2002. A reevaluation of the oceanic uranium budget for the Holocene. Chem. Geol. 190, 45–67. https://doi.org/10.1016/S0009-2541(02)00110-9.
Eigl, R., Srncik, M., Steier, P., Wallner, G., 2013. ^{236}U/^{238}U and ^{240}Pu/^{239}Pu isotopic ratios in small (2*L*) sea and river water samples. J. Environ. Radioact. 116, 54–58. https://doi.org/10.1016/j.jenvrad.2012.09.013.
Fine, R.A., 2011. Observations of CFCs and SF6 as Ocean tracers. Annu. Rev. Mar. Sci. 3, 173–195. https://doi.org/10.1146/annurev.marine.010908.163933.
Gjelstrup, C.V.B., Sejr, M.K., Christiansen, J.S., Dodd, P.A., Granskog, M.A., Koch, B., Møller, E.F., de Steur, L., Winding, M.S., Stedmon, C.A., 2022. Warm Meets Fresh: Decadal Changes in Water Properties on the Northeast Greenland Shelf (in review).
Hain, K., Steier, P., Froehlich, M.B., Golser, R., Hou, X., Lachner, J., Qiao, J., Quinto, F., Sakaguchi, A., 2020. ^{233}U/^{236}U signature allows to distinguish environmental emissions of civil nuclear industry from weapons fallout. Nat. Commun. 11 https://doi.org/10.1038/s41467-020-15008-2.
Hansen, H.P., Koroleff, F., 1999. Determination of nutrients. In: Grasshoff, K., Kremling, K., Ehrhardt, M. (Eds.), Methods of Seawater Analysis, 3rd ed. Wiley-VCH, Weinheim, Germany, pp. 159–228. https://doi.org/10.1002/9783527613984.ch10.
HELCOM MORS Discharge database [WWW Document]. n.d. https://helcom.fi/baltic-sea-trends/data-maps/databases/ (accessed 5.20.2020).
Ionita, M., Scholz, P., Lohmann, G., Dima, M., Prange, M., 2016. Linkages between atmospheric blocking, sea ice export through Fram Strait and the Atlantic Meridional Overturning Circulation. Sci. Rep. 6 (1), 32881. https://doi.org/10.1038/srep32881.
Jones, E.P., Anderson, L.G., Swift, J.H., 1998. Distribution of Atlantic and Pacific waters in the upper Arctic Ocean: implications for circulation. Geophys. Res. Lett. 25, 765–768. https://doi.org/10.1029/98GL00464.
Klimkhammer, G.P., Palmer, M.R., 1991. Uranium in the oceans: where it goes and why. Geochim. Cosmochim. Acta 55, 1799–1806.
Lin, M., Qiao, J.X., Hou, X.L., Dellwig, O., Steier, P., Hain, K., Golser, R., Zhu, L.C., 2021a. 70-Year anthropogenic uranium imprints of nuclear activities in Baltic Sea sediments. Environ. Sci. Technol. 55 (13), 8918–8927. https://doi.org/10.1021/acs.est.1c02136.
Lin, M., Qiao, J.X., Hou, X.L., Golser, R., Hain, K., Steier, P., 2021b. On the quality control for the determination of ultratrace-level ^{236}U and ^{233}U in environmental samples by accelerator mass spectrometry. Anal. Chem. 93, 3362–3369. https://doi.org/10.1021/acs.analchem.0c03623.
Polyakov, I.V., Pnyushkov, A.V., Alkire, M.B., Ashik, I.M., Baumann, T.M., Carmack, E.C., Goszczko, I., Guthrie, J., Ivanov, V.V., Kanzow, T., Krishfield, R., Kwok, R., Sundfjord, A., Morison, J., Rember, R., Yulin, A., 2017. Greater role for Atlantic inflows on sea ice loss in the Eurasian Basin of the Arctic Ocean. Science 356 (6335), 285–291. https://doi.org/10.1126/science.aai8204.
Qiao, J.X., Ransby, D., Steier, P., 2022. Deciphering anthropogenic uranium sources in the equatorial northwest Pacific margin. Sci. Total Environ. 806, 150482. https://doi.org/10.1016/j.scitotenv.2021.150482.
Qiao, J.X., Xu, Y.H, 2018. Direct measurement of uranium in seawater by inductively coupled plasma mass spectrometry. Talanta 183, 18–23. https://doi.org/10.1016/j.talanta.2018.02.045.
Qiao, J.X., Hou, X.L., Steier, P., Nielsen, S., Golser, R., 2015. Method for ^{236}U determination in seawater using flow injection extraction chromatography and accelerator mass spectrometry. Anal. Chem. 87, 7411–7417. https://doi.org/10.1021/acs.analchem.5b01608.
Qiao, J.X., Hain, K., Steier, P., 2020. First dataset of ^{236}U and ^{233}U around the Greenland coast: A 5-year snapshot (2012–2016). Chemosphere 257, 127185. https://doi.org/10.1016/j.chemosphere.2020.127185.
Rahmstorf, S., 2002. Ocean circulation and climate during the past 120,000 years. Nature 419, 207–214. https://doi.org/10.1038/nature01090.
Rudels, B., 2009. Arctic Ocean circulation. In: Encyclopedia of Ocean Sciences, pp. 211–225. https://doi.org/10.1016/B978-012374473-9.00601-9.
Rudels, B., Jones, E.P., Schauer, U., Eriksson, P., 2004. Atlantic sources of the Arctic Ocean surface and halocline waters. Polar Res. 23 (2), 181–208. https://doi.org/10.3402/polar.v23i2.6278.
Rutgers van der Loeff, M.M., Geibert, W., 2008. U-and Th-series nuclides as tracers of particle dynamics, scavenging and biogeochemical cycles in the Oceans. In: Krishnaswami, S., Cochran, J.K. (Eds.), Radioactivity in the Environment, 13, pp. 227–268. https://doi.org/10.1016/S1569-4860(07)00007-1.
Sakaguchi, A., Kawai, K., Steier, P., Quinto, F., Mino, K., Tomita, J., Hoshi, M., Whitehead, N., Yamamoto, M., 2009. First results on ^{236}U levels in global fallout. Sci. Total Environ. 407, 4238–4242. https://doi.org/10.1016/j.scitotenv.2009.01.058.
Sakaguchi, A., Kadokura, A., Steier, P., Takahashi, Y., Shizuma, K., Hoshi, M., Nakakuki, T., Yamamoto, M., 2012. Uranium-236 as a new oceanic tracer: a first depth profile in the Japan Sea and comparison with caesium-137. Earth Planet. Sci. Lett. 333, 165–170. https://doi.org/10.1016/j.epsl.2012.04.004.
Sakaguchi, A., Nomura, T., Steier, P., Golser, R., Sasaki, K., Watanabe, T., Nakakuki, T., Takahashi, Y., Yamano, H., 2016. Temporal and vertical distributions of anthropogenic ^{236}U in the Japan Sea using a coral core and seawater samples. J. Geophys. Res. Oceans 121, 4–13. https://doi.org/10.1002/2015JC011109.
Schaffer, J., von Appen, W.-J., Dodd, P.A., Hofstede, C., Mayer, C., de Steur, L., Kanzow, T., 2017. Warm water pathways toward Nioghalvfjerdsfjorden Glacier, Northeast Greenland. J. Geophys. Res. Oceans 122 (5), 4004–4020. https://doi.org/10.1002/2016JC012462.
Schaffer, J., Kanzow, T., von Appen, W.-J., von Albedyll, L., Arndt, J.E., Roberts, D.H., 2020. Bathymetry constrains ocean heat supply to Greenland's largest glacier tongue. Nat. Geosci. 13, 227–231. https://doi.org/10.1038/s41561-019-0529-x.
Schwehr, K.A., Scantschi, P.H., Elmore, D., 2005. The dissolved organic iodine species of the isotopic ratio of 129I/127I: a novel tool for tracing terrestrial organic carbon in the estuarine surface waters of Galveston Bay, Texas. Limnol. Oceanogr. Methods 3, 326–337. https://doi.org/10.4319/lom.2005.3.326.
Sejr, M.K., Stedmon, C.A., Bendtsen, J., Abermann, J., Juul-Pedersen, T., Mortensen, J., Rysgaard, S., 2017. Evidence of local and regional freshening of Northeast Greenland coastal waters. Sci. Rep. 7, 13183. https://doi.org/10.1038/s41598-017-10610-9.
Serreze, M.C., Barrett, A.P., Slater, A.G., Woodgate, R.A., Aagaard, K., Lammers, R.B., Steele, M., Moritz, R., Meredith, M., Lee, C.M., 2006. The large-scale freshwater cycle of the Arctic. J. Geophys. Res. 111, C11010. https://doi.org/10.1029/2005JC003424.
Skagseth, Ø., Eldevik, T., Årthun, M., Asbjørnsen, H., Lien, V.S., Smedsrud, L.H., 2020. Reduced efficiency of the Barents Sea cooling machine. Nat. Clim. Chang. 10, 661–666. https://doi.org/10.1038/s41558-020-0772-6.
Smith, J.N., McLaughlin, F.A., Smethie, W.M., Moran, S.B., Lepore, K., 2011. Iodine-129, ^{137}Cs, and CFC-11 tracer transit time distributions in the Arctic Ocean. J. Geophys. Res. 116 (C04024), 2011. https://doi.org/10.1029/2010JC006471.
Steier, P., Bichler, M., Keith Fifield, L., Golser, R., Kutschera, W., Priller, A., Quinto, F., Richter, S., Srncik, M., Terrasi, P., Wacker, L., Wallner, A., Wallner, G., Wilcken, K. M., Maria Wild, E., 2008. Natural and anthropogenic ^{236}U in environmental samples. Nucl. Inst. Methods Phys. Res. B 266, 2246–2250. https://doi.org/10.1016/j.nimb.2008.03.002.
Steier, P., Dellinger, F., Forstner, O., Golser, R., Knie, K., Kutschera, W., Priller, A., Quinto, F., Srncik, M., Terrasi, F., Vockenhuber, C., Wallner, A., Wallner, G., Wild, E. M., 2010. Analysis and application of heavy isotopes in the environment. Nucl. Inst. Methods Phys. Res. B 268 (7–8), 1045–1049. https://doi.org/10.1016/j.nimb.2009.10.094.
Steier, P., Hain, K., Klötzli, U., Lachner, J., Priller, A., Winkler, S., Golser, R., 2019. The Actinide Beamline at VERA. Nucl. Instrum. Methods Phys. Res. Sect. B Beam Interact. Mater. At. 458, 82–89. https://doi.org/10.1016/j.nimb.2019.07.031.
Tsubouchi, T., Våge, K., Hansen, B., Larsen, K.M.H., Østerhus, S., Johnson, C., Jonsson, S., Valdimarsson, H., 2021. Increased ocean heat transport into the Nordic Seas and Arctic Ocean over the period 1993–2016. Nat. Clim. Chang. 11, 21–26. https://doi.org/10.1038/s41558-020-00941-3.
Tsungogai, S., Henmi, T., 1971. Iodine in the surface water of the Ocean. J. Oceanogr. Soc. Jpn. 27, 67–72.
Villa-Alfageme, M., Chamizo, E., Kenna, T.C., López-Lora, M., Casacuberta, N., Chang, C., Masqué, P., Christl, M., 2019. Distribution of ^{236}U in the U.S. GEOTRACES Eastern Pacific Zonal Transect and its use as a water mass tracer. Chem. Geol. 517, 44–57. https://doi.org/10.1016/j.chemgeo.2019.04.003.
Wang, Q., 2021. Stronger variability in the Arctic Ocean induced by sea ice decline in a warming climate: Freshwater storage, dynamic sea level and surface circulation. J. Geophys. Res. Oceans 126. https://doi.org/10.1029/2020JC016886 e2020JC016886.

Wefing, A.-M., Christl, M., Vockenhuber, C., Rutgers van der Loeff, M., Casacuberta, N., 2019. Tracing Atlantic waters using ^{129}I and ^{236}U in the Fram Strait in 2016. J. Geophys. Res. Oceans 124, 882–896. https://doi.org/10.1029/2018JC014399.

Wefing, A.-M., Casacuberta, N., Christl, M., Gruber, N., Smith, J.N., 2021. Circulation timescales of Atlantic Water in the Arctic Ocean determined from anthropogenic radionuclides. Ocean Sci. 17, 111–129. https://doi.org/10.5194/os-17-111-2021.

Whitmore, L.M., Pasqualini, A., Newton, R., Shiller, A.M., 2020. Gallium: a new tracer of Pacific Water in the Arctic Ocean. J. Geophys. Res. Oceans 125. https://doi.org/10.1029/2019JC015842 e2019JC015842.

Supporting Information

Estimation of Atlantic Water transit times in East Greenland fjords using a ^{233}U-^{236}U tracer approach

Gang Lin[a], Mu Lin[a], Jixin Qiao[a,*], Mikael K. Sejr[b,c], Peter Steier[d], Lorenz Meire[e,f], Colin A. Stedmon[g]

[a]Department of Environmental and Resource Engineering, Technical University of Denmark, DK-4000 Roskilde, Denmark

[b]Department of Bioscience, Aarhus University, Vejlsøvej 25, 8600 Silkeborg, Denmark

[c]Arctic Research Centre, Aarhus University, Aarhus, Denmark

[d]VERA Laboratory, Faculty of Physics, Isotope Physics, University of Vienna, Währinger Straße 17, A-1090 Vienna, Austria

[e]Greenland Climate Research Centre, Greenland Institute of Natural Resources, Kivioq 2, P.O. Box 570, 3900 Nuuk, Greenland

[f]Department of Estuarine and Delta Systems, Royal Netherlands Institute of Sea Research, Yerseke, Netherlands

[g]National Institute of Aquatic Resources, Technical University of Denmark, Kemitorvet, 2800 Kgs. Lyngby, Denmark

*Corresponding author

E-mail address: jiqi@dtu.dk (J. Qiao).

Introduction

The supporting information (in total of 6 pages) includes supplementary text for detailed methods in this work, Table S1 (See excel) summarizing all analytical results and Table S2 presenting the contributions of different water masses in Norwegian Coastal Current and Norwegian Atlantic Current. The details for the reconstruction of ^{236}U input functions in Norwegian Coastal Current and Norwegian Atlantic Current are also described.

1. The Chemical Procedure of Extracting U Isotopes From Seawater

After filtration with filter paper (Munktell Filtrak, Grade 00K), seawater samples were acidified to pH = 2 with 14 M HNO_3 to decompose the existing uranyl carbonate complexes in seawater. After adding 500 – 1000 mg of Fe^{3+} ($FeCl_3$ solution, 0.05 g/mL for Fe^{3+}, purified with a UTEVA® resin column) as a carrier for U isotopes and bubbling with compressed air for 10 min to remove CO_2, 25% $NH_3 \cdot H_2O$ solution was added to adjust pH to 8 - 9 to quantitatively co-precipitate U with $Fe(OH)_3$. After keeping still for 30 min, the supernatant was decanted, and the slurry was centrifuged at 3000 rpm for 5 min. The precipitate was dissolved by 14M HNO_3, and the sample solution was diluted to a final HNO_3 concentration of 3M with ultrapure water. The sample solution was loaded to a 2-mL UTEVA® resin column pre-conditioned with 20 mL of 3M HNO_3. The UTEVA® column was successively rinsed with 40 mL of 3M HNO_3 and 20 mL of 6M HCl. The retained U on the UTEVA® resin column was eluted by 10 mL of 0.025M HCl. After adding 2 mg Fe^{3+} and adjusting pH to 8-9, U in the sample eluate was co-precipitated with $Fe(OH)_3$. The $Fe(OH)_3$ precipitate was dried in an oven at 90 ℃ for at least 4 h and combusted at 800 °C for 12 h. Finally, the combusted sample was pressed into an aluminum sputter target holder for ^{233}U and ^{236}U analyses.

2. The Combined Uncertainties of $^{233}U/^{238}U$ and $^{236}U/^{238}U$

To subtract the contribution of ^{236}U and ^{233}U from laboratory background, the actual ratios of $^{233}U/^{238}U$ (R_S^{233}) and $^{236}U/^{238}U$ (R_S^{236}) in seawater samples were calculated according to the following equation (Lin et al., 2021):

$$R_S^x = \frac{(m_m^{238} R_m^x - m_b^{238} R_b^x)}{m_m^{238} - m_b^{238}} \quad \text{(S1)}$$

where x is 233 or 236, R_m^x is the measured atomic ratio of ^{236}U or ^{233}U to ^{238}U in the sputter target and m_m^{238} is the mass of ^{238}U in the seawater sample; R_b^x and m_b^{238} are the corresponding atomic ratios and mass of ^{238}U in the sputter target of corresponding blank sample. As the recovery of target preparation step is quantitative (recovery > 99%) (Qiao et al., 2015), we assumed that m_m^{238} or m_b^{238} was equal to the ^{238}U mass in the eluate, which was determined by ICP-MS. Calculation results indicate that the contribution of ^{236}U and ^{233}U from procedure blanks was negligible (< 2%) to the real seawater samples.

The combined uncertainties of $^{233}U/^{238}U$ and $^{236}U/^{238}U$ is calculated from eq. S2 based on the law of uncertainty propagation, The combined uncertainties contain the uncertainties of ^{238}U contents ($u(m_m^{238})$ and $u(m_b^{238})$) and the uncertainties of determined $^{236}U/^{238}U$ or $^{233}U/^{238}U$ atomic ratio ($u(R_m^x)$ and $u(R_b^x)$) in the eluates of sample and blank (Lin et al., 2021).

$$u\left(R_s^{236(233)}\right) = \sqrt{\left[\frac{\partial R_s^{236(233)}}{\partial R_m^{236(233)}} u\left(R_m^{236(233)}\right)\right]^2 + \left[\frac{\partial R_s^{236(233)}}{\partial R_b^{236(233)}} u\left(R_b^{236(233)}\right)\right]^2 + \left[\frac{\partial R_s^{236(233)}}{\partial m_m^{238}} u(m_m^{238})\right]^2 + \left[\frac{\partial R_s^{236(233)}}{\partial m_b^{238}} u(m_b^{238})\right]^2}$$

$$= \sqrt{\left[\frac{m_m^{238}}{m_m^{238} - m_b^{238}} u\left(R_m^{236(233)}\right)\right]^2 + \left[\frac{m_b^{238}}{m_m^{238} - m_b^{238}} u\left(R_b^{236(233)}\right)\right]^2 + \left[\frac{m_b^{238}\left(R_m^{236(233)} - R_b^{236(233)}\right)}{(m_m^{238} - m_b^{238})^2} u(m_m^{238})\right]^2 + \left[\frac{m_m^{238}\left(R_m^{236(233)} - R_b^{236(233)}\right)}{(m_m^{238} - m_b^{238})^2} u(m_b^{238})\right]^2} \quad (S2)$$

3. The Reconstruction of Reprocessing Plants-derived ^{236}U Concentrations in Norwegian Coastal Current and Norwegian Atlantic Current in the Arctic Entrance

The RP-derived ^{236}U and GF-derived ^{236}U concentrations have been reconstructed in Sellafield (SF) branch water and La Hague (LH) branch water (Christl et al., 2015). Based on these results, Wefing et al. (2021) reconstructed two input functions for ^{236}U in the Arctic. This is composed of Norwegian Coastal Current (NCC) and Norwegian Atlantic Current (NwAC), each with their own specific contributions from Sellafield (SF) and La Hague (LH) (Casacuberta et al., 2018) (Table S2 and equation S3 and S4).

Table S2. Sellafield Branch Water, La Hague Branch Water and Atlantic Water Contributions in Norwegian Coastal Current (NCC) and Norwegian Atlantic Current (NwAC) in the Arctic Entrance

Current*	Water composition	LH branch (%)	SF branch (%)	AW (%)
NwAC	Barents Sea Branch Water	1.7 ± 0.2	0.5 ± 0.1	97.7 ± 0.2
	Fram Strait Branch Water	0.8 ± 0.1	0.4 ± 0.1	98.7 ± 0.2
NCC	Arctic Shelf Break Branch	5.2 ± 1.1	2.7 ± 0.4	92.1 ± 1.1

** NCC was also defined as Arctic Shelf Break Branch (Casacuberta et al., 2018), and the contributions of Barents Sea Branch Water and Fram Strait Branch Water were averaged as the contribution of NwAC (Wefing et al., 2021). Atlantic Water (AW) only contains global fallout background level ($^{236}U_{AW}$: 10 × 10^6 atom/L) (Casacuberta et al., 2018).*

$$^{236}U_{NCC} = 5.2\% \times {}^{236}U_{LH} + 2.7\% \times {}^{236}U_{SF} + 92.1\% \times {}^{236}U_{AW} \quad (S3)$$

$$^{236}U_{NwAC} = ((1.7\% \times {}^{236}U_{LH} + 0.5\% \times {}^{236}U_{SF} + 97.7\% \times {}^{236}U_{AW}) + (0.8\% \times {}^{236}U_{LH} + 0.4\% \times {}^{236}U_{SF} + 98.7\% \times {}^{236}U_{AW})) \times \frac{1}{2} \quad (S4)$$

We only used RP-derived ^{236}U concentrations based on the above equations to obtain the input functions of RP-derived ^{236}U concentrations in NCC and NwAC in the Arctic entrance (Fig. S1). And RP-derived ^{236}U concentration in Atlantic Water (i.e., $^{236}U_{AW}$ in equations S3 and S4) is assumed as 0 due to the pure global fallout signal in Atlantic Water. Recently, the ^{236}U discharges from SF were reconstructed based on shell records by Castrillejo et al. (2020). Therefore, we used the newest reconstruction of total ^{236}U concentrations from SF branch water and LH branch water (Castrillejo et al., 2020), and subtracted the estimated GF-derived ^{236}U concentrations in the North Sea (Christl et al., 2015) to obtain the RP derived $^{236}U_{LH}$ and $^{236}U_{SF}$ in equations S3 and S4. The uncertainty of $^{236}U_{RP\text{-}AW}$ was propagated from uncertainties of the shell record of $^{236}U/^{238}U$ ratios near SF and LH and marine mixing pattern of SF branch water, LH branch water and GF in the Arctic entrance (Casacuberta et al., 2018; Castrillejo et al., 2020).

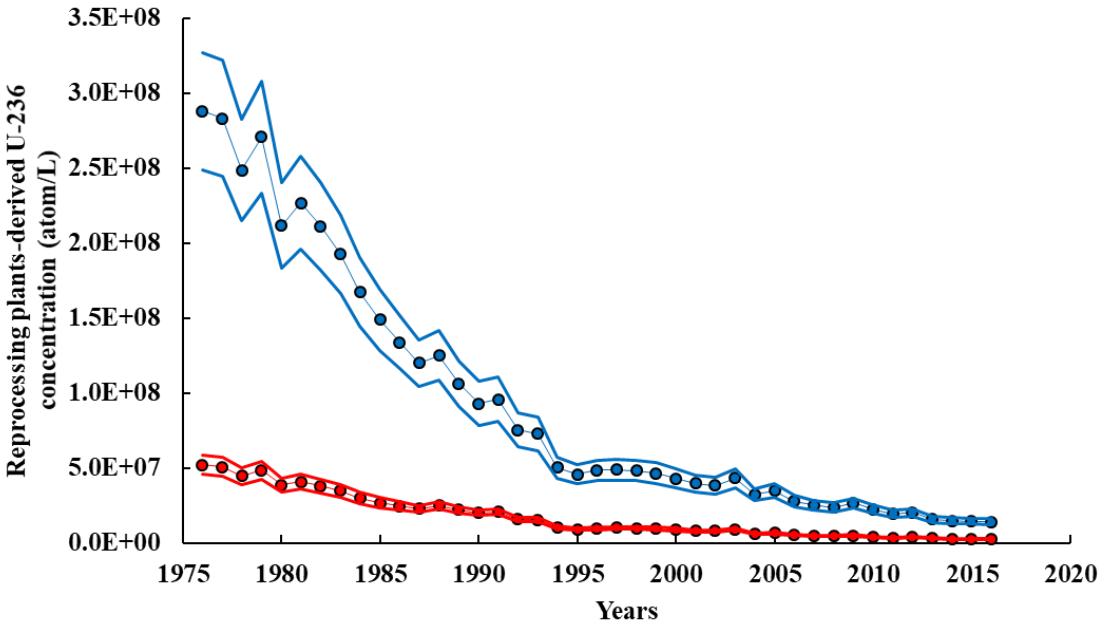

Fig. S1. The input function of Norwegian Coastal Current (NCC) (blue) and Norwegian Atlantic Current (NwAC) (red) in the entrance of the Arctic Ocean during 1976 – 2016 (dots with thin line) with

uncertainties (thick lines) (Christl et al., 2015; Casacuberta et al., 2018; Castrillejo et al., 2020; Wefing et al., 2021); and from Norwegian Atlantic Current (NwAC)

References

Casacuberta, N., Christl, M., Vockenhuber, C., Wefing, A.-M., Wacker, L., Masqué, P., Synal, H.-A., van der Loeff, M.R., 2018. Tracing the three Atlantic branches entering the Arctic Ocean with ^{129}I and ^{236}U. Journal of Geophysical Research: Oceans 123, 6909–6921. https://doi.org/10.1029/2018JC014168.

Castrillejo, M., Witbaard, R., Casacuberta, N., Richardson, C.A., Dekker, R., Synal, H.-A., Christl, M., 2020. Unravelling 5 Decades of Anthropogenic ^{236}U Discharge from Nuclear Reprocessing Plants, Sci. Total Environ. 717, 137094, https://doi.org/10.1016/j.scitotenv.2020.137094, 2020.

Christl, M., Casacuberta, N., Vockenhuber, C., Elsässer, C., Bailly du Bois, P., Herrmann, J., Synal, H. A., 2015. Reconstruction of the ^{236}U input function for the Northeast Atlantic Ocean: Implications for ^{129}I/^{236}U and ^{236}U/^{238}U-based tracer ages. Journal of Geophysical Research: Oceans 120, 7282–7299. https://doi.org/10.1002/2015JC011116.

Lin, M., Qiao, J.X., Hou, X.L., Golser, R., Hain, K., Steier, P., 2021. On the Quality Control for the Determination of Ultratrace-Level ^{236}U and ^{233}U in Environmental Samples by Accelerator Mass Spectrometry. Analytical chemistry 93, 3362 – 3369. https://doi.org/10.1021/acs.analchem.0c03623.

Qiao, J.X., Hou, X.L., Steier, P., Nielsen, S., Golser, R., 2015. Method for ^{236}U determination in seawater using flow injection extraction chromatography and accelerator mass spectrometry. Anal. Chem. 87, 7411–7417. https://doi.org/10.1021/acs.analchem.5b01608.

Wefing, A.-M., Casacuberta, N., Christl, M., Gruber, N., Smith, J.N., 2021. Circulation timescales of Atlantic Water in the Arctic Ocean determined from anthropogenic radionuclides. Ocean Science 17, 111 -129. https://doi.org/10.5194/os-17-111-2021.

Paper II

Tracing Atlantic water transit time in the subarctic and Arctic Atlantic using ^{99}Tc-^{233}U-^{236}U

Gang Lin[a], Jixin Qiao[a,*], Peter Steier [b], Magnús Danielsen[c], Kjartan Guðnason[d], Hans Pauli Joensen[e], Colin A. Stedmon[f]

[a]Department of Environmental and Resource Engineering, Technical University of Denmark, DK-4000 Roskilde, Denmark

[b]VERA Laboratory, Faculty of Physics, Isotope Physics, University of Vienna, Währinger Straße 17, A-1090 Vienna, Austria

[c]Marine and Freshwater Research Institute, Iceland

[d]Icelandic Radiation Safety Authority, Iceland

[e]University of the Faroe Islands, FO - 110 Tórshavn, Faroe Islands

[f]National Institute of Aquatic Resources, Technical University of Denmark, Kemitorvet, 2800 Kgs. Lyngby, Denmark

Science of the Total Environment 851 (2022) 158276

Contents lists available at ScienceDirect

Science of the Total Environment

journal homepage: www.elsevier.com/locate/scitotenv

Tracing Atlantic water transit time in the subarctic and Arctic Atlantic using ^{99}Tc-^{233}U-^{236}U

Gang Lin [a], Jixin Qiao [a,*], Peter Steier [b], Magnús Danielsen [c], Kjartan Guðnason [d], Hans Pauli Joensen [e], Colin A. Stedmon [f]

[a] Department of Environmental and Resource Engineering, Technical University of Denmark, DK-4000 Roskilde, Denmark
[b] VERA Laboratory, Faculty of Physics, Isotope Physics, University of Vienna, Währinger Straße 17, A-1090 Vienna, Austria
[c] Marine and Freshwater Research Institute, Iceland
[d] Icelandic Radiation Safety Authority, Iceland
[e] University of the Faroe Islands, FO-110 Tórshavn, Faroe Islands
[f] National Institute of Aquatic Resources, Technical University of Denmark, Kemitorvet, 2800 Kgs. Lyngby, Denmark

HIGHLIGHTS

- New ^{99}Tc^{-233}U-^{236}U radiotracer approach to estimate Atlantic water transit time.
- Time-dependent ratios of ^{99}Tc and ^{236}U from reprocessing discharge applied.
- Reprocessing plants ^{236}U is isolated from global fallout using ^{233}U.
- Atlantic water transit times from Sellafield to Greenland coast are 16–22 years.

GRAPHICAL ABSTRACT

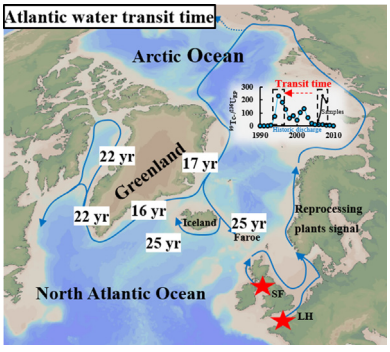

ARTICLE INFO

Editor: Jay Gan

Keywords:
^{99}Tc
^{233}U
^{236}U
Atlantic water
Transit time
Greenland-Iceland-Faroe Islands coast

ABSTRACT

The pathway and transport time of Atlantic water passing northern Europe can be traced via anthropogenic radioisotopes released from reprocessing of spent nuclear fuels at Sellafield (SF) and La Hague (LH). These reprocessing derived radioisotopes, with extremely low natural background, are source specific and unique fingerprints for Atlantic water. This study explores a new approach using ^{99}Tc-^{233}U-^{236}U tracer to estimate the transit time of Atlantic water in the coast of Greenland. We isolate the reprocessing plants (RP) signal of ^{236}U ($^{236}U_{RP}$) by incorporating ^{233}U measurements and combine this with ^{99}Tc which solely originates from RP, to estimate the transit time of Atlantic water circulating from Sellafield to the coast of Greenland-Iceland-Faroe Islands. Both being conservative radioisotopes, the temporal variation of ^{99}Tc/$^{236}U_{RP}$ ratio in Atlantic water is only influenced by their historic discharges from RP, thus ^{99}Tc/$^{236}U_{RP}$ can potentially be a robust tracer to track the transport of Atlantic water in the North Atlantic-Arctic region. Based on our observation data of ^{99}Tc-^{233}U-^{236}U in seawater and the proposed ^{99}Tc/$^{236}U_{RP}$ tracer approach, Atlantic water transit times were estimated to be 16–22, 25 and 25 years in the coast of Greenland, Iceland and Faroe Island, respectively. Our estimates from northeast Greenland coastal waters agree with earlier results (17–22 years). Therefore, this work provides an independent approach to estimate Atlantic water transit time with which to compare estimates from ocean modelling and other radiotracer approaches.

* Corresponding author.
E-mail address: jiqi@dtu.dk (J. Qiao).

http://dx.doi.org/10.1016/j.scitotenv.2022.158276
Received 20 May 2022; Received in revised form 18 August 2022; Accepted 21 August 2022
Available online 25 August 2022

1. Introduction

Atlantic water plays a key role in the Arctic climate due to the transport of entrained heat from lower latitudes (Muilwijk et al., 2018). Atlantic water enters the Arctic through the Fram Strait and Barents Sea, and exits along East Greenland coast. Variations in the properties and intensity of the Atlantic inflow influences sea-ice formation and melt, hereby effecting spatial and vertical distribution of heat and salt (and freshwater) in the region, which has a great potential to influence global circulation and climate (Polyakov et al., 2017; Halloran et al., 2020). Similarly, changes in circulation and stratification patterns have the potential to influence the marine food web, by altering nutrient supply (Hátún et al., 2017) and by supporting migration of species into new areas (Carscadden et al., 2013; Hátún et al., 2016).

Anthropogenic radionuclides (such as ^{90}Sr, ^{137}Cs, ^{99}Tc, ^{129}I and ^{236}U) emitted from the European reprocessing plants (RP) at Sellafield (SF) and La Hague (LH) are useful tracers for Atlantic water in the Arctic Ocean (Aarkrog et al., 1987; Dahlgaard, 1994; Hou et al., 2000; Smith et al., 2011, 2021; Casacuberta et al., 2014, 2018; Wefing et al., 2019, 2021), as Arctic seawater has contributions from various sources (Atlantic water, Pacific water and freshwater), and only Atlantic water is tagged with RP derived radioisotopes signals. ^{90}Sr and ^{137}Cs are good examples of RP specific marine tracers (Dahlgaard, 1995a; Smith et al., 2011; Rozmaric et al., 2022) as both were released in significant amounts during 1970s – 1980s. In this light the RP signal of ^{90}Sr and ^{137}Cs from SF can be used to estimate Atlantic water transit time in the Arctic and subpolar region (Dahlgaard, 1995a; OSPAR, 2019). However, their application is limited by their relatively short half-lives (^{90}Sr t½ = 28.8 yr and ^{137}Cs t½ = 30.2 yr). In contrast, long-lived radioisotopes such as ^{233}U, ^{236}U, ^{129}I and ^{99}Tc, can trace ocean circulation over longer time scales. In addition, ^{137}Cs is readily attached to particles, thereby scavenged from water columns into sediments (distribution coefficient (K_d) for ^{137}Cs between sediment and seawater is 2000. This also urges us to explore other more conservative radioisotopes to trace water mass movement, such as ^{99}Tc (K_d = 100), ^{129}I (K_d = 200) and U isotopes (K_d = 500) (International Atomic Energy Agency IAEA, 2004).

In recent years, ^{236}U (t½ = 23.4 Myr) has been recognized as a powerful Atlantic water tracer, especially when combing with another long-lived RP derived tracer ^{129}I (t½ = 15.7 Myr) (Christl et al., 2012; Casacuberta et al., 2014, 2016, 2018; Wefing et al., 2019, 2021). Several studies demonstrated the successful application of ^{236}U—^{129}I tracer pair to identify and trace the flow of water from the North Atlantic into the Arctic Ocean. For instance, the transit times of Atlantic water in the Arctic surface layer from the entrance of the Arctic Ocean (74°N, 19°E) have been reported in the range of 3–12 years in the Nansen Basin, 9–16 years in the Amundsen Basin, 2–14 years in the Makarov Basin, 14–20 years in the Canada Basin and 12–17 years in the Fram Strait via the combination of ^{129}I and ^{236}U as tracers (Wefing et al., 2021).

Anthropogenic ^{236}U is mainly derived from RP (115–200 kg, with majority from SF) and global fallout (GF, 900–1400 kg) (Steier et al., 2008; Sakaguchi et al., 2009, 2012). The reconstructed discharge of ^{236}U from RP showed a gradually decreasing trend since the 1970s, varying within 1–31.3 kg/yr at SF during 1971–2018, and 0.2–2.1 kg/yr at LH during 1967–2017 (Fig. S1) (Castrillejo et al., 2020). Due to rapid atmospheric mixing, GF-derived ^{236}U is a ubiquitous source affecting all regions in the world with a gradually decreasing deposition after the 1970s (Fig. S2) (Christl et al., 2015). Previous studies using ^{236}U as an oceanic tracer have assumed GF ^{236}U contribution to be constant after 1990 (Wefing et al., 2019, 2021) and this may introduce uncertainties in the transit time estimation.

The development of advanced accelerator mass spectrometry (AMS) technique allows the quantification of another long-lived uranium isotope, ^{233}U (t½ = 0.159 Ma) in environmental samples. Anthropogenic ^{233}U is primarily produced through the ^{235}U (n,3n) ^{233}U reaction by fast neutrons or directly by ^{233}U-fueled devices in thermonuclear explosions. The ^{233}U production in nuclear power reactors or reprocessing plants is negligible (Hain et al., 2020). Therefore, the ^{233}U/^{236}U ratios in the RP and GF endmembers are very different, and the coupling of ^{233}U with ^{236}U signature presents the possibility to distinguish between the two different ^{236}U source terms, RP and GF through a linear mixing model (detailed explanation see Section 2.7, Hain et al., 2020; Qiao et al., 2020a). Although previous study shows that sediment in the shallow European Shelf Seas acts as minor sinks of ^{236}U (Periáñez et al., 2018), isotopic fractionate between ^{233}U and ^{236}U is not expected to occur as any alternations in biogeochemical behavior will equally affect all the isotopes of uranium, highlighting the robustness of ^{233}U—^{236}U pair in oceanic tracer studies.

Radioisotopes from the two RPs in Europe have been released at different concentrations in different years, and this can be used to trace Atlantic water transit times. Combining estimates of RP-derived ^{236}U with another conservative RP-derived radioisotope with a different discharge profile, enables one to use their ratios to determine Atlantic water transit time. This is because the ratios of RP-derived isotopes in Atlantic water is only dependent on the RP discharge histories and not affected by the dilution of other waters along the transport. This has been demonstrated earlier with coupled measurements of ^{129}I and ^{236}U (Wefing et al., 2021). However, ^{129}I is primarily released from LH, whereas ^{236}U is predominantly released from SF (Fig. S1). Different transport passage and transit times of Atlantic water to Arctic from LH compared with from SF may complicate the application. It is therefore, relevant to consider other source specific radioisotopes with which to compare current estimates of Atlantic water transit times.

Since the early 1980s, the long-lived and conservative ^{99}Tc (t½ = 0.211 Myr) has been applied to trace Atlantic water transport in the Nordic seas and Arctic Ocean (Aarkrog et al., 1987; Kershaw et al., 1999; Karcher et al., 2004). ^{99}Tc has a dominant source (> 90 %) from RP (cumulative emission of 1720 TBq from SF and 154 TBq from LH, Fig. S1) (Shi et al., 2012) and only a minor contribution from GF (140 TBq) and other sources such as nuclear power plants, medical applications of ^{99m}Tc and nuclear accidents (e.g., Chernobyl (ca. 0.75 TBq ^{99}Tc) and Fukushima) (Shi et al., 2012). The discharge histories of ^{99}Tc from RP are characterized by two peak-release periods in 1970–1980 and 1994–2003, respectively, both were related to the operation of SF (Fig. S1). Therefore, the combination of ^{99}Tc and RP-derived ^{236}U has a potential to assess transport time scales of Atlantic water in the Arctic Ocean while eliminating uncertainties from GF ^{236}U and avoiding the reconstruction of combined RP ^{236}U input function from SF and LH contributions based on certain assumptions for the water mixing in the North Sea and Norwegian Sea.

In this study, we aim to apply a ^{99}Tc-^{233}U-^{236}U approach to estimate the transit time of Atlantic water across the Nordic Seas to the coast of Greenland, Iceland and Faroe Islands. The approach isolated RP-derived ^{236}U signal through ^{233}U measurement avoids potential interference from the GF ^{236}U signal, which is supplied in Pacific water exiting the Arctic Ocean and in glacial and sea-ice meltwater. In addition, some ^{137}Cs and ^{90}Sr seawater data obtained from an earlier marine radioactivity monitoring program were compiled to support our interpretation on the potential current transport in the study area.

2. Material and methods

2.1. Study area and sampling

The study area includes the coastal waters of Greenland, southern Iceland and the Faroe Islands (Fig. 1A). The eastern and western Greenland coastal waters are dominated by the southwards flowing East Greenland Current and northward flowing West Greenland Current, respectively. East and West Greenland Currents mainly consist of outflowing Polar Surface Water and returning Atlantic waters. In the southeast of the region, Atlantic mode water directly transports waters from the North Atlantic to the southern coast of Iceland and Faroe Islands (Daniault et al., 2016). One branch of direct Atlantic water moves westward to the southeastern Greenland coast, while another branch water continuously transports to the Norwegian Sea (Daniault et al., 2016).

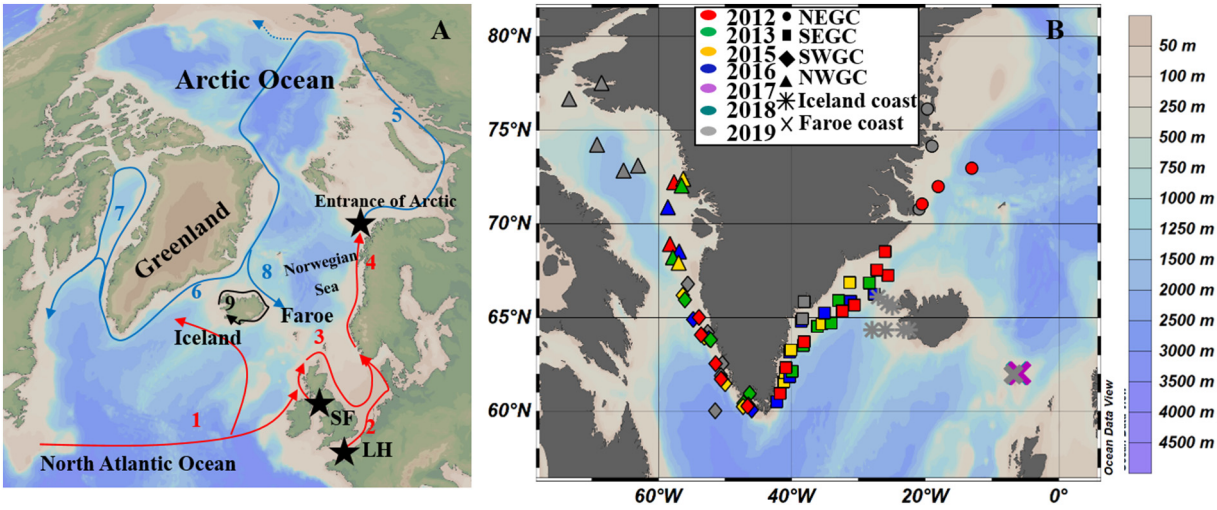

Fig. 1. The selected surface currents transporting RP signal in the Arctic-North Atlantic region (A). The sites of sampling location (B). Currents are labelled by the number: 1. North Atlantic Current; 2. La Hague branch water; 3.Sellafield branch water; 4. Norwegian Coastal Current; 5. Norwegian Coastal Current in the Arctic Ocean; 6. East Greenland Current; 7. West Greenland Current; 8. A branch of East Greenland Current to the northern coast of Iceland (Casanova-Masjoan et al., 2020); 9. The coastal current of Iceland. Red lines refer to the transport of surface Atlantic water in the North Atlantic Ocean, and blue lines refer to the transport of surface Atlantic water in the Arctic Ocean and Greenland coast. NEGC: north-eastern Greenland coast; SEGC: south-eastern Greenland coast; SWGC: south-western Greenland coast; NWGC: north-western Greenland coast.

Sampling was carried out in 1991–1999 and 2012–2019 through the collaboration of Technical University of Denmark, Marine and Freshwater Research Institute, Iceland, and University of Faroe Islands. In total of 96 seawater samples were collected at 0–10 m depth along the coasts of Greenland-Iceland-Faroe in 2012–2019 (Fig. 1B), and processed for ^{99}Tc, ^{233}U, ^{236}U and ^{238}U analysis. Twelve additional samples were collected earlier in Faroe Islands coastal waters (1991–1999), and prepared for ^{90}Sr and ^{137}Cs measurement within a marine radioactivity monitoring program at Technical University of Denmark (DTU). ^{233}U–^{236}U-^{238}U measurements from Greenland coastal waters during 2012–2016 have been published earlier (Qiao et al., 2020a). More detailed sample information is provided in Table S1 (Supporting Information).

2.2. Standards and materials

Uranium standard solution (1.000 g/L in 2 mol/L HNO_3) was purchased from NIST (Gaithersburg, MD) and used as a standard for ^{238}U measurement after dilution with 0.5 mol/L HNO_3. ^{99m}Tc tracer was obtained from 2 to 4 GBq commercial ^{99}Mo-^{99m}Tc generators (Amersham, UK) and was purified using alumina cartridges. All reagents used in the experiment were of analytical reagent grade and prepared using ultra-pure water (18 MΩ·cm). UTEVA resin (100–150 μm particle size) was purchased from Triskem International, Bruz, France and packed in 2-mL Econo-Columns (0.7 cm i.d. × 5 cm length, Bio-Rad Laboratories Inc., Hercules, CA) for the chemical purification of uranium isotopes. Anion exchange chromatography (AG 1 × 4 resin, 100–150 mesh particle size, Bio-Rad Laboratory, USA) was used to concentrate ^{99}Tc from seawater samples.

2.3. Determination of ^{99}Tc

The determination of ^{99}Tc in seawater is based on the procedure reported earlier (Chen et al., 1994), which is briefly described below. After spiking with ^{99m}Tc as a yield monitor, each seawater (ca. 200 L) was preconcentrated using anion exchange chromatography (AG 1 × 4 resin). ^{99}Tc was further purified using a second anion exchange chromatographic separation followed by solvent extraction (5 % triisooctylamine (TIOA)-xylene). After the source preparation using electrodeposition, the activity of ^{99}Tc was measured using an anticoincidence gas flow Geiger-Müller (GM) counter (Risø, Denmark). The chemical yields of technetium for the whole procedure were measured by counting the ^{99m}Tc tracer using a NaI detector.

2.4. Determination of ^{233}U, ^{236}U and ^{238}U

The radiochemical separation of uranium isotopes from seawater samples was performed according to earlier studies (Qiao et al., 2015; Lin et al., 2021a). To 5–10 L of filtered seawater, 14 M HNO_3 was added to adjust pH = 2 to release uranium ion from the uranyl carbonate complexes. 500–1000 mg Fe^{3+} (0.05 g/mL purified $FeCl_3$ solution using UTEVA® resin) was added, and the sample was vigorously stirred (10 min) with air to expel the dissolved CO_2. pH value was adjusted to 8–9 through 25 % $NH_3{\cdot}H_2O$ solution for co-precipitating iron hydroxides with uranium. The sample was kept still for 1–2 h to allow the iron hydroxide co-precipitate to settle down. The supernatant was decanted and the remaining sludge was centrifuged at 3000 rpm for 10 min. The obtained precipitate was dissolved with 14 M HNO_3 and then diluted to 3 M HNO_3. A 2-mL UTEVA® resin column was preconditioned with 20 mL of 3 M HNO_3 and used for the chromatographic separation of uranium. The column was rinsed with 40 mL of 3 M HNO_3 and 20 mL of 6 M HCl, respectively. Uranium was eluted by 10 mL of 0.025 M HCl. 2 mg of Fe^{3+} was added to the eluate to form iron hydroxide co-precipitate after adjusting the pH to 8–9 with 25 % $NH_3{\cdot}H_2O$. The precipitate was separated via centrifugation, dried in an oven at 90 °C for 4 h, and combusted in a muffle furnace at 800 °C for 12 h. After cooling, the combusted sample was pressed into an aluminum sputter target holder for ^{233}U/^{238}U and ^{236}U/^{238}U measurement. The measurement was carried out by accelerate mass spectrometry (AMS) at the Vienna Environmental Research Accelerator (VERA) facility, in the University of Vienna (Steier et al., 2010; Hain et al., 2020).

To monitor the laboratory background (Lin et al., 2021a), one procedure blank was processed with the same procedure for every seven seawater samples. All chemical separations were carried out in a laminar flow bench with the use of purified chemicals and carefully cleaned (with acid boiling) glassware for reducing the background level. The ^{233}U (0) and ^{236}U (< 0.1) count rates of all blank samples were significantly low (< 2 %) compared to those in seawater samples. The uncertainties of ^{233}U and ^{236}U were expanded uncertainties (with a coverage factor k = 1) including the measurement uncertainties of ^{238}U contents, ^{233}U/^{238}U and ^{236}U/^{238}U in the eluates of seawater and blank samples. The detailed description was reported in the previous work (Lin et al., 2021a).

^{238}U concentration in the raw seawater and the U eluate from UTEVA column was diluted with 0.5 M HNO_3 and measured by the inductively coupled plasma mass spectrometry (ICP-MS) (ICP-QQQ 8800, Agilent) using indium or bismuth as an internal standard (Qiao and Xu, 2018).

2.5. Determination of ^{90}Sr

The detailed procedure of ^{90}Sr in seawater is reported in a previous study (Chen et al., 2002), and it is briefly described below. The ^{85}Sr tracer and $SrCl_2{\cdot}H_2O$ carrier were added into 45 L seawater with stirring for 10 min. NaOH was added to adjust pH = 8–10. After boiling, 2 M $(NH_4)_2CO_3$ was added with stirring to form $SrCO_3/CaCO_3$ precipitation. After siphoning off the supernatant, the $SrCO_3/CaCO_3$ precipitate was dissolved in 4 M HNO_3 followed by addition of Fe^{3+}. 6 M NaOH was then added to a concentration of 0.5 M NaOH to separate Ca (as $Ca(OH)_2$) from Sr. After centrifuging, 0.2 M NaOH was used to wash the $Ca(OH)_2$ precipitate. The supernatant and washes were combined and heated at 250 °C for 1 h. Na_2CO_3 was added to precipitate Sr as $SrCO_3$ which was thereafter dissolved with 8 M HNO_3. The $Ca(OH)_2$ and $SrCO_3$ precipitation were repeated to ensure a sufficient remove of Ca. The finally obtained $SrCO_3$ precipitate was dissolved with 6 M HNO_3, and after addition of $FeCl_3$, adjusted to pH 10 with NaOH. The supernatant was added with Y^{3+} carrier and Ba^{2+} carrier after centrifuging. After waiting (approximately 3 weeks) for the ingrowth of ^{90}Y (daughter radionuclide of ^{90}Sr), Sr and Ba in the sample solution were separated from Y via $BaSO_4$ and $SrSO_4$ precipitation. Y was finally prepared as $Y_2(C_2O_4)_3$ for the ^{90}Y radioactivity measurement using an anti-coincident gas flow GM counter (Risø, Denmark). The ^{90}Sr radioactivity concentration in the sample was thereby obtained via ^{90}Y based on the decay equilibrium.

2.6. Determination of ^{137}Cs

^{137}Cs determination in seawater is based on a previous report (Qiao et al., 2020b). To 45 L of filtered seawater, 14 M HNO_3 was added to acidify seawater to pH = 2. 30 mg of Cs carrier (CsCl) and 50 mg of ammonium molybdophosphate (AMP) were added with stirring for 1 h. After allowing the AMP to settle overnight and discarding the supernatant, the slurry was filtered and dried in an oven under 105 °C. The dried AMP powder was measured for ^{137}Cs by gamma spectrometry using high-purity germanium detectors. The Cs chemical yield was calculated through weighing the AMP powder (Eq. (1)) and results indicated high recovery (> 95 %).

$$Yield_{Cs} = \frac{Final\ weight_{AMP\ powder}}{Initial\ weight_{AMP\ powder}} \times 100\% \quad (1)$$

2.7. Estimation of reprocessing plants contribution to ^{236}U

The contributions of RP and GF in ^{236}U can be distinguished through the atomic ratio of $^{233}U/^{236}U$ and the following Eqs. (2)–(3) resolved from a two-endmember mixing algorithm (Qiao et al., 2020a).

$$P_{RP} = \frac{R_{GF} - R_S}{R_{GF} - R_{RP}} \quad (2)$$

$$^{236}U_{RP} = {}^{236}U_S \times P_{RP} \quad (3)$$

where P_{RP} is the fraction of RP-derived ^{236}U in the seawater sample (Table S1); R_S is the measured $^{233}U/^{236}U$ atomic ratio in the seawater sample; R_{RP} is the $^{233}U/^{236}U$ atomic ratio in RP endmember (1×10^{-7}) (HELCOM MORS Discharge database, 2020); R_{GF} is the $^{233}U/^{236}U$ atomic ratio in GF endmember ($1.4 \pm 0.15 \times 10^{-2}$) (Hain et al., 2020); $^{236}U_{RP}$ is the RP-derived ^{236}U concentration in the seawater sample, $^{236}U_S$ is the measured ^{236}U concentration in the seawater sample.

2.8. Estimation of Atlantic water transit times based on $^{99}Tc/^{236}U_{RP}$ ratios

The temporal change of $^{99}Tc/^{236}U_{RP}$ ratios is established based on the ^{99}Tc and ^{236}U annual discharges from SF and LH, considering a 2-year lag time for the SF release to be mixed with LH release during transport northwards along the Norwegian coast (Fig. 2). The ^{236}U discharges from SF and LH were based on the data reported by Castrillejo et al. (2020). The discharges of ^{99}Tc from SF and LH were compiled from several earlier works (Jackson, 2000; OSPAR, 2019; Shi et al., 2012). Based on our hypothesis that $^{99}Tc/^{236}U_{RP}$ ratio tagged in the Atlantic water is only dependent on their release pattern from RP, by comparing the measured $^{99}Tc/^{236}U_{RP}$ in seawater samples with the established temporal variation of $^{99}Tc/^{236}U_{RP}$ in the RP release, we could allocate the source year of the Atlantic water. However, the temporal variation of $^{99}Tc/^{236}U_{RP}$ in RP release has several peaks in 1993–2005 (Fig. 2). To constrain the source year, a time series of $^{99}Tc/^{236}U_{RP}$ measurements from the same region can be used to compare with the temporal trend of $^{99}Tc/^{236}U_{RP}$ in the RP discharge (Fig. 2).

3. Results

3.1. The temporal and spatial distribution of radioisotopes in the coastal waters of Greenland, Iceland and Faroe Islands

To facilitate the data interpretation, we divided the study region into four areas around Greenland: the north-eastern Greenland coast (NEGC), the south-eastern Greenland coast (SEGC), the south-western Greenland coast (SWGC) and the north-western Greenland coast (NWGC); and Icelandic and Faroe Island coastal waters (Fig. 3, Table 1). ^{99}Tc concentrations in surface waters ranged from 0.01 to 0.94 Bq/m^3 during 2012–2019 (Fig. 3A). Highest values were detected in the SEGC in 2013 and NEGC in 2019 while the lowest concentrations were measured in NWGC in 2012 and Faeroe Island waters in 2019. The range of ^{236}U concentrations (8.98–120.27 $\times 10^6$ atom/L) from the coastal waters of Greenland and Iceland in 2019 and Faroe Islands waters in 2016–2019 were comparable with reported earlier results (7.38–128.60 $\times 10^6$ atom/L) for Greenlandic waters in 2012–2016, but a narrower range of ^{233}U (4.10–23.66 $\times 10^4$ atom/L) was reported for the earlier study (^{233}U concentrations: 2.64–45.70 $\times 10^4$ atom/L) (Fig. 3B and C) (Qiao et al., 2020a). And the range of $^{233}U/^{236}U$ ratios obtained in this work are 0.05–1.71 $\times 10^{-2}$ (Fig. 3D). Based on the Eq. (2), the RP fractions of ^{236}U can be calculated and were for Greenland samples (0.18–0.92 during 2012–2019), Iceland (0.24–0.64 in 2019) and Faroe Islands (0–0.96 during 2016–2019). For some samples, the ratios of $^{233}U/^{236}U$ are even higher than the GF endmember value ($1.40 \pm 0.15 \times 10^{-2}$). This may be induced by either uncertainties from measurement or the spatiotemporal variation of $^{233}U/^{236}U$ ratios in GF signals as observed in other studies (Qiao et al., 2022; Lin et al., 2021b). The ratio of $^{233}U/^{236}U$ in GF endmember was estimated from corals and sediments in the low-mid latitudes (Hain et al., 2020), and the nuclear weapons testing in the high latitude (i.e. Novaya Zemlya Island in the Arctic) may also potentially contribute to ^{233}U budget to the Arctic Ocean (Chamizo et al., 2022), resulting in such variability of $^{233}U/^{236}U$ ratios in different latitudes belts.

3.2. The temporal and spatial trends in $^{99}Tc/^{236}U_{RP}$ atomic ratios

$^{99}Tc/^{236}U_{RP}$ atomic ratios ranged from 2 to 525 during 2012–2019 in Greenland coastal waters. (Fig. 3E, Table 2). The highest average value was obtained in NEGC in 2019, and the lowest values were seen in NWGC in the years of 2012. In general, $^{99}Tc/^{236}U_{RP}$ atomic ratios show a gradual decrease trend from NEGC to NWGC in the same year during 2012–2019. In contrast, $^{99}Tc/^{236}U_{RP}$ ratios in Icelandic and Faroe Islands coastal waters were much less variable, ranging between 26 and 94 and 2–139, respectively (Fig. 3E, Table 2).

It is worth noting that there is extremely low $^{99}Tc/^{236}U_{RP}$ atomic ratio in SEGC (2013, 2 ± 1) and Faroe Island (2019, 2 ± 1) due to the

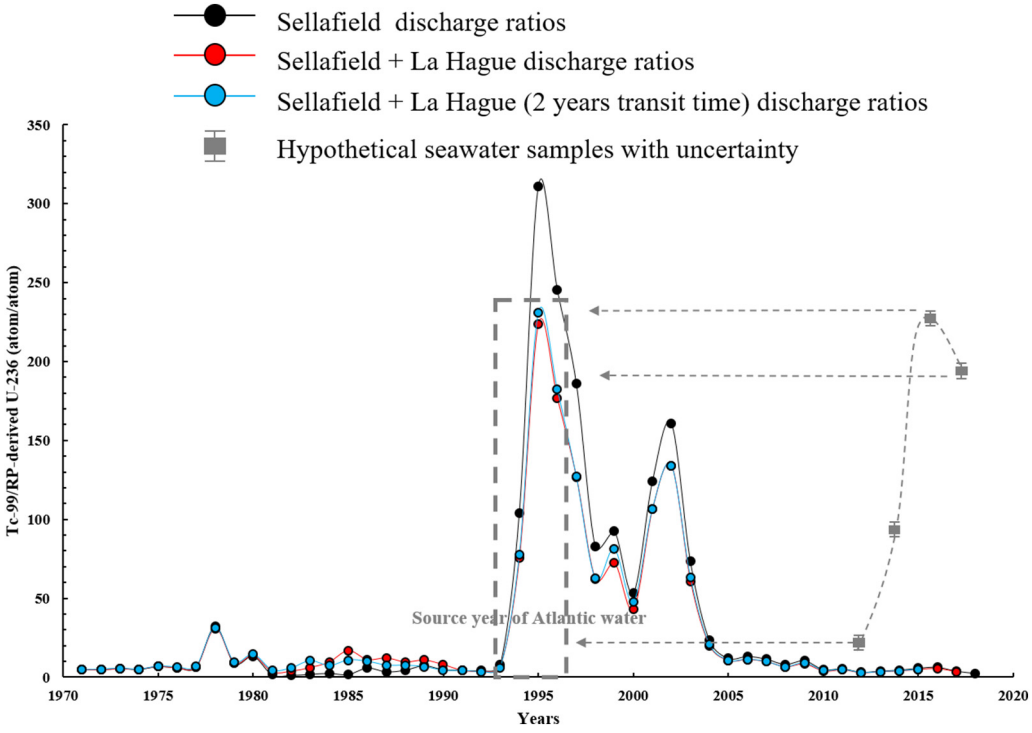

Fig. 2. An example of the approach to estimate Atlantic water source year by comparing times series $^{99}Tc/^{236}U_{RP}$ atomic ratios in samples from a specific region with the temporal changes of ratios in the RP discharge from Sellafield (black line), Sellafield and La Hague (red line), Sellafield and La Hague (with 2 year delay to account for transport time from SF to LH) (light blue line) discharge ratios. The year in the x-axis corresponds to the year of radioactive release from Sellafield. In this figure, the $^{99}Tc/^{236}U_{RP}$ atomic ratios in seawater samples are hypothetical data for better explanation.

significantly high concentration of $^{236}U_{RP}$ (117.7 ± 15.8 and 115.9 ± 7.9 × 10^6 atom/L, respectively). This extremely high concentration of $^{236}U_{RP}$ may be derived from another transport pathway (see Section 4.2 in detail), thus was not included in the initial estimation for Atlantic water transit time.

(data marked with * are from Qiao et al., 2020a, data marked with # are presented as value ± uncertainty as only a single sample was obtained in the corresponding region)

3.3. The temporal distribution of ^{90}Sr and ^{137}Cs in the coastal water of Faroe Islands

The continuous observation of ^{90}Sr and ^{137}Cs was performed in same location of Faroe Islands coast during 1991–1999. ^{90}Sr concentrations in surface waters varied within 0.55–1.44 Bq/m^3, while ^{137}Cs concentrations ranged from 1.47 to 9.96 Bq/m^3 (Table S1). The lowest concentration of ^{90}Sr (0.55 ± 0.0003 Bq/m^3) was measured in 1992, and the highest

Table 1
^{99}Tc, ^{233}U and ^{236}U average concentrations and $^{233}U/^{236}U$ average ratios with standard deviations (SD) or uncertainties in the coastal water of Greenland, Iceland and Faroe Islands ("average" refers to arithmetic mean).

Station	^{99}Tc (Bq/m^3)	^{233}U (× 10^4 atom/L)	^{236}U (× 10^6 atom/L)	$^{233}U/^{236}U$ (× 10^{-2})
The NEGC in 2012	0.14 ± 0.03 (*n* = 3)	3.8 ± 1.2*#	11.1 ± 3.0* (n = 3)	0.42 ± 0.14*#
The SEGC in 2012	0.13 ± 0.06 (*n* = 8)	9.3 ± 2.5*#	16.3 ± 7.2* (n = 8)	0.32 ± 0.09*#
The SWGC in 2012	0.13 ± 0.07 (*n* = 5)	5.3 ± 1.0* (n = 5)	26.5 ± 4.5* (n = 5)	0.21 ± 0.07* (n = 5)
The NWGC in 2012	0.02 ± 0.01 (*n* = 2)	7.2 ± 3.4* (*n* = 2)	22.1 ± 1.6* (*n* = 2)	0.34 ± 0.18* (*n* = 2)
The SEGC in 2013	0.25 ± 0.35 (*n* = 7)	15.8 ± 14.4* (n = 7)	48.0 ± 39.7* (n = 7)	0.42 ± 0.38* (n = 7)
The SWGC in 2013	0.14 ± 0.06 (n = 5)	7.7 ± 3.8* (n = 5)	29.8 ± 11.1* (n = 5)	0.26 ± 0.05* (n = 5)
The NWGC in 2013	0.10 ± 0.02 (*n* = 2)	13.6 ± 1.2* (n = 2)	26.2 ± 1.7* (n = 2)	0.52 ± 0.01* (n = 2)
The SEGC in 2015	0.09 ± 0.04 (*n* = 6)	9.0 ± 1.9* (n = 6)	18.5 ± 4.9* (n = 6)	0.50 ± 0.09* (n = 6)
The SWGC in 2015	0.10 ± 0.03 (*n* = 4)	9.0 ± 1.2* (*n* = 4)	25.7 ± 6.6* (n = 4)	0.37 ± 0.12* (n = 4)
The NWGC in 2015	0.10 ± 0.02 (*n* = 2)	6.5 ± 1.4* (n = 2)	22.2 ± 4.6* (*n* = 2)	0.29 ± 0.00* (n = 2)
The SEGC in 2016	0.12 ± 0.09 (n = 6)	4.5 ± 1.4* (n = 6)	13.9 ± 3.3* (*n* = 7)	0.33 ± 0.05* (n = 6)
The SWGC in 2016	0.12 ± 0.06 (*n* = 4)	9.5 ± 2.8* (*n* = 4)	15.5 ± 4.0* (n = 4)	0.61 ± 0.06* (n = 4)
The NWGC in 2016	0.08 ± 0.00 (n = 2)	7.7 ± 4.8* (n = 2)	16.2 ± 5.8* (n = 2)	0.45 ± 0.13* (n = 2)
The NEGC in 2019	0.17 ± 0.14 (n = 4)	11.0 ± 1.5 (n = 4)	15.5 ± 1.7 (n = 4)	0.71 ± 0.09 (n = 4)
The SEGC in 2019	0.07 ± 0.00#	8.2 ± 0.1 (n = 2)	13.3 ± 3.7 (n = 2)	0.64 ± 0.17 (n = 2)
The SWGC in 2019	0.08 ± 0.01 (n = 6)	9.0 ± 1.7 (n = 7)	14.6 ± 1.3 (n = 7)	0.62 ± 0.11 (n = 7)
The NWGC in 2019	0.07 ± 0.04 (n = 4)	9.3 ± 1.9 (*n* = 5)	15.7 ± 1.6 (n = 5)	0.59 ± 0.11 (n = 5)
Iceland in 2019	0.05 ± 0.05 (n = 2)	8.4 ± 1.7 (*n* = 9)	11.1 ± 2.4 (n = 9)	0.79 ± 0.19 (n = 9)
Faroe island in 2016		4.1 ± 1.9#	11.7 ± 1.3#	0.35 ± 0.17#
Faroe island in 2017	0.04 ± 0.02 (n = 4)	11.4 ± 2.0 (n = 2)	21.5 ± 12.4 (*n* = 3)	0.49 ± 0.19 (n = 2)
Faroe island in 2018	0.04 ± 0.00#	15.4 ± 5.8 (n = 4)	16.2 ± 6.6 (n = 4)	1.07 ± 0.54 (n = 4)
Faroe island in 2019	0.02 ± 0.01 (n = 4)	7.3 ± 2.5 (n = 4)	37.4 ± 55.3 (n = 4)	0.60 ± 0.44 (n = 4)

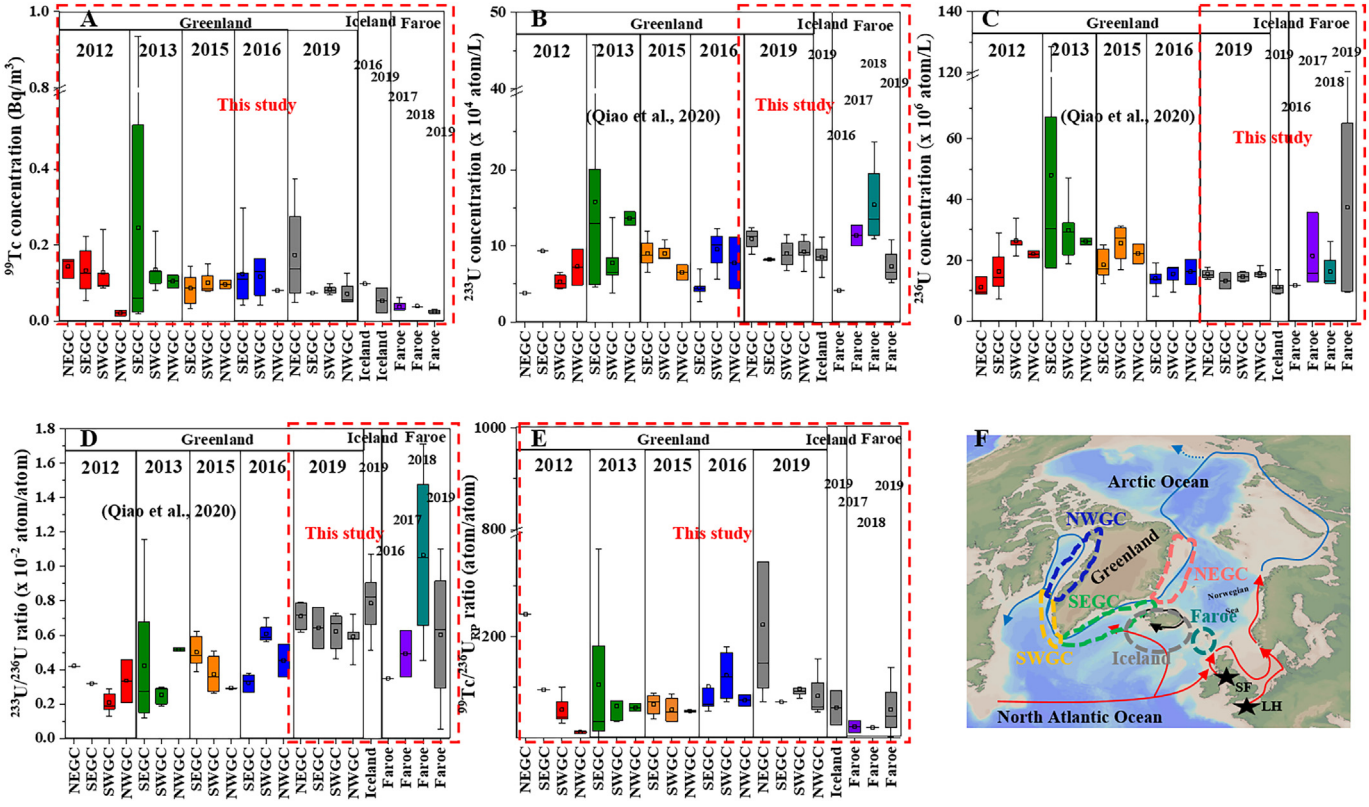

Fig. 3. The boxplot distributions of ^{99}Tc (A), ^{233}U (B) and ^{236}U (C) concentrations, ^{233}U/^{236}U atomic ratio (D), and ^{99}Tc/$^{236}U_{RP}$ atomic ratio (E) in coastal waters of Greenland, Iceland and Faroe Islands during 2012–2019, and the definition of the different areas in the study region (F). NEGC: north-eastern Greenland coast; SEGC: south-eastern Greenland coast; SWGC: south-western Greenland coast; NWGC: north-western Greenland coast. Data from Qiao et al. (2020a) are shown together with the results from this study.

value of ^{137}Cs (9.96 ± 0.43 Bq/m^3) was detected in 1997. The ^{137}Cs/^{90}Sr activity ratios were significantly higher in 1992 (4.36 ± 0.76) and 1997 (6.92 ± 0.34), compared to the other years where it remained between 1.03 and 2.21.

4. Discussion

4.1. Constraining the transit time of Atlantic water in Greenland-Iceland-Faroe Island coastal water using ^{99}Tc/$^{236}U_{RP}$ atomic ratio

Greenland coastal surface seawater is dominated by the outflowing Polar Surface Water entraining RP signal from the Norwegian Coastal Current (NCC) (Fig. 1) (Qiao et al., 2020a; Wefing et al., 2019, 2021). The use of discharge data from SF and LH enables a straightforward construction of the temporal variation of ^{99}Tc/$^{236}U_{RP}$ atomic ratio in the Atlantic water. Previous studies have reconstructed the input function in Atlantic water entering the Arctic Ocean by assuming a constant marine mixing proportion Casacuberta et al. (2018), which may introduce uncertainty in estimating transit time. However, the approach applied here is an attempt to circumnavigate this.

Based on the ^{236}U and ^{99}Tc historical data from SF and LH (Fig. S1), we calculated the temporal evolution of ^{99}Tc/$^{236}U_{RP}$ atomic ratio under three different scenarios: i) considering SF as the sole source of discharge; ii) considering both SF and LH contribute to discharge; and iii), considering both but with a 2-year transit time for SF to mix with LH discharge. For this latter scenario the discharge from SF for a given year was combined with the LH

Table 2
The estimation of Atlantic water transit time from Sellafield with ^{99}Tc/$^{236}U_{RP}$ average ratios and standard deviations (SD) or uncertainties in Greenland-Iceland-Faroe Islands coastal seawater.

Region	^{99}Tc/$^{236}U_{RP}$ average ratio in 2012	^{99}Tc/$^{236}U_{RP}$ average ratio in 2013	^{99}Tc/$^{236}U_{RP}$ average ratio in 2015	^{99}Tc/$^{236}U_{RP}$ average ratio in 2016	^{99}Tc/$^{236}U_{RP}$ average ratio in 2017	^{99}Tc/$^{236}U_{RP}$ average ratio in 2018	^{99}Tc/$^{236}U_{RP}$ average ratio in 2019	Transit time of Atlantic water (year)	Uncertainty of transit time (year)
Northeast Greenland coast (NEGC)	244 ± 61#						223 ± 205	17	
Southeast Greenland coast (SEGC)	95 ± 20#	122 ± 140 (105 ± 135)	66 ± 20	102 ± 72			71 ± 12#	16	±2
Southwest Greenland coast (SWGC)	56 ± 29	63 ± 46	56 ± 27	123 ± 53			97 ± 20	22	±2
Northwest Greenland coast (NWGC)	12 ± 3	60 ± 10	53 ± 2	74 ± 16			82 ± 49	22	±2
Iceland coast (IC)							60 ± 48	25	
Faroe Island coast (FIC)					22 ± 17	21 ± 3#	74 ± 20 (56 ± 59)	25	

Data marked with # show uncertainty due to only one data this year; data in parentheses contained the abnormal values with unexpected 236U concentrations.

discharge from two years later to account for transit between sites. Two year lag was chosen as previous work has showed that the transit times from SF and LH to the Arctic entrance were 5 and 3 years, respectively (Casacuberta et al., 2018). Fig. 2 shows how these scenarios influence the calculated temporal trend in $^{99}Tc/^{236}U_{RP}$ atomic ratios in the discharges. The ratios are comparable across these three scenarios, with two notable peaks in 1993–2000 and 2000–2005, respectively. Comparison of $^{99}Tc/^{236}U_{RP}$ atomic ratio for each sample with that reconstructed from the RP discharge allows us to constrain the source year, and the transit time of Atlantic water is estimated by aligning the time series of measurements to the discharge histories (Fig. 4).

The RP signal from SF and LH partly mixes in the North Sea and moves northward to the Arctic along the Norwegian coast (Fig. 1) (Christl et al., 2017; Casacuberta et al., 2018). The Norwegian Coastal Current carries RP signal onwards to the Barents Sea overflow and towards the Siberian shelf, whereafter it moves into the central Arctic Ocean along the Lomonosov ridge (Casacuberta et al., 2018). It dominates the RP signal input in surface seawater of the Arctic Ocean and outflows along the eastern Greenland coast (Wefing et al., 2021; Qiao et al., 2020a). Pacific water and freshwater, in contrast, carry a GF signal and also contribute to the outflow along the eastern Greenland coast.

Due to the westward water transport pathway from the northeastern Greenland coast to the northwestern Greenland coast, the samples in NEGC in same sampling years should be younger than those in other regions (namely, NEGC < SEGC < SWGC < NWGC) and this is indeed the case (Fig. 4). However, no significant statistical correlation was observed when using the annually-varied RP discharge ratios to align with our time-series observation. Instead correlations between the measurements and 3-year, 5-year and 7-year running averages of $^{99}Tc/^{236}U_{RP}$ ratios from the RP release were tested. The best correlation was obtained when using the 5-year running (i.e., the release year ±2 years) average of $^{99}Tc/^{236}U_{RP}$ ratios from the RP release. The results show that the transit times of Atlantic water reached SEGC, SWGC and NWGC are 16 ± 2, 22 ± 2 and 22 ± 2 years (R^2 = 0.73, 0.75 and 0.77, respectively) from SF (Fig. S3, Table S2). For NEGC, although correlation analysis was not possible due to limited dataset, the observed $^{99}Tc/^{236}U_{RP}$ atomic ratios appear to match well with the two peaks in 1995 and 2002 in the discharge ratios based on visual estimation, indicating a 17 years transit time (Fig. 4D). These transport time estimates agree with previous estimates based the combination of ^{129}I and ^{236}U (17–22 years) in the west Fram Strait in northeastern Greenland (Wefing et al., 2021). Our findings also confirm that the water transport from east to northwest Greenland takes 5–6 years (Dahlgaard, 1995a; Hou et al., 2000).

An anticyclonic coastal current circulates around Iceland (Logenmann et al., 2013), with a branch of East Greenland Current from the NEGC transports south-eastward along the ridge of Iceland- Faroe Islands (Logenmann et al., 2013; Casanova-Masjoan et al., 2020). This branch of East Greenland Current may entrain RP signal to the southern coast of Iceland through Iceland Coastal Current and further return to SEGC. The mean $^{99}Tc/^{236}U_{RP}$ atomic ratio in 2019 Iceland costal water is comparable with that in Faroe Islands water in 2019, possibly indicating a similar Atlantic water transit time between Faroe Islands and Iceland. However, the dataset limits the application of correlation analysis in the coast of Faroe Islands and Iceland, so the mean $^{99}Tc/^{236}U_{RP}$ atomic ratios are also directly compared to historic RP discharge ratios. Our observation of mean $^{99}Tc/^{236}U_{RP}$ atomic ratios in the coast of Faroe Islands during 2017–2019

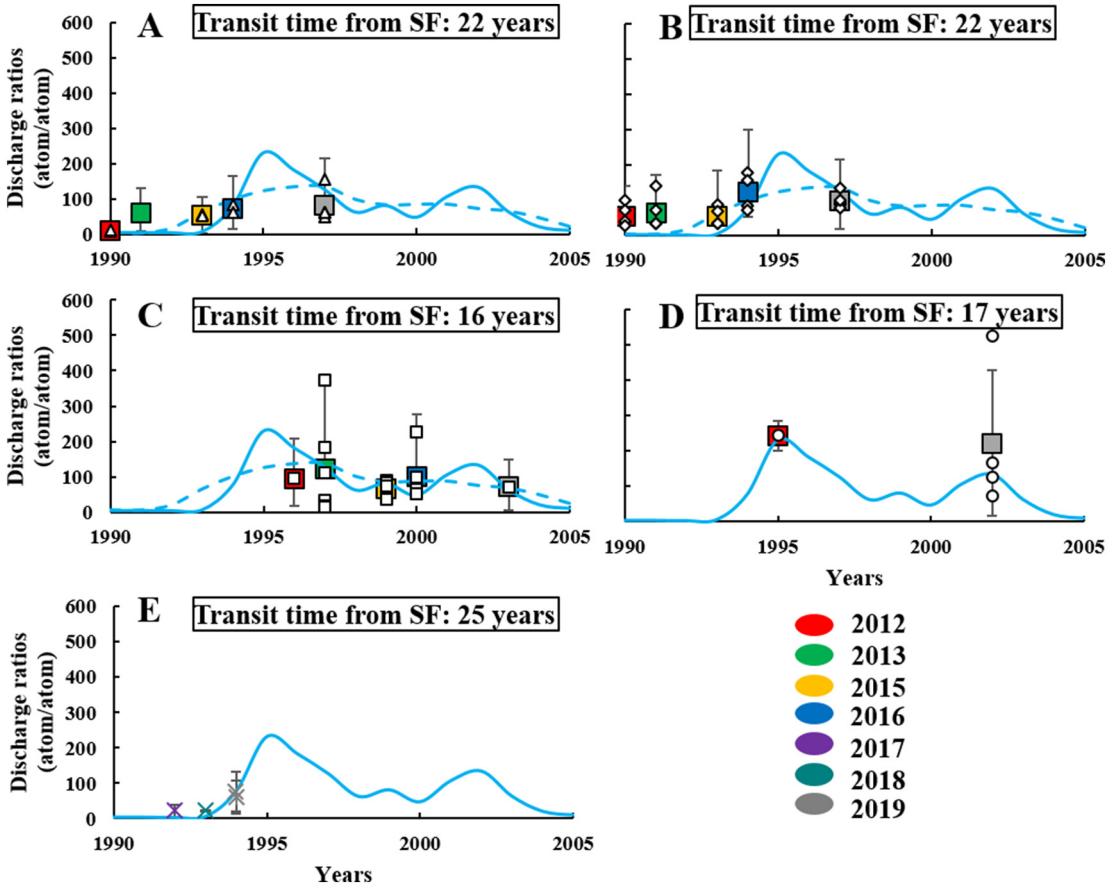

Fig. 4. The distribution of $^{99}Tc/^{236}U_{RP}$ atomic ratios in the NWGC (A), SWGC (B), SEGC (C), NEGC (D), IC and FIC (E) during 2012–2019. The temporal change of 5-year running average (dashed) and annual (solid) $^{99}Tc/^{236}U_{RP}$ atomic ratios from RP discharge is shown as a blue line. The colored boxes are the mean values of $^{99}Tc/^{236}U_{RP}$ ratios in seawater samples, where the colour depends on the year. The smaller symbols are individual observations. NWGC: north-western Greenland coast; SWGC: south-western Greenland coast; SEGC: south-eastern Greenland coast; NEGC: north-eastern Greenland coast; IC: Iceland coast; FIC: Faroe Islands coast.

shows an increasing trend with time, which appears to match well with the trend of discharge ratios in the period during 1992–1994 (Fig. 4). Thereby Atlantic water transit times from SF to Faroe Islands and Iceland are roughly estimated to be both 25 years.

4.2. The potential reason of unexpected ^{236}U concentration in the region of Greenland and Faroe Island

Anthropogenic ^{236}U in seawater is solely derived from GF and RP. Among the observations of ^{236}U concentrations during 2012–2019, an extremely high value was obtained in SEGC in 2013 ($128.6 \pm 17.3 \times 10^6$ atom/L of ^{236}U, 92 % of RP contribution, $0.12 \pm 0.01 \times 10^{-2}$ of $^{233}U/^{236}U$) (Fig. 3C, Table S1). Similarly, measurements from the coastal waters of the Faroe Islands also show an extremely high ^{236}U concentration ($115.9 \pm 7.9 \times 10^6$ atom/L, December 2nd, 2019) with significant RP contribution (96 %, $^{233}U/^{236}U$: $0.05 \pm 0.01 \times 10^{-2}$) (Fig. S4A and B). Although the deposition of GF in the world is not homogenous, GF ^{236}U concentration in mid-high latitude region decreases to relatively low level (10×10^6 atom/L in the North Sea) (Christl et al., 2015), suggesting that the extremely high ^{236}U concentration in surface seawater is unlikely to be derived from GF.

Generally, RP-derived ^{236}U in Greenland coast water derives from the outflowing polar water of the Arctic Ocean (Wefing et al., 2019; Qiao et al., 2020a). Previous studies also show that the current circulation pattern in the North Atlantic Ocean and the Arctic Ocean facilitates the transport of RP-derived ^{236}U with relatively higher level, but ^{236}U concentration is significantly diluted (10^6–10^7 atom/L) during the transport in the Arctic Ocean (Casacuberta et al., 2014, 2016, 2018; Wefing et al., 2021).

The high concentrations of ^{236}U are comparable to levels in LH branch water (10^8 atom/L in 2010) and the reconstructed ^{236}U concentration in SF branch water ($2.8–3.2 \times 10^8$ atom/L during 2012–2018) (Christl et al., 2017; Castrillejo et al., 2020). This indicates that an additional RP signal may be transported northwestwards from northern Europe without first entering the Arctic Ocean.

The unexpectedly high RP signal is also supported by other anthropogenic radioisotopes (^{90}Sr and ^{137}Cs). For instance, according to time-series monitoring data, $^{137}Cs/^{90}Sr$ activity ratios of 1.03–6.92 in Faroe Island coastal water appeared in 1990s (Fig. S4D) (AMAP 2010). A typical $^{137}Cs/^{90}Sr$ ratio for GF is approximately 1.5, as measured in seawater from the North Atlantic Ocean (Dahlgaard et al., 1995b). RP release results in much higher values. Considering the long residence time (~ 16 years) of ^{137}Cs, the sub-tidal sediments of Irish Sea are a continuous source of ^{137}Cs (Jenkinson et al., 2014), resulting in consistently high $^{137}Cs/^{90}Sr$ ratios in the ambient seawater in 1990s. The cumulative discharges from SF indicate $^{137}Cs/^{90}Sr$ activity ratios of 6.43–6.55 during 1991–1999 (OSPAR, 2019). Since GF was prevailing source for ^{137}Cs and ^{90}Sr in Faroe Islands coastal water, higher $^{137}Cs/^{90}Sr$ activity ratios in 1992 (4.36 ± 0.76) and 1997 (6.92 ± 0.34) reveal the existence of RP signal from SF (Fig. S4D). Combined this implies that there must be, at least sporadic, more direct connectivity between the waters leaving the North Sea and the SEGC. All these facts from anthropogenic radioisotopes suggest the sporadic connectivity of Faroe Island and Greenland coastal waters to the seawater in the western European coast, which could potentially explain the unexpected ^{236}U concentrations in Greenland and Faroe Islands coastal water (Fig. S4).

4.3. Perspectives

Anthropogenic radioisotopes with long half-lives (such as ^{99}Tc, ^{233}U and ^{236}U) offer a unique tool to study ocean currents and transit times. This is due to the combination of well-defined point sources (i.e., RP), high sensitivity of measurement (counting atoms per L), transient discharges ratios (time-dependent variations) and great specificity of sources (isotopic ratios). The major hurdle is the large sample volume (especially the case for ^{99}Tc) required a laborious sample preparation procedure. Further improvement of measurement techniques thus reducing sample volume requirements e.g., advanced AMS measurement for ^{99}Tc using ≤10 L of seawater (Hain et al., 2022), may permit the future use of tracking dispersion of RP signal further into the Atlantic and Arctic, and potentially into deep waters.

The ^{99}Tc-^{233}U-^{236}U approach tested here holds potential as it can easily isolate the RP signal, separating the contribution to ^{236}U from GF. The ubiquitous GF contribution may introduce uncertainties in estimating transit times of Atlantic water. Downstream, far from reprocessing plants, such as in the Arctic, the GF contribution continuously increases with water transport, and additional inputs from GF in Siberian catchments and glacial meltwater may play a greater role. The testing of the approach in the subarctic and Arctic Atlantic, near to point sources indicates that it gives similar transit times to that from $^{129}I/^{236}U$, confirming that GF interference since 1990s is not significant for estimating Atlantic water transit time in these waters. Finally due to the extreme specificity of the radiotracer approach, these measurements can offer the only empirical evidence of connectivity across ocean basins, which can be used to verify ocean circulation modelling and indicate new dispersion pathways for contaminants and organisms.

5. Conclusion

In this work, we report the first application to estimate the Atlantic water transit time in the Greenland coast based on a purely RP-derived dual-tracer ($^{99}Tc/^{236}U_{RP}$ transformed from ^{99}Tc-^{233}U-^{236}U). The estimated range of Atlantic water transit time in the Greenland coast (16–22 years) supports earlier estimates using different radioisotopes from samples in the western Fram Strait of the northeastern Greenland coast. The transit times of Atlantic water from northern Europe to both Iceland and Faroe Islands are estimated to be 25 years. The proposed radiotracer approach isolated the RP signal thus excludes the interference from the ubiquitous GF signal. This method provides independent validation to the existing ^{129}I—^{236}U tracer approach where GF ^{236}U was not isolated. The ^{99}Tc-^{233}U-^{236}U radiotracer approach is expected to be robust in estimating Atlantic water transit times in the North Atlantic-Arctic region. With the continuous transport of outflowing polar water, the use of long-lived ^{99}Tc-^{233}U-^{236}U is a potential tool to trace the outflowing water in a large-scale region, such as the tropical Atlantic Ocean and the South Atlantic Ocean.

Supplementary data to this article can be found online at https://doi.org/10.1016/j.scitotenv.2022.158276.

CRediT authorship contribution statement

Gang Lin: Conceptualization, Data curation, Formal analysis, Investigation, Methodology, Writing – original draft. **Jixin Qiao:** Conceptualization, Data curation, Formal analysis, Funding acquisition, Investigation, Methodology, Resources, Supervision, Writing – review & editing. **Peter Steier:** Data curation, Investigation, Methodology, Resources. **Magnús Danielsen:** Investigation, Resources. **Kjartan Guðnason:** Investigation, Resources. **Hans Pauli Joensen:** Investigation, Resources. **Colin A. Stedmon:** Conceptualization, Formal analysis, Investigation, Methodology, Supervision, Writing – review & editing.

Declaration of competing interest

The authors declare that they have no known competing financial interests or personal relationships that could have appeared to influence the work reported in this paper.

Acknowledgements

We thank employees at National Institute of Aquatic Resources, Denmark, Marine and Freshwater Research Institute, Iceland, and University of Faroe Islands for the help in seawater samples collection. This study was supported by the Independent Research Fund Denmark (9040-00266B). J. Qiao wishes to thank the 'Radioactivity, AMAP 2018-2019'

project (J. nr. MST-113-00080) and 'Radioactivity, AMAP-2015' project (J. nr. MST-112-00223) granted by Environmental Protection Agency, Danish Ministry of the Environment for financial support. The RADIATE project (21002412-ST) from the EU Research and Innovation programme HORIZON 2020 under grant agreement No 824096 supports part of the AMS measurements.

References

Aarkrog, A., Boelskifthe, S., Dahlgaard, H., Duniec, S., Hallstadius, L., Holm, E., Smith, J.N., 1987. Technetium-99 and Caesium-134 as long distance tracers in Arctic water. Estuar. Coast. Shelf Sci. 24, 637–647. https://doi.org/10.1016/0272-7714(87)90103-X.

Carscadden, J.E., Gjøsæter, H., Vilhjálmsson, H., 2013. A comparison of recent changes in distribution of capelin (Mallotus villosus) in the Barents Sea, around Iceland and in the Northwest Atlantic. Prog. Oceanogr. 114, 64–83. https://doi.org/10.1016/j.pocean.2013.05.005.

Casacuberta, N., Christl, M., Lachner, J., van der Loeff, M.R., Masqué, P., Synal, H.-A., 2014. A first transect of 236U in the North Atlantic Ocean. Geochim. Cosmochim. Acta 133, 34–46. https://doi.org/10.1016/j.gca.2014.02.012.

Casacuberta, N., Masqué, P., Henderson, G., van-der-Loeff, M.R., Bauch, D., Vockenhuber, C., Daraoui, A., Walther, C., Synal, H.A., Christl, M., 2016. First 236U data from the Arctic Ocean and use of 236U/238U and 129I/236U as a new dual tracer. Earth Planet. Sci. Lett. 440, 127–134. https://doi.org/10.1016/j.epsl.2016.02.020.

Casacuberta, N., Christl, M., Vockenhuber, C., Wefing, A.-M., Wacker, L., Masqué, P., Synal, H.-A., van der Loeff, M.R., 2018. Tracing the three Atlantic branches entering the Arctic Ocean with 129I and 236U. J. Geophys. Res. Oceans 123, 6909–6921. https://doi.org/10.1029/2018JC014168.

Casanova-Masjoan, M., Pérez-Hernández, M.D., Pickart, R.S., Valdimarsson, H., Ólafsdóttir, S.R., Macrander, A., et al., 2020. Along-stream, seasonal, and interannual variability of the North Icelandic Irminger Current and East Icelandic Current around Iceland. J. Geophys. Res. Oceans 125, e2020JC016283. https://doi.org/10.1029/2020JC016283.

Castrillejo, M., Witbaard, R., Casacuberta, N., Richardson, C.A., Dekker, R., Synal, H.-A., Christl, M., 2020. Unravelling 5 decades of anthropogenic 236U discharge from nuclear reprocessing plants. Sci. Total Environ. 717 (137094), 2020. https://doi.org/10.1016/j.scitotenv.2020.137094.

Chamizo, E., Christl, M., López-Lora, M., Casacuberta, N., Wefing, A.-M., Kenna, T.C., 2022. The potential of 233U/236U as a water mass tracer in the Arctic Ocean. J. Geophys. Res. Oceans 127, e2021JC017790. https://doi.org/10.1029/2021JC017790.

Chen, Q., Dahlgaard, H., Nielsen, S.P., 1994. Determination of 99Tc in sea water at ultra low levels. Anal. Chim. Acta 285, 177–180. https://doi.org/10.1016/0003-2670(94)85021-6.

Chen, Q., Hou, X., Yu, Y., Dahlgaard, H., Nielsen, S.P., 2002. Separation of Sr from Ca, Ba and Ra by means of Ca(OH)2 and Ba(Ra)Cl2 or Ba(Ra)SO4 for the determination of radiostrontium. Anal. Chim. Acta 466, 109–116. https://doi.org/10.1016/S0003-2670(02)00571-8.

Christl, M., Lachner, J., Vockenhuber, C., Lechtenfeld, O., Stimac, I., van der Loeff, M.R., Synal, H.-A., 2012. A depth profile of uranium-236 in the Atlantic Ocean. Geochim. Cosmochim. Acta 77, 98–107. https://doi.org/10.1016/j.gca.2011.11.009.

Christl, M., Casacuberta, N., Vockenhuber, C., Elsässer, C., Bailly du Bois, P., Herrmann, J., Synal, H.A., 2015. Reconstruction of the 236U input function for the Northeast Atlantic Ocean: implications for 129I/236U and 236U/238U-based tracer ages. Journal of Geophysical Research: Oceans 120, 7282–7299. https://doi.org/10.1002/2015JC011116.

Christl, M., Casacuberta, N., Lachner, J., Herrmann, J., Synal, H.-A., 2017. Anthropogenic 236U in the North Sea – a closer look into a source region. Environ. Sci. Technol. 51, 12146–12153. https://doi.org/10.1021/acs.est.7b03168.

Dahlgaard, H., 1994. Source of 137Cs, 90Sr and 99Tc in the East Greenland Current. J. Environ. Radioact. 25, 37–55. https://doi.org/10.1016/0265-931X(94)90006-X.

Dahlgaard, H., 1995a. Transfer of European coastal pollution to the arctic: radioactive tracers. Mar. Pollut. Bull. 31, 3–7. https://doi.org/10.1016/0025-326X(95)00003-6.

Dahlgaard, H., Chen, Q., Herrmann, J., Nies, H., Ibbett, R.D., Kershaw, P.J., 1995b. On the background level of 99Tc, 90Sr and 137Cs in the North Atlantic. J. Mar. Syst. 6, 571–578. https://doi.org/10.1016/0924-7963(95)00025-K.

Daniault, N., Mercier, H., Lherminier, P., Sarafanov, A., Falina, A., Zunino, P., et al., 2016. The northern North Atlantic Ocean mean circulation in the early 21st century. Prog. Oceanogr. 146, 142–158. https://doi.org/10.1016/j.pocean.2016.06.007.

Hain, K., Steier, P., Froehlich, M.B., Golser, R., Hou, X., Lachner, J., Qiao, J., Quinto, F., Sakaguchi, A., 2020. 233U/236U signature allows to distinguish environmental emissions of civil nuclear industry from weapons fallout. Nat. Commun. 11. https://doi.org/10.1038/s41467-020-15008-2.

Hain, K., Martschini, M., Gülce, F., Honda, M., Lachner, J., Kern, M., Pitters, J., Quinto, F., Sakaguchi, A., Steier, P., Wiederin, A., 2022. Developing accelerator mass spectrometry capabilities for anthropogenic radionuclide analysis to extend the set of oceanographic tracers. Front. Mar. Sci. 9, 837515. https://doi.org/10.3389/fmars.2022.837515.

Halloran, P.R., Hall, I.R., Menary, M., Reynolds, D.J., Scourse, J.D., Screen, J.A., et al., 2020. Natural drivers of multidecadal Arctic sea ice variability over the last millennium. Sci. Rep. 10 (668), 1–9. https://doi.org/10.1038/s41598-020-57472-2.

Hátún, H., Lohmann, K., Matei, D., Jungclaus, J., Pacariz, S., Bersch, M., Gislason, A., Ólafsson, J., Reid, P.C., 2016. An inflated subpolar gyre blows life towards the northeastern Atlantic. Prog. Oceanogr. 147, 49–66. https://doi.org/10.1016/j.pocean.2016.07.009.

Hátún, H., Azetsu-Scott, K., Somavilla, R., Rey, F., Johnson, C., Mathis, M., Mikolajewicz, U., Coupel, P., Tremblay, J.-É., Hartman, S., Pacariz, S.V., Salter, I., Ólafsson, J., 2017. The subpolar gyre regulates silicate concentrations in the North Atlantic. Sci. Rep. 7, 14576. https://doi.org/10.1038/s41598-017-14837-4.

Hou, X.L., Dahlgaard, H., Nielsen, S.P., 2000. Iodine-129 time series in Danish, Norwegian and northwest Greenland coast and the Baltic Sea by seaweed. Estuar. Coast. Shelf Sci. 51, 571–584. https://doi.org/10.1006/ecss.2000.0698.

International Atomic Energy Agency (IAEA), 2004. Sediment distribution coefficients and concentration factors for biota in the marine environment. Technical Reports Series No. 422 9–25.

Jackson, D., 2000. Related content radiation doses to members of the public near to Sellafield, Cumbria, from liquid discharges 1952-. J. Radiol. Prot. 20, 139–167.

Jenkinson, S.B., McCubbin, D., Kennedy, P.H.W., Dewar, A., Bonfield, R., Leonard, K.S., 2014. An estimate of the inventory of technetium-99 in the sub-tidal sediments of the Irish Sea. J. Environ. Radioact. 133, 40–47. https://doi.org/10.1016/j.jenvrad.2013.05.004.

Karcher, M.J., Gerland, S., Harms, I.H., Iosjpe, M., Heldal, H.E., Kershaw, P.J., Sickel, M., 2004. The dispersion of 99Tc in the Nordic Seas and the Arctic Ocean: a comparison of model results and observations. Journal of Environmental Radioactivity 74, 185–198. https://doi.org/10.1016/j.jenvrad.2004.01.026.

Kershaw, P.J., McCubbin, D., Leonard, K.S., 1999. Continuing contamination of North Atlantic and Arctic waters by sellafield radionuclides. Sci. Total Environ. 237 (238), 119–132. https://doi.org/10.1016/S0048-9697(99)00129-1.

Lin, M., Qiao, J.X., Hou, X.L., Golser, R., Hain, K., Steier, P., 2021a. On the quality control for the determination of ultratrace-level 236U and 233U in environmental samples by accelerator mass spectrometry. Anal. Chem. 93, 3362–3369. https://doi.org/10.1021/acs.analchem.0c03623.

Lin, M., Qiao, J., Hou, X., Dellwig, O., Steier, P., Hain, K., Golser, R., Zhu, L., 2021b. 70-year anthropogenic uranium imprints of nuclear activities in Baltic Sea sediments. Environ. Sci. Technol. 55 (13), 8918–8927. https://doi.org/10.1021/acs.est.1c02136.

Logenmann, K., Ólafsson, J., Snorrason, Á., Valdimarsson, H., Marteinsdóttir, G., 2013. The circulation of icelandic waters – a modelling study. Ocean Sci. 9, 931–955. https://doi.org/10.5194/os-9-931-2013.

Muilwijk, M., Smedsrud, L.H., Ilicak, M., Drange, H., 2018. Atlantic water heat transport variability in the 20th century Arctic Ocean from a global ocean model and observations. J. Geophys. Res. Oceans 123, 8159–8179. https://doi.org/10.1029/2018JC014327.

OSPAR, 2019. Liquid Discharges from Nuclear Installations [WWW Document]. https://www.ospar.org.

Periáñez, R., Suh, K.S., Min, B.I., Villa-Alfageme, M., 2018. The behaviour of 236U in the North Atlantic Ocean assessed from numerical modelling: a new evaluation of the input function into the Arctic. Sci. Total Environ. 626, 255–263. https://doi.org/10.1016/j.scitotenv.2018.01.058.

Polyakov, I.V., Pnyushkov, A.V., Alkire, M.B., Ashik, I.M., Baumann, T.M., Carmack, E.C., Goszczko, I., Guthrie, J., Ivanov, V.V., Kanzow, T., Krishfield, R., Kwok, R., Sundfjord, A., Morison, J., Rember, R., Yulin, A., 2017. Greater role for Atlantic inflows on sea ice loss in the Eurasian Basin of the Arctic Ocean. Science 356 (6335), 285–291. https://doi.org/10.1126/science.aai8204.

Qiao, J.X., Xu, Y.H., 2018. Direct measurement of uranium in seawater by inductively coupled plasma mass spectrometry. Talanta 183, 18–23. https://doi.org/10.1016/j.talanta.2018.02.045.

Qiao, J.X., Hou, X.L., Steier, P., Nielsen, S., Golser, R., 2015. Method for 236U determination in seawater using flow injection extraction chromatography and accelerator mass spectrometry. Anal. Chem. 87, 7411–7417. https://doi.org/10.1021/acs.analchem.5b01608.

Qiao, J.X., Hain, K., Steier, P., 2020a. First dataset of 236U and 233U around the Greenland coast: a 5-year snapshot (2012–2016). Chemosphere 257, 127185. https://doi.org/10.1016/j.chemosphere.2020.127185.

Qiao, J.X., Andersson, K., Nielsen, S., 2020b. A 40-year marine record of 137Cs and 99Tc transported into the Danish Straits: significance for oceanic tracer studies. Chemosphere 244, 125595. https://doi.org/10.1016/j.chemosphere.2019.125595.

Qiao, J., Ransby, D., Steier, P., 2022. Deciphering anthropogenic uranium sources in the equatorial northwest Pacific margin. Sci. Total Environ. 806, 150482. https://doi.org/10.1016/j.scitotenv.2021.150482.

Rozmaric, M., Chamizo, E., Louw, D.C., López-Lora, M., Blinova, O., Levy, I., Mudumbi, B., van der Plas, A.K., Tenorio, R.G., McGinnity, P., Osvath, I., 2022. Fate of anthropogenic radionuclides (90Sr, 137Cs, 238Pu, 239Pu, 240Pu, 241Am) in seawater in the northern Benguela upwelling system off Namibia. Chemosphere 286, 131514. https://doi.org/10.1016/j.chemosphere.2021.131514.

Sakaguchi, A., Kawai, K., Steier, P., Quinto, F., Mino, K., Tomita, J., Hoshi, M., Whitehead, N., Yamamoto, M., 2009. First results on 236U levels in global fallout. Sci. Total Environ. 407, 4238–4242. https://doi.org/10.1016/j.scitotenv.2009.01.058.

Sakaguchi, A., Kadokura, A., Steier, P., Takahashi, Y., Shizuma, K., Hoshi, M., Nakakuki, T., Yamamoto, M., 2012. Uranium-236 as a new oceanic tracer: a first depth profile in the Japan Sea and comparison with caesium-137. Earth Planet. Sci. Lett. 333, 165–170. https://doi.org/10.1016/j.epsl.2012.04.004.

Shi, K., Hou, X., Roos, P., Wu, W., 2012. Determination of technetium-99 in environmental samples: a review. Anal. Chim. Acta 709, 1–20. https://doi.org/10.1016/j.aca.2011.10.020.

Smith, J.N., McLaughlin, F.A., Smethie, W.M., Moran, S.B., Lepore, K., 2011. Iodine-129, 137Cs, and CFC-11 tracer transit time distributions in the Arctic Ocean. J. Geophys. Res. 116, C04024. https://doi.org/10.1029/2010JC006471.

Smith, J.N., Karcher, M., Casacuberta, N., Williams, W.J., Kenna, T., Smethie Jr., W.M., 2021. A changing Arctic Ocean: how measured and modeled 129I distributions indicate fundamental shifts in circulation between 1994 and 2015. J. Geophys. Res. Oceans 126, e2020JC016740. https://doi.org/10.1029/2020JC016740.

Steier, P., Bichler, M., Keith Fifield, L., Golser, R., Kutschera, W., Priller, A., Quinto, F., Richter, S., Srncik, M., Terrasi, P., Wacker, L., Wallner, A., Wallner, G., Wilcken, K.M., Maria Wild, E., 2008. Natural and anthropogenic 236U in environmental samples. Nucl. Inst. Methods Phys. Res. B 266, 2246–2250. https://doi.org/10.1016/j.nimb.2008.03.002.

Steier, P., Dellinger, F., Forstner, O., Golser, R., Knie, K., Kutschera, W., Priller, A., Quinto, F., Srncik, M., Terrasi, F., Vockenhuber, C., Wallner, A., Wallner, G., Wild, E.M., 2010. Analysis and application of heavy isotopes in the environment. Nucl. Inst. Methods Phys. Res. B 268 (7–8), 1045–1049. https://doi.org/10.1016/j.nimb.2009.10.094.

Wefing, A.-M., Christl, M., Vockenhuber, C., Rutgers van der Loeff, M., Casacuberta, N., 2019. Tracing Atlantic waters using 129I and 236U in the Fram Strait in 2016. J. Geophys. Res. Oceans 124, 882–896. https://doi.org/10.1029/2018JC014399.

Wefing, A.-M., Casacuberta, N., Christl, M., Gruber, N., Smith, J.N., 2021. Circulation timescales of Atlantic water in the Arctic Ocean determined from anthropogenic radionuclides. Ocean Sci. 17, 111–129. https://doi.org/10.5194/os-17-111-2021.

Supporting Information

Tracing Atlantic water transit time in the subarctic and Arctic Atlantic using ^{99}Tc-^{233}U-^{236}U

Gang Lin[a], Jixin Qiao[a,*], Peter Steier [b], Magnús Danielsen[c], Kjartan Guðnason[d], Hans Pauli Joensen[e], Colin A. Stedmon[f]

a. Department of Environmental and Resource Engineering, Technical University of Denmark, DK-4000 Roskilde, Denmark
b. VERA Laboratory, Faculty of Physics, Isotope Physics, University of Vienna, Währinger Straße 17, A-1090 Vienna, Austria
c. Marine and Freshwater Research Institute, Iceland
d. Icelandic Radiation Safety Authority, Iceland
e. University of the Faroe Islands, FO - 110 Tórshavn, Faroe Islands
f. National Institute of Aquatic Resources, Technical University of Denmark, Kemitorvet, 2800 Kgs. Lyngby, Denmark

Corresponding author*: E-mail address: jiqi@dtu.dk (J. Qiao).

Contents of the file

The supporting information (8 pages in total) contains all integrated data of seawater samples in Table S1 (see attached excel file), the correlation analysis for estimating Atlantic water transit time (Table S2), annual discharges of ^{99}Tc (A) and ^{236}U (B) from Sellafield and La Hague (Fig. S1), global fallout derived-^{236}U concentration in the North Sea (Fig. S2), the coefficient of correlation analysis in different transit times (Fig. S3), ^{236}U concentrations, $^{233}U/^{236}U$ in East Greenland, Iceland and Faroe Islands coastal water and $^{137}Cs/^{90}Sr$ ratios in Faroe Islands coastal water (Fig. S4)

Table S2

The correlation analysis between our time-series observation and historic RP discharge ratios (5-year running average for SEGC, SWGC and NWGC)

Difference between discharge and sampling year (Transit time)	SEGC	SWGC	NWGC
41			
40			
39	-0.64	0.68	0.75
38	-0.39	0.59	0.53
37	0.00	0.26	0.51
36	0.33	-0.17	-0.25
35	0.27	-0.90	-0.57
34	0.60	-0.64	-0.71
33	0.60	-0.66	-0.70
32	0.28	-0.32	-0.84
31	0.36	-0.12	-0.50
30	0.09	-0.29	-0.49
29	0.52	-0.28	-0.31
28	0.50	-0.68	-0.68
27	-0.42	0.15	0.36
26	-0.47	0.30	0.50
25	-0.48	0.32	0.51
24	-0.47	0.44	0.57
23	-0.46	0.69	0.72
22	-0.58	**0.75**	**0.77**
21	-0.52	0.71	0.74
20	-0.31	0.56	0.70
19	-0.13	0.36	0.51
18	0.06	-0.60	-0.17
17	0.65	-0.73	-0.67
16	**0.73**	-0.59	-0.71
15	0.47	-0.54	-0.91
14	0.42	-0.55	-0.76
13	0.56	-0.51	-0.65
12	0.55	-0.68	-0.74
11	0.49	-0.79	-0.85
10	0.60	-0.70	-0.79
9	0.56	-0.63	-0.84
8	0.40	-0.59	-0.93
7	0.35	-0.60	-0.96
6	0.49	-0.72	-0.90
5			
4			
3			
2			
1			

(SEGC: south-eastern Greenland coast; SWGC: south-western Greenland coast; NWGC: north-western Greenland coast)

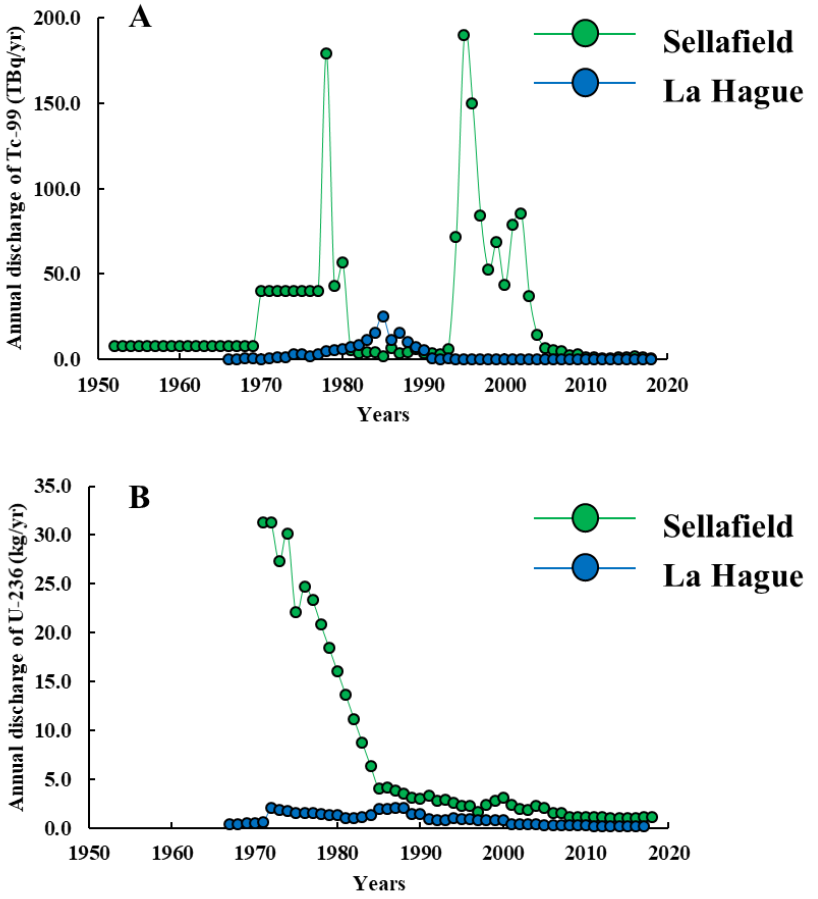

Fig. S1. Annual discharges of ^{99}Tc (A) and ^{236}U (B) from Sellafield and La Hague (Jackson, 2000; Shi et al., 2012; OSPAR, 2019; Castrillejo et al., 2000).

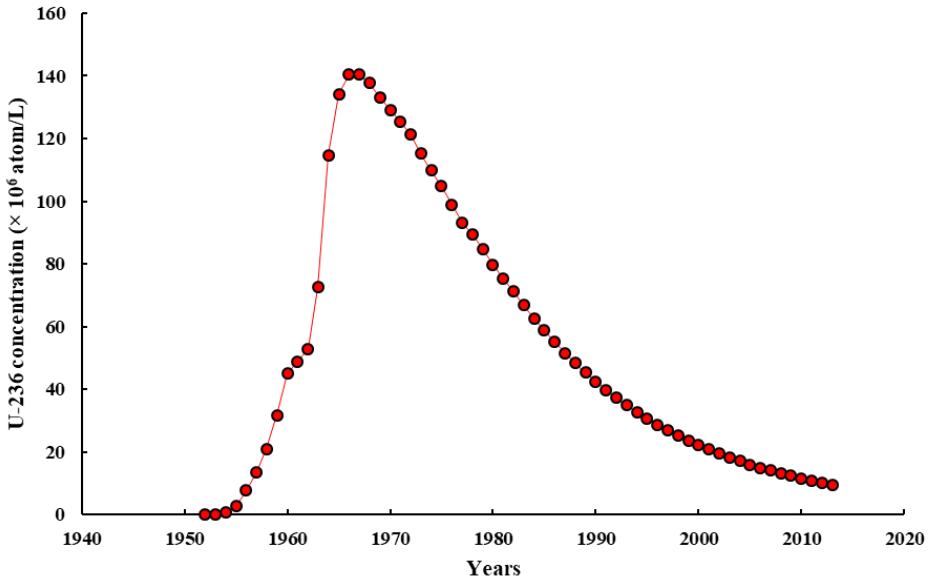

Fig. S2. Global fallout derived-^{236}U concentration in the North Sea (Christl et al., 2015).

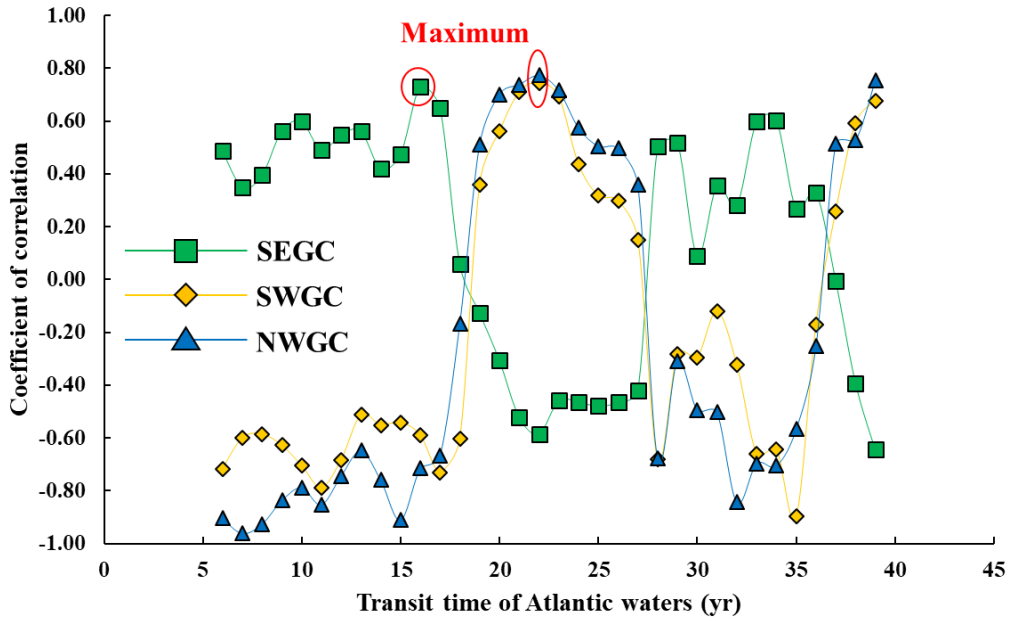

Fig.S3 The coefficient of correlation analysis in different transit times (5-year running average for SEGC, SWGC and NWGC). SEGC: south-eastern Greenland coast; SWGC: south-western Greenland coast; NWGC: north-western Greenland coast.

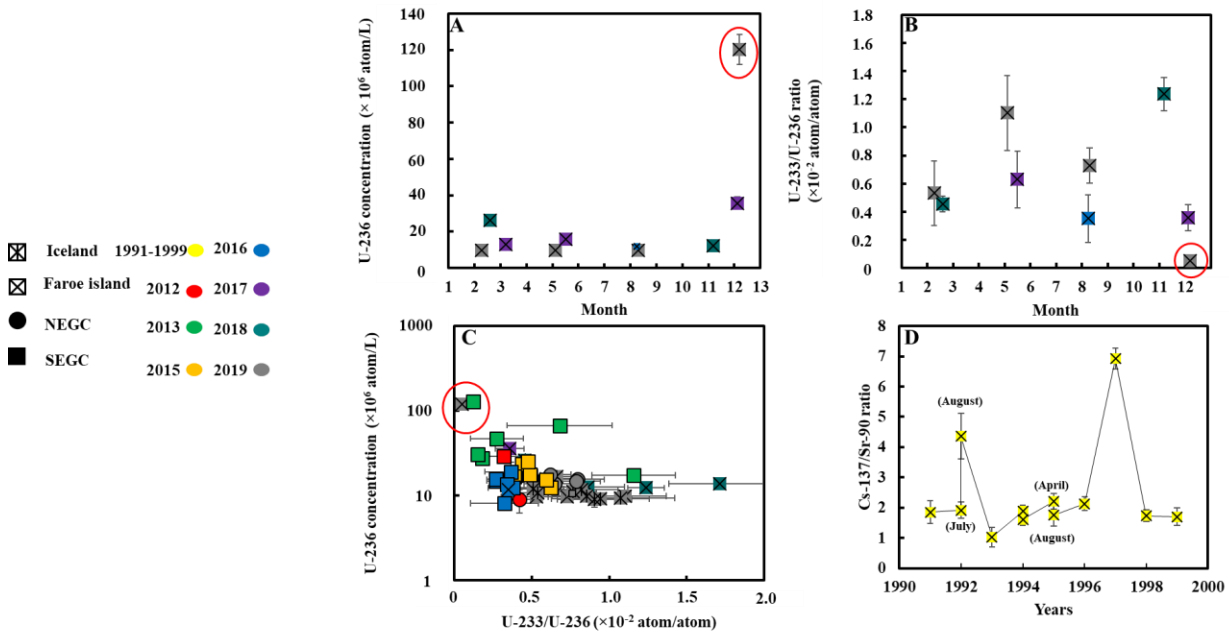

Fig. S4. Seasonal variations of ^{236}U concentrations (A) and $^{233}U/^{236}U$ atomic ratios (B) in Faroe Islands coastal waters. Variation of ^{236}U concentration with $^{233}U/^{236}U$ atomic ratio in coastal waters of Greenland, Iceland and Faroe Islands (C). Annual variation of $^{137}Cs/^{90}Sr$ activity ratios in Faroe Islands coastal waters during 1990-2000 (D). NEGC: north-eastern Greenland coast; SEGC: south-eastern Greenland coast.

References

Castrillejo, M., Witbaard, R., Casacuberta, N., Richardson, C.A., Dekker, R., Synal, H.-A., Christl, M., 2020. Unravelling 5 Decades of Anthropogenic ^{236}U Discharge from Nuclear Reprocessing Plants, Sci. Total Environ. 717, 137094, https://doi.org/10.1016/j.scitotenv.2020.137094, 2020.

Christl, M., Casacuberta, N., Vockenhuber, C., Elsässer, C., Bailly du Bois, P., Herrmann, J., Synal, H. A., 2015. Reconstruction of the ^{236}U input function for the Northeast Atlantic Ocean: Implications for ^{129}I/^{236}U and ^{236}U/^{238}U-based tracer ages. Journal of Geophysical Research: Oceans 120, 7282–7299. https://doi.org/10.1002/2015JC011116.

Jackson, D., 2000. Related content Radiation doses to members of the public near to Sellafield , Cumbria , from liquid discharges 1952-. J. Radiol. Prot. 20, 139–167.

OSPAR, 2019. Liquid Discharges from Nuclear Installations [WWW Document]. https://www.ospar.org.

Shi, K., Hou, X., Roos, P., Wu, W., 2012. Determination of technetium-99 in environmental samples: A review. Anal. Chim. Acta, 709, 1–20.

Paper III

Tracing Atlantic water transit times in the Arctic Ocean: coupling reprocessing-derived ^{236}U and colored dissolved organic matter to distinguish different pathways

Gang Lin[a], Jixin Qiao[a,*], Paul A. Dodd[b], Rafael Gonçalves-Araujo[c], Mats A. Granskog[b], Peter Steier[d], Colin A. Stedmon[c]

[a]Department of Environmental and Resource Engineering, Technical University of Denmark, DK-4000 Roskilde, Denmark

[b]Norwegian Polar Institute, Fram Centre, Tromsø, Norway

[c]National Institute of Aquatic Resources, Technical University of Denmark, Kemitorvet, 2800 Kgs. Lyngby, Denmark

[d]VERA Laboratory, Faculty of Physics, Isotope Physics, University of Vienna, Währinger Straße 17, A-1090 Vienna, Austria

Earth and Planetary Science Letters ••• (••••) ••••••

Contents lists available at ScienceDirect

Earth and Planetary Science Letters

journal homepage: www.elsevier.com/locate/epsl

Tracing Atlantic water transit times in the Arctic Ocean: Coupling reprocessing-derived ^{236}U and colored dissolved organic matter to distinguish different pathways

Gang Lin [a], Jixin Qiao [a,*], Paul A. Dodd [b], Rafael Gonçalves-Araujo [c], Mats A. Granskog [b], Peter Steier [d], Colin A. Stedmon [c]

[a] Department of Environmental and Resource Engineering, Technical University of Denmark, DK-4000 Roskilde, Denmark
[b] Norwegian Polar Institute, Fram Centre, Tromsø, Norway
[c] National Institute of Aquatic Resources, Technical University of Denmark, Kemitorvet, 2800 Kgs. Lyngby, Denmark
[d] VERA Laboratory, Faculty of Physics, Isotope Physics, University of Vienna, Währinger Straße 17, A-1090 Vienna, Austria

ARTICLE INFO

Article history:
Received 29 June 2023
Received in revised form 14 September 2023
Accepted 17 September 2023
Available online xxxx
Editor: A. Jacobson

Keywords:
^{233}U
^{236}U
colored dissolved organic matter
Atlantic water transit times
transport pathways
Arctic Ocean

ABSTRACT

The Fram Strait is a key region for investigating the exchange of Atlantic water with the Arctic Ocean. Uranium-236 (^{236}U) from the two European nuclear reprocessing plants (NRPs) at La Hague and Sellafield provides a unique fingerprint in Atlantic water which can be used for studying its circulation patterns in the Arctic Ocean. And NRPs-derived ^{236}U ($^{236}U_{NRPs}$) can be identified by its $^{233}U/^{236}U$ signature. In this study, we use colored dissolved organic matter (CDOM) absorption to constrain the selection of three Atlantic branch waters that carried different inputs of $^{236}U_{NRPs}$ in Fram Strait. This can potentially provide better estimates of transit times of Atlantic waters in the Arctic Ocean. High CDOM levels ($a_{350} \geq 0.35\ m^{-1}$) in Fram Strait reflect the passage of Atlantic water transported to the Arctic by the Norwegian Coastal Current and its extension (NCC) and subsequently along the Siberian continental slope and shelf where the Ob, Yenisei and Lena rivers supply terrestrial organic matter with significantly high CDOM content. Conversely, low CDOM water represents Atlantic water that has remained off the shelf. Based on CDOM absorption, potential temperature (Θ), potential density (σ_Θ) and ^{236}U concentration, the path of a given body of Atlantic water could be inferred and an appropriate NRPs input function constrained so that transit times could be estimated. Our results indicate that Arctic High CDOM Water ($a_{350} \geq 0.35\ m^{-1}$) sourced from the NCC and Barents Sea Branch Water (BSBW) in the Barents Sea Opening has an average of 7–27 yrs transit time in the upper ~200 m of the western shelf of the Fram Strait. Atlantic Low CDOM Water ($a_{350} < 0.35\ m^{-1}$, $\Theta > 2\,°C$) sourced from the Fram Strait Branch Water (FSBW) has a short pathway from the eastern Fram Strait. Arctic Low CDOM / High ^{236}U Water ($a_{350} < 0.35\ m^{-1}$, $\Theta \leq 2\,°C$, $\sigma_\Theta \leq 27.97$ or ^{236}U concentration $\geq 15 \times 10^6$ atom/L) sourced from the BSBW and the FSBW has an average of 22–28 yrs transit time. These findings demonstrate how combining measurements of CDOM with $^{236}U_{NRPs}$ can improve the robustness in estimation of transit times of different Atlantic water pathways in the Arctic Ocean. There are limited ways to empirically derive estimates and the values provided offer unique data for comparison with estimates from regional circulation models.

1. Introduction

Heat carried by Atlantic water flowing northwards from lower latitudes has an impact on sea-ice and glacier melt, and air temperatures in the Arctic (Smedsrud et al., 2022). This in turn influences the quantity and distribution of freshwater leaving the Arctic into the subpolar North Atlantic which can in turn threaten the Atlantic Meridional Overturning Circulation (AMOC) and thus change global climate (Rahmstorf, 2002; Tsubouchi et al., 2021; Wang, 2021). The majority of water in the Arctic Ocean originates from the Atlantic, and understanding its transport pathways and transit times is important (Karcher and Oberhuber, 2002; Karcher et al., 2011; Smith et al., 2021). The Fram Strait, located between Svalbard and Greenland is an important gateway for the exchange of salt and heat between the Arctic and North Atlantic oceans (e.g. Marnela et al., 2013; Timmermans and Marshall, 2020). Therefore,

* Corresponding author.
E-mail address: Jiqi@dtu.dk (J. Qiao).

https://doi.org/10.1016/j.epsl.2023.118415

sustained observations in the western Fram Strait in the Arctic outflow are relevant for investigating and monitoring environmental changes in the upstream Arctic Ocean (e.g. Dodd et al., 2012; Karpouzoglou et al., 2022; Sumata et al., 2023). These include the effects of changing freshwater budgets, ice conditions and biogeochemical cycling of elements.

Anthropogenic radioisotopes provide transient signals which can be used to trace water mass movement (Aarkrog et al., 1987; Dahlgaard, 1994; Smith et al., 1998; Casacuberta et al., 2014). In general, anthropogenic radioisotopes in North Atlantic and Arctic seawater have two main sources: a point source from nuclear reprocessing plants (NRPs); and a diffuse source of global fallout (GF) which is a legacy of atmospheric nuclear weapon tests. NRPs derived radioisotopes in the Arctic Ocean predominantly originate from the two European facilities at La Hague and Sellafield, and provide unique signature to trace the passage of Atlantic water northwards (Casacuberta et al., 2016). NRPs release a suite of radioisotopes with a range in half-lives and behavior in seawater (International Atomic Energy Agency IAEA, 2004). Both ^{236}U and ^{129}I have proven to be useful tracers due to their long half-lives (t 1/2 = 23.4 Myr and 15.7 Myr, respectively) and variable (and differing) discharge rates (Raisbeck et al., 1995; Christl et al., 2015a; Casacuberta et al., 2018). The weaknesses of the ^{236}U-^{129}I tracer approach are that iodine has different biogeochemical properties than uranium (Andersson et al., 1995; Schwehr et al., 2005) and that ^{236}U distributions are influenced by both NRPs and GF (Christl et al., 2015b).

Recently, measurements of ^{233}U have been used to resolve this and isolate the NRPs contribution of ^{236}U from that of GF (Hain et al., 2020; Qiao et al., 2020). The ^{233}U contribution from thermal-neutron nuclear reactors is nearly negligible compared to that from GF (Hain et al., 2020) and by using a two end-member algorithm the contribution from each can be derived (Qiao et al., 2020). Compared with the total ^{236}U, NRPs-derived ^{236}U ($^{236}U_{NRPs}$) could offer a more refined approach to trace Atlantic water in the Arctic (Lin G. et al., 2022a, 2022b; Chamizo et al., 2022).

Based on the historic ^{236}U concentrations in Sellafield and La Hague branch waters reconstructed from records in sea shells (Castrillejo et al., 2020), the temporal variations of $^{236}U_{NRPs}$ concentrations in different branches of Atlantic water in the Barents Sea Opening can be reconstructed and used as input functions for Atlantic water transit time estimates (Fig. S1). The monotonically decrease of the $^{236}U_{NRPs}$ input functions since 1970s provides high reliability to anchor the source year of the Atlantic water (before 1990s) entering the Arctic. The natural ^{236}U concentration in seawater of the ocean is estimated to on the order of 10^3 atom/L (Steier et al., 2008). This is more than thousand times lower than the anthropogenic contribution and therefore be considered negligible.

According to Casacuberta et al. (2018), the Norwegian Coastal Current (NCC) carries a significantly stronger NRPs signal into the Arctic Ocean compared with other Atlantic branch waters (Barents Sea branch water (BSBW) and Fram Strait branch water (FSBW)) (Fig. 1). Earlier studies show that the NRPs input functions can be selectively applied for different water layers in the Arctic Ocean based on the spatio-temporal distribution of radioisotopes in water column profiles (Smith et al., 2011; Wefing et al., 2019). However, this distribution is not only influenced by fluctuations in NRPs input from the Atlantic Ocean but also by the dilution with variable contributions of Pacific water and freshwater, resulting in the indistinguishable influence of different NRPs input functions in the downstream seawater. Therefore, selection of reasonable NRPs input functions is crucial to obtain viable estimates on Atlantic water transit times (Smith et al., 2011; Casacuberta et al., 2018; Wefing et al., 2019), and a direct tracer solely impacted by the NCC or the BSBW/FSBW is important for distinguishing them.

Colored dissolved organic matter (CDOM) is the light-absorbing fraction of dissolved organic matter. In the Arctic Ocean there is a weak background signal from marine organic matter and a very prominent signal associated with terrestrial organic matter supplied by Arctic rivers (e.g. Stedmon et al., 2011). The CDOM contribution from terrestrial organic matter can be used as a tracer of riverine freshwater (Granskog et al., 2012; Stedmon et al., 2015; Gonçalves-Araujo et al., 2016; Charette et al., 2020). High CDOM levels in surface and intermediate waters (<500 m) exiting the Arctic Ocean reflect the fact that a portion of the Atlantic water flowing into the Arctic is transported along or on the Siberian shelf where it accumulates CDOM (and riverine freshwater) and is subsequently exported off shelf and across the basin towards the Fram Strait as part of the Transpolar drift (Charette et al., 2020). During this transit the waters are cooled down because they experience sea ice formation during Arctic winter.

In this study we combine measurements of uranium and CDOM in an attempt to provide improved estimates of Atlantic water transit times. The goal was to trace and estimate Atlantic water transport pathways and transit times in the Arctic Ocean, using CDOM as an additional novel constraint for appropriate NRPs input functions based on circulation pathways of waters exiting the Arctic Ocean in Fram Strait. If successful this would provide valuable auxiliary data which can be easily routinely measured together with temperature and salinity, and assist distinguishing circulation pathways for different Arctic water bodies.

2. Materials and methods

2.1. Setting and sampling

The study region is located in the Fram Strait, which is a gateway for water exchange between the Arctic Ocean and the North Atlantic Ocean (Fig. 1). Fram Strait has ~450 km width with a maximum depth of ~2600 m (Rudels et al., 2015). The Atlantic inflow (West Spitsbergen Current, WSC) is constrained to the eastern side of the strait where Svalbard Branch Water (SBW) splits from the WSC and flows into the Arctic Ocean. To the west Arctic water flows out southwards and consists of Atlantic water that has had a long passage in the Arctic Ocean; and Recirculating Atlantic Water (RAW) in Return Atlantic Current (RAC) which has a short passage in the Arctic turning just north of the Fram Strait and exiting (Rudels et al., 2005). In this study, we define Atlantic branch waters through their $^{236}U_{NRPs}$ tracer signals. The $^{236}U_{NRPs}$ signals in both RAW and SBW originate from Fram Strait Branch Water (FSBW), so the waters carrying FSBW-derived $^{236}U_{RP}$ signals in the Arctic Ocean are defined as FSBW. The river signal that the Atlantic waters acquire when circulating in the Arctic basin originates predominantly from six major Arctic rivers from the Eurasian (Ob, Yenisei, Lena and Kolyma rivers) and American continent (Yukon and Mackenzie rivers). Inflowing Pacific water from the Bering Strait also contributes to dilute Atlantic waters as it has a lower salinity. Pacific water properties are modified as it passes over the shallow shelf and a contribution is exported into the central Arctic Ocean (Jones et al., 2003). A mixture of Atlantic water, Pacific water, river water and sea ice meltwater constitute the polar surface waters that exit the Arctic in the western Fram Strait as the East Greenland Current (Jones et al., 2008; Dodd et al., 2012).

Sampling of seawater was carried out in August and September during the period 2019–2021 on expeditions aboard R/V Kronprins Haakon by the Norwegian Polar Institute. Temperature and salinity were measured using a SeaBird (SBE911+) CTD. A rosette water sampler was used to collect 247 seawater samples (5-10 L) for uranium isotopes (^{233}U-^{236}U-^{238}U) measurement and 832 samples for colored dissolved organic matter absorption measurement. Additionally, three sea-ice core samples were collected in the western

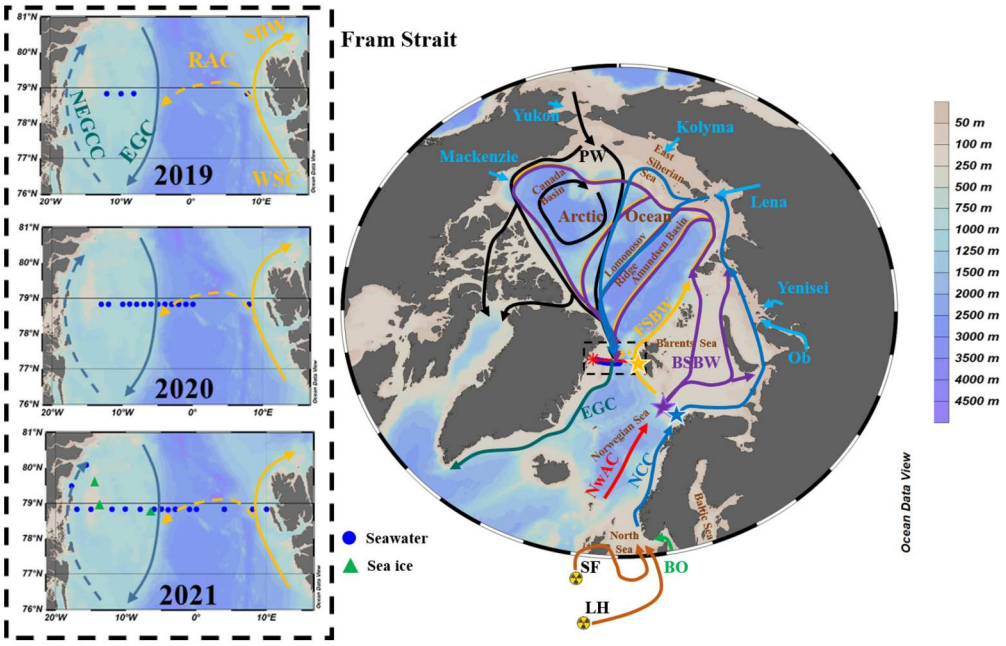

Fig. 1. Left: Location of the sampling stations in the Fram Strait in 2019, 2020 and 2021. Blue dots indicate seawater samples and green triangles refer to sea ice samples (latter all collected in 2021). Right: Simplified circulation patterns for surface and intermediate waters in the Arctic (Rudels, 2009). Four Arctic inflows are indicated as Barents Sea Branch Water (purple, BSBW); Fram Strait Branch Water (yellow, FSBW), Pacific water (black, PW), Norwegian Coastal Current and its extension (blue, NCC) in the Arctic Ocean. The BSBW and FSBW have their origins in the Norwegian Atlantic Current (red, NwAC). The East Greenland Current (EGC) is shown in dark green. Light blue arrows indicate the discharge from major Arctic rivers; Light green arrow indicates the Baltic outflow (BO); Stars refer to the location of the derived $^{236}U_{NRPs}$ input functions in the Barents Sea Opening with contributions from NCC and NwAC. SF and LH refer to two main reprocessing plants at Sellafield and La Hague. RAC: Return Atlantic Current; SBW: Svalbard Branch Water; NEGCC: North East Greenland Coastal Current. Produced with Ocean Data View (Schlitzer, 2016).

Fram Strait in 2021. The length of sea ice cores was 1.31 m, 1.92 m and 3.13 m, respectively. Complete sea ice cores were slowly melted in precleaned plastic containers for the measurement of uranium isotopes.

2.2. Determination of ^{233}U, ^{236}U and ^{238}U

Seawater samples (5-10 L) and sea ice samples (10 L) were processed for ^{233}U and ^{236}U measurement based on an optimized procedure developed in an earlier study (Qiao et al., 2015). The pH value of filtered water was adjusted to 2 using 14 M HNO_3 and stirred with air (10 min) for separating uranium ion from uranyl carbonate complex and expelling CO_2. After adding 10-20 mL of 0.05 g/mL Fe^{3+} ($FeCl_3$ solution pre-purified by UTEVA® resin) dissolved in 3 M HNO_3, the pH value was adjusted to 8-9 using $NH_3{\cdot}H_2O$ solution, forming iron hydroxides to co-precipitate with uranium. The precipitation was dissolved by 14 M HNO_3 and diluted to 3 M HNO_3. To purify uranium, the dissolved sample solution was load on a 2 mL UTEVA® resin preconditioned with 20 mL of 3 M HNO_3. 40 mL of HNO_3 and 20 mL of 6 M HCl were used to rinse the column sequentially, and 10 mL of 0.025 M HCl was used to elute uranium. 2 mg of Fe^{3+} was added to the eluate to co-precipitate uranium with iron hydroxides again. Finally, after drying for 4 h at 90 °C and combustion for 12 h at 800 °C, the sample was pressed into a sputter cathode and measured by accelerator mass spectrometry (AMS) at the Vienna Environmental Research Accelerator (VERA) facility at University of Vienna (Steier et al., 2010; Hain et al., 2020).

One procedural blank was prepared to monitor every seven samples with the same analytical procedure (Lin et al., 2021). To reduce the background level in the experiment, all procedures were performed in a laminar flow bench. All acid solutions were purified by an in-house distillation system, and glassware was cleaned by acid boiling using 6 M HCl. In addition, 0.1 mL aliquots of each raw sample and U eluate were diluted with 1 ppb Indium (internal standard)-0.5 M HNO_3 solution and prepared for ^{238}U measurement through the inductively coupled plasma mass spectrometry (ICP-MS, ICP-QQQ 8800, Agilent) (Qiao and Xu, 2018).

2.3. Measurement of colored dissolved organic matter absorption and nutrients

Water samples were filtered through 0.2 μm Millipore filter cartridges (part # KVGLA04HH3) into precombusted amber glass vials, then stored refrigerated (4 °C) in the dark and measured onboard within a few days using a Shimadzu UV-2401PC spectrophotometer. Measurements were performed using a 10 cm quartz cuvette with ultrapure water (Milli Q with UV lamp) as reference (Stedmon and Markager, 2001). Absorbance between 240 and 700 nm was recorded and converted to Naperian absorption coefficients. The CDOM absorption coefficient at 350 nm (a_{350}, units, m^{-1}) in the ultra-violet wavelength range is used here as a proxy for DOM concentration due to the correlations with concentrations of dissolved organic carbon and lignin (which is a terrestrial dissolved organic matter molecule) (Spencer et al., 2009; Stedmon et al., 2011; Gonçalves-Araujo et al., 2020).

Nitrite and phosphate were measured on board using a SmartChem 200 discrete analyzer following the reagent concentrations for the manual method in Hansen and Koroleff (1999), with the inclusion of a 150 g/L solution of sodium dodecylsulfate as a dispersant for the phosphate analysis. Nitrate was measured following the vanadium chloride reduction technique (Schnetger and Lehners, 2014). Community reference material for nutrients in seawater supplied by Kanso Technos Co. LTD, Japan, was used for assuring accuracy and assessing precision.

2.4. Isolating $^{236}U_{NRPs}$

The contribution of NRPs and GF in ^{236}U could be isolated through ^{233}U based on the following equations (Qiao et al., 2020):

$$P_{GF} = \frac{(R_{NRPs}^{233/236} - R_S^{233/236})}{(R_{NRPs}^{233/236} - R_{GF}^{233/236})} \approx \frac{R_S^{233/236}}{R_{GF}^{233/236}} \quad (1)$$

$$P_{NRPs} = 1 - P_{GF} \quad (2)$$

$$C_{s,GF}^{236} = C_s^{236} \times P_{GF} = \frac{C_S^{233}}{R_{GF}^{233/236}} \quad (3)$$

$$C_{s,NRPs}^{236} = C_s^{236} \times P_{NRPs} = C_s^{236} - C_{s,GF}^{236} \quad (4)$$

where P_{GF} and P_{NRPs} are the proportions of GF and NRPs in ^{236}U; $R_S^{233/236}$, $R_{NRPs}^{233/236}$ and $R_{GF}^{233/236}$ are the ^{233}U/^{236}U atomic ratio of the sample, and the representative values of 1×10^{-7} in NRPs endmember and $1.40 \pm 1.5 \times 10^{-2}$ in GF endmember, respectively (Hain et al., 2020; HELCOM MORS Discharge basement, 2020); C_s^{233}, C_s^{236}, C_{GF}^{236}, and C_{RP}^{236} are measured ^{233}U concentration, and total, GF-derived ($^{236}U_{GF}$) and NRPs-derived ($^{236}U_{NRPs}$) ^{236}U concentrations in the sample, respectively. The calculation of uncertainties is based uncertainty propagation (BIPM et al., 2008), and the detailed equations were summarized in our earlier study (Supporting information, Lin G. et al., 2022a).

2.5. Atlantic water endmember concentration of $^{236}U_{NRPs}$ and transit time estimation

The $^{236}U_{NRPs}$ input functions for the three Atlantic branch waters (NCC, BSBW, FSBW) were constructed (Casacuberta et al., 2018; Castrillejo et al., 2020; Lin G. et al., 2022a). The approach is summarized in the supporting information (Fig. S1 and Table S2). Three input functions showed a monotonically decreasing trend since 1970s, and the NCC input function carried a significantly stronger NRPs signal (14.34–287.92 $\times 10^6$ atom/L during 1976–2016 in the Barents Sea Opening) compared with the BSBW (3.54–61.31 $\times 10^6$ atom/L) and FSBW (2.16–42.98 $\times 10^6$ atom/L) input functions (Fig. S1). Based on the end-member mixing algorithm, the NRPs discharge concentration of ^{236}U could be constructed as below.

$$f_{aw}^{236}U_{NRPs\text{-}aw} + f_{pw}^{236}U_{NRPs\text{-}pw} + f_{fw}^{236}U_{NRPs\text{-}fw} = {}^{236}U_{NRPs} \quad (5)$$

where $^{236}U_{NRPs\text{-}aw}$, $^{236}U_{NRPs\text{-}pw}$ and $^{236}U_{NRPs\text{-}fw}$ are $^{236}U_{NRPs}$ endmember concentrations in Atlantic water, Pacific water and freshwater, respectively. f_{AW}, f_{PW} and f_{FW} are the fractions of Atlantic water, Pacific water and freshwater. As Pacific water and freshwater are assumed not to contain any reprocessing signal, the values of $^{236}U_{NRPs\text{-}pw}$ and $^{236}U_{NRPs\text{-}fw}$ are considered to be zero. Atlantic water fraction (f_{AW}) can be calculated through nitrate, phosphate and salinity (Jones et al., 2003; Dodd et al., 2012), and the method is described in supporting information.

Therefore,

$$f_{aw}{}^{236}U_{NRPs\text{-}aw} = {}^{236}U_{NRPs} \quad (6)$$

$${}^{236}U_{NRPs\text{-}aw} = {}^{236}U_{NRPs}/f_{aw} \quad (7)$$

The Atlantic water endmember of $^{236}U_{NRPs}$ ($^{236}U_{NRPs\text{-}aw}$) concentration could then be compared to the NRPs discharge input functions to provide an estimate of transit time. It can be inferred from equations ((6)–(7)) that, $^{236}U_{NRPs}$ concentration in the downstream seawater of the Arctic Ocean is only dependent on Atlantic water fraction and transit time. $^{236}U_{NRPs}$ is only presented in waters from the Atlantic, so the measured $^{236}U_{NRPs}$ concentration in the downstream seawater is a function of dilution by Pacific water and freshwater, and discharge date. The $^{236}U_{NRPs}$ discharge from SF (237 ± 21 kg) and LH (46 kg) (Castrillejo et al., 2020), are at least two orders of magnitude greater than the $^{236}U_{NRPs}$ output in the Baltic outflow (~407 g during 1981-2018) (Lin M. et al., 2022). The contribution of Baltic outflow to U in the Barents Sea Opening is deemed negligible.

3. Results and interpretations

3.1. Hydrography

Potential temperature (Θ) in Fram Strait ranged within −1.79–9.12 °C (Fig. 2d-f), while seawater salinity (practical salinity, S_P) varied between 28.55 and 35.05 (Fig. 2g-i). Overall, in the upper 200 m, seawater west of the meridian was dominated by outflowing cold and less saline Polar Surface Water (PSW) ($\sigma_\Theta \leq 27.70$, $\Theta \leq 0$, Rudels et al., 2005) with low S_P (<34.5). In contrast, surface waters east of the meridian were warmer and more saline. Seawater off the East Greenland Shelf at depths of 200–~1000 m was characterized by intermediate temperatures (0–2 °C) and high S_P (34.5–35) reflecting Arctic Atlantic Water (AAW) (Rudels et al., 2005). At depth > ~1000 m, waters were cold (<0 °C) and saline (>34.5) (Table S1). On the East Greenland Shelf, Θ therefore increased with depth with bottom waters having positive temperatures. Observations in the Fram Strait during 2019–2021 showed that the distribution of the outflowing PSW extended to the meridian in 2019 and 2021 and deeper than 200 m in 2020 and 2021 (Fig. 2d-i).

3.2. CDOM absorption

CDOM absorption, a_{350}, varied between 0.06 and 0.86 m^{-1}. Higher absorption values of a_{350} (≥0.35 m^{-1}) where generally associated with PSW in the upper 200 m of the western Fram Strait, primarily on the East Greenland Shelf (Fig. 2j-l). For the remainder of the section a_{350} was less than 0.35 m^{-1}, and in contrast to the low salinity waters in western Fram Strait, the higher salinity waters in the eastern Fram Strait were associated with low CDOM. For the samples analyzed for uranium isotopes, it indicated that the data could be split into two groups: samples with a_{350} above 0.35 m^{-1} and those below 0.35 m^{-1}. The coverage of high CDOM waters expanded from 2019 to 2021, and on average the values of a_{350} were notably higher in 2021 than in the other two years (Fig. 2j, k, and l).

3.3. Uranium isotopes

^{238}U concentrations in the seawater samples ranged between 2.64–3.52 μg/L, and the concentrations of ^{233}U (1.90–22.48 $\times 10^4$ atom/L) and ^{236}U (3.67–39.01 $\times 10^6$ atom/L) showed different distribution patterns in the Fram Strait during 2019–2021 (Fig. 3a-l, Table S1). ^{236}U concentrations were higher at depths between 100 – ~1000 m on the western shelf, while the distribution of ^{233}U was more even across the Fram Strait. The lowest concentrations of ^{233}U and ^{236}U were found in deep water (below ~1000 m) (Table S1). ^{233}U/^{236}U ratios across the Fram Strait varied between 0.13–1.46 $\times 10^{-2}$ (Fig. 3m-o). The highest concentrations of ^{233}U and ^{236}U, and highest ^{233}U/^{236}U ratio were measured in 2020.

Compared with seawater, sea ice cores had very low concentrations of ^{233}U (0.15–1.01 $\times 10^4$ atom/L), ^{236}U (0.23–0.95 $\times 10^6$ atom/L) and ^{238}U (0.01–0.15 μg/L), but the range in ^{233}U/^{236}U ratios was comparable to that observed in seawater (0.29–1.06 $\times 10^{-2}$) (Table S1).

GF fraction was between 0.09–1 of the ^{236}U in the samples measured (Fig. 4a-c), and conversely the NRPs fractions ranged from 0 to 0.91 (Fig. 4d-f). $^{236}U_{GF}$ concentrations were calculated between 1.36–16.06 $\times 10^6$ atom/L (Fig. 4g-i), and $^{236}U_{NRPs}$ concentrations varied within 0–29.38 $\times 10^6$ atom/L (Fig. 4j-l). Highest $^{236}U_{NRPs}$ concentrations were observed between 100 – ~1000 m around the western shelf region of the Fram Strait and $^{236}U_{NRPs}$ concentrations in 2021 were more variable than in the previous two years. The Atlantic water fractions were between 0.34–1. Estimated $^{236}U_{NRPs\text{-}aw}$ concentrations varied between 0.47–40.82 ×

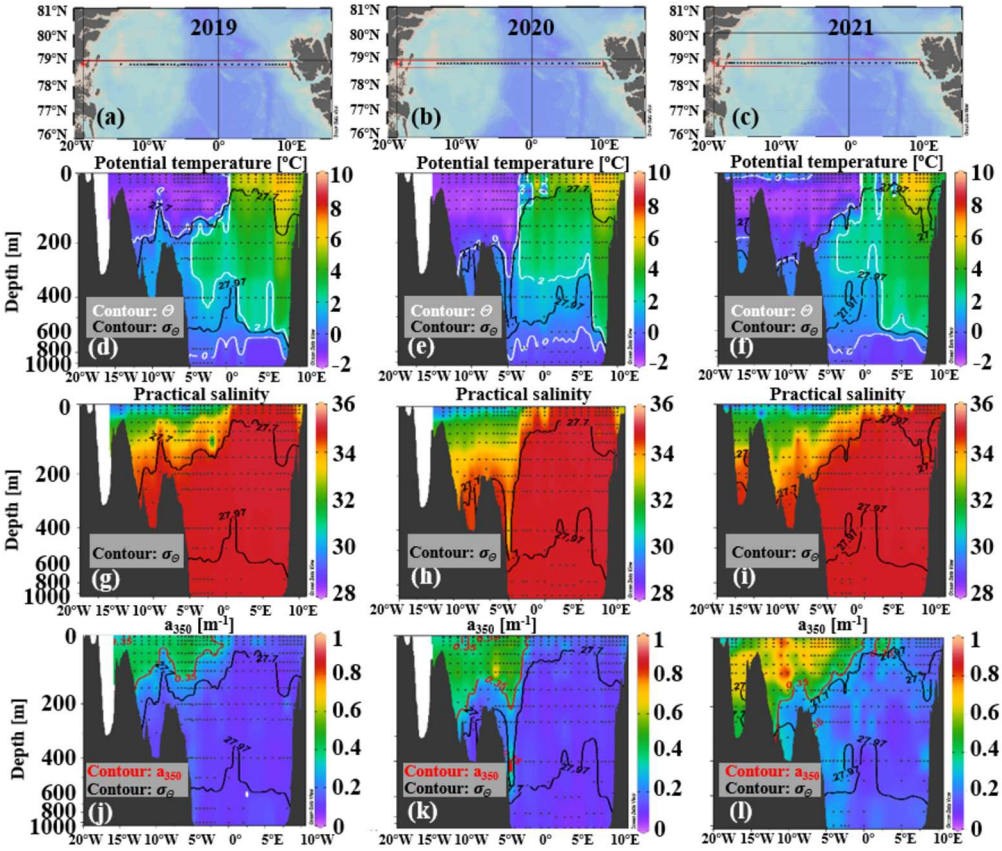

Fig. 2. Transects (a-c) of potential temperature (d-f), practical salinity (g-i) and a_{350} (j-l) in the upper ~1000 m across the Fram Strait in 2019 (left panels), 2020 (middle panels) and 2021 (right panels). White isolines are the value of Θ at 0 °C or 2 °C; Black isolines are the value of σ_Θ at 27.70 or 27.97; Red isolines are the value of a_{350} at 0.35 m^{-1}.

10^6 atom/L, and concentrations in the western Fram Strait were higher in 2021 than in 2019 and 2020 (Fig. 4m-o).

3.4. The merits of $^{236}U_{NRPs}$ as a tracer for Atlantic water

Comparison of the distribution of $^{236}U_{NRPs}$ and total ^{236}U reveals that higher total ^{236}U level in the Fram Strait is not necessarily a direct influence of Atlantic water due to interference from $^{236}U_{GF}$. The distribution of $^{236}U_{GF}$ across the Fram Strait transect is heterogeneous, as can be seen clearly from Fig. 4g-i. The average contributions of $^{236}U_{GF}$ to the total ^{236}U in 2019 (47%), 2020 (53%) and 2021 (36%) indicate that at approximate half of the ^{236}U is from GF. In such cases, the use of $^{236}U_{NRPs}$ is more advantageous reducing uncertainties in tracing transit times for Atlantic water. $^{236}U_{NRPs}$ provides a direct signal for Atlantic water movement in the Arctic Ocean, so it is better to use $^{236}U_{NRPs}$ to replace total ^{236}U.

3.5. The correlation between estimated $^{236}U_{NRPs\text{-}aw}$ and CDOM

To understand the relation of Atlantic waters transit times and pathways with CDOM levels, the estimated $^{236}U_{NRPs\text{-}aw}$ concentration vs. a_{350} is plotted in Fig. 5a. The observational data during 2019–2021 shows a general positive correlation between $^{236}U_{NRPs\text{-}aw}$ vs. a_{350} (Fig. 5a). Two clusters of data stand out: one with CDOM ≥0.35 m^{-1} and another with CDOM <0.25 m^{-1}. While at intermediate CDOM levels ($0.25 < a_{350} < 0.35$ m^{-1}), no robust trend can be seen between $^{236}U_{NRPs\text{-}aw}$ vs. a_{350} across both groups. A linear regression between estimated $^{236}U_{NRPs\text{-}aw}$ and a_{350} indicates the slopes of low and high CDOM clusters differed by approximately a factor of two (Fig. 5a).

3.6. Constraining NRPs input functions in the Fram Strait using CDOM

CDOM absorption was used to support the selection of different input functions. The amount of marine CDOM in Atlantic water can be constrained from observations in northward flowing waters west of Svalbard, which reveal that absorption at 350 nm is less than 0.35 m^{-1} (Fig. 2). Conversely the Arctic outflow in the western Fram Strait has high CDOM levels (≥0.35 m^{-1}) representing waters that have entrained terrestrial CDOM from Arctic rivers. Waters from the NCC enter the Arctic Ocean along the Siberian coast (Fig. 1), which is supported by the model results of ^{129}I (Karcher et al., 2012; Smith et al., 2021). In this branch with Atlantic water supplied by the NCC, CDOM levels are influenced by the subsequent circulation along the Siberian shelf (Fig. 1). We therefore define them here as 'Arctic High CDOM Water' (Table 1). A recent study proposes that there is the potential for mixing of waters from the NCC and BSBW or FSBW in the Barents Sea based on an analysis of ^{129}I and ^{236}U in the Amundsen Basin and the NCC input function (Wefing et al., 2022). The circulation in the Barents Sea shows that BSBW may be divided into two branches (see Fig. 1) (Loeng, 1991). One branch moves coastward and partially mix with waters from the NCC on the Arctic shelf. Thus, a mixture of NCC and BSBW signals should be considered as the input function for Arctic High CDOM Water (Table 1). The samples in this group were associated with surface waters on the east Greenland Shelf (Fig. 6a-d). In addition, two seawater samples (2020) located in very surface layer (5–25 m) of the shelf have low CDOM levels (<0.35 m^{-1}) (Table S1). This may be related to a strong local dilution from sea ice meltwater, which has a freshening effect in the upper ~40 m of the Fram Strait (Dodd et al., 2012;

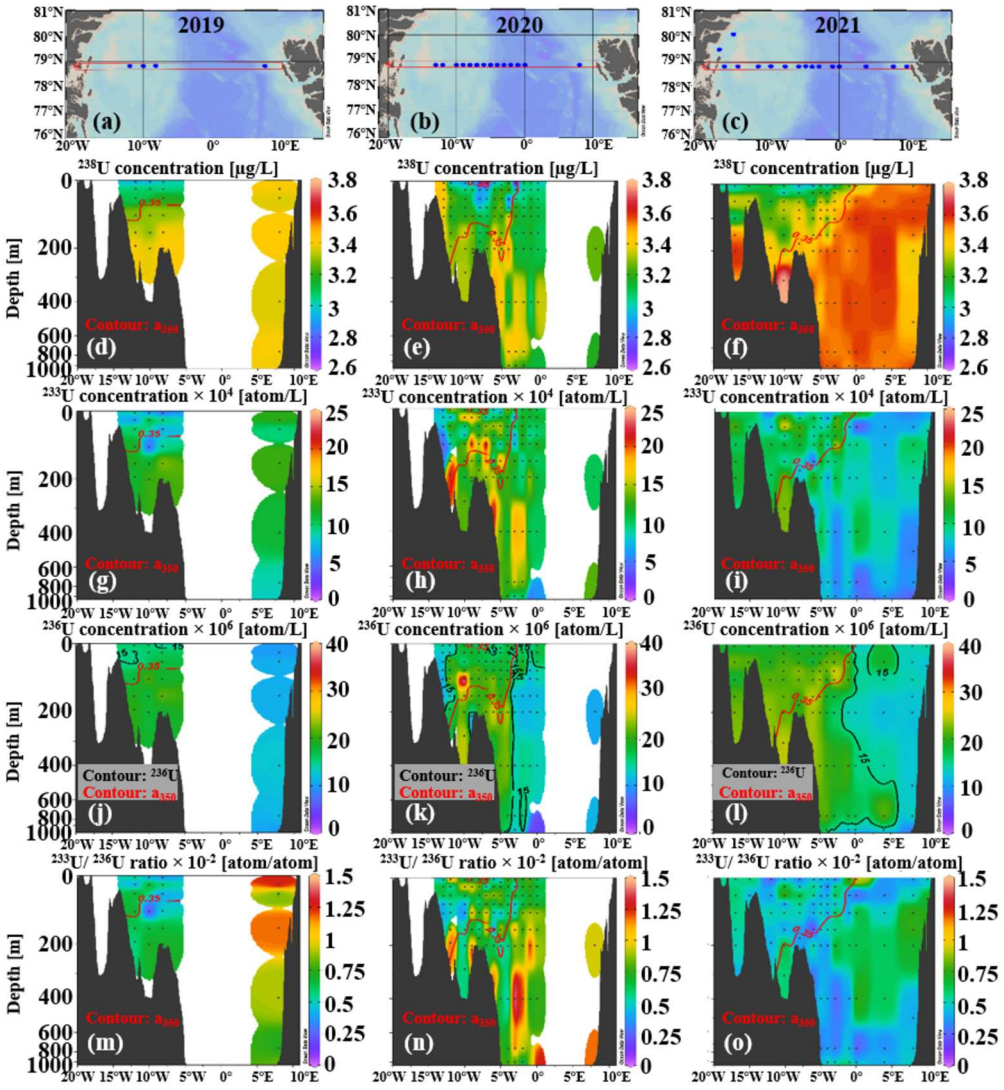

Fig. 3. Transects (a-c) of the concentrations of ^{238}U (d-f), ^{233}U (g-i) and ^{236}U (j-l) and the ^{233}U/^{236}U ratio (m-o) in the upper ~1000 m across the Fram Strait in 2019 (left panels), 2020 (middle panels) and 2021 (right panels). Red isolines are the value of a_{350} at 0.35 m^{-1}; Black isolines are the value of ^{236}U concentration at 15 × 10^6 atom/L.

Gonçalves-Araujo et al., 2016). Therefore, they are still characterized as 'Arctic High CDOM Water' here.

The remainder of waters in the Fram Strait had low CDOM levels ($a_{350} < 0.35$ m^{-1}) but could be further distinguished through Θ, σ_Θ and ^{236}U concentration. Low CDOM seawater in the Fram Strait originates from the Arctic Ocean and the North Atlantic Ocean, and their sources can be identified through different Θ. The inflowing Atlantic water in the eastern Fram Strait flows northwards with Θ over 2 °C and low-intermediate σ_Θ ($\sigma_\Theta \leq 27.97$). North of the Fram Strait, a portion of this current turns west to return southwards as RAW ($2 < \Theta$, $27.7 < \sigma_\Theta \leq 27.97$) (Rudels 2005 and 2009; Marnela et al., 2013). As this has only had a short transit in the Arctic, it is still relatively warm ($\Theta > 2$ °C). The RAW derives from the inflowing Atlantic water of the West Spitsbergen Current without entering the Arctic Ocean proper. These waters originate from the North Atlantic Ocean and thus are defined as 'Atlantic Low CDOM Water' affected by the input function of FSBW (Table 1, Fig. 6e-h).

The Arctic-derived low CDOM water characterized by low Θ (≤2 °C) represents the seawater which has taken a longer passage through the Arctic Ocean (Rudels 2005 and 2009) without passing over shelf or interacting with waters with high CDOM from the shelves (Table 1, Fig. 6i-l). Consequently, the input function of the offshore BSBW and FSBW should match with the Arctic-derived low CDOM rather than the NCC input function. For the Arctic-derived low CDOM water, the ~1000 m of the Fram Strait is characterized by lower σ_Θ (≤27.97) or high ^{236}U concentration (≥ 15 × 10^6 atom/L) and thus is defined as 'Arctic Low CDOM / High ^{236}U Water'. In contrast, the deepest waters (> ~1000 m) in the Fram Strait are characterized higher σ_Θ (>27.97) and low ^{236}U concentration (≤10 × 10^6 atom/L) (Table 1), and this is derived from a mixture of anthropogenic ^{236}U and natural ^{236}U. These waters form the basis of the fourth water class 'Arctic Low CDOM / Low ^{236}U Water'.

Although the average $^{236}U_{NRPs}$ for the cold waters representing Atlantic water with a longer passage in the Arctic (Arctic High CDOM Water and Arctic Low CDOM / High ^{236}U Water) are comparable in magnitude, the $^{236}U_{NRPs\text{-}aw}$ values were more distinctly different, with higher values for Arctic High CDOM Water, in part reflecting the removal of the effect of dilution of the Atlantic water signal with Pacific water and freshwater (Table 1).

3.7. Estimating Atlantic water transit time with constrained input functions

The corresponding NRPs input functions for different water classes in the Fram Strait were applied based on the categorization

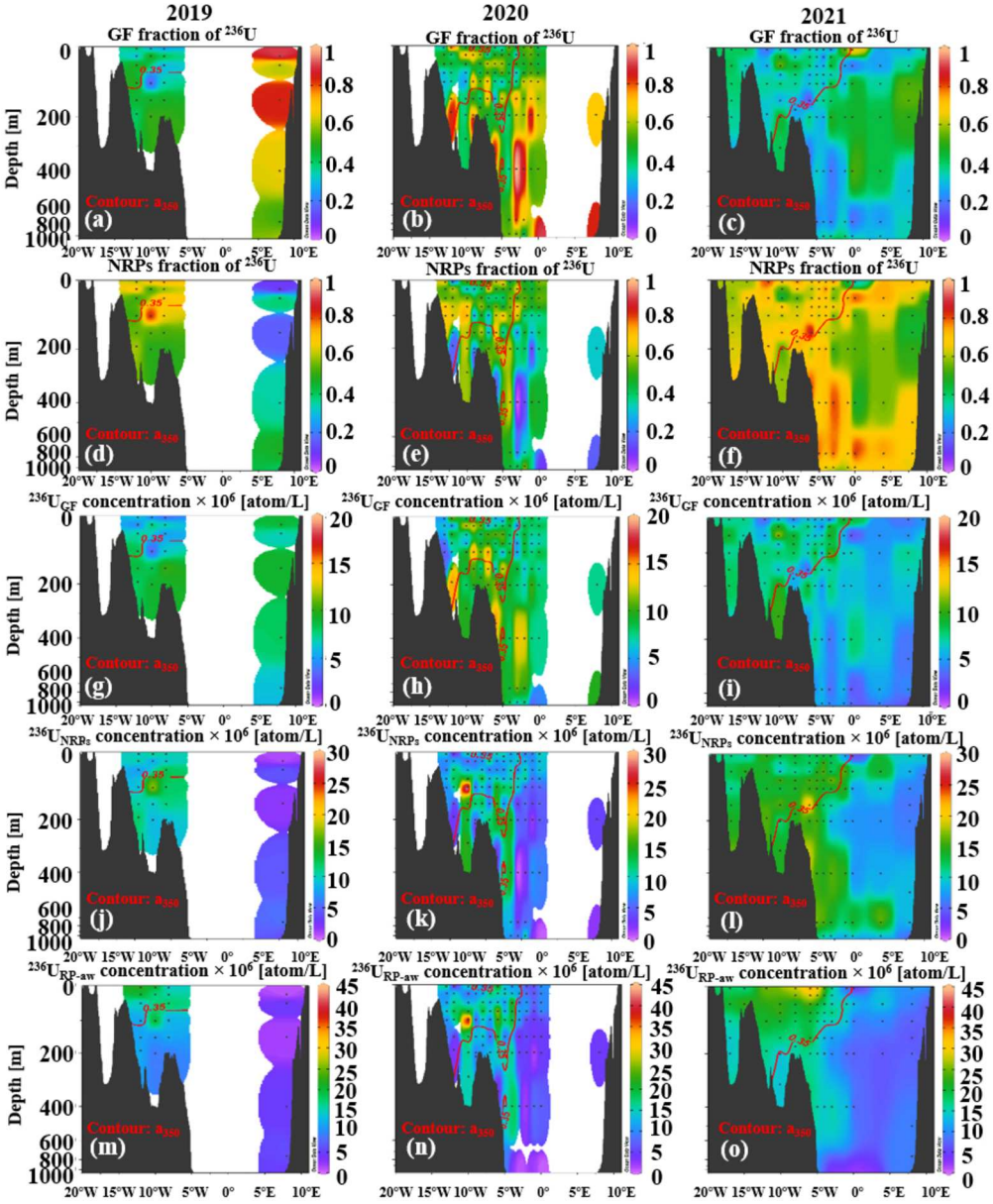

Fig. 4. Transects of the fractions of GF (a-c) and NRPs (d-f), the concentrations of $^{236}U_{GF}$ (g-i) and $^{236}U_{NRPs}$ (j-l), and estimated $^{236}U_{NRPs\text{-}aw}$ concentration (m-o) in the upper ~1000 m across the Fram Strait in 2019 (left panels), 2020 (middle panels) and 2021 (right panels). Red isolines are the value of a_{350} at 0.35 m^{-1}.

in Table 1 and using the derived average $^{236}U_{NRPs\text{-}aw}$ concentrations (Table 2). Here the Arctic Low CDOM / Low ^{236}U Water is not considered as it is essentially devoid of $^{236}U_{NRPs}$. The average estimated $^{236}U_{NRPs\text{-}aw}$ concentration for each water class was matched to the input functions of $^{236}U_{NRPs}$ concentration, to determine the source year of Atlantic water entering the Arctic Ocean (Fig. 7). The uncertainty of source year is estimated through the match of uncertainties of the input functions and standard deviation of estimated $^{236}U_{NRPs\text{-}aw}$ concentration, obtaining the potentially oldest and earliest source years. In addition, due to the unclear mixing patterns for two input functions, we examine the impact of varying their relative contributions from 0%–100% on estimates of source year.

Although the NCC and BSBW regulate the supply of $^{236}U_{NRPs}$ to Arctic High CDOM Water class, their relative contributions are unclear and must be assumed. In Fig. 7a and Table 2, we provide the full potential range in expected input function values from mixing of both. This results in a wide range in potential source years from 1993 to 2013 depending on the assumed mixture of source waters. A 50:50 contribution of NCC and BSBW results in an estimated source year of 2006 (uncertainties: 2000–2015) which results in a transit time of 14 (5–20) yrs (assuming measurement year to be 2020). The greater assumed contribution of BSBW in source waters is the older the estimated age is (Fig. 7a), due to the low $^{236}U_{NRPs\text{-}aw}$ concentration in BSBW.

The situation is much simpler for Atlantic Low CDOM Water as it is only affected by the FSBW, and its transit time is calculated to be 20 (8–27) yrs (Fig. 7b and Table 2). For Arctic Low CDOM / High ^{236}U Water, the contribution of the BSBW and the FSBW is assumed to vary between 0–100% (Fig. 7c and Table 2), although previously this has been assumed to have an equal contribution from each (Wefing et al. (2021). Based on different contributions of the BSBW and the FSBW, the potential range in average source years was between 1992 (1986–1994) and 1998 (1993–2004) and this resulted in a transit time of 22–28 (16–34) yrs. Younger age is estimated from a larger BSBW contribution due to relative higher $^{236}U_{NRPs\text{-}aw}$ concentration (with the FSBW).

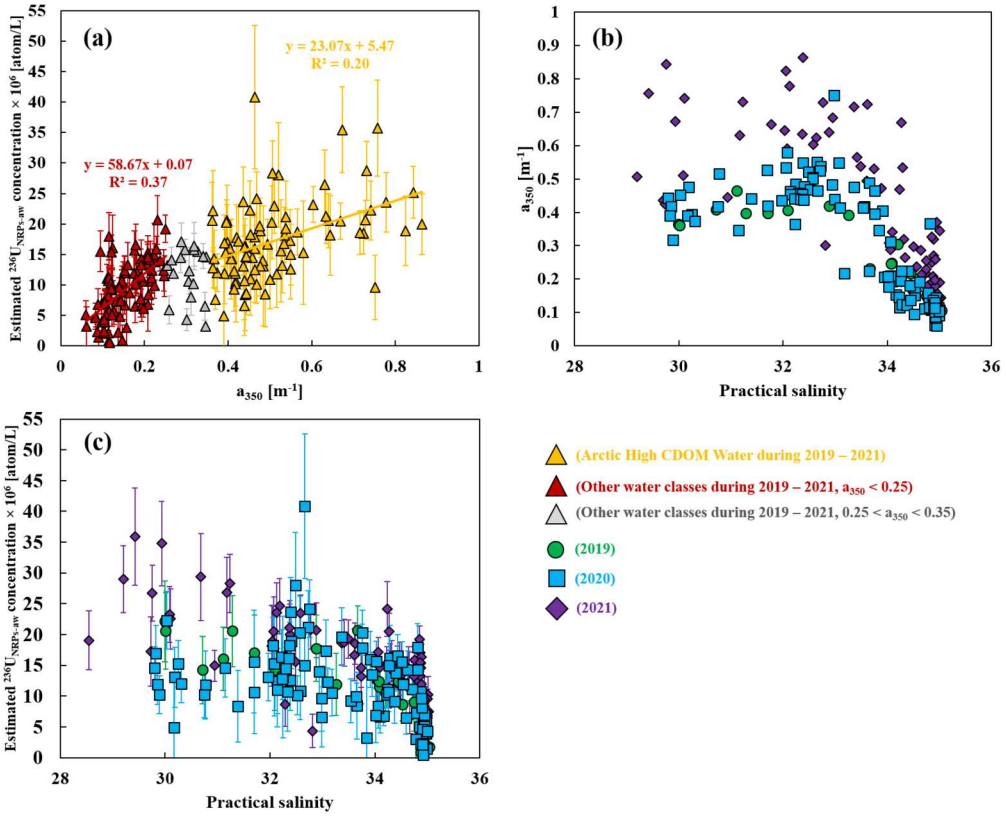

Fig. 5. The pairwise relationship between the estimated $^{236}U_{NRPs\text{-}aw}$ concentration, a_{350} and practical salinity (a-c).

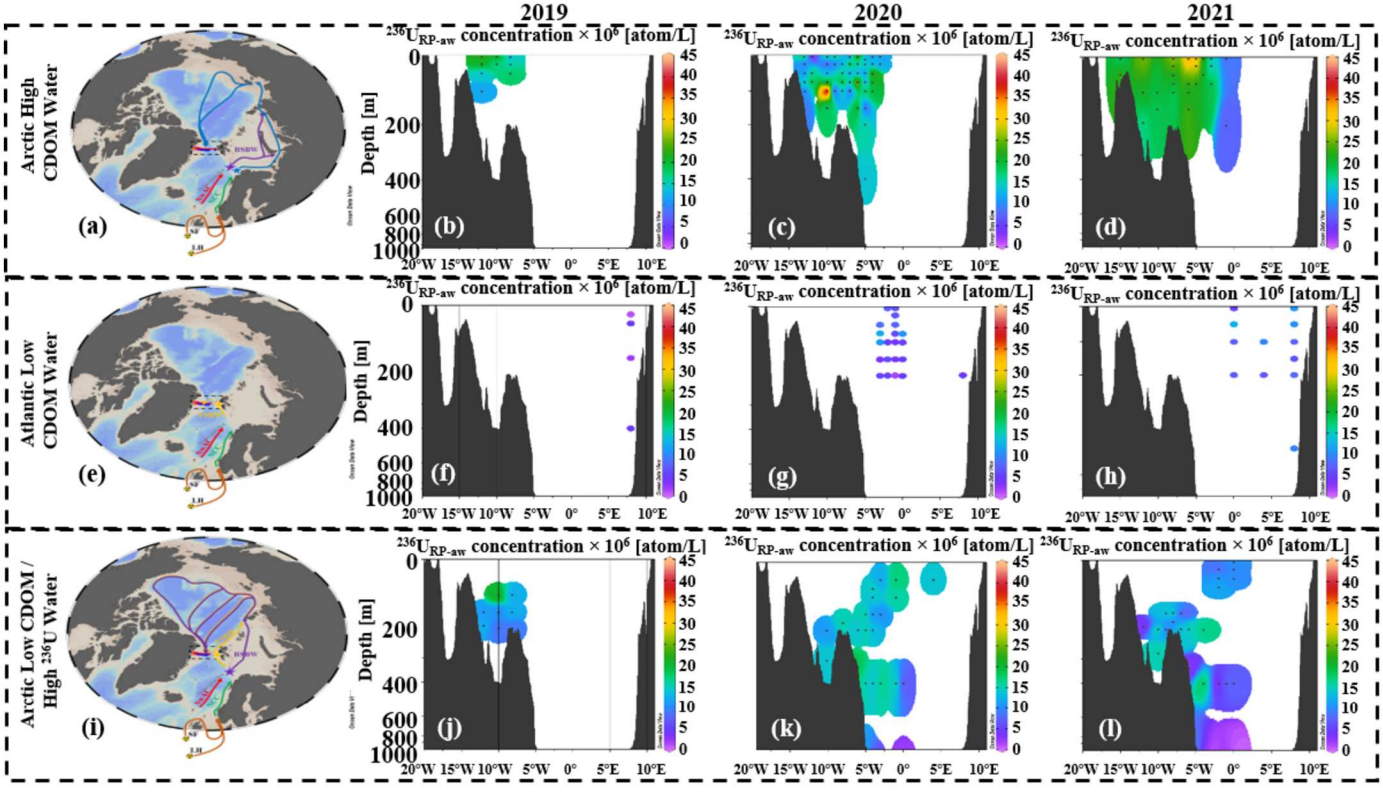

Fig. 6. The distribution of the estimated $^{236}U_{NRPs\text{-}aw}$ concentration in different water classes in the Fram Strait and their proposed transport pathways in the Arctic Ocean.

Table 1
Characteristics of the different water classes in the Fram Strait.

Properties	Years	Arctic High CDOM Water* (n = 108)	Atlantic Low CDOM Water (n = 40)	Arctic Low CDOM / High ^{236}U Water (n = 79)	Arctic Low CDOM / Low ^{236}U Water (n = 14)
Average Θ [°C]	2019	−1.3 ± 0.23	5.62 ± 1.43	−0.19 ± 0.74	
	2020	−1.36 ± 0.65	3.32 ± 0.71	0.12 ± 0.90	−0.71 ± 0.02
	2021	−0.84 ± 1.03	3.55 ± 1.40	0.33 ± 0.92	−0.65 ± 0.08
Average S_p	2019	31.45 ± 1.16	34.95 ± 0.09	34.28 ± 0.34	
	2020	32.11 ± 1.23	34.75 ± 0.30	34.41 ± 0.53	34.92 ± 0.003
	2021	32.12 ± 1.63	34.78 ± 0.55	34.69 ± 0.27	34.92 ± 0.01
Average a_{350} [m^{-1}]	2019	0.40 ± 0.03	0.12 ± 0.02	0.22 ± 0.05	
	2020	0.46 ± 0.07	0.13 ± 0.06	0.17 ± 0.06	0.11 ± 0.02
	2021	0.61 ± 0.13	0.16 ± 0.08	0.24 ± 0.07	0.18 ± 0.08
Average $^{236}U_{NRPs}$ concentration × 10^6 [atom/L]	2019	9.82 ± 1.48	2.86 ± 1.83	11.38 ± 3.01	
	2020	9.48 ± 4.02	5.63 ± 2.10	8.86 ± 4.50	1.27 ± 0.76
	2021	13.49 ± 2.83	7.64 ± 1.72	13.67 ± 2.54	3.92 ± 1.64
Average estimated $^{236}U_{NRPs\text{-}aw}$ concentration× 10^6 [atom/L]	2019	17.16 ± 3.43	2.90 ± 1.87	12.17 ± 3.73	
	2020	14.92 ± 5.89	6.11 ± 2.67	11.38 ± 5.06	1.47 ± 0.91
	2021	20.74 ± 6.18	8.12 ± 2.09	14.16 ± 2.47	3.26 ± 2.35
Corresponding source waters		NCC-BSBW	FSBW	BSBW-FSBW	

* Two surface seawater samples in 2020 with lower a_{350} values (<0.35 m^{-1}) are also included in Arctic High CDOM Water due to the local dilution from sea ice meltwater.

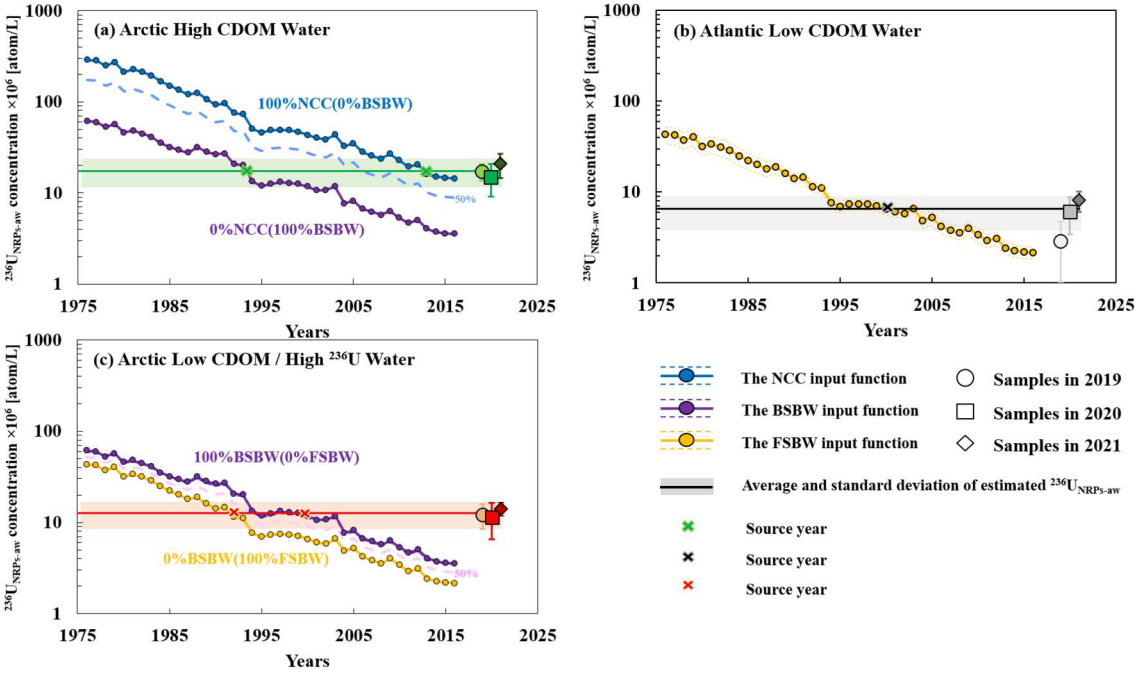

Fig. 7. The average estimated $^{236}U_{NRPs\text{-}aw}$ concentration in 2019–2021 and Atlantic water transit time estimates for Arctic High CDOM Water (a), Atlantic Low CDOM Water (b) and Arctic Low CDOM / High ^{236}U Water (c) through comparing the input functions of $^{236}U_{NRPs}$ concentration in the Barents Sea Opening. The dashed line in (a) and (c) indicates a 50:50 mixture of contribution from NCC/FSBW and BSBW assumed by Wefing et al. (2021).

4. Discussion

4.1. The variation of estimated $^{236}U_{NRPs\text{-}aw}$ and CDOM

The fact that there are clear correlations between $^{236}U_{NRPs\text{-}aw}$ and a_{350}, reflects the water mass mixing patterns (Fig. 5a). Arctic High CDOM Water has a high degree of scatter but there is an indication of a positive relationship suggesting that in these waters the highest CDOM contribution is associated to older water with the highest Atlantic end member $^{236}U_{NRPs}$ concentration. The scatter is most likely due to the inclusion of nutrient and salinity data to subtract the effect of dilution and derive $^{236}U_{NRPs\text{-}aw}$ concentrations. The scatter is less for the lower CDOM waters as the corresponding correction factor is also lower (greater proportion of Atlantic water). The linear fittings indicate a significantly lower slope for $^{236}U_{NRPs\text{-}aw}$ vs. a_{350} in Arctic High CDOM Water (slope = 23.07) compared to other lower CDOM waters (slope = 58.67). The low slope observed for Arctic High CDOM Water suggests that the levels of CDOM increase rapidly as the transit time and transport pathway become longer.

The longer transit time and transport pathway of Atlantic water facilitate the contribution of high levels of CDOM from Siberian rivers. In contrast, the high slope in the sample from the other lower CDOM water classes reveals that CDOM levels increase only

Table 2
Estimates of source year and transit times for each water class and an indication of how the assumption of source water mixing influences estimates. (Arctic Low CDOM / Low ^{236}U Water is not estimated here due to the essential lack of $^{236}U_{NRPs}$).

Water classes	Average $^{236}U_{NRPs\text{-}aw} \times 10^6$ [atom/L]	Input function assumption	Source year	Transit time* (from 2020)
Arctic High CDOM Water	17.49 ± 6.41	100% NCC	2013 (2009 - >2016)	7 (<4 - 11)
		50:50 NCC:BSBW	2006 (2000 - 2015)	14 (5 - 20)
		100% BSBW	1993 (1991 - 2001)	27 (19 - 29)
Atlantic Low CDOM Water	6.51 ± 2.82	FSBW	2000 (1993 - 2012)	20 (8 - 27)
Arctic Low CDOM / High ^{236}U Water	12.70 ± 4.03	100% BSBW	1998 (1993 - 2004)	22 (16 - 27)
		50:50 BSBW:FSBW	1994 (1990 - 2002)	26 (18 - 30)
		100% FSBW	1992 (1986 - 1994)	28 (26 - 34)

* Transit time in this study only considers the advective transport due to strong water stratification in the Arctic Ocean and thus refers to tracer age.

slightly with longer transit time and transport pathway. These waters are transported by the offshore waters, passing through the regions with relatively low CDOM levels and limited entrainment of high CDOM shelf waters. Consequently, we can get a positive correlation between $^{236}U_{NRPs\text{-}aw}$ and a_{350} but with a different slope.

To analyze for any systematic differences between years a_{350}-S_p and $^{236}U_{NRPs\text{-}aw}$-S_p plots were made (Fig. 5b and c). There was a notable difference in the estimated $^{236}U_{NRPs\text{-}aw}$ in seawaters with lower S_p (<32) between 2019–2020 and 2021, while the estimated $^{236}U_{NRPs\text{-}aw}$ concentration appears comparable at higher S_p (>32). To test for statistical difference, all estimated $^{236}U_{NRPs\text{-}aw}$ concentrations in Arctic High CDOM Water in 2019–2021 were subjected to T-Test. The results indicate that the estimated $^{236}U_{NRPs\text{-}aw}$ values for 2019 and 2020 are similar ($p > 0.05$), but significantly different from those in 2021 ($p < 0.05$). Higher $^{236}U_{NRPs\text{-}aw}$ concentration suggests a longer Atlantic water transit time and pathway in the Arctic Ocean in 2021 compared to 2019-2020 (Fig. 5c). CDOM levels at low and intermediate salinities also appear to be higher in 2021 than in the preceding years. While this could be explained by variability in contribution of river water, Pacific water and sea ice melt water, this is not true for $^{236}U_{NRPs\text{-}aw}$ which remains unaffected. The fact that there is a tendency for both $^{236}U_{NRPs\text{-}aw}$ and a_{350} values to be higher at low salinities in 2021 suggests that there may be a difference in Atlantic waters transit times and pathways.

4.2. Comparison of derived Atlantic water transits times

Estimates of transit time of Atlantic water entering the Arctic and traveling along the Siberian shelf (High CDOM Arctic waters) are very sensitive to the selection of proportions of water from NCC and BSBW, as these are expected to differ considerably in their U concentrations. The transit time estimate derived ranges between 7 and 27 yrs. If we assume a 50-50 contribution the estimate in Arctic High CDOM Water (upper ~200 m) is 14 yrs which is comparable with earlier estimates (12–19 yrs) in NCC-influenced PSW using ^{129}I-^{236}U tracer approach (Wefing et al., 2019) and longer than that estimated for surface waters near the North Pole using ^{129}I-^{137}Cs (Smith et al., 2011). The latter technique estimated a transit time of 8–11 yrs in NCC-influenced surface water (upper 60 m), assuming a 1-yr delay from 60°N on the Norwegian coast (Smith et al., 2011). As the gateway for the outflowing water, estimated transit time would be longer in the Fram Strait. However, Atlantic water transit time in the Fram Strait can be expected to vary depending on dominant transport pathways, which are in part associated with circulation pattern changes induced by regional phenomena such as the Arctic Oscillation (AO) (Karcher et al., 2012). A positive mean AO index in January – March facilitates longer transport pathways of water Arctic High CDOM Water in the East Siberian Sea and the Mendeleev Ridge (Karcher et al., 2012; Smith et al., 2021). The movement along shorter pathways along the Lomonosov Ridge is related to a negative mean AO index (Karcher et al., 2012; Smith et al., 2021). Therefore, we can expect that the AO index likely has a partial impact on CDOM and U levels. Longer transit time for the Arctic High CDOM Water estimated from higher $^{236}U_{NRPs\text{-}aw}$ concentration in the Fram Strait reveals that more Siberian rivers-derived terrestrial CDOM can be entrained and exported.

For Arctic Low CDOM / High ^{236}U Water, our estimates show longer transit times (22–28 yrs) compared with Arctic High CDOM Water, and they are also longer than that reported for BSBW-influenced intermediate Atlantic water (16–23 yrs, ^{129}I-^{236}U tracer) in the western Fram Strait (Wefing et al., 2019). An earlier study based on tracer ages from ^{129}I-^{137}Cs obtained transit times ranging within 8–14 yrs for the intermediate Atlantic water (depth: ~200–~1000 m) in the central Arctic Ocean near the North Pole affected by BSBW and FSBW, and relatively longer transit times (17–20 yrs) in the Canada Basin (Smith et al., 2011). Transport pathway of intermediate Atlantic water is also partly influenced by the AO index (Karcher et al., 2012; Smith et al., 2021), so the slightly longer transit times in our estimates may be related to the change of transport pathways in different periods.

The Atlantic Low CDOM Water has the lowest $^{236}U_{NRPs\text{-}aw}$ concentration which would at first suggest that it has the shortest transit time. However, it has its origins in the FSBW which is assumed to have a very low NRPs contribution, and this results in a transit time estimate of 20 yrs which is surprisingly long when taking into account the fact that this water is relatively warm and represents RAW. The overestimated result may be due to the fact that the $^{236}U_{NRPs\text{-}aw}$ concentrations overlap with a period of consistently low levels ($<10 \times 10^6$ atom/L) in the input function of FSBW since 1994 (Fig. S2), resulting from reduced discharges from the reprocessing plants. Our observations of $^{236}U_{NRPs}$ in the upper 200 m depth at 8°E show variable values during 2019–2021 (Fig. S2), and deviate from the FSBW input function available for the latest years (2015-2016), implying that $^{236}U_{NRPs}$ is not suitable for tracing "young" Atlantic water, such as that in the RAW in the Fram Strait.

4.3. Limitations

There are several limitations in the method applied that deserve highlighting and contribute to the variability in the transit times estimated. The low concentrations of ^{233}U necessitate large sample volumes and introduce uncertainties in the derived $^{233}U/^{236}U$ ratios and isolation of $^{236}U_{NRPs}$. Improvement of the detection methods in the future can help rectify this issue. The further isolation of the Atlantic water endmember concentration of $^{236}U_{NRPs}$ is depended on the correction for dilution by freshwater and Pacific water. Here Pacific water is estimated from its assumed nitrate deficit relative to Atlantic water and there is a discussion of how precise this method of identifying Pacific water contributions is (Jones et

al., 1998; Alkire et al., 2019). To overcome this, new methods for water fractionation in the Arctic may be used, such as dissolved gallium and neodymium isotopes (Laukert et al., 2017; Whitmore et al., 2020). Some of the large range in transit time estimates is also due to the unfortunate period of constant $^{236}U_{NRPs}$ concentrations in the input functions of all Atlantic branch waters between 1994–2003. A longer time series of measurements from the region will help to refine transit time estimates. Finally as our calculations have shown, the transit time estimates are very sensitive to the assumption of the extent of dilution and mixing of NRPs input functions. An effort to improve estimates of $^{236}U_{NRPs}$ concentrations in Atlantic water at high latitudes would be highly beneficial for the use of ^{233}U and ^{236}U as tracers for Arctic ocean circulation.

5. Conclusion

In this work, $^{236}U_{NRPs}$ was applied, instead of the total ^{236}U, to trace Atlantic water in the Fram Strait thus to avoid interference from GF-^{236}U signal. Additionally CDOM content was included to aid the selection of appropriate input functions, reflecting the different source branch waters and pathways. The estimated transit times on the whole agree with earlier estimates but their accuracy and reliability can still be affected by the inherent uncertainty in the composition of input function (source waters). A reconstruction of $^{236}U_{NRPs}$ concentration through model result or records from sea shells or coral in the Arctic is useful for understanding the mixing pattern of different input functions and thus is expected to consummate our estimate. In addition, $^{236}U_{NRPs\text{-}aw}$ concentrations in 2019 and 2020 are very similar, but the significant difference in 2021 indicates a shift in transit pathways of Arctic High CDOM Water. Older water ages we estimate in Arctic High CDOM Water, higher CDOM contents we find. However, other water classes do not show changes.

CRediT authorship contribution statement

Gang Lin: Writing – original draft, Methodology, Investigation, Formal analysis, Data curation, Conceptualization. **Jixin Qiao:** Writing – review & editing, Supervision, Resources, Methodology, Data curation, Conceptualization. **Paul A. Dodd:** Writing – review & editing, Resources, Investigation. **Rafael Gonçalves-Araujo:** Writing – review & editing, Resources, Methodology, Investigation, Data curation. **Mats A. Granskog:** Writing – review & editing, Resources, Investigation. **Peter Steier:** Writing – review & editing, Resources, Methodology, Investigation, Data curation. **Colin A. Stedmon:** Writing – review & editing, Supervision, Resources, Methodology, Investigation, Data curation, Conceptualization.

Declaration of competing interest

The authors declare that they have no known competing financial interests or personal relationships that could have appeared to influence the work reported in this paper.

Data availability

Data will be made available on request.

Acknowledgements

We thank the captain and crews of the expedition aboard R/V Kronprins Haakon of the Norwegian Polar Institute. And part of the ship-time leading to these results (2020 and 2021) was funded by the European Union H2020 as part of the EU Project ARICE grant agreement No. 730965. We also acknowledge the financial support of Independent Research Fund Denmark (9040-00266B), the RADIATE project from the EU Research and Innovation programme Horizon 2020 under grant agreement No 824096, proposal No. 21002394-ST.

Appendix A. Supplementary material

Supplementary material related to this article can be found online at https://doi.org/10.1016/j.epsl.2023.118415.

References

Aarkrog, A., Boelskifthe, S., Dahlgaard, H., Duniec, S., Hallstadius, L., Holm, E., Smith, J.N., 1987. Technetium-99 and caesium-134 as long distance tracers in Arctic water. Estuar. Coast. Shelf Sci. 24, 637–647. https://doi.org/10.1016/0272-7714(87)90103-X.

Alkire, M.B., Rember, R., Polyakov, I., 2019. Discrepancy in the identification of the Atlantic/Pacific front in the central Arctic Ocean: NO versus nutrient relationships. Geophys. Res. Lett. 46 (7), 3843–3852. https://doi.org/10.1029/2018GL081837.

Andersson, P.S., Wasserburg, G.J., Chen, J.H., Papanastassiou, D.A., Ingri, J., 1995. ^{238}U-^{234}U and ^{232}Th-^{230}Th in the Baltic Sea and in river water. Earth Planet. Sci. Lett. 130, 217–234. https://doi.org/10.1016/0012-821X(94)00262-W.

BIPM, I., IFCC, I., ISO, I., IUPAP, O., 2008. Evaluation of Measurement Data—Guide to the expression of Uncertainty in Measurement, JCGM 100: 2008 GUM 1995 with Minor Corrections. Jt. Comm. Guid. Metrol.

Casacuberta, N., Christl, M., Lachner, J., van der Loeff, M.R., Masqué, P., Synal, H.-A., 2014. A first transect of ^{236}U in the North Atlantic Ocean. Geochim. Cosmochim. Acta 133, 34–46. https://doi.org/10.1016/j.gca.2014.02.012.

Casacuberta, N., Masqué, P., Henderson, G., van-der-Loeff, M.R., Bauch, D., Vockenhuber, C., Daraoui, A., Walther, C., Synal, H.A., Christl, M., 2016. First ^{236}U data from the Arctic Ocean and use of $^{236}U/^{238}U$ and $^{129}I/^{236}U$ as a new dual tracer. Earth Planet. Sci. Lett. 440, 127–134. https://doi.org/10.1016/j.epsl.2016.02.020.

Casacuberta, N., Christl, M., Vockenhuber, C., Wefing, A.-M., Wacker, L., Masqué, P., Synal, H.-A., van der Loeff, M.R., 2018. Tracing the three Atlantic branches entering the Arctic Ocean with ^{129}I and ^{236}U. J. Geophys. Res., Oceans 123, 6909–6921. https://doi.org/10.1029/2018JC014168.

Castrillejo, M., Witbaard, R., Casacuberta, N., Richardson, C.A., Dekker, R., Synal, H.-A., Christl, M., 2020. Unravelling 5 decades of anthropogenic ^{236}U discharge from nuclear reprocessing plants. Sci. Total Environ. 717, 137094. https://doi.org/10.1016/j.scitotenv.2020.137094.

Chamizo, E., Christl, M., López-Lora, M., Casacuberta, N., Wefing, A.M., Kenna, T.C., 2022. The potential of $^{233}U/^{236}U$ as a water mass tracer in the Arctic Ocean. J. Geophys. Res., Oceans 127 (3), e2021JC017790. https://doi.org/10.1029/2021JC017790.

Charette, M.A., Kipp, L.E., Jensen, L.T., Dabrowski, J.S., Whitmore, L.M., Fitzsimmons, J.N., Williford, T., Ulfsbo, A., Jones, E., Bundy, R.M., Vivancos, S.M., et al., 2020. The transpolar drift as a source of riverine and shelf-derived trace elements to the central Arctic Ocean. J. Geophys. Res., Oceans 125 (5), e2019JC015920. https://agupubs.onlinelibrary.wiley.com/doi/abs/10.1029/2019JC015920.

Christl, M., Casacuberta, N., Lachner, J., Maxeiner, S., Vockenhuber, C., Synal, H.A., Goroncy, I., Herrmann, J., Daraoui, A., Walther, C., Michel, R., 2015a. Status of ^{236}U analyses at ETH Zurich and the distribution of ^{236}U and ^{129}I in the North Sea in 2009. Nucl. Instrum. Methods Phys. Res., Sect. B, Beam Interact. Mater. Atoms 361, 510–516. https://doi.org/10.1016/j.nimb.2015.01.005.

Christl, M., Casacuberta, N., Vockenhuber, C., Elsässer, C., Bailly du Bois, P., Herrmann, J., Synal, H.A., 2015b. Reconstruction of the ^{236}U input function for the Northeast Atlantic Ocean: implications for $^{129}I/^{236}U$ and $^{236}U/^{238}U$-based tracer ages. J. Geophys. Res., Oceans 120 (11), 7282–7299. https://doi.org/10.1002/2015JC011116.

Dahlgaard, H., 1994. Source of ^{137}Cs, ^{90}Sr and ^{99}Tc in the East Greenland Current. J. Environ. Radioact. 25, 37–55. https://doi.org/10.1016/0265-931X(94)90006-X.

Dodd, P.A., Rabe, B., Hansen, E., Falck, E., Mackensen, A., Rohling, E., Stedmon, C.A., Kristiansen, S., 2012. The freshwater composition of the Fram Strait outflow derived from a decade of tracer measurements. J. Geophys. Res. 117, C11005. https://doi.org/10.1029/2012JC008011.

Gonçalves-Araujo, R., Granskog, M.A., Bracher, A., Azetsu-Scott, K., Dodd, P.A., Stedmon, C.A., 2016. Using fluorescent dissolved organic matter to trace and distinguish the origin of Arctic surface waters. Sci. Rep. 6 (1), 1–12. https://doi.org/10.1038/srep33978.

Gonçalves-Araujo, R., Stedmon, C.A., de Steur, L., Osburn, C.L., Granskog, M.A., 2020. A decade of annual Arctic DOC export with polar surface water in the East Greenland current. Geophys. Res. Lett. 47 (20), e2020GL089686. https://onlinelibrary.wiley.com/doi/10.1029/2020GL089686.

Granskog, M.A., Stedmon, C.A., Dodd, P.A., Amon, R.M.W., Pavlov, A.K., de Steur, L., et al., 2012. Characteristics of colored dissolved organic matter (CDOM) in the Arctic outflow in the Fram Strait: assessing the changes and fate of terrigenous CDOM in the Arctic Ocean. J. Geophys. Res. 117, C12021. https://doi.org/10.1029/2012JC008075.

Hain, K., Steier, P., Froehlich, M.B., Golser, R., Hou, X., Lachner, J., Qiao, J., Quinto, F., Sakaguchi, A., 2020. $^{233}U/^{236}U$ signature allows to distinguish environmental emissions of civil nuclear industry from weapons fallout. Nat. Commun. 11. https://doi.org/10.1038/s41467-020-15008-2.

Hansen, H.P., Koroleff, F., 1999. Determination of nutrients. In: Grasshoff, K., Kremling, K., Ehrhardt, M. (Eds.), Methods of Seawater Analysis, 3rd ed. Wiley-VCH, Weinheim, Germany, pp. 159–228.

HELCOM, 2020. HELCOM MORS discharge database. https://helcom.fi/%20baltic-sea-trends/data-maps/databases/. (Accessed 1 May 2020).

International Atomic Energy Agency (IAEA), 2004. Sediment distribution coefficients and concentration factors for biota in the marine environment. Technical Reports Series No. 422.

Jones, E.P., Anderson, L.G., Swift, J.H., 1998. Distribution of Atlantic and Pacific waters in the upper Arctic Ocean: implications for circulation. Geophys. Res. Lett. 25, 765–768. https://doi.org/10.1029/98GL00464.

Jones, E.P., Swift, J.H., Anderson, L.G., Lipizer, M., Civitarese, G., Falkner, K.K., Kattner, G., McLaughlin, F., 2003. Tracing Pacific water in the North Atlantic Ocean. J. Geophys. Res., Oceans 108 (C4). http://doi.wiley.com/10.1029/2001JC001141.

Jones, E.P., Anderson, L.G., Jutterström, S., Swift, J.H., 2008. Sources and distribution of fresh water in the East Greenland Current. Prog. Oceanogr. 78 (1), 37–44. https://doi.org/10.1016/j.pocean.2007.06.003.

Karcher, M., Oberhuber, J.M., 2002. Pathways and modification of the upper and intermediate waters of the Arctic Ocean. J. Geophys. Res., Oceans 107 (C6), 2-1–2-13. https://doi.org/10.1029/2000JC000530.

Karcher, M., BeszczynskaMöller, A., Kauker, F., Gerdes, R., Heyen, S., Rudels, B., Schauer, U., 2011. Arctic Ocean warming and its consequences for the Denmark Strait overflow. J. Geophys. Res., Oceans 116 (C2). https://doi.org/10.1029/2010JC006265.

Karcher, M., Smith, J.N., Kauker, F., Gerdes, R., Smethie Jr, W.M., 2012. Recent changes in Arctic Ocean circulation revealed by iodine-129 observations and modeling. J. Geophys. Res., Oceans 117 (C8). https://doi.org/10.1029/2011JC007513.

Karpouzoglou, T., de Steur, L., Smedsrud, L.H., Sumata, H., 2022. Observed changes in the Arctic freshwater outflow in Fram Strait. J. Geophys. Res., Oceans 127 (3), e2021JC018122. https://doi.org/10.1029/2021jc018122.

Laukert, G., Frank, M., Bauch, D., Hathorne, E.C., Rabe, B., von Appen, W.J., Wegner, C., Zieringer, M., Kassens, H., 2017. Ocean circulation and freshwater pathways in the Arctic Mediterranean based on a combined Nd isotope, REE and oxygen isotope section across Fram Strait. Geochim. Cosmochim. Acta 202, 285–309. https://doi.org/10.1016/j.gca.2016.12.028.

Loeng, H., 1991. Features of the physical oceanographic conditions of the Barents Sea. Polar Res. 10 (1), 5–18. https://doi.org/10.3402/polar.v10i1.6723.

Lin, G., Lin, M., Qiao, J., Sejr, M.K., Steier, P., Meire, L., Stedmon, C.A., 2022a. Estimation of Atlantic water transit times in East Greenland fjords using a U-U tracer approach. Chem. Geol. 607, 121007. https://doi.org/10.1016/j.chemgeo.2022.121007.

Lin, G., Qiao, J., Steier, P., Danielsen, M., Guðnason, K., Joensen, H.P., Stedmon, C.A., 2022b. Tracing Atlantic water transit time in the subarctic and Arctic Atlantic using ^{99}Tc-^{233}U-^{236}U. Sci. Total Environ. 851, 158276.

Lin, M., Qiao, J.X., Hou, X.L., Golser, R., Hain, K., Steier, P., 2021. On the quality control for the determination of ultratrace-level ^{236}U and ^{233}U in environmental samples by accelerator mass spectrometry. Anal. Chem. 93, 3362–3369. https://doi.org/10.1021/acs.analchem.0c03623.

Lin, M., Qiao, J., Hou, X., Steier, P., Golser, R., Schmidt, M., Dellwig, O., Hansson, M., Bäck, Ö., Vartti, V.P., Stedmon, C., She, J., Murawski, J., Aldahan, A., Schmied, S.A.K., 2022. Anthropogenic ^{236}U and ^{233}U in the Baltic Sea: distributions, source terms, and budgets. Water Res. 210, 117987. https://doi.org/10.1016/j.watres.2021.117987.

Marnela, M., Rudels, B., Houssais, M.N., Beszczynska-Möller, A., Eriksson, P.B., 2013. Recirculation in the Fram Strait and transports of water in and north of the Fram Strait derived from CTD data. Ocean Sci. 9 (3), 499–519. https://doi.org/10.5194/os-9-499-2013.

Qiao, J.X., Hou, X.L., Steier, P., Nielsen, S., Golser, R., 2015. Method for ^{236}U determination in seawater using flow injection extraction chromatography and accelerator mass spectrometry. Anal. Chem. 87, 7411–7417. https://doi.org/10.1021/acs.analchem.5b01608.

Qiao, J., Xu, Y., 2018. Direct measurement of uranium in seawater by inductively coupled plasma mass spectrometry. Talanta 183, 18–23. https://doi.org/10.1016/j.talanta.2018.02.045.

Qiao, J.X., Hain, K., Steier, P., 2020. First dataset of ^{236}U and ^{233}U around the Greenland coast: a 5-year snapshot (2012 - 2016). Chemosphere 257, 127185. https://doi.org/10.1016/j.chemosphere.2020.127185.

Rahmstorf, S., 2002. Ocean circulation and climate during the past 120,000 years. Nature 419, 207–214. https://doi.org/10.1038/nature01090.

Raisbeck, G.M., Yiou, F., Zhou, Z.Q., Kilius, L.R., 1995. ^{129}I from nuclear fuel reprocessing facilities at Sellafield (UK) and La Hague (France); potential as an oceanographie tracer. J. Mar. Syst. 6 (5–6), 561–570. https://doi.org/10.1016/0924-7963(95)00024-J.

Rudels, B., Björk, G., Nilsson, J., Winsor, P., Lake, I., Nohr, C., 2005. The interaction between waters from the Arctic Ocean and the Nordic Seas north of Fram Strait and along the East Greenland Current: results from the Arctic Ocean-02 Oden expedition. J. Mar. Syst. 55 (1–2), 1–30. https://doi.org/10.1016/j.jmarsys.2004.06.008.

Rudels, B., 2009. Arctic Ocean circulation. In: Encyclopedia of Ocean Sciences, pp. 211–225.

Rudels, B., Korhonen, M., Schauer, U., Pisarev, S., Rabe, B., Wisotzki, A., 2015. Circulation and transformation of Atlantic water in the Eurasian Basin and the contribution of the Fram Strait inflow branch to the Arctic Ocean heat budget. Prog. Oceanogr. 132, 128–152. https://doi.org/10.1016/j.pocean.2014.04.003.

Schlitzer, R., 2016. Ocean data view. Retrieved from http://odv.awi.de.

Schnetger, B., Lehners, C., 2014. Determination of nitrate plus nitrite in small volume marine water samples using vanadium(III)chloride as a reduction agent. Mar. Chem. 160, 91–98. https://doi.org/10.1016/j.marchem.2014.01.010.

Schwehr, K.A., Scantschi, P.H., Elmore, D., 2005. The dissolved organic iodine species of the isotopic ratio of 129I/127I: a novel tool for tracing terrestrial organic carbon in the estuarine surface waters of Galveston Bay, Texas. Limnol. Oceanogr., Methods 3, 326–337. https://doi.org/10.4319/lom.2005.3.326.

Smedsrud, L.H., Muilwijk, M., Brakstad, A., Madonna, E., Lauvset, S.K., Spensberger, C., Born, A., Eldevik, T., Drange, H., Jeansson, E., Li, C., Olsen, A., Skagseth, Ø, Slater, D.A., Straneo, F., Våge, K., Årthun, M., 2022. Nordic seas heat loss, Atlantic inflow, and Arctic sea ice cover over the last century. Rev. Geophys. 60 (1), e2020RG000725. https://onlinelibrary.wiley.com/doi/abs/10.1029/2020RG000725.

Smith, J.N., Ellis, K.M., Kilius, L.R., 1998. 129I and 137Cs tracer measurements in the Arctic Ocean. Deep-Sea Res., Part 1, Oceanogr. Res. Pap. 45 (6), 959–984. https://doi.org/10.1016/S0967-0637(97)00107-6.

Smith, J.N., Karcher, M., Casacuberta, N., Williams, W.J., Kenna, T., Smethie, W.M., 2021. A changing Arctic Ocean: how measured and modeled 129I distributions indicate fundamental shifts in circulation between 1994 and 2015. J. Geophys. Res., Oceans 126, e2020JC016740. https://doi.org/10.1029/2020JC016740.

Smith, J.N., McLaughlin, F.A., Smethie, W.M., Moran, S.B., Lepore, K., 2011. Iodine-129, ^{137}Cs, and CFC-11 tracer transit time distributions in the Arctic Ocean. J. Geophys. Res. 116, C04024. https://doi.org/10.1029/2010JC006471.

Spencer, R.G.M., Aiken, G.R., Butler, K.D., Dornblaser, M.M., Striegl, R.G., Hernes, P.J., 2009. Utilizing chromophoric dissolved organic matter measurements to derive export and reactivity of dissolved organic carbon exported to the Arctic Ocean: a case study of the Yukon River, Alaska. Geophys. Res. Lett. 36 (6), L06401. https://doi.org/10.1029/2008GL036831.

Stedmon, C.A., Markager, S., 2001. The optics of chromophoric dissolved organic matter (CDOM) in the Greenland Sea: an algorithm for differentiation between marine and terrestrially derived organic matter. Limnol. Oceanogr. 46 (8), 2087–2093. https://doi.org/10.4319/lo.2001.46.8.2087.

Stedmon, C.A., Amon, R.M.W., Rhinehart, A.J., Walker, S.A., 2011. The supply and characteristics of colored dissolved organic matter (CDOM) in the Arctic Ocean. Mar. Chem. 124, 108–118. https://doi.org/10.1016/j.marchem.2010.12.007.

Stedmon, C.A., Granskog, M.A., Dodd, P.A., 2015. An approach to estimate the freshwater contribution from glacial melt and precipitation in East Greenland shelf waters using colored dissolved organic matter (CDOM). J. Geophys. Res., Oceans 120 (2), 1107–1117. http://doi.wiley.com/10.1002/2014JC010501.

Steier, P., Bichler, M., Fifield, L.K., Golser, R., Kutschera, W., Priller, A., Quinto, F., Richter, S., Srncik, M., Terrasi, P., Wacker, L., 2008. Natural and anthropogenic ^{236}U in environmental samples. Nucl. Instrum. Methods Phys. Res., Sect. B, Beam Interact. Mater. Atoms 266 (10), 2246–2250. https://doi.org/10.1016/j.nimb.2008.03.002.

Steier, P., Dellinger, F., Forstner, O., Golser, R., Knie, K., Kutschera, W., Priller, A., Quinto, F., Srncik, M., Terrasi, F., Vockenhuber, C., Wallner, A., Wallner, G., Wild, E.M., 2010. Analysis and application of heavy isotopes in the environment. Nucl. Instrum. Methods Phys. Res., Sect. B 268 (7–8), 1045–1049. https://doi.org/10.1016/j.nimb.2009.10.094.

Sumata, H., de Steur, L., Divine, D.V., Granskog, M.A., Gerland, S., 2023. Regime shift in Arctic Ocean sea ice thickness. Nature 615 (7952), 443–449. https://doi.org/10.1038/s41586-022-05686-x.

Timmermans, M.-L., Marshall, J., 2020. Understanding Arctic oceancirculation: a review of oceandynamics in a changing climate. J. Geophys. Res., Oceans 125, e2018JC014378. https://doi.org/10.1029/2018JC014378.

Tsubouchi, T., Våge, K., Hansen, B., Larsen, K.M.H., Østerhus, S., Johnson, C., Jonsson, S., Valdimarsson, H., 2021. Increased ocean heat transport into the nordic seas and Arctic Ocean over the period 1993–2016. Nat. Clim. Change 11, 21–26. https://doi.org/10.1038/s41558-020-00941-3.

Wang, Q., 2021. Stronger variability in the Arctic Ocean induced by sea ice decline in a warming climate: freshwater storage, dynamic sea level and surface circulation. J. Geophys. Res., Oceans 126, e2020JC016886. https://doi.org/10.1029/2020JC016886.

Wefing, A.-M., Christl, M., Vockenhuber, C., Rutgers van der Loeff, M., Casacuberta, N., 2019. Tracing Atlantic waters using ^{129}I and ^{236}U in the Fram Strait in 2016. J. Geophys. Res., Oceans 124, 882–896. https://doi.org/10.1029/2018JC014399.

Wefing, A.-M., Casacuberta, N., Christl, M., Gruber, N., Smith, J.N., 2021. Circulation timescales of Atlantic water in the Arctic Ocean determined from anthropogenic radionuclides. Ocean Sci. 17, 111–129. https://doi.org/10.5194/os-17-111-2021.

Wefing, A-M., Casacuberta, N., Christl, M., Dodd, P.A., 2022. Water mass composition in Fram Strait determined from the combination of ^{129}I and ^{236}U: changes between 2016, fmars. 2022.9735072018, and 2019. Front. Mar. Sci. 9, 973507. https://doi.org/10.3389/fmars.2022.973507.

Whitmore, L.M., Pasqualini, A., Newton, R., Shiller, A.M., 2020. Gallium: a new tracer of Pacific water in the Arctic Ocean. J. Geophys. Res., Oceans 125, e2019JC015842. https://doi.org/10.1029/2019JC015842.

XMLVIEW: extended

Appendix A. Supplementary material

The following is the Supplementary material related to this article.

begin ecomponent begin ecomponent begin ecomponent begin ecomponent begin ecomponent begin ecomponent begin ecomponent begin ecomponent begin ecomponent begin ecomponent begin ecomponent begin ecomponent begin ecomponent begin ecomponent begin ecomponent begin ecomponent begin ecomponent

Label: Supporting information

caption: The supporting information (in total of 10 pages) includes detailed methods for data process and water fractionation, 2 supplementary figure (Fig. S1 and S2), text (Table S1, See excel) summarizing all analytical results and Table S2 showing the mixing pattern of different branch waters in the Barents Sea Opening. Figs. S1 and S2 show the reconstructed input functions of historic nuclear reprocessing plants-derived ^{236}U ($^{236}U_{NRPs}$) concentrations in different branch waters of the Barents Sea Opening and the comparison with our observations.

link: **APPLICATION : mmc1**

end ecomponent end ecomponent

begin ecomponent begin ecomponent begin ecomponent begin ecomponent begin ecomponent begin ecomponent begin ecomponent begin ecomponent begin ecomponent begin ecomponent begin ecomponent begin ecomponent begin ecomponent begin ecomponent begin ecomponent begin ecomponent begin ecomponent

Label: Table S1

Dataset in the Fram Strait.

link: **APPLICATION : mmc2**

end ecomponent end ecomponent end ecomponent end ecomponent end ecomponent end ecomponent end ecomponent end ecomponent end ecomponent end ecomponent end ecomponent end ecomponent end ecomponent end ecomponent end ecomponent end ecomponent end ecomponent end ecomponent end ecomponent end ecomponent

Sponsor names

Do not correct this page. Please mark corrections to sponsor names and grant numbers in the main text.

H2020, *country*=European Union, *grants*=730965

Independent Research Fund Denmark, *country*=Denmark, *grants*=9040-00266B

Horizon 2020, *country*=European Union, *grants*=824096

Highlights

- New approach defining water classes by combining CDOM and ^{236}U.
- ^{233}U applied to isolate the reprocessing plant signal of ^{236}U in the Fram Strait.
- Atlantic water reaching Siberian shelf has 14 yrs transit time in the Arctic Ocean.
- Siberian shelf water with longer transit time has higher CDOM content.
- Atlantic water remaining off-shelf has a transit time of 22–28 yrs.

Supporting Information

Tracing Atlantic water transit times in the Arctic Ocean: coupling reprocessing-derived ^{236}U and colored dissolved organic matter to distinguish different pathways

Gang Lin[a], Jixin Qiao[a,*], Paul A. Dodd[b], Rafael Gonçalves-Araujo[c], Mats A. Granskog[b], Peter Steier[d], Colin A. Stedmon[c]

[a]Department of Environmental and Resource Engineering, Technical University of Denmark, DK-4000 Roskilde, Denmark

[b]Norwegian Polar Institute, Fram Centre, Tromsø, Norway

[c]National Institute of Aquatic Resources, Technical University of Denmark, Kemitorvet, 2800 Kgs. Lyngby, Denmark

[d]VERA Laboratory, Faculty of Physics, Isotope Physics, University of Vienna, Währinger Straße 17, A-1090 Vienna, Austria

* Corresponding author: Jiqi@dtu.dk

The supporting information (in total of 10 pages) includes detailed methods for data process and water fractionation, 2 supplementary figure (Fig. S1 and S2), text (Table S1, See excel) summarizing all analytical results and Table S2 showing the mixing pattern of different branch waters in the Barents Sea Opening. Figures S1 and S2 show the reconstructed input functions of historic nuclear reprocessing plants-derived

^{236}U ($^{236}U_{NRPs}$) concentrations in different branch waters of the Barents Sea Opening and the comparison with our observations.

1. The Reconstruction of the input functions of $^{236}U_{NRPs}$ in the Barents Sea Opening

The input function of $^{236}U_{NRPs}$ in the Barents Sea Opening has been reconstructed in our earlier study (Lin et al., 2022). The historic ^{236}U concentrations in Sellafield (SF) branch water and La Hague (LH) branch water are reconstructed through the record in shells (Castrillejo et al., 2020). Their $^{236}U_{NRPs}$ concentrations are obtained by subtracting the estimated $^{236}U_{GF}$ concentration (Christl et al., 2015, Lin et al., 2022). And the input functions of $^{236}U_{NRPs}$ are reconstructed through the branch water mixing pattern in the Barents Sea Opening (modified from Casacuberta et al., 2018) (Table S1, equation S7 – S9). The uncertainties of $^{236}U_{RP}$ concentrations in the Barents Sea Opening are propagated from the marine mixing pattern of SF branch water, LH branch water and NRPs-free Atlantic water in the Barents Sea Opening and the uncertainties of $^{236}U/^{238}U$ ratios in the shell record near SF and LH (Casacuberta et al., 2018; Castrillejo et al., 2020).

Table S2. The mixing pattern of Sellafield branch water, La Hague branch water and Atlantic water in the Barents Sea Opening for different reprocessing plants input functions (Casacuberta et al., 2018).

Input functions	LH branch (%)	SF branch (%)	AW (%)
Barents Sea Branch Water (BSBW)	1.7 ± 0.2	0.5 ± 0.1	97.7 ± 0.2
Fram Strait Branch Water (FSBW)	0.8 ± 0.1	0.4 ± 0.1	98.7 ± 0.2

Norwegian Coastal Current (NCC)	5.2 ± 1.1	2.7 ± 0.4	92.1 ± 1.1

** Arctic Shelf Break Branch is refined as Norwegian Coastal Current (Wefing et al., 2019). Atlantic water (AW) refers to RP-free Atlantic water with pure GF signal (Casacuberta et al., 2018), so its $^{236}U_{RP}$ concentration is assumed as zero.*

$$^{236}U_{NRPs\text{-}NCC} = 5.2\% \times {}^{236}U_{NRPs\text{-}LH} + 2.7\% \times {}^{236}U_{NRPs\text{-}SF} + 92.1\% \times {}^{236}U_{NRPs\text{-}AW} \quad (S7)$$

$$^{236}U_{NRPs\text{-}BSBW} = 1.7\% \times {}^{236}U_{NRPs\text{-}LH} + 0.5\% \times {}^{236}U_{NRPs\text{-}SF} + 97.7\% \times {}^{236}U_{NRPs\text{-}AW} \quad (S8)$$

$$^{236}U_{NRPs\text{-}FSBW} = 0.8\% \times {}^{236}U_{NRPs\text{-}LH} + 0.4\% \times {}^{236}U_{NRPs\text{-}SF} + 98.7\% \times {}^{236}U_{NRPs\text{-}AW} \quad (S9)$$

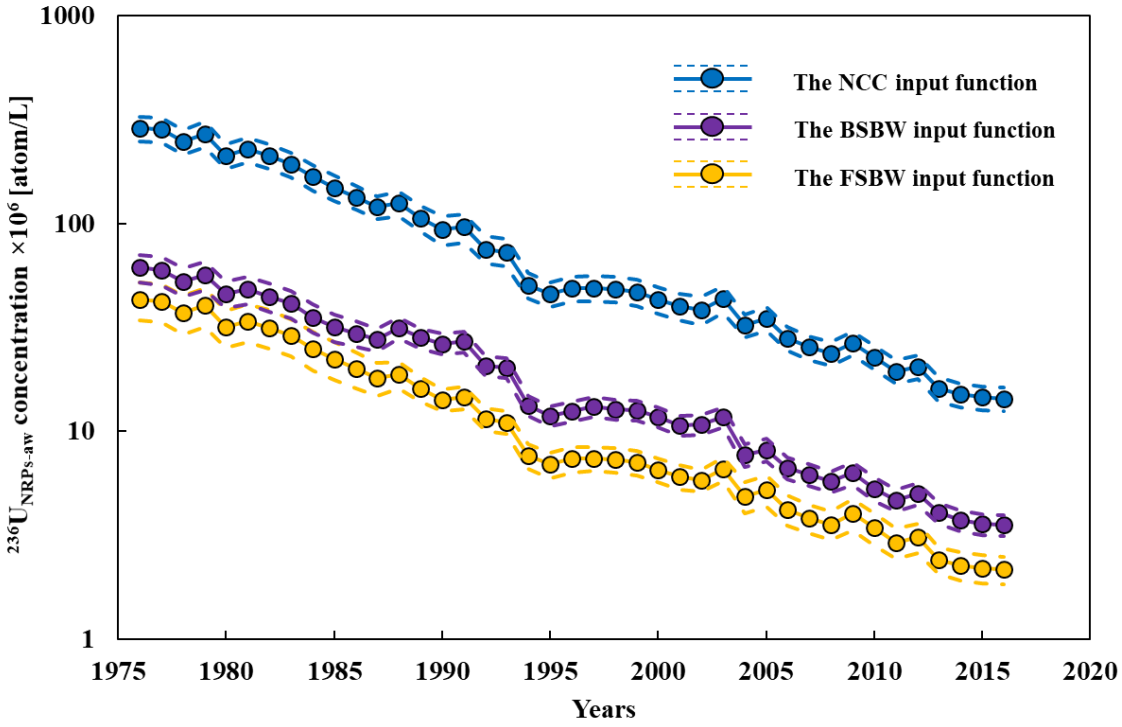

Fig. S1. The reconstructed input function of historic reprocessing plants-derived ^{236}U ($^{236}U_{NRPs}$) concentrations in different Atlantic branch waters of the Barents Sea Opening during 1976 – 2016. Their uncertainties are propagated from the $^{236}U/^{238}U$ ratios in the shell closed to the reprocessing plants at Sellafield and La Hague and the water mixing pattern in the Barents Sea Opening (Casacuberta et al., 2018; Castrillejo et al., 2020). NCC: Norwegian Coastal Current; BSBW: Barents Sea Branch Water; FSBW: Fram Strait Branch Water; Dashed lines are their uncertainties, and lines with circles are actual values.

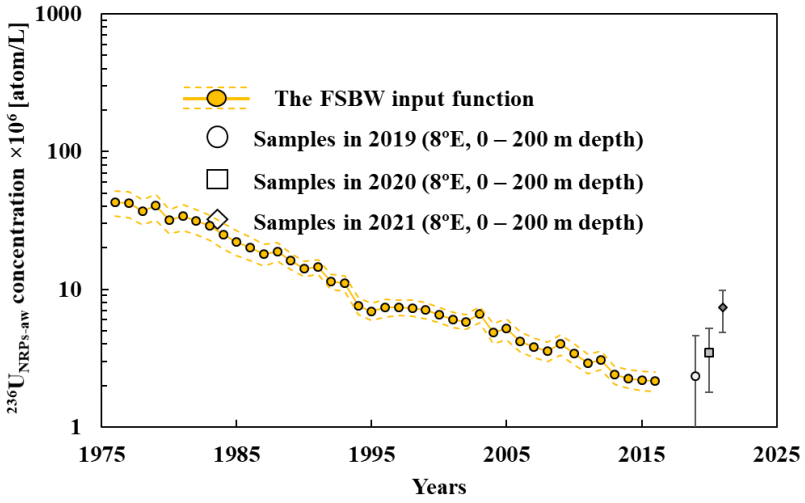

Fig. S2 The constructed input function of historic $^{236}U_{NRPs}$ concentration in Fram Strait Branch Water with our observation during 2019 – 2021. Dashed lines are their uncertainties, and lines with circles are actual values.

2. Quality control of uranium isotopes

To obtain the actual $^{233}U/^{238}U$ (R_S^{233}) and $^{236}U/^{238}U$ (R_S^{236}) ratios in the samples, the influence from the laboratory background should be removed through the equation S1 (Lin et al., 2021a):

$$R_S^x = \frac{(m_m^{238} R_m^x - m_b^{238} R_b^x)}{m_m^{238} - m_b^{238}} \quad \text{(S1)}$$

where R_m^x and R_b^x are the measured $^{233}U/^{238}U$ or $^{236}U/^{238}U$ atomic ratio in the sputter target of seawater sample and blank, respectively; x refers to 233 or 236; m_m^{238} and m_b^{238} are ^{238}U mass in the sputter target of seawater sample and blank, respectively. m_m^{238} or m_b^{238} are assumed as the same values with the mass of ^{238}U in the eluate due to the high recovery (> 99%) of target preparation (Qiao et al., 2015). After calculating, a negligible contribution (< 2%) from the procedure blanks of ^{233}U and ^{236}U is obtained in the seawater samples.

In addition, the combined uncertainties of actual $^{233}U/^{238}U$ and $^{236}U/^{238}U$ atomic ratios can be calculated through the law of uncertainty propagation (equation S2). And the influences of ^{238}U contents uncertainties (u(m_m^{238}) and u(m_b^{238})) and the uncertainties from measured atomic ratios of $^{236}U/^{238}U$ and $^{233}U/^{238}U$ in the eluates of sample and blank are considered in the combined uncertainties (Lin et al., 2021b)

$$u\left(R_s^{236(233)}\right) = \sqrt{\left[\frac{\partial R_s^{236(233)}}{\partial R_m^{236(233)}} u\left(R_m^{236(233)}\right)\right]^2 + \left[\frac{\partial R_s^{236(233)}}{\partial R_b^{236(233)}} u\left(R_b^{236(233)}\right)\right]^2 + \left[\frac{\partial R_s^{236(233)}}{\partial m_m^{238}} u(m_m^{238})\right]^2 + \left[\frac{\partial R_s^{236(233)}}{\partial m_b^{238}} u(m_b^{238})\right]^2}$$

$$= \sqrt{\left[\frac{m_m^{238}}{m_m^{238} - m_b^{238}} u\left(R_m^{236(233)}\right)\right]^2 + \left[\frac{m_b^{238}}{m_m^{238} - m_b^{238}} u\left(R_b^{236(233)}\right)\right]^2 + \left[\frac{m_b^{238}\left(R_m^{236(233)} - R_b^{236(233)}\right)}{(m_m^{238} - m_b^{238})^2} u(m_m^{238})\right]^2 + \left[\frac{m_m^{238}\left(R_m^{236(233)} - R_b^{236(233)}\right)}{(m_m^{238} - m_b^{238})^2} u(m_b^{238})\right]^2} \quad (S2)$$

3. Calculation of uncertainties of nuclear reprocessing plants (NRPs)-derived and global fallout (GF)-derived ^{236}U concentrations ($^{236}U_{NRPs}$, $^{236}U_{GF}$)

$^{236}U_{RP}$ and $^{236}U_{GF}$ concentrations are obtained through multiplying by the fractions of RP and GF with total ^{236}U concentration, so the uncertainties of the fractions of NRPs and GF should be calculated at first (Lin et al., 2022). Based on the law of uncertainty propagation (BIPM et al., 2008), the combined uncertainties of the fractions of NRPs and GF are estimated through the following equations (S3 – S4):

$$\mathrm{u}(P_{GF}) = \sqrt{\left(\frac{\partial P_{GF}}{\partial R_S^{233/236}}\right)^2 \times u^2\left(R_S^{233/236}\right) + \left(\frac{\partial P_{GF}}{\partial R_{GF}^{233/236}}\right)^2 \times u^2\left(R_{GF}^{233/236}\right)}$$

$$= \sqrt{\left(\frac{1}{R_{GF}^{233/236}}\right)^2 \times u^2\left(R_S^{233/236}\right) + \frac{(R_S^{233/236})^2}{(R_{GF}^{233/236})^4} \times u^2\left(R_{GF}^{233/236}\right)} \quad (S3)$$

$$\mathrm{u}(P_{NRPs}) = \sqrt{\left(\frac{\partial P_{NRPs}}{\partial P_{GF}}\right)^2 \times u^2(P_{GF})} = \mathrm{u}(P_{GF}) \quad (S4)$$

where $\mathrm{u}(P_{GF})$ and $\mathrm{u}(P_{NRPs})$ are the combined uncertainties for GF and NRPs fractions of ^{236}U, respectively; and $u\left(R_S^{233/236}\right)$ and $u\left(R_{GF}^{233/236}\right)$ are the uncertainties of the ^{233}U/^{236}U ratios in the measured samples and GF endmember (1.4×10^{-2}) (Hain et al., 2020).

Therefore, the combined uncertainties of $^{236}U_{GF}$ and $^{236}U_{RP}$ concentrations can be calculated by these equations (S5 – S6):

$$\mathrm{u}\left(C_{S,GF}^{236}\right) = \sqrt{\left(\frac{\partial C_{S,GF}^{236}}{\partial C_S^{233}}\right)^2 \times u^2(C_S^{233}) + \left(\frac{\partial C_{S,GF}^{236}}{\partial R_{GF}^{233/236}}\right)^2 \times u^2\left(R_{GF}^{233/236}\right)}$$

$$= \sqrt{\left(\frac{1}{R_{GF}^{233/236}}\right)^2 \times u^2(C_S^{233}) + \frac{(C_S^{233})^2}{(R_{GF}^{233/236})^4} \times u^2\left(R_{GF}^{233/236}\right)} \quad (S5)$$

$$\mathrm{u}\left(C_{S,NRPs}^{236}\right) = \sqrt{\left(\frac{\partial C_{S,NRPs}^{236}}{\partial C_S^{236}}\right)^2 \times u^2(C_S^{236}) + \left(\frac{\partial C_{S,NRPs}^{236}}{\partial C_{S,GF}^{236}}\right)^2 \times u^2\left(C_{S,GF}^{236}\right)}$$

$$= \sqrt{u^2(C_S^{236}) + u^2\left(C_{S,GF}^{236}\right)} \quad (S6)$$

where $\mathrm{u}\left(C_{S,GF}^{236}\right)$ and $\mathrm{u}\left(C_{S,NRPs}^{236}\right)$ are the combined uncertainties for $^{236}U_{GF}$ and $^{236}U_{NRPs}$ concentrations, respectively; $u(C_S^{233})$ and $u(C_S^{233})$ are the uncertainties of measured ^{233}U and ^{236}U concentrations, respectively; and $u\left(R_{GF}^{233/236}\right)$ is the uncertainty of the ^{233}U/^{236}U ratio in GF endmember (0.12×10^{-2}) (Hain et al., 2020).

4. Water fractionation

According to Dodd et al. (2012), the fraction of Atlantic water in the Fram Strait could be estimated based on the following equations (S7 – S11).

$$f_{AW} + f_{PW} + f_{FW} = 1 \qquad (S7)$$

$$f_{AW}P_{AW} + f_{FW}P_{AW} + f_{PW}P_{PW} = P_S \qquad (S8)$$

$$f_{AW}S_{AW} + f_{PW}S_{PW} + f_{FW}S_{FW} = S_S \qquad (S9)$$

$$P_{AW} = M_{AW}N + C_{AW} \qquad (S10)$$

$$P_{PW} = M_{PW}N + C_{PW} \qquad (S11)$$

where f_{AW}, f_{PW} and f_{FW} are the fractions of Atlantic water, Pacific water and freshwater in the Fram Strait; P_{AW}, P_{PW} and P_S are the corresponding phosphate concentrations in the Atlantic water, Pacific water and the measured seawater sample; S_{AW}, S_{PW}, S_{FW} *and* S_s are the corresponding salinities in the Atlantic water (34.9), Pacific water (32), freshwater (0) and the measured seawater sample; M_{AW} and M_{PW} are the slopes of the N:P relationship in the Atlantic water (0.53) and Pacific water (0.65); C_{AW} and C_{PW} are the intercepts of the N:P relationship in the Atlantic water (0.170) and Pacific water (0.940).

Therefore, f_{AW}, f_{PW} and f_{FW} could be expressed as:

$$f_{aw} = S_s/S_{aw} - f_{pw}S_{pw}/S_{aw} \qquad (S12)$$

5. Calculation method of the total uncertainties of nuclear reprocessing plants-derived ^{236}U endmember concentration in Atlantic water ($^{236}U_{NRPs\text{-}aw}$) and the estimated Atlantic water transit times in different waters

According to the equations 6 – 7 in context, the total uncertainty of $^{236}U_{NRPs\text{-}aw}$ concentration is propagated from $^{236}U_{NRPs}$ concentration and Atlantic water fraction and thus can be obtained through the equation S13:

$$u\left(C_{s,NRPs-aw}^{236}\right) = \sqrt{\left(\frac{u\left(C_{s,NRPs}^{236}\right)}{C_{s,NRPs}^{236}}\right)^2 + \left(\frac{u(f_{aw})}{f_{aw}}\right)^2} \quad (S13)$$

where $u\left(C_{s,NRPs-aw}^{236}\right)$, $u\left(C_{s,NRPs}^{236}\right)$ and $u(f_{aw})$ are uncertainties of $^{236}U_{NRPs\text{-}aw}$ concentration, $^{236}U_{NRPs}$ concentration and Atlantic water fraction, respectively ; $C_{s,NRPs}^{236}$ and f_{aw} are $^{236}U_{NRPs}$ concentration and Atlantic water fraction. Atlantic water fraction is estimated through using nitrate and phosphate, and the approach gives 10 % of uncertainty for the obtained Atlantic water fraction (Dodd et al., 2012).

In addition, the total uncertainties of Atlantic water transit times can not simply be calculated by equations. For Arctic High CDOM Water and Arctic Low CDOM / High ^{236}U Water, the total uncertainties of the analytical procedures for Atlantic water transit times derive from three parts: 1) standard deviation of $^{236}U_{NRPs\text{-}aw}$ concentrations, 2) the relative contributions of two Atlantic branch waters and 3) the uncertainty of the $^{236}U_{NRPs\text{-}aw}$ input functions in the Barents Sea Opening. The decreasing trends of $^{236}U_{NRPs\text{-}aw}$ input functions are changed with times, so the specific uncertainties depend on the actual Atlantic water source year. The potential maximum and minimum $^{236}U_{NRPs\text{-}aw}$ concentrations can be matched with the corresponding values in the $^{236}U_{NRPs\text{-}aw}$ input functions of two branch waters (NCC/BSBW or BSBW/FSBW), and the potential oldest (longest) and youngest (shortest) Atlantic water source years (transit times) are therefore obtained. The potential longest and shortest Atlantic water transit times reveal the total uncertainties. Therefore, the total uncertainties of Atlantic water transit times in Arctic High CDOM Water and Arctic Low CDOM / High ^{236}U Water are provided to be 7 – 64 % and 7 – 31 %, respectively. For Atlantic Low CDOM Water, the total uncertainty derives from standard deviation of $^{236}U_{NRPs\text{-}aw}$ concentrations and the uncertainty of the $^{236}U_{NRPs\text{-}aw}$ input function in FSBW of the Barents Sea Opening. Similarly, due to the various decreasing rates for the $^{236}U_{NRPs\text{-}aw}$ input function, the specific

uncertainty is also influenced by the actual Atlantic water source year. The potential longest and shortest Atlantic water transit times can be estimated through using the maximum and minimum $^{236}U_{NRPs\text{-}aw}$ concentrations to anchor the FSBW input function. And the total uncertainties for Atlantic Low CDOM Water is 35 – 60 %.

Reference

BIPM, I.; IFCC, I.; ISO, I.; IUPAP, O., 2008. Evaluation of Measurement Data—Guide to the Expression of Uncertainty in Measurement, JCGM 100: 2008 GUM 1995 with Minor Corrections. Jt. Comm. Guid. Metrol..

Casacuberta, N., Christl, M., Vockenhuber, C., Wefing, A.-M., Wacker, L., Masqué, P., Synal, H.-A., van der Loeff, M.R., 2018. Tracing the three Atlantic branches entering the Arctic Ocean with ^{129}I and ^{236}U. Journal of Geophysical Research: Oceans 123, 6909–6921. https://doi.org/10.1029/2018JC014168.

Castrillejo, M., Witbaard, R., Casacuberta, N., Richardson, C.A., Dekker, R., Synal, H.-A., Christl, M., 2020. Unravelling 5 Decades of Anthropogenic ^{236}U Discharge from Nuclear Reprocessing Plants, Sci. Total Environ. 717, 137094, https://doi.org/10.1016/j.scitotenv.2020.137094, 2020.

Christl, M., Casacuberta, N., Vockenhuber, C., Elsässer, C., Bailly du Bois, P., Herrmann, J., Synal, H.A., 2015. Reconstruction of the 236 U input function for the N ortheast A tlantic O cean: Implications for 129I/236 U and 236U/238 U-based tracer ages. *Journal of Geophysical Research: Oceans*, *120*(11), 7282-7299. https://doi.org/10.1002/ 2015JC011116.

Dodd, P.A., Rabe, B., Hansen, E., Falck, E., Mackensen, A., Rohling, E., Stedmon, C.A., Kristiansen, S., 2012. The freshwater composition of the Fram Strait outflow derived from a decade of tracer measurements, J. Geophys. Res. 117, C11005. https://doi.org/10.1029/2012JC008011.

Hain, K., Steier, P., Froehlich, M.B., Golser, R., Hou, X., Lachner, J., Qiao, J., Quinto, F., Sakaguchi, A., 2020. $^{233}U/^{236}U$ signature allows to distinguish environmental emissions of civil nuclear industry from weapons fallout. Nat. Commun. 11. https://doi.org/10.1038/s41467-020-15008-2.

Lin, G., Lin, M., Qiao, J., Sejr, M.K., Steier, P., Meire, L., Stedmon, C.A., 2022. Estimation of Atlantic water transit times in East Greenland fjords using a U- U tracer approach. Chem. Geol. 607, 121007. https://doi.org/10.1016/j.chemgeo.2022.121007.

Lin, M., Qiao, J.X., Hou, X.L., Dellwig, O., Steier, P., Hain, K., Golser, R., Zhu, L.C., 2021a. 70-Year Anthropogenic Uranium Imprints of Nuclear Activities in Baltic Sea Sediments. Envir. Scien. & Techno. 55, 13, 8918 – 8927. https://doi.org/10.1021/acs.est.1c02136.

Lin, M., Qiao, J.X., Hou, X.L., Golser, R., Hain, K., Steier, P., 2021b. On the Quality Control for the Determination of Ultratrace-Level ^{236}U and ^{233}U in Environmental Samples by Accelerator Mass Spectrometry. Analytical chemistry 93, 3362 – 3369. https://doi.org/10.1021/acs.analchem.0c03623.

Qiao, J.X., Hou, X.L., Steier, P., Nielsen, S., Golser, R., 2015. Method for ^{236}U determination in seawater using flow injection extraction chromatography and accelerator mass spectrometry. Anal. Chem. 87, 7411–7417. https://doi.org/10.1021/acs.analchem.5b01608.

Paper IV

Tracing Atlantic water in and out of the Nordic Seas with reprocessing-derived ^{236}U

Gang Lin[a], Jixin Qiao[a,*], Peter Steier[b], Magnús Danielsen[c], Kjartan Guðnason[d]

[a]Department of Environmental and Resource Engineering, Technical University of Denmark, DK-4000 Roskilde, Denmark

[b]VERA Laboratory, Faculty of Physics, Isotope Physics, University of Vienna, Währinger Straße 17, A-1090 Vienna, Austria

[c]Marine and Freshwater Research Institute, Iceland

[d]Icelandic Radiation Safety Authority, Iceland

Tracing Atlantic water in and out of the Nordic Seas with reprocessing-derived ^{236}U

Gang Lin[a], Jixin Qiao[a,*], Peter Steier[b], Magnús Danielsen[c], Kjartan Guðnason[d]

[a]Department of Environmental and Resource Engineering, Technical University of Denmark, DK-4000 Roskilde, Denmark

[b]VERA Laboratory, Faculty of Physics, Isotope Physics, University of Vienna, Währinger Straße 17, A-1090 Vienna, Austria

[c]Marine and Freshwater Research Institute, Iceland

[d]Icelandic Radiation Safety Authority, Iceland

* Corresponding author: Jiqi@dtu.dk

Abstract: The Nordic Seas is a critical region for monitoring the Atlantic Meridional Overturning Circulation (AMOC), so we use the ^{233}U to isolate the reprocessing plants signal in ^{236}U ($^{236}U_{RP}$) to trace the pathways of in-and-out flowing Atlantic waters in the Norwegian Sea and the sea around Iceland for understanding the AMOC. Based on our observation of $^{236}U_{RP}$, the inflowing Atlantic water dominates the Norwegian offshore area and has an impact on the Norwegian coast, especially at ~62°N and ~68 °N. And the dispersion of Norwegian Coastal Water is limited in the Norwegian coastal shelf, and its volume fractions in the coastal and offshore areas are quantified to be 0 – 0.42 and 0 – 0.11, respectively. In addition, the distribution of $^{236}U_{RP}$ concentration in the sea around Iceland suggests the predominant Atlantic water in the southern coast of Iceland, but the water in the northern Iceland is influenced by the outflowing water from the Arctic Ocean. The first observation of a transient signal from $^{236}U_{RP}$ supports the earlier modelling result that a stronger RP signal in the intermediate layer of the continental slope region, and provide a observed evident for the view that the North Icelandic Jet transports along the continental slope of Iceland and feeds the Denmark Strait Overflow Water.

Keywords: ^{233}U; ^{236}U; Atlantic water pathways; the sea around Iceland and Norway; AMOC

1. Introduction

Atlantic Meridional Overturning Circulation (AMOC) is an important component for global thermohaline circulation, which has a great impact on global climate change. A large amount of heat is transported from low to high latitude region through the polarward Atlantic water, and the variability of AMOC influences sea ice melt and extent in the Arctic Ocean (Polyakov et al., 2017; Sévellec et al., 2017; Lozier et al., 2017). Atlantic water gradually sinks in the Nordic Seas with the loss of heat. Recent study shows that changes of deep water formation in the sea between the eastern Greenland and Scotland dominate AMOC rather than those in the Labrador Sea (Lozier et al., 2019). As a critical gateway, the Greenland-Iceland-Faroe-Scotland Ridge (Greenland-Scotland Ridge, GSR) facilitates the exchange of inflowing Atlantic water from the North Atlantic Ocean with outflowing water from the Arctic Ocean (Østerhus et al., 2001; Zhang et al., 2004; Jungclaus et al., 2008). A appropriate 90% northward upper limb AMOC locates in the Iceland Basin (Sarafanov et al., 2012; Mercier et al., 2015; Daniault et al., 2016). This suggests that the sea around Iceland may be a core region in the GSR for the northward Atlantic water. After passing across the GSR, the northward Atlantic water enters the Norwegian Sea as Norwegian Atlantic Current (NwAC) and further bifurcates into two branch (Poulain et al., 1996). The eastern branch water of the NwAC merges with the Norwegian Coastal Current in various speed (< 8 cm/s, 8 – 15 cm/s, and > 15 cm/s) (Ribergaad et al., 2004), implying a different mixing pattern at each latitude, but their detailed mixing pattern is still not clear. In addition, Demark Strait is a main exit for the outflowing Atlantic water. The Denmark Strait Outflow Water (DSOW) outflowed from the Nordic Seas is critical for feeding the lower limb of AMOC, and its source may be the East Greenland Current (EGC) or the North Icelandic Jet transported along the continental slope of Iceland depending on the wind stress curl (Jonsson and Valdimarsson, 2004; Våge et al., 2011; de Jong et al., 2018). These uncertain understandings for the AMOC highlight the significance of tracing Atlantic water in the entire Norwegian Sea and the sea around Iceland of the central GSR. Uncovering transport pathways of in-and-out flowing Atlantic waters in the Nordic Seas is useful to understand the AMOC and thus an appropriate tracer to track their transport in this transition zone is needed.

Anthropogenic radioisotopes as transient tracers have been increasingly used to trace Atlantic water in the Arctic-North Atlantic Ocean. These radioisotopes are originated from two main sources: 1) global fallout (GF) from nuclear weapons testing and 2) reprocessing plants (RP) at Sellafield (SF) and La

Hague (LH) (Aarkrog et al., 1987; Dahlgaard, 1994; Smith et al., 1998; Casacuberta et al., 2014). Tracing Atlantic water in a large scale urges us to utilize conservative and long-lived radioisotope tracers, such as ^{99}Tc: t½ = 0.211Myr, K_d (distribution coefficient)= 100; ^{129}I: t½ = 15.7 Myr, K_d = 200; ^{236}U: t½ = 23.4 Myr, K_d = 500 (Dahlgaard, 1994; International Atomic Energy Agency IAEA, 2004; Casacuberta et al., 2018). However, the historic RP discharges of ^{99}Tc peaked in two different periods, giving rise to difficulties in anchoring the source year of Atlantic water entering the Arctic Ocean (G. Lin et al., 2022a). In addition, the current measurement techniques for ^{99}Tc still require a large volume (100-200 L) of water sample, thus limiting the oceanic tracer application of ^{99}Tc. The RP discharge of ^{129}I increased continuously after 1990s, providing a useful tool to trace Atlantic water. However, the contribution of GF-derived ^{129}I can not be distinguished from the RP-derived ^{129}I. Differently, RP-derived ^{236}U ($^{236}U_{RP}$) had peak discharge in 1970s with a monotonous decreasing trend (Casacuberta et al., 2018; Castrillejo et al., 2020). With the use of ^{233}U/^{236}U isotope ratio, RP-derived ^{236}U can be isolated from GF-derived ^{236}U (Hain et al., 2020; HELCOM MORS Discharge database, 2020; Qiao et al., 2020). Considering the potential old water age in deep and bottom water in the North Atlantic-Arctic Ocean, the use of $^{236}U_{RP}$ is expected suitable to track the large-scale advective transport of Atlantic water in our study region (Wefing et al., 2021).

RP signal from SF and LH mixes in the North Sea and transports northward into the Arctic Ocean along the coast of Norway (Karcher et al., 2004; Christl et al., 2017). It is divided into three Atlantic branch waters, which disperse in surface and intermediate layers of the Arctic Ocean (Casacuberta et al., 2018). These Atlantic waters finally outflow from the western Fram Strait, and transport to the North Atlantic Ocean along the coast of Greenland (Wefing et al., 2019; G. Lin et al., 2022a). RP signal was also found in the North Atlantic Deep Water (Casacuberta et al., 2014; Castrillejo et al., 2022). Although some modeling work based on the dispersion of RP signal in the Arctic-subarctic region have been reported (Orre et al., 2010; Simonsen et al., 2017), the detailed sink process of Atlantic water from surface to deep and bottom layers is still not clear in the Nordic Seas, especially the sea around the GSR. In our earlier studies, we used $^{236}U_{RP}$ to trace Atlantic water in the coastal surface seawater of Greenland, Iceland and Faroe Islands (Qiao et al., 2020; G. Lin, 2022). However, a knowledge gap still exists in terms of deep and bottom water transport in these regions, which impedes our understanding of the AMOC.

In this study, we aim to trace the transport of the inflowing Atlantic water from the North Atlantic Ocean and the outflowing Atlantic water from Arctic Ocean for better understanding the ventilation of AMOC. The observation of $^{236}U_{RP}$ in the Norwegian Sea and the water column of the GSR is expected to provide new insights and validation for previous modelling results in the North Atlantic Ocean.

2. Materials and methods

2.1 Setting and sampling in study area

The GSR is located in the gateway for Atlantic water exchange between the North Atlantic Ocean and the Arctic Ocean (Fig. 1). Warm northward Atlantic water is divided into two branch waters in the subpolar region. One branch water moves westward along the GSR to the southeastern Greenland coast as the Subpolar Mode Water (SPMW), and a part of it as the North Icelandic Irminger Current (NIIC) flows into the northern coast of Iceland along its western coast. One branch water directly passes through the GSR into the Norwegian Sea as the Norwegian Atlantic Current (NwAC), which transports in the offshore area and is parallel to the Norwegian Coastal Current (NCC). The NwAC and the NCC mix in a different proportion and form three branch waters (Norwegian Coastal Current branch water, Barents Sea branch water and Fram Strait branch water), which transport in surface and intermediate layers of the Arctic Ocean and outflow from the western Fram Strait along the East Greenland coast as East Greenland Current (EGC). One branch of EGC moves southward on the coast of East Greenland, but another one transports eastward to the North of Iceland as East Iceland Current (EIC). In addition, the sinking Atlantic water in the Nordic Sea outflows from the Denmark Strait and the ridge between Iceland and Scotland as Denmark Strait Outflow Water (DSOW) and Iceland Scotland Outflow Water (ISOW), respectively. And they move southward to the North Atlantic Ocean as the North Atlantic Deep Water (NADW).

A total of 77 seawater samples were collected in the sea around Iceland, the Norwegian Sea and the coast of Faroe Islands by the Niskin bottles equipped on a CTD (conductivity-temperature-depth). Sampling was carried out through the R/V Bjarni Sæmundsson during May-August, 2020 and the R/V G.O. Sars in May, 2020.

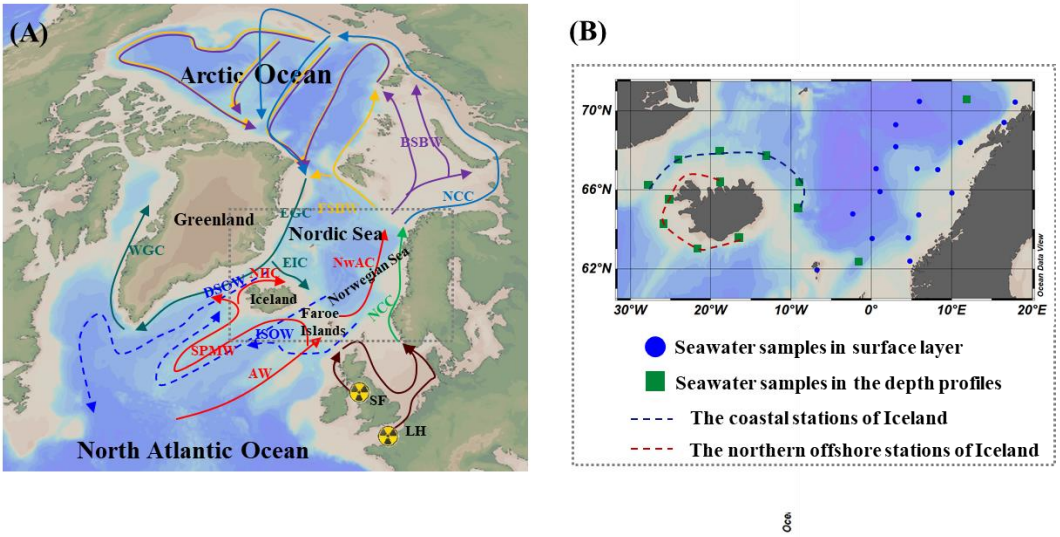

Fig. 1 The current circulation in the Arctic-subpolar region (A) and the sites of sampling location in the Norwegian Sea and the sea around Iceland (B). AW: (RP-free) Atlantic water; SPMW: Subpolar Mode Water; NIIC: North Icelandic Irminger Current; NwAC: Norwegian Atlantic Current; NCC: Norwegian Coastal Current; BSBW: Barents Sea branch water; FSBW: Fram Strait branch water; EGC: East Greenland Current; WGC: West Greenland Current; EIC: East Iceland Current; DSOW: Denmark Strait Overflow Water; ISOW: Iceland Scotland Outflow Water; SF: Sellafield; LH: La Hague; solid arrows refer to waters in surface and intermediate layers, and dash arrows refer to waters in deep and bottom layers.

2.2. Measurement of uranium isotopes (^{233}U, ^{236}U and ^{238}U)

We used the developed method to process 5 – 10 L seawater for the measurement of ^{233}U and ^{236}U (Qiao et al., 2015). 14 M HNO_3 was added into the filtered seawater until the pH value changed to be 2, and uranium ion was released from uranyl carbonate complex. 0.05 g/mL Fe^{3+} ($FeCl_3$ solution pre-purified by UTEVA® resin) was added 10 – 20 mL with expelling of CO_2 through stirring. $NH_3 \cdot H_2O$ solution was added until the pH value became 8 – 9, resulting in co-precipitation with uranium through the iron hydroxides. The iron hydroxides were dissolved in 3 M HNO_3 for loading on UTEVA® resin. 2 mL UTEVA® resin was enough for purifying uranium, and it should be rinsed with 20 mL of 3 M HNO_3

before loading the samples. And we added 40 mL of HNO_3 and 20 mL of 6 M HCl for removing the interfering radioisotopes. Uranium was eluted by 10 mL of 0.025 M HCl. We added 2 mg of Fe^{3+} was added for co-precipitating uranium. The iron hydroxides was dried for 4 h at 90 ºC and combusted for 12 h at 800 ºC. Before measuring in the accelerate mass spectrometry (AMS), the samples should be pressed into a sputter. And the measurement of ^{233}U and ^{236}U was carried out at the Vienna Environmental Research Accelerator (VERA) facility in University of Vienna (Steier et al., 2010; Hain et al., 2020).

The contamination was effectively reduced through our reported procedures, and we used same procedures to prepare one procedure blank with every seven seawater samples (M. Lin et al., 2021). For the measurement of ^{238}U, 1 ppb Indium-0.5 M HNO_3 solution was added to dilute 0.1 mL of filtered seawater, and the samples were measured by the inductively coupled plasma mass spectrometry (ICP-MS, ICP-QQQ 9900, Agilent) (Qiao and Xu, 2018).

2.3 Separate the RP and GF contributions in ^{236}U

Our earlier study has showed that fractions of RP and GF could be estimated through a two-endmember mixing algorithm (equations 1 – 4) (Qiao et al., 2020).

$$P_{GF} = \frac{(R_{RP}^{233/236} - R_S^{233/236})}{(R_{RP}^{233/236} - R_{GF}^{233/236})} \approx \frac{R_S^{233/236}}{R_{GF}^{233/236}} \qquad (1)$$

$$P_{RP} = 1 - P_{GF} \qquad (2)$$

$$C_{S,GF}^{236} = C_S^{236} \times P_{GF} = R_{GF}^{236/233} \times C_S^{233} \quad (3)$$

$$C_{S,RP}^{236} = C_S^{236} \times P_{RP} = C_S^{236} - C_{S,GF}^{236} \quad (4)$$

where P_{GF} and P_{RP} are GF and RP fractions in ^{236}U, respectively; $R_{GF}^{233/236}$, $R_{RP}^{233/236}$ and $R_S^{233/236}$ are the atomic ratio of $^{233}U/^{236}U$ in the GF endmember ($1.40 \pm 1.5 \times 10^{-2}$), RP endmember ($1 \times 10^{-7}$) and seawater

sample, respectively (Hain et al., 2020; HELCOM MORS Discharge basement, 2020); C_s^{233}, C_s^{236}, $C_{s,GF}^{236}$, and $C_{s,RP}^{236}$ are ^{233}U, ^{236}U, GF-derived ($^{236}U_{GF}$) and $^{236}U_{RP}$ concentrations in the seawater sample, respectively. The uncertainties are calculated through the law of uncertainty propagation, and the detailed calculation is reported in our earlier study (BIPM et al., 2008; G. Lin et al., 2022b).

3. Results

3.1 Properties of water in the Norwegian Sea and the sea around Iceland

Temperature and salinity ranged from -0.50 – 11.64 ℃ and 34 – 35.14 PSU in the sea around Iceland, and -0.64 – 8.80 °C and 34 – 35.27 PSU in the Norwegian Sea, respectively (Fig. 2B and 2C, Fig. 3B and 3C). Seawater on the southern coast of Iceland has a warmer temperature and higher salinity. In contrast, the relatively low temperature and salinity were found in the seawater of the North Iceland. In addition, for surface seawater in the Norwegian Sea, temperature is warmer in the southern area, and salinity is lower on the northeastern coast of Norway. And the bottom water is characterized by subzero temperature and high salinity.

3.2 The distribution of uranium isotopes in the Norwegian Sea

^{238}U concentration in surface water of the Norwegian Sea ranged from 3.06 – 3.42 μg/L (Fig. 2D). And ^{233}U and ^{236}U concentrations were measured between 2.74 – 22.79 × 10^4 atom/L and 8.46 – 53.01 × 10^6 atom/L, respectively (Fig. 2E and 2F). Different from the distribution pattern of ^{233}U concentration, significantly higher ^{236}U concentration was observed along the shelf of Norway. The ratios of $^{233}U/^{236}U$ varied from 0.09 – 2.63 × 10^{-2}, and lower ratios were distinct in the Norwegian coastal water (Fig. 2G). In bottom water, concentrations of ^{238}U, ^{233}U and ^{236}U were 3.41 – 3.42 μg/L, 6.48 – 6.76 × 10^4 atom/L and 8.15 – 10.24 × 10^6 atom/L, respectively, and their ratios ranged within 0.63 – 0.83 × 10^{-2} (Fig. 3D-G).

For surface water, GF fraction and concentration of ^{236}U varied within 0.07 – 1 and 1.95 – 15.90 × 10^6 atom/L. The distribution of RP fraction (0 – 0.93) and $^{236}U_{RP}$ concentration (0 – 37.11 × 10^6 atom/L) was clearly separated between the coastal and offshore water (water in the continental shelf, and the continental slope-basin regions) (Fig. 2H-K), with higher values in coastal water than those in offshore water. In bottom water, GF and RP fractions of ^{236}U were calculated in 0.45 – 0.59 and 0.41 – 0.55 (Fig.

3H and 3I), and the ranges of $^{236}U_{GF}$ and $^{236}U_{RP}$ were 4.63 – 4.83 × 10^6 atom/L and 3.32 – 5.61 × 10^6 atom/L, respectively (Fig. 3J and 3K).

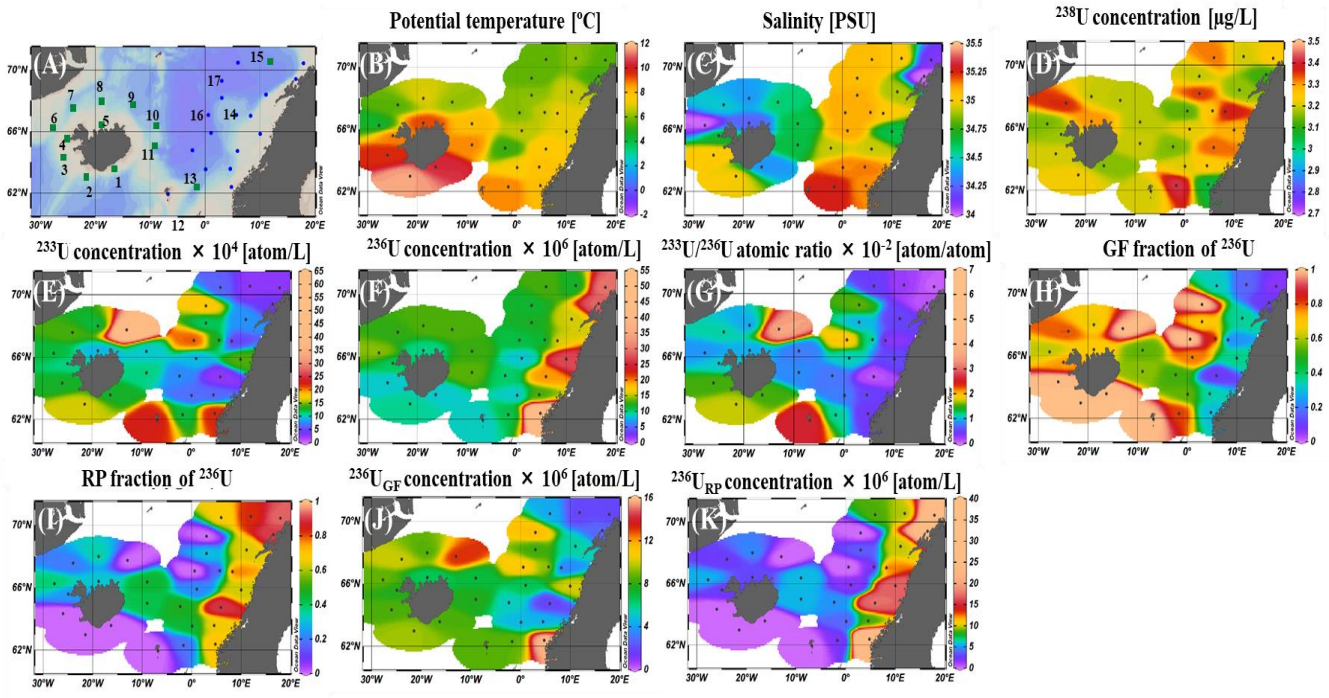

Fig. 2 The distribution of sample sites (A), potential temperature (B), salinity (C), ^{238}U concentration (D), ^{233}U concentration (E), ^{236}U concentration (F) and $^{233}U/^{236}U$ atomic ratio (G), GF fraction of ^{236}U (H), RP fraction of ^{236}U (I), $^{236}U_{GF}$ concentration (J) and $^{236}U_{RP}$ concentration (K) in surface seawater.

3.3 The distribution of uranium isotopes in seawater around the Iceland

^{238}U concentrations of the water profiles around the Iceland were 2.78 – 3.48 µg/L (Fig. 2D and 3D). Concentrations of ^{233}U and ^{236}U ranged within 3.65 – 62.85 × 10^4 atom/L and 7.56 – 17.85 × 10^6 atom/L, and their ratios varied within 0.31 – 6.73 × 10^{-2} (Fig. 2E-G and 3E-G). The level of ^{233}U concentrations along the coastal water columns was comparable, but the ^{236}U level in the northern offshore water columns was uniformly higher than that in the coastal water columns (Fig 4).

GF fraction of ^{236}U was obtained in the range of 0.22 – 1, with the rest as RP fraction (0 – 0.78) (Fig. 2H and 2I, Fig. 3H and 3I). $^{236}U_{GF}$ concentration ranged from 2.61 – 14.30 × 10^6 atom/L, and $^{236}U_{RP}$ were 0 – 12.71 × 10^6 atom/L (Fig. 2J and 2K, Fig. 3J and 3K). The regional difference of $^{236}U_{RP}$ concentration was similar to ^{236}U concentration (Fig. 4).

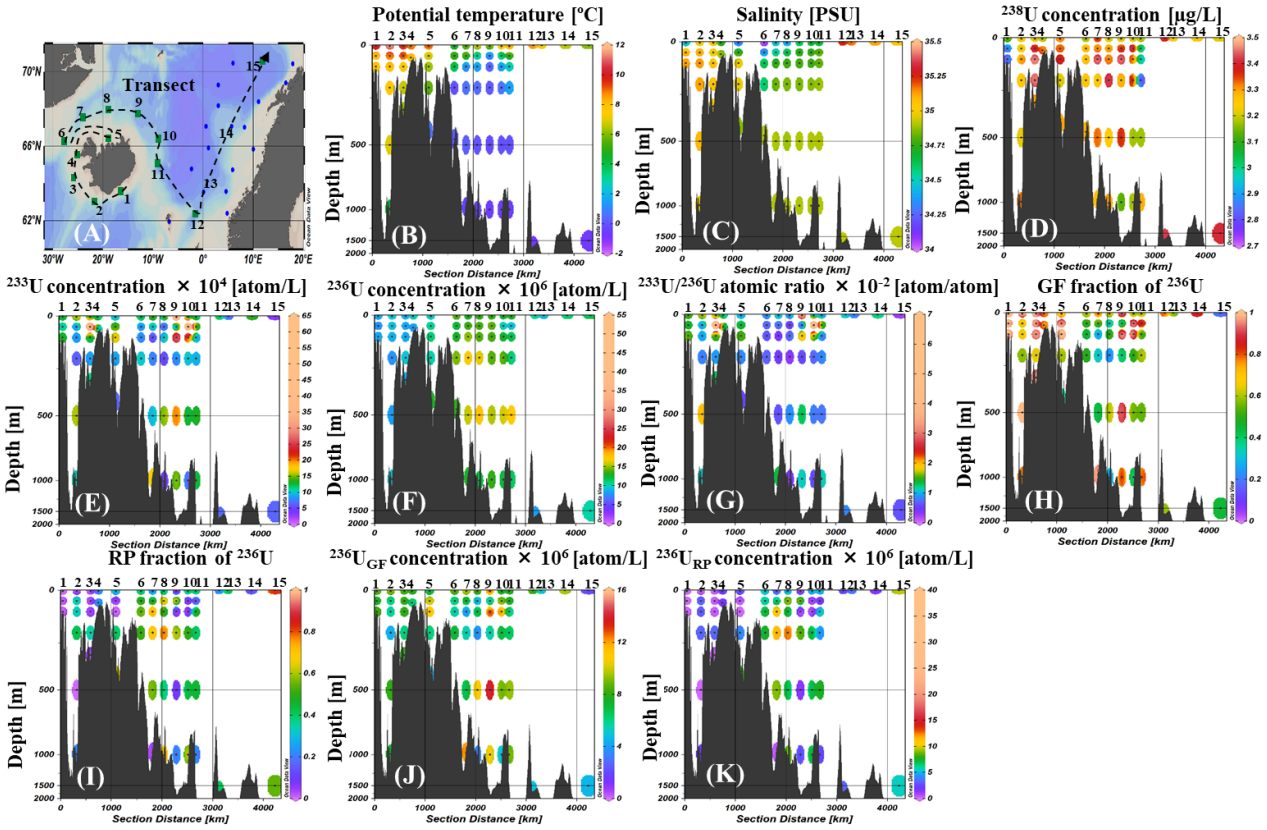

Fig. 3 The transect of samples (A) and the depth profiles of potential temperature (B), salinity (C), ^{238}U concentration (D), ^{233}U concentration (E), ^{236}U concentration (F) and $^{233}U/^{236}U$ atomic ratio (G), GF fraction of ^{236}U (H), RP fraction of ^{236}U (I), $^{236}U_{GF}$ concentration (J) and $^{236}U_{RP}$ concentration (K).

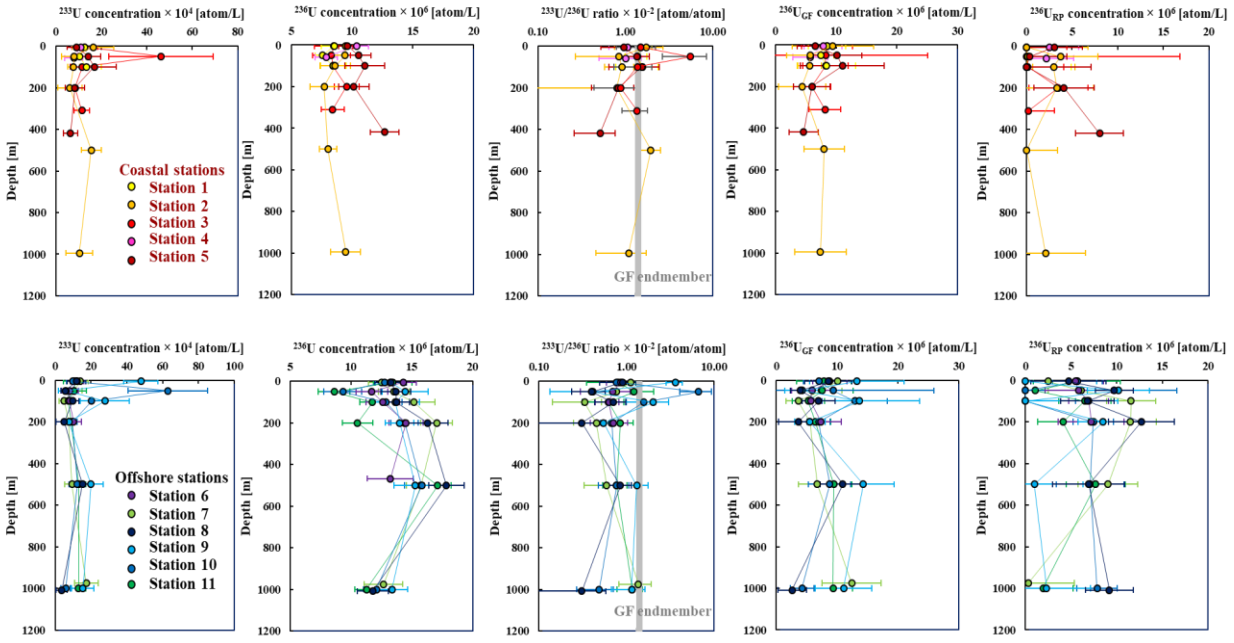

Fig. 4 Comparison of anthropogenic uranium isotopes in the coastal seawater and the offshore seawater of Iceland

4. Discussion

4.1 Tracing surface Atlantic water in the transition zone between the Arctic Ocean and the North Atlantic Ocean using $^{236}U_{RP}$

The original Atlantic water from the Atlantic Ocean is assumed to contain a pure-GF signal and defined as RP-free Atlantic water in this study. Atlantic water is only tagged with RP signal when flowing from the North Sea and consequently the Arctic Ocean, thus $^{236}U_{RP}$ can be used to indicate the transport pathways of Atlantic water. According to our observations, low concentration of $^{236}U_{RP}$ was found in seawaters from the Norwegian offshore, revealing a strong influence of RP-free Atlantic water in these areas (Fig. 2K). Conversely, high $^{236}U_{RP}$ concentration was observed in the Norwegian coastal seawater due to strong RP contribution in the NCC from the release of SF and LH (Fig. 2K). Our observation supports earlier model results for the dispersion of RP signal from SF and LH (Orre et al., 2010; Simonsen et al., 2017).

Clear boundary in $^{236}U_{RP}$ distribution between the coastal (> 10×10^6 atom/L) and offshore (< 10×10^6 atom/L) areas suggests that the RP-carried NCC is constrained in the coastal area without the notably westward dispersion in the offshore area (Fig. 2K). Simulated $^{236}U_{RP}$ concentrations in surface water (0 – 100 m depth) in the southern coast of Norway have showed a relative stable annual variability since

2010s (M. Lin et al., 2022). Thereby, we used the average of simulated $^{236}U_{RP}$ concentrations during 2010 – 2017 as an endmember of the NCC (88.31 × 10^6 atom/L) at 60°N of Norwegian coast to derive the mixing pattern of the NCC and RP-free Atlantic water. No $^{236}U_{RP}$ was detected in the coast of Faroe Islands (Fig. 2K), agreeing with the assumption that the Atlantic water has no RP signal before entering the Norwegian Sea. Volume fractions of the NCC and the RP-free Atlantic water calculated by the following equation (5) range from 0 – 0.42 and 0.58 – 1, respectively (Fig. 5).

$$f_{NCC}{}^{236}U_{RP\text{-}NCC} + f_{RP\text{-}free\text{-}aw}{}^{236}U_{RP\text{-}free\text{-}aw} = {}^{236}U_{RP\text{-}s} \qquad (5)$$

where f_{NCC} and $f_{RP\text{-}free\text{-}aw}$ are fractions of the NCC and RP-free Atlantic water, respectively; $^{236}U_{RP\text{-}NCC}$, $^{236}U_{RP\text{-}free\text{-}aw}$ and $^{236}U_{RP\text{-}total}$ are the endmember concentrations of $^{236}U_{RP}$ in the NCC, RP-free Atlantic water and measured seawater sample, respectively. $^{236}U_{RP\text{-}free\text{-}aw}$ is assumed as zero.

Higher fraction of the NCC was observed in the coastal region (0.10 – 0.42) than that in the offshore region (0 – 0.11). Less NCC fractions in coastal area at ~ 62°N and ~68 °N are influenced by a strong impact from the RP-free Atlantic water. The RP-free Atlantic water merges with the NCC with a high current vector (> 15 cm/s), even greater than 110 cm/s at 68°N (Ribergaad et al., 2004). Interestingly, the NCC contributions increased notably in both coastal and offshore areas at the northernmost stations in the study region. This is related to the decline of the eastward RP-free Atlantic water with a lower speed (8 – 15 cm/s, even < 8 cm/s) (Ribergaad et al., 2004), and thus allows more NCC contributions to the coastal and offshore areas.

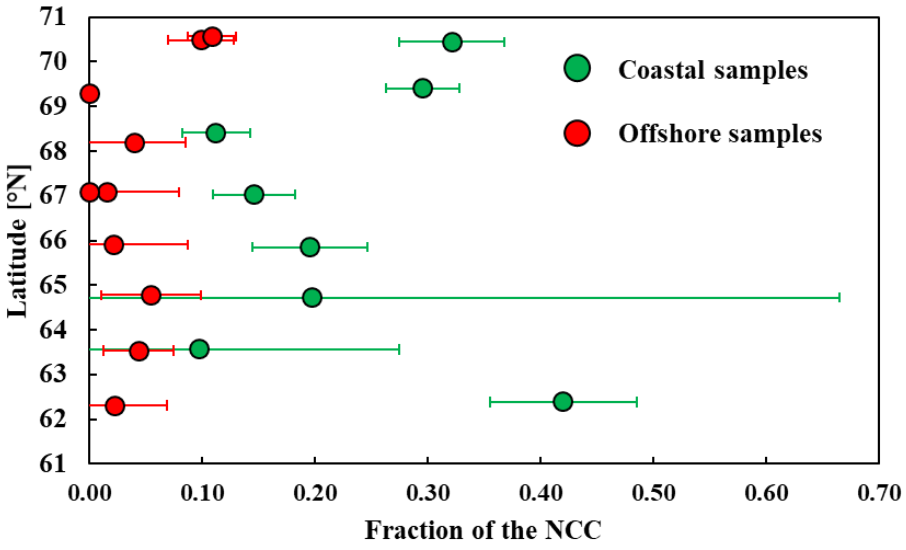

Fig. 5 The fraction of the NCC in surface seawater of the Norwegian Sea

Different from the southern Iceland coast without the RP signal in seawater, $^{236}U_{RP}$ could be detected in the northern Iceland coast, which is related to the outflowing polar water carried RP signal (Fig. 2K). RP signal in polar water is gradually diluted in the Arctic Ocean by Pacific water, river water and sea ice melted (Smith et al., 2011; Wefing et al., 2021). Outflowing polar water exits from the Arctic Ocean along the eastern coast of Greenland, and splits into two branches: 1) a southward East Greenland Current (EGC) and 2) a southeastward East Iceland Current (EIC) (Casanova-Masjoan et al., 2020). Compared with $^{236}U_{RP}$ concentration (~ 10×10^6 atom/L) in surface seawater (0 – 10 m) of the Fram Strait in 2020 (Lin et al., in submission), $^{236}U_{RP}$ concentration in surface water of the northern Iceland decreases to a lower level (~5×10^6 atom/L), suggesting a further dilution with the freshwater from East Greenland and the northward RP-free North Icelandic Irminger Current (EIIC) from the southern Iceland coast in the transport from the Fram Strait. In addition, $^{236}U_{RP}$ concentrations were very low at stations 9, 16 and 17 (Fig. 2K), implying that this area is dominated by RP-free Atlantic water from the North Atlantic Ocean without the impact of the NCC and the outflowing polar water.

4.2 $^{236}U_{RP}$ evidence for tracing the outflowing Atlantic water from the Nordic Seas

One of RP-free Atlantic branch water transports westward along the Greenland-Scotland Ridge and thus dominates the southern coast of Iceland. And a part of it further transports northward to the northern coast of Iceland as (NIIC). It is noted that $^{236}U_{RP}$ was detected in bottom water of the northern coast (station 5), suggesting the influence of the invaded NIIC is primarily in the overlying water (Fig. 3K). And the detected $^{236}U_{RP}$ in bottom water is transported by the outflowing water from the Arctic Ocean carrying RP signal.

Although the outflowing Polar Surface Water is dominated by the NCC carrying stronger RP signal (Casacuberta et al., 2018), higher $^{236}U_{RP}$ concentration is distributed at 100 – 500 m depth rather than in surface seawater due to the dilution of Pacific water, river water and sea ice melt (Casacuberta et al., 2016 and 2018; Chamizo et al., 2022; Wefing et al., 2022). The outflowing water in the intermediate layer (100 – 1000 m) solely consists of Atlantic water and originates from the BSBW and the FSBW (Wefing et al., 2019). The outflowing Atlantic water have two pathways from the Norwegian Sea: 1) long pathway in the Arctic Ocean passing through the shelf break and edge of Barents Sea and Eurasian and American Basins, and 2) short pathway across the Fram Strait from the east to the west, resulting in the distribution of RP signal from different pathways in the northern offshore water of Iceland.

Low level of $^{236}U_{RP}$ in the southern water profiles of Iceland suggests that the southward transport of outflowing Atlantic water is limited (Fig. 3K). However, vertical mixing in the northern Iceland coast

maybe prevailing, which is supported by gradually increased $^{236}U_{total}$ and $^{236}U_{RP}$ concentration along the water column from surface to bottom layers (Fig. 3F and 3K). The gradual decrease in $^{236}U_{RP}$ concentration from stations 7 and 8 at 100 – 500 m depth to the northeastern and northwestern stations 6, 9, 10 and 11 may indicate the dispersion of the westward North Icelandic Jet (NIJ) and the eastward EIC (Fig. 6). NJI is hypothesized to derive from the overturning loop in North of Iceland (Våge et al., 2011). Higher $^{236}U_{RP}$ and $^{236}U_{total}$ concentrations at 100 – 500 m depth support the previous view that overflows along the continental slope of Iceland and passes through the Denmark Strait (Våge et al., 2011). In addition, the EIC continuously moves southeastward and outflows from the Iceland-Faroe Ridge, even the Faroe Shetland Channel (Fig. 6) (Orre et al., 2010; Jong et al., 2018). Interestingly, compared with other stations at 500 m and 1000 m depths, $^{236}U_{RP}$ concentration at station 9 is lower. This may be related to the influence of terrain, as station 9 is located in the basin, whereas the other northern offshore stations are distributed along the continental slope (Fig. 6). The terrain of continental slope strengths the sink of the outflowing Atlantic water, and the outflowing water from the Fram Strait transports along the edge of the continent. The simulated dispersion of ^{129}I from RP discharge also shows a higher concentration in the continental slope at the intermediate layer, which is consistent with our observation (Orre et al., 2010). The ventilation of Atlantic water in the continental slope is expected to be stronger than that in the basin.

For the water at ~ 1000 m depth, $^{236}U_{RP}$ concentrations are still higher at stations 8 and 10 (7.87 – 9.19 $\times 10^6$ atom/L), but their decline is distinct at other northern offshore stations of Iceland ($< 2.5 \times 10^6$ atom/L). The low $^{236}U_{RP}$ concentrations at station 9 maybe related to weaker ventilation in the basin. While the low level of $^{236}U_{RP}$ at stations 7 and 11 maybe due to the influence of the DSOW and the IOSW. The sill of Greenland-Faroe Ridge is generally shallower than 1000 m (Østerhus et al., 2001; Jónsson and Valdimarsson, 2004), thus the sinking RP-tagged Atlantic water nearby the ridge (stations 7 and 11) flows out from the Denmark Strait and the strait between Iceland and Faroe Islands rather than sinking to the bottom layer (Fig. 6). These outflows carrying strong RP signal from the straits transport southward along the terrain to the North Atlantic Ocean as the North Atlantic Deep Water (Orre et al., 2010; Castrillejo et al., 2018). In addition, $^{236}U_{RP}$ concentration in the northern bottom water of the Norwegian Sea is higher than that in the southern bottom water, which may be related to a higher $^{236}U_{RP}$ concentration in the northern surface water of the same station. $^{236}U_{RP}$ in bottom water of the northern and southern Norwegian Sea derives from surface Atlantic water, and the continental slope facilitates the sink of $^{236}U_{RP}$.

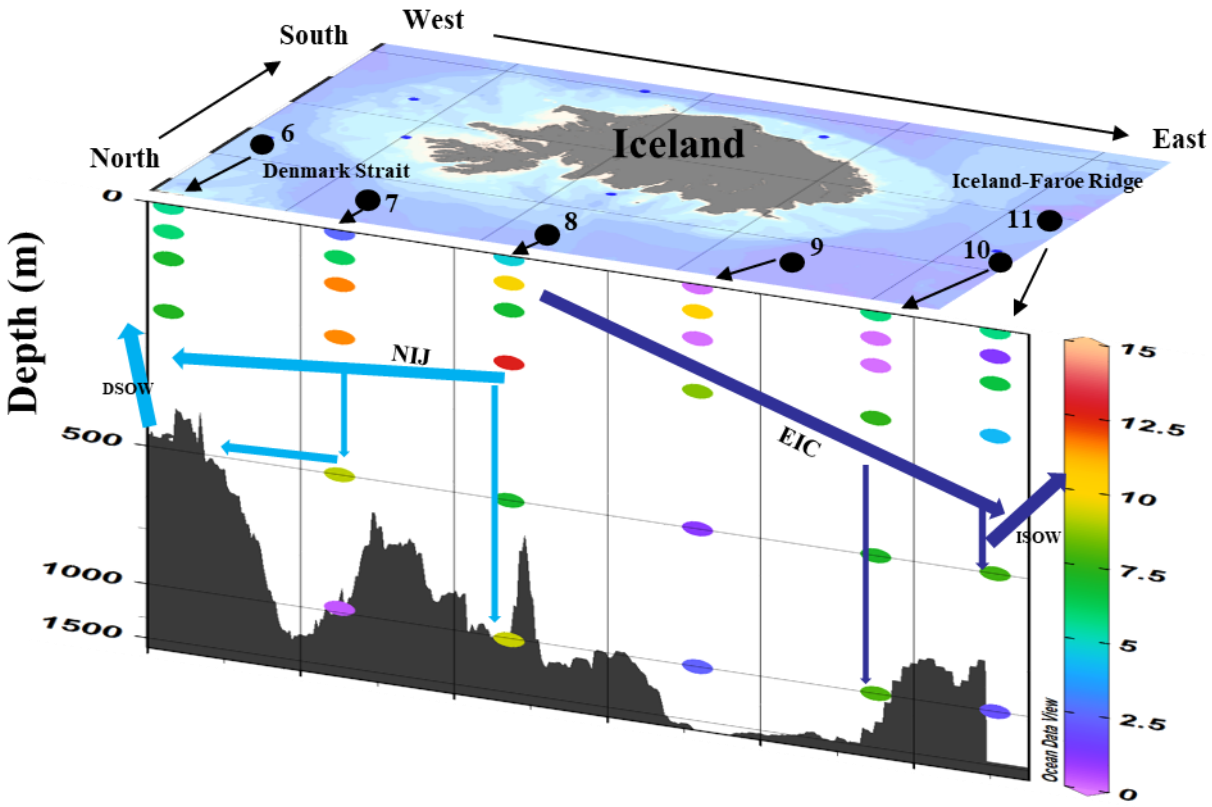

Fig. 6 The dispersion of the outflowing Atlantic water in the northern offshore area of Iceland based on the $^{236}U_{RP}$ concentration (× 10^6 atom/L). NIJ: North Iceland Jet; EIC: East Iceland Current; DSOW: Denmark Strait Overflow Water; ISOW: Iceland Scotland Outflow Water.

5. Conclusion and perspectives

Our work presents a wider investigation of uranium isotopes in the Norwegian Sea, where the fraction of the NCC is quantified through the distribution of $^{236}U_{RP}$ concentration and the dispersion of inflowing Atlantic water. The NCC fraction is estimated to be 0 – 0.11 in the offshore area, but the significantly elevated fraction of NCC (0.10 – 0.42) is constrained in the coastal area of Norway. Our investigation provides the first observation of a transient signal from RP signal to present the visualized dispersion of the outflowing Atlantic water in the sea around Iceland, supporting earlier modelling result of a stronger RP in the intermediate layer of the northern offshore water and the view that NIJ contributes to the DSOW along the continental slope (Orre et al., 2010; Våge et al., 2011).

However, the uncertainties of $^{236}U_{RP}$ ask us to use a larger water volume and improve the technology of AMS measurement on ^{233}U in the future. High uncertainties of $^{236}U_{RP}$ limit our further estimate and

investigation based on RP signal, even if the correlation between $^{236}U_{total}$ concentration and $^{236}U_{RP}$ concentration is high in this study (R^2 = 0.80). Compared with other seas and basins in the Nordic Seas, earlier study shows a stronger ventilation of Atlantic water in the Greenland Sea through the use of CFCs and SF_6 (Jeansson et al., 2023). These sinking Atlantic waters with different mean ages outflowed from the straits in the GSR are also the important constitute of the AMOC, but the process of advective transport from these basins to the GSR is unclear. Therefore, more works on investigating anthropogenic radioisotopes in the transects between Greenland and Norway are significant for understanding AMOC.

Reference

Aarkrog, A., Boelskifthe, S., Dahlgaard, H., Duniec, S., Hallstadius, L., Holm, E., Smith, J.N., 1987. Technetium-99 and Caesium-134 as long distance tracers in Arctic water. Estuar. Coast. Shelf Sci. 24, 637–647. https://doi.org/10.1016/0272-7714(87)90103-X.

BIPM, I.; IFCC, I.; ISO, I.; IUPAP, O., 2008. Evaluation of Measurement Data—Guide to the Expression of Uncertainty in Measurement, JCGM 100: 2008 GUM 1995 with Minor Corrections. Jt. Comm. Guid. Metrol..

Casacuberta, N., Christl, M., Lachner, J., van der Loeff, M.R., Masqué, P., Synal, H.-A., 2014. A first transect of ^{236}U in the north Atlantic Ocean. Geochim. Cosmochim. Acta 133, 34 - 46. https://doi.org/10.1016/j.gca.2014.02.012.

Casacuberta, N., Masqué, P., Henderson, G., van-der-Loeff, M.R., Bauch, D., Vockenhuber, C., Daraoui, A., Walther, C., Synal, H.A., Christl, M., 2016. First ^{236}U data from the Arctic Ocean and use of $^{236}U/^{238}U$ and $^{129}I/^{236}U$ as a new dual tracer. Earth and Planetary Science Letters 440, 127-134. http://dx.doi.org/10.1016/j.epsl.2016.02.020.

Casacuberta, N., Christl, M., Vockenhuber, C., Wefing, A.-M., Wacker, L., Masqué, P., Synal, H.-A., van der Loeff, M.R., 2018. Tracing the three Atlantic branches entering the Arctic Ocean with ^{129}I and ^{236}U. Journal of Geophysical Research: Oceans 123, 6909–6921. https://doi.org/10.1029/2018JC014168.

Casanova-Masjoan, M., Pérez-Hernández, M.D., Pickart, R.S., Valdimarsson, H., Ólafsdóttir, S.R., Macrander, A., et al., 2020. Along-stream, seasonal, and interannual variability of the North Icelandic Irminger Current and East Icelandic Current around Iceland. J. Geophys. Res. Oceans 125, e2020JC016283. https://doi.org/10.1029/2020JC016283.

Castrillejo, M., Casacuberta, N., Christl, M., Vockenhuber, C., Synal, H.A., García-Ibáñez, M.I., Lherminier, P., Sarthou, G., Garcia-Orellana, J. and Masqué, P., 2018. Tracing water masses with 129I and 236U in the subpolar North Atlantic along the GEOTRACES GA01 section. *Biogeosciences*, *15*(18), pp.5545-5564.

Castrillejo M, Casacuberta N, Vockenhuber C and Lherminier P (2022) Rapidly Increasing Artificial Iodine Highlights Pathways of Iceland-Scotland Overflow Water and Labrador Sea Water. Front. Mar. Sci. 9:897729. doi: 10.3389/fmars.2022.897729.

Chamizo, E., Christl, M., López-Lora, M., Casacuberta, N., Wefing, A.-M., Kenna, T.C., 2022. The potential of 233U/236U as a water mass tracer in the Arctic Ocean. J. Geophys. Res. Oceans 127, e2021JC017790. https://doi.org/10.1029/2021JC017790.

Christl, M., Casacuberta, N., Lachner, J., Herrmann, J., Synal, H.-A., 2017. Anthropogenic 236U in the North Sea− a closer look into a source region. Environ. Sci. Technol. 51, 12146–12153. https://doi.org/10.1021/acs.est.7b03168. Dahlgaard, H., 1994. Source of 137Cs, 90Sr and 99Tc in the East Greenland Current. J. Environ. Radioact. 25, 37–55. https://doi.org/10.1016/0265-931X(94)90006-X.

Daniault, N., Mercier, H., Lherminier, P., Sarafanov, A., Falina, A., Zunino, P., et al., 2016. The northern North Atlantic Ocean mean circulation in the early 21st century. Progress in Oceanography, 146, 142–158. https://doi.org/10.1016/j.pocean.2016.06.007.

de Jong, M. F., Søiland, H., Bower, A. S., & Furey, H. H., 2018. The subsurface circulation of the Iceland Sea observed with RAFOS floats. Deep Sea Research Part I: Oceanographic Research Papers, 141, 1–10. https://doi.org/10.1016/j.dsr.2018.07.008

Fine, R.A., 2011. Observations of CFCs and SF6 as Ocean tracers. Annu. Rev. Mar. Sci. 3, 173–195. https://doi.org/10.1146/annurev.marine.010908.163933.

Hain, K., Steier, P., Froehlich, M.B., Golser, R., Hou, X., Lachner, J., Qiao, J., Quinto, F., Sakaguchi, A., 2020. $^{233}U/^{236}U$ signature allows to distinguish environmental emissions of civil nuclear industry from weapons fallout. Nat. Commun. 11. https://doi.org/10.1038/s41467-020-15008-2.

HELCOM. HELCOM MORS Discharge database https:// helcom.fi/%20baltic-sea-trends/data-maps/databases/ (accessed May 1, 2020).

International Atomic Energy Agency (IAEA), 2004. Sediment distribution coefficients and concentration factors for biota in the marine environment. Technical Reports Series No. 422.

Jeansson, E., Tanhua, T., Olsen, A., Smethie Jr, W.M., Rajasakaren, B., Ólafsdóttir, S.R. and Ólafsson, J., Decadal Changes in Ventilation and Anthropogenic Carbon in the Nordic Seas. *Journal of Geophysical Research: Oceans*, p.e2022JC019318. . https://doi. org/10.1029/2022JC019318.

Jungclaus, J.H., Macrander, A. and Käse, R.H., 2008. Modelling the overflows across the Greenland–Scotland Ridge. *Arctic–Subarctic Ocean Fluxes: Defining the Role of the Northern Seas in Climate*, pp.527-549.

Jónsson, S., Valdimarsson, H., 2004. An ocean current over the continental slope northwest of Iceland carrying Denmark Strait overflow water from the Iceland Sea to Denmark Strait. *ICES Document CM*, (04), p.11.

Karcher, M.J., Gerland, S., Harms, I.H., Iosjpe, M., Heldal, H.E., Kershaw, P.J., Sickel, M., 2004. The dispersion of 99Tc in the Nordic Seas and the Arctic Ocean: a comparison of model results and observations. Journal of Environmental Radioactivity 74, 185–198. https://doi.org/10.1016/j.jenvrad.2004.01.026.

Lin, G., Qiao, J., Steier, P., Danielsen, M., Guðnason, K., Joensen, H.P. and Stedmon, C.A., 2022a. Tracing Atlantic water transit time in the subarctic and Arctic Atlantic using 99Tc-233U-236U. *Science of the Total Environment*, *851*, p.158276.

Lin, G., Lin, M., Qiao, J., Sejr, M.K., Steier, P., Meire, L., Stedmon, C.A., 2022b. Estimation of Atlantic water transit times in East Greenland fjords using a U- U tracer approach. Chem. Geol. 607, 121007. https://doi.org/10.1016/j.chemgeo.2022.121007.

Lin, G., Qiao, J., Gonçalves-Araujo, R., Steier, P., Dodd, P., Stedmon, C.A., in submission. Tracing Atlantic water exiting the Arctic Ocean: coupling reprocessing-derived ^{236}U and colored dissolved organic matter.

Lin, M., Qiao, J.X., Hou, X.L., Golser, R., Hain, K., Steier, P., 2021. On the Quality Control for the Determination of Ultratrace-Level ^{236}U and ^{233}U in Environmental Samples by Accelerator Mass Spectrometry. Analytical chemistry 93, 3362 – 3369. https://doi.org/10.1021/acs.analchem.0c03623.

Lin, M., Qiao, J., Hou, X., Steier, P., Golser, R., Schmidt, M., Dellwig, O., Hansson, M., Bäck, Ö., Vartti, V.P. and Stedmon, C., 2022. Anthropogenic 236U and 233U in the Baltic Sea: Distributions, source terms, and budgets. *Water Research*, *210*, p.117987.

Lozier, M. S., Bacon, S., Bower, A. S., Cunningham, S. A., Femke de Jong, M., de Steur, L., et al., 2017. Overturning in the Subpolar North Atlantic Program: a new international ocean observing system. Bulletin of the American Meteorological Society, 98(4), 737–752. https://doi.org/10.1175/BAMS-D-16-0057.1.

Lozier, M.S., Li, F., Bacon, S., Bahr, F., Bower, A.S., Cunningham, S.A., de Jong, M.F., de Steur, L., deYoung, B., Fischer, J. and Gary, S.F., 2019. A sea change in our view of overturning in the subpolar North Atlantic. *Science*, *363*(6426), pp.516-521.

Mercier, H., Lherminier, P., Sarafanov, A., Gaillard, F., Daniault, N., Desbruyères, D., et al., 2015. Variability of the meridional overturning circulation at the Greenland–Portugal OVIDE section from 1993 to 2010. Progress in Oceanography, 132, 250–261. https://doi.org/10.1016/j.pocean.2013.11.001.

Orre, S., Smith, J.N., Alfimov, V. and Bentsen, M., 2010. Simulating transport of 129 I and idealized tracers in the northern North Atlantic Ocean. *Environmental fluid mechanics*, *10*, pp.213-233.

Poulain, P. M., Warn-Varnas, A., & Niiler, P. P., 1996. Near-surface circulation of the Nordic seas as measured by Lagrangian drifters. Journal of Geophysical Research, 101(C8), 18,237–18,258. https://doi.org/10.1029/96JC00506.

Qiao, J.X., Hou, X.L., Steier, P., Nielsen, S., Golser, R., 2015. Method for ^{236}U determination in seawater using flow injection extraction chromatography and accelerator mass spectrometry. Anal. Chem. 87, 7411–7417. https://doi.org/10.1021/acs.analchem.5b01608.

Qiao, J., Xu, Y., 2018. Direct measurement of uranium in seawater by inductively coupled plasma mass spectrometry. Talanta 183, 18–23. https://doi.org/10.1016/j.talanta.2018.02.045.

Qiao, J.X., Hain, K., Steier, P., 2020. First dataset of ^{236}U and ^{233}U around the Greenland coast: A 5-year snapshot (2012 - 2016). Chemosphere 257, 127185. https://doi.org/10.1016/j.chemosphere.2020.127185.

Ribergaard, M.H., 2004. On the coupling between hydrography and larval transport in the Southwest Greenland waters. Ph.D. thesis. University of Copenhagen. Re-issued as DMI scientific report, 05-05.

Sarafanov, A., Falina, A., Mercier, H., Sokov, A., Lherminier, P., Gourcuff, C., et al., 2012. Mean full-depth summer circulation and transports at the northern periphery of the Atlantic Ocean in the 2000s. Journal of Geophysical Research, 117, C01014. https://doi.org/ 10.1029/2011JC007572.

Smith, J.N., Ellis, K.M., Kilius, L.R., 1998. 129I and 137Cs tracer measurements in the Arctic Ocean. Deep Sea Research Part I: Oceanographic Research Papers, 45(6), 959-984. https://doi.org/10.1016/S0967-0637(97)00107-6.

Simonsen, M., Saetra, Ø., Isachsen, P.E., Lind, O.C., Skjerdal, H.K., Salbu, B., Heldal, H.E. and Gwynn, J.P., 2017. The impact of tidal and mesoscale eddy advection on the long term dispersion of 99Tc from Sellafield. *Journal of environmental radioactivity*, *177*, 100-112.

Smith, J. N., McLaughlin, F. A., Smethie, W. M., Moran, S. B., Lepore, K., 2011. Iodine-129, 137Cs, and CFC-11 tracer transit time distributions in the Arctic ocean. J. Geophysical Res. 116, C04024. https://doi.org/10.1029/2010JC006471.

Steier, P., Dellinger, F., Forstner, O., Golser, R., Knie, K., Kutschera, W., Priller, A., Quinto, F., Srncik, M., Terrasi, F., Vockenhuber, C., Wallner, A., Wallner, G., Wild, E.M., 2010. Analysis and application of heavy isotopes in the environment. Nucl. Inst. and Methods Phys. Res. B 268 (7–8), 1045–1049. https://doi.org/10.1016/j.nimb.2009.10.094.

Sévellec, F., Fedorov, A.V. and Liu, W., 2017. Arctic sea-ice decline weakens the Atlantic meridional overturning circulation. *Nature Climate Change*, *7*(8), pp.604-610.

Våge, K., Pickart, R. S., Spall, M. A., Valdimarsson, H., Jónsson, S., Torres, D. J., et al., 2011. Significant role of the North Icelandic Jet in the formation of Denmark Strait overflow water. Nature Geoscience, 4(10), 723–727. https://doi.org/10.1038/ngeo1234.

Wefing, A.- M., Christl, M., Vockenhuber, C., Rutgers van der Loeff, M., Casacuberta, N., 2019. Tracing Atlantic waters using ^{129}I and ^{236}U in the Fram Strait in 2016. Journal of Geophysical Research: Oceans, 124, 882–896. https://doi.org/10.1029/2018JC014399.

Wefing, A.-M., Casacuberta, N., Christl, M., Gruber, N., Smith, J.N., 2021. Circulation timescales of Atlantic Water in the Arctic Ocean determined from anthropogenic radionuclides. Ocean Science 17, 111-129. https://doi.org/10.5194/os-17-111-2021.

Wefing, A-M., Casacuberta, N., Christl, M., Dodd, P.A., 2022. Water mass composition in Fram Strait determined from the combination of ^{129}I and ^{236}U: Changes between 2016, fmars.2022.9735072018, and 2019. Front. Mar. Sci. 9:973507. http://dx.doi.org/10.3389/fmars.2022.973507.

Zhang, J., Steele, M., Rothrock, D.A. and Lindsay, R.W., 2004. Increasing exchanges at Greenland-Scotland Ridge and their links with the North Atlantic Oscillation and Arctic sea ice. *Geophysical research letters*, *31*(9).

Østerhus, S., Turrell, W.R., Hansen, B., Lundberg, P. and Buch, E., 2001. Observed transport estimates between the North Atlantic and the Arctic Mediterranean in the Iceland–Scotland region. *Polar Research*, *20*(2), pp.169-175.

Department of Environmental and Resource Engineering is one of the largest university departments specializing in environmental and resource engineering in Europe. The department conducts research, development & scientific advice and provides educational programs and service to society. We are working to develop new environmentally friendly and sustainable technologies, methods and solutions, and to disseminate this knowledge to society and future generations of engineers. The Department has approximately 300 staff of more than 30 nationalities.

Department of Environmental and Resource Engineering

Bygningstorvet, Building 115
DK-2800 Kgs. Lyngby
Tlf. +45 4525 1600

www.sustain.dtu.dk